INHIBITION OF α-AMYLASE AND α-GLUCOSIDASE BY ALKALOIDS AND PHENOLICS FROM STEM BARK OF *Zanthoxylum chalybeum* and *Zanthoxylum gilletii*

BY

OTIENO KEVIN YAMO

A THESIS SUBMITTED IN PARTIAL FULFILMENT OF THE REQUIREMENTS FOR THE DEGREE OF MASTER OF SCIENCE IN CHEMISTRY

SCHOOL OF PHYSICAL AND BIOLOGICAL SCIENCES

MASENO UNIVERSITY

DECLARATION

This thesis is my original work and has never been previously submitted for examination for a degree in Maseno University or any other institution.

Otieno Kevin Yamo

MSC/SC/00006/2018

Sign…….. Date……

Declaration by Supervisors

This thesis has been submitted with our approval as Maseno University Supervisors

Dr. Charles O. Ochieng

Department of Chemistry

Maseno University

Sign…….. Date……

Dr. Joab Otieno Onyango

Department of Chemistry

Technical University of Kenya

Sign:…….. Date: …….

ACKNOWLEDGEMENT

The study was supported by the Third World Academy of Science TWAS, Research Grant (RGA NO. 18-192 RG/CHE/AF/ AC_G_FR3240303660 dated 24, September 2018) of which I am much indebted to my supervisors Dr. Charles O. Ochieng of Maseno University and Dr. Joab Otieno Onyango of Technical University of Kenya for offering me the scholarship. Acknowledgements goes of the technical support team: Dr. Moses Langat of the Jodrell Laboratory Royal Botanic Gardens, UK who performed the spectroscopic analysis of (MS and NMR) analysis on isolated compounds; and Dr. Philip Onyango of Botany Department, Maseno University for his taxonomic services at Maseno University herbarium. Thanks for social, moral and general academic development gratitudes to: The Chairman of the Department of Chemistry, Dr. Bowa Kwach; Chemistry Research group under leadership of Dr. Dorothy Okoth Professor Kowenje, Daniel Wasiali and Mr. Bernard Goga of Maseno University who guided me to Homa hills for plant sampling.

DEDICATION

This thesis is dedicated to my family, and to all that supported me throughout the study period.

ABSTRACT

Diabetes prevalence is on the rise with conventional drugs either being unaffordable, unavailable or having undesirable side effects. The plants *Zanthoxylum chalybeum* (ZC) and *Zanthoxylum giletii* (ZG) are reported for management of diabetes by local communities. Root bark and stem bark extract from two plants has shown *in vivo* anti-diabetic activity against alloxan streptozotocin–induced diabetic rats. Two benzophenanthridine alkaloids and a phenolic were established to inhibit the α-amylase and α-glucosidase activities. Based on the molecular variations of benzophenanthridine alkaloids and phenolics, the inhibitory effects of only three compounds were not predictive enough for the trends of inhibition against α-amylase and α-glucosidase. Molecular structural requirement including enzymatic inhibitory modes of alkaloids and phenolics from *Zanthoxylum* plants was also unknown. Further research to establish the structural characteristics exhibiting the enzymatic inhibition of these compounds is thus necessary to provide insight into their potential in hyperglycemic management. Therefore, the study intends to determine the structures of these compounds, their relative α-amylase and α-glucosidase inhibitory activities, and kinetic modes of inhibition of the active molecule. The stem bark of ZC was collected from Homa Hills, Kenya and stem bark of ZG from Kakamega forest, Kenya. Both the samples were air dried, ground into fine powder followed by acid-base alkaloid extraction comprising of 25% v/v of aq.NH_4OH: ethyl acetate-petroleum ether: 2% v/v H_2SO_4; chloroform fractionation into alkaloid and non-alkaloids extracts. The fractions were subjected to chromatographic separations then characterization of the pure isolates using mass spectrometry, NMR, and UV-vis spectroscopic techniques. Eleven compounds were isolated: six alkaloids {Norchelerythrine (**9**), Phenanthridine A (**42**), chalybemide A (**39**), chalybemide B (**40**), chalybemide C (**41**) and skimmianine (**21**); two phenolics {2,3-epoxy-6,7-methylenedioxy coniferyl alcohol (**10**) and sesamine(**46**})} from *Z. chalybeum*. Whereas *Z. gilettii* yielded six compounds: four alkaloids {**9**, **42**, Zanthocapensine (**43**), Zanthoamide D (**45**)}; and two phenolics {Zanthocapensol (**44**) and sesamine (**46**)}. Ten compounds showed inhibitory activities against α-amylase and α-glycosidase in the range of IC_{50} = 43.22-49.36 µM which had no significant difference ($P > 0.05$) relative to acarbose (IC_{50} = 42.67, 44.88) following *in vitro* bioassay by Worthington Enzyme assay protocols except sesamine (IC_{50} = 54.67, 54.77) which showed lower activity. The kinetic analysis based on Lineweaver-Burk plots {1/velocity vs 1/[Substrate] at constant [Inhibitor] (sample compounds)} established modes of inhibition and on each kinetic mode, Dixon plots {1/velocity vs [Inhibitor] at constant [Substrate]} were used to establish the respective enzymatic dissociation constants (Ki). Compound **10** showed competitive inhibition with Ki of 5.54 and 17.21 µM as acarbose (Ki = 6.14 and 22.40 µM) against α-amylase and α-glucosidase, respectively. Alkaloids **9, 21, 42**, and **43** showed mixed modes of inhibitions (Ki ranges 2.74-3.10 µM and 4.73-9.17 µM) in α-amylase and α-glucosidase enzymes, respectively. Compounds with amides functionality **39, 40, 41, 45** showed non-competitive inhibition (Ki = 11.05-26.69 and 17.56-44.58) against α-amylase and α-glucosidase, respectively, except compound **40** which showed uncompetitive inhibition (Ki = 44.58 µM) against α-glucosidase same as **44** (Ki = 26.28 and 20.62 µM). Compounds showing competitive inhibition similarly exhibited stronger binding (lower Ki values) to the enzymes followed by mixed inhibitors and noncompetitive modes while uncompetitive inhibitors showed the highest Ki. Compounds **10, 9, 21, 42** and **43** exhibited good activity against α-amylase and α-glucosidase thus were considered as lead compounds for management of hyperglycemia. The study offers guidance for future investigations into drug discovery using these kinds of molecular templates.

TABLE OF CONTENTS

LIST OF ABBREVIATIONS AND ACRONYMS

^{13}C NMR	-	Carbon-13 Nuclear Magnetic Resonance
^{1}H NMR	-	Proton Nuclear Magnetic Resonance
ANOVA	-	Analysis of Variance
br	-	broad
CC	-	Column Chromatography
$CDCl_3$	-	Deutrated trichloromethane
COSY	-	Correlation Spectroscopy
DMSO	-	Dimethylsulfoxide
d	-	doublet
DBP	-	Dihydrobenzo[c]phenanthridine
DCM	-	Dichloromethane
dd	-	doublet of doublet
DEPT	-	Distortionless Enhancement Polarization Transfer
DM	-	Diabetes Mellitus
DNA	-	Deoxyribonucleic Acid
DNS	-	Dinitrosalycilic acid
EIMS	-	Electron Ionization Mass Spectroscopy
ES	-	Enzyme-substrate
ESI	-	Enzyme-Substrate-Inhibitor
ESIMS	-	Electron spray Ionization Mass Spectrometry
EtOAc	-	Ethyl acetate
GC/MS	-	Gas Chromatography/Mass Spectrometry
GH	-	Glycoside Hydrolase
HBP	-	Hexahydrobenzo[c]phenanthridine
HIV	-	Human Immunodeficiency Virus
HMBC	-	Heteronuclear Multiple Bond Correlation
HMQC	-	Heteronuclear Multiple Quantum Correlation
HPLC	-	High Performance Liquid Chromatography
HREIMS	-	High Electron Ionization Mass Spectroscopy
HSQC	-	Heteronuclear Single Quantum Correlation

Hz	-	Hertz
IC_{50}	-	Inhibitory Concentration of 50%
J	-	Coupling constant
K_i	-	Dissociation constant
[M]+	-	Molecular ion
m	-	multiplet
MeOH	-	Methanol
mg	-	milligram
MHz	-	Mega Hertz
mL	-	Milliliter
mM	-	millimole
m.p	-	melting point
MS	-	Mass spectrometry
m/z	-	Mass to charge ratio
NMR	-	Nuclear Magnetic Resonance
NOE	-	Nuclear Overhauser Effect
NOESY	-	Nuclear Overhauser Effect Spectroscopy
ppm	-	parts per million
PTLC	-	Preparative Thin Layer Chromatography
QBP	-	Quaternary benzo[c]phenanthridine
Rf	-	Retention factor
s	-	singlet
SAR	-	Structure-Activity Relations
t	-	triplet
TLC	-	Thin Layer chromatography
TMS	-	Tetramethylsilane
UV-Vis	-	Ultraviolet-visible
WHO	-	World Health Organization
ZC	-	*Zanthoxylum chalybeum*
ZG	-	*Zathoxylum gilletii*
δ	-	Chemical shift in pp

LIST OF TABLES

LIST OF FIGURES

LIST OF APPENDICES

CHAPTER ONE

INTRODUCTION

1.1 Background Information

Diabetes mellitus, a metabolic disease resulting from irregularities in insulin secretion and activity, is characterized by chronic hyperglycemia (WHO, 1999). This occurs when the pancreas is unable to produce enough insulin (Ünal *et al*, 2012; Gardner and Shoback, 2011). Insulin receptor sensitivity or insufficiency is a major factor in type 1 and type 2 diabetes as well as gestational diabetes. Type 1 diabetes is brought about by the pancreas' incapacity to produce enough insulin, whereas gestational diabetes develops during pregnancy. Type 2 diabetes is a complex metabolic disorder marked by prolonged hyperglycemia (Fernandez-Mejıa, 2013) and defective insulin action (Lin and Sun, 2010), often linked to overproduction of free radicals (Johansen *et al*, 2005). Despite being less common than Type 1, Type 2 diabetes remains a significant challenge and requires more research attention.

By the year 2016, 422 million people had been diagnosed with diabetes (WHO, 2016). In addition 80% of deaths from the disease in low- and middle-income nations had occurred by 2006 (Mathers and Loncar, 2006). Factors contributing to this increase include a shift towards processed foods, urbanization, and a decline in physical activities, as well as inadequate management techniques and faulty diagnosis (WHO, 2016). Type 1 diabetes is normally managed by insulin injection therapy (Gough and Narendan, 2010), while type 2 diabetes is managed by oral anti-diabetic medications like sulphonylureas, biguanides, thiazolidinediones, and α-glucosidase inhibitors (Krentz and Bailey, 2005). However, many reports of unsuccessful all-round therapy suggest the need for further research on more effective treatments.

Diabetes management involves managing starch digestion and absorption rates using starch digestive enzyme inhibitors moderate postprandial hyperglycemia (Ye *et al*., 2008). These enzymes including Glycosidase Hydrolases (GH), break down glycosidic bonds in starch, producing simple sugars (Lombard *et al*, 2013). The key enzymes include α-amylase which break down internal α-1,4-glycosidic bonds (Rajagopalan and Krishnan, 2008; Gupta *et al*, 2011), while brush border hydrolases (sucrase-amylase, maltase-gluco-amylase, α-glucosidase and amylase) digest dietary carbohydrates in the small intestine (Hooton *et al*, 2015). Modulating these enzymes may predispose the body to positive pathophysiological conditions, potentially aiding in diabetes type 2 management. The search for natural modulators of these enzymes is thus envisaged as safe avenue for discovery alternative anti-diabetic options (Gupta *et al*, 2011).

Shai *et al.* (2010) suggested that employing natural α-amylase inhibitors derived from food and medicinal plants is a better option for controlling hyperglycemia by decreasing post-prandial serum glucose levels. Notably, a number of α-amylase inhibitors, including nojirimycin, valiolamine, voglibose, and acarbose (Niwa *et al*., 1970) as well as Miglitol (**6**), salacinol (**2**) and kotalanol (**3**) (Yoshikawa *et al*, 1998), which were isolated either from higher plants or lower plants then later synthesized. However, many of the synthetic analogues have shown certain limitations including being non-specific, displaying serious side effects and failure to manage hyperglycemia successfully.

Grant (2003), highlighted the limitations and high costs of prescription drugs, particularly insulin, in managing diabetes. Furthermore, with prolonged management of diabetes mellitus with insulin has specific disadvantages, including brain atrophy, insulin resistance, anorexia nervosa, fatty liver tissues and (Verspohl, 2012). It is therefore necessary to look at alternative therapy and management approaches in light of these restrictions. Natural sources like plants offer an alternative management resources, but their applications are limited due to insufficient coherent scientific information to support the usage.

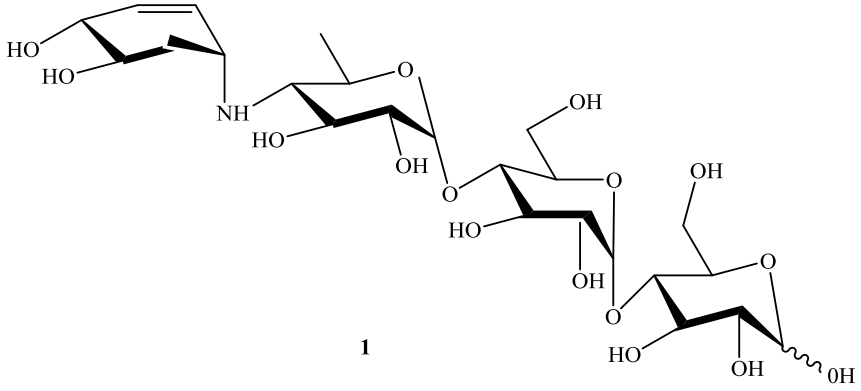

1

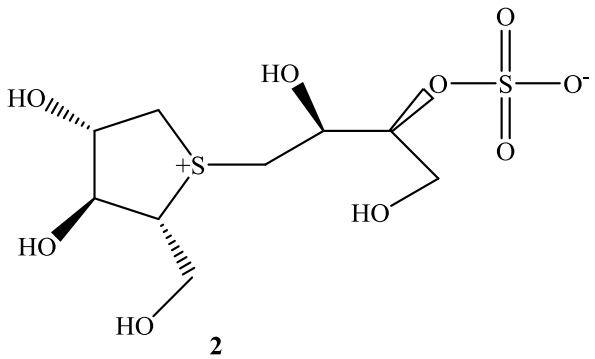

2

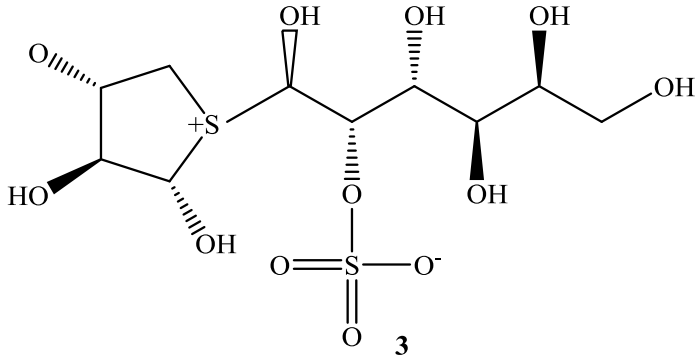

3

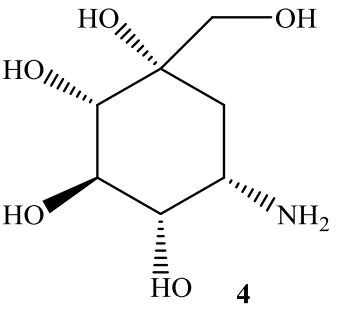

4

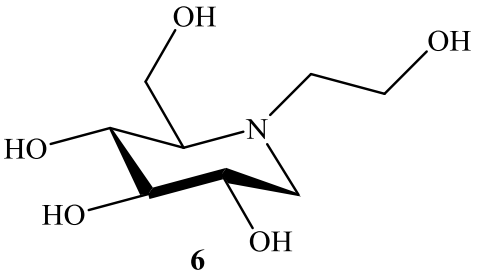

6

Traditional medicine suggests that various plants have anti-diabetic properties, benefiting patients with diabetic retinopathy, insulin-dependent and non-insulin-dependent diabetes as well as diabetic peripheral neuropathy (Trojan-Rodrigues *et al,*. 2012). Among these plants are *Zanthoxylum chalybeum* and *Zanthoxylum gilletii* (Agwaya et al, 2016; Kokwaro, 2009). *Z. chalybeum* has anti-hyperglycemic effects *in vivo*, while *Z. gilletii* manages various ailments such as malaria, tuberculosis, including viral and cancerous (Kokwaro, 2009). Both plants have anticancer, anti-leukemia, antimicrobial (Nakanishi *et al*, 1998), anti-viral (Tan *et al*, 1991), and anti-diabetic properties (Mbaze *et al*, 2007). The plants were separately noted to be used in management diabetic cardiomyopathy (Agwaya *et al*, 2016). However, possible chemical leads displaying these different beneficial effects remain uncertain.

The phytochemical information on *Z. gilletii* and *Z. chalybeum* and their anti-diabetic activities are inconsistent, with only 3-β-acetoxy-16-β-hydroxybetulinic acid showing mild α-glucosidase inhibitory effects. Triterpenoids isolated from *Z. chalybeum* displayed mild inhibitory activities against α-amylase. This previous study pointed out *in vitro* inhibitory effects against α-glucosidase and α-amylase activities of two benzophenanthridine alkaloids, while lupeol, 3α, 20-hydroxy-3-oxo-28-lupanoic acid, 20-dihydroxy-28-lupanoic acid and 3α,20,28-trihydroxylupane registered low activity (Wasiali, 2019).

Phytochemical information linking the two plants to management of diabetic conditions are inconsistent, for instance *Z. gilletii* is known for furoquinoline alkaloids, cinnamic acid amides and benzophenathridine alkaloids (Islam *et al*, 2001) which have not been evaluated for anti-

hyperglycemic potential. Except for 3-β-acetoxy-16-β -hydroxybetulinic acid (**7**), a triterpenoid from the *Z. gilletii* stem bark that showed mild α-glucosidase inhibitory effects (Mbaze *et al*, 2007). Conversely, triterpenoids isolated from *Z. chalybeum* showed mild activities against α-amylase inhibitory effects relative to benzophenthridine alkaloids against α-amylase inhibitory effects (Wasiali, 2019). Two benzophenanthridine alkaloids {6-hydroxy-N-methyl decarine (**8**) and norchelerynthrine **9**)} and a phenolic {2,3-epoxy-6,7-methylenedioxyconiferyl (**10)}** showed potent *in vitro* inhibitory effects against α-glucosidase and α-amylase activities, while lupeol, 3α,20-dihydroxy-28-lupanoic acid, 20-hydroxy-3-oxo-28-lupanoic acid, and 3α,20,28-trihydroxylupane registered low activity (Wasiali, 2019). This means that the most active compounds were not actually the triterpenoids in *Z. gilletti*, but since triterpenoids are stable and are easy to isolate, consequently the only pure isolate that was tested but in the crude some other compounds could have been active as well but might have not been isolated.

The anti-hyperglycemic potentials of *Zanthoxylum* has been attributed to the existence of benzophenanthridine alkaloids together with additive effects of phenolics compounds (Wasiali, 2019). However, the genus is known to elaborate different classes of benzophenanthridine alkaloids with marked structural variation that normally exhibit variable biological activities (Tavares *et al*, 2014). Generally, benzophenanthridine alkaloids are classified into three classes: dihydrobenzo[c]phenanthridine-type (DBP), quaternary benzo[c]phenanthridine-type (QBP), and hexahydrobenzo[c]phenanthridine-type (HBP) (Krane *et al*, 1984). The two alkaloids (**8** and **9)** reported as active against α-glucosidase and α-amylase structurally belong to the DBP although the other two (HBP and QBP) forms are also noted with scaffold necessary for specific biological activities (Tavares *et al*, 2014). Since all these benzophenanthridine alkaloids types and their various derivatives have been isolated from the genus *Zanthoxylum*, it implies existences of interesting molecular chromophores worth exploring. The activity of only one type cannot qualify that all the benzophenanthridine alkaloids and phenolic from *Zanthoxylum* plants are active against α-glucosidase and α-amylase hydrolytic effects on carbohydrates. To this extent, the varied functionalities among benzophenanthridine alkaloids and phenolic that predispose inhibition of both α –amylase and α-glucosidase are unknown.

Based on chemotaxonomic similarities, the benzophenathridine alkaloids and phenolics from *Z. gilletti* and that of *Z. chalybeum* presumably should display common biological activities which vary depending on difference in molecular structures. Such an assertion, endorses structure-activity relationship study on benzophenathridine alkaloids and phenolics from these plants, which then require targeted systematic extraction and separation procedures for alkaloids and phenolics.

Besides, establishing the possible activity trends among these benzophenathridine alkaloids and phenolics together with their possible inhibitory kinetics parameters would determine the precise mode of inhibition as either uncompetitive, noncompetitive, mixed inhibition or competitive inhibition, are unknown.

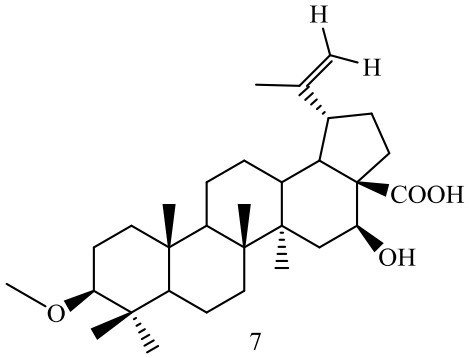

7

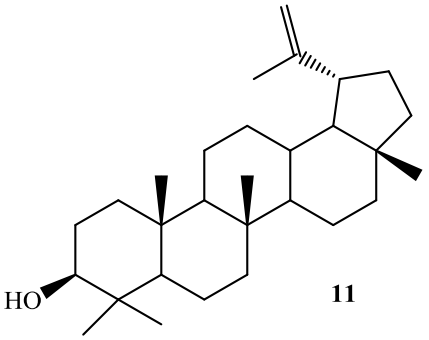

11

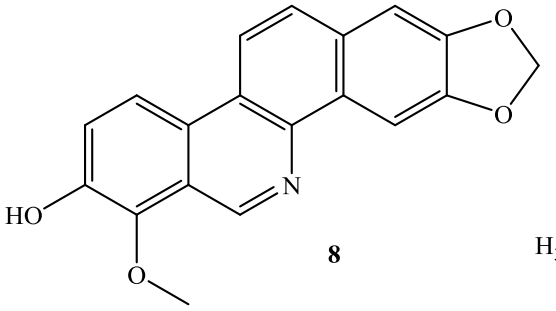

8

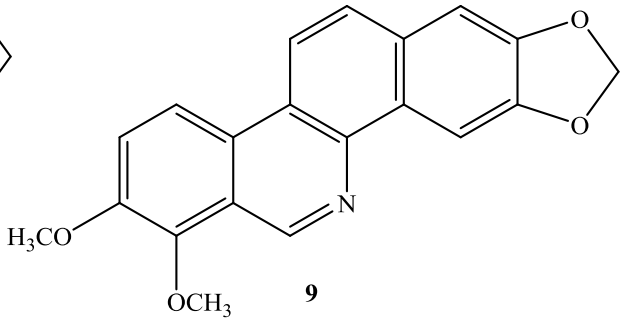

9

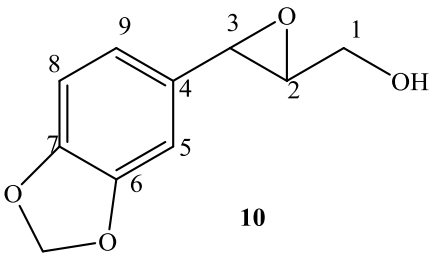

10

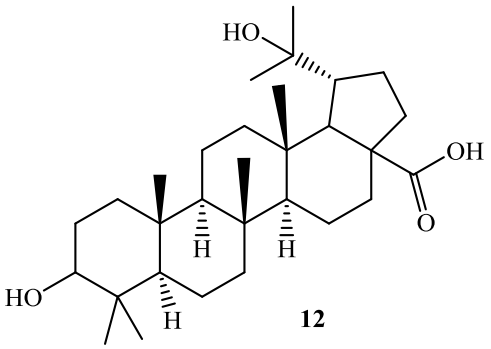

12

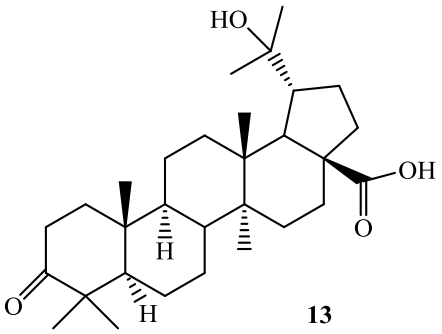

13

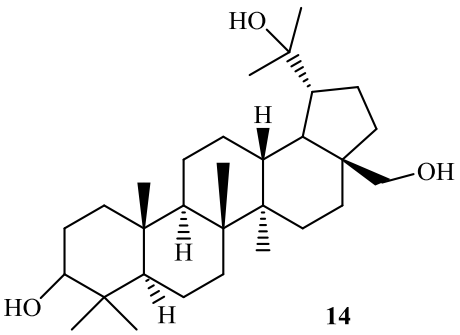

14

1.2 Statement of the Problem

The plants, *Zanthoxylum chalybeum* and *Zanthoxylum gilletii* have been identified as medicinal plants with potential for managing diabetes including hyperglycemia although there is scanty pharmacological evidence to validate the claims. Reported data indicate two benzophenanthridine alkaloids and a phenolic from *Zanthoxylum chalybeum* as active against α-amylase activity despite the different classes of these compounds elaborated by the genus. Based on the varied classes of benzophenanthridine alkaloids and phenolics, inhibitory effects of only one class cannot qualify that all benzophenanthridine alkaloids from *Zanthoxylum* genus are active as α-glucosidase and α-amylase inhibitors hydrolytic effects on carbohydrates. Data that can be used for predicting the activities of these compounds is lacking. In other words, the varied functionalities among benzophenanthridine alkaloids and phenolic that predispose inhibitory effects on both α-glucosidase and α-amylase are unknown. Besides, the possible enzymatic inhibitory activities trends, the inhibitory kinetics modes have not been established among these compounds.

1.3 Objectives

1.3.1 General Objective

To determine molecular structures of alkaloids and phenolics from the stem barks of *Zanthoxylum chalybeum* and *Zanthoxylum gilletii* and their kinetic modes of inhibition towards α-amylase and α-glucosidase activities.

1.3.2 Specific Objectives

i. To isolate and elucidate structures of compounds from the stem bark of *Zanthoxylum chalybeum* and *Zanthoxylum gilletii* using chromatographic and spectroscopic techniques.

ii. To ascertain the relative inhibitory activity of the isolated compounds from objective (i) against α-amylase and α-glucosidase activities on carbohydrate substrate.

iii. To determine the modes of inhibition of the active isolated compounds from the objective (ii) against α-amylase and α-glucosidase activities on carbohydrates substrate.

1.4 Null Hypothesis

Benzophenanthridine alkaloids and phenolics from *Zanthoxylum chalybeum* and *Zanthoxylum gilletii* do not significantly inhibit activities α-amylase and α-glucosidase relative to a standard drug (acarbose).

1.4.1 Research Questions

What are the molecular structural variations of alkaloids and phenolic compounds present in the stem bark of *Z. chalybeum* and *Z. gilletii* which are responsible for amylase and glucosidase inhibition?

What are the modes/mechanism of inhibition of α-amylase and α-glucosidase enzymes by alkaloids and phenolics from *Z. chalybeum* and *Z. gilletii* stem bark*?*

1.5 Justification of the Study

Diabetes mellitus is a global epidemic for which there are no effective treatments or their side effects are either unfavorable. Because most people in underdeveloped countries find herbal medications to be acceptable, economical, and easily available, they are growing in popularity. Establishing an efficient supplementary and alternative diabetes management strategy is necessary for the impoverished communities in developing nations, as the current anti-hyperglycemic medicines are not very effective and have undesirable side effects. Herbal remedies, of which *Zanthoxylum spp*. are a plentiful source, may provide such safe and efficient substitutes. Based on the few reports inclining the metabolites from these plants especially alkaloids and phenolics which vary depending on difference in molecular structural features. Molecular variation normally predisposes varied biological activities, which require predictive structure-activity relationship (SAR) study which can be used for development of active drug

components. Moreover, establishment of the possible activity trends among these alkaloids and phenolics together with their possible kinetics modes of inhibition would provide necessary information relevant for the development of the urgently need alternative medicinal remedies from natural resource.

CHAPTER TWO
LITERATURE REVIEW

2.1 Diabetes Mellitus

Mammals must digest complex carbohydrates, starch, for provision of energy the body needs (Quezada *et al.,* 2007). During starch metabolism, complex pathophysiological conditions can interfere with starch hydrolysis, leading to diabetes mellitus. This condition is associated with hyperglycemia, or elevated blood glucose levels, is a complication of this chronic illness (Gerich *et al*, 2006; Zeyana *et al*, 2013). In 2016, over 360 million people worldwide were diagnosed with diabetes due to unhealthy lifestyles, obesity, and ageing (WHO, 2016). Prolonged hyperglycemia can cause organ failure including kidneys, heart, blood vessels, nerves, eyes, and kidneys (Gerich, 2006).

In 2014, 8.5% of people who were 18 years of age or older had diabetes. In 2019, diabetes-related mortality accounted for 1.5 million deaths, with 48% of these deaths occurring in those under the age of 70. Diabetes was responsible for 20% of deaths from cardiovascular disease and 460,000 deaths from renal disease, according to the (WHO, 2016). Between 2000 and 2019, there was a 22% global drop in non-communicable diseases, however diabetes raised age-standardized death rates by 3%, leading to a 13% increase in mortality in lower-middle income nations (WHO, 2020).

Type 1, type 2, and gestational diabetes are three types of diabetes. Type 1 causes insufficient insulin production due to pancreatic β-cell destruction occasioned by genetic susceptibility (Eckel *et al*, 2011), while type 2 results from malfunctions and insulin resistance (Lin and Sun, 2010). Gestational diabetes occurs during pregnancy due to hormonal changes (Eckel *et al*, 2011). Treatments include insulin from outside sources to manage type 1 diabetes whereas healthy diet, exercise, and administration hypoglycemic agents are applied for type 2 (Krentz and Bailey, 2005). To date, finding a safe, efficacious drug to combat all conditions simultaneously without side effects is a challenge to be addressed.

A part from insulin administration other oral anti-hyperglycemia therapeutic options available include sulphonylureas (**15**) and meglitinides (**16**) drugs which stimulate pancreatic insulin secretion. Biguanides (**17**) and metformin (**18**) medication reduce hepatic glucose production and thiazolidinediones (**19**) improve insulin action. While Miglitol (**6**) and acarbose (**1**) delay digestion and absorption of glucose (Luna and Feinglos, 2001). The latter option has not received much attention due to several options and its mild effectiveness, although it may prove to be safe in terms of preventive measures.

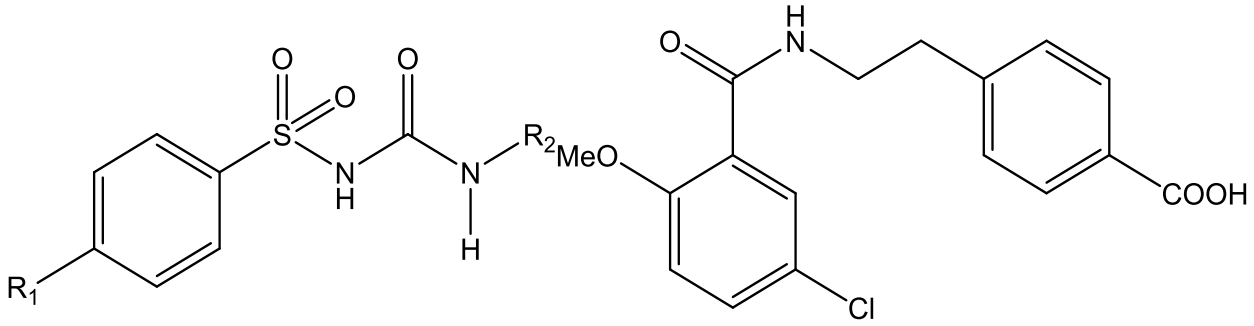

15 **16**

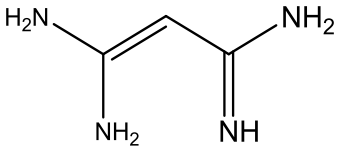

17

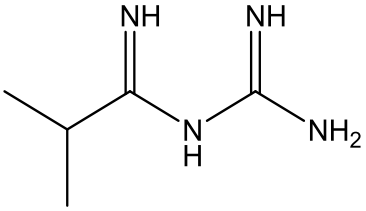

18

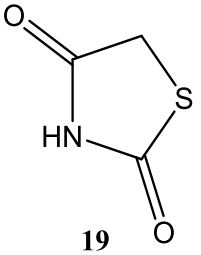

19

2.2 Carbohydrate metabolism

Carbohydrates is key dietary component for energy provision for animals is broken down by enzymes at the small intestine. (Haque and Tan, 2017). Enzymatic hydrolysis of glycosidic bonds in disaccharides and polysaccharides is crucial for metabolism to simple sugars. Management of the rate of carbohydrate digestion to avoid too much or less glucose in the bloodstream has thus been regarded as an option in management of diabetes mellitus (Ünal *et al*, 2012).

2.2.1 Glycoside Hydrolases

Glycoside hydrolases are enzymes that break down the glycosidic bond between carbohydrates or carbohydrate and non-carbohydrate components. Glycoside hydrolases have been categorized using a similarity in sequence, which has resulted in the identification of more than a thousand distinct enzyme families that are selective to various substrates (Henrissat and Davies, 1995).

2.2.2 α-Amylase

α-amylases are found in saliva and pancreatic secretions. They are responsible for breaking down the internal α-1,4-glycosidic linkages in starch (Fig. 1(a)). Amylases convert starch into low-molecular-weight products. These low-molecular products are in form of maltose, short oligosaccharides, and limit dextrins, they are branch points of amylopectin (Rajagopalan and Krishnan, 2008). The main function of α-Amylase is to reduce workload in the small intestines and

prevent oligosaccharide accumulation (Horton and Tomasik, 2015; Wickham *et al*, 2015). However, high amylase activities may lead to excess oligosaccharides, requiring control to avoid excess glucose generation.

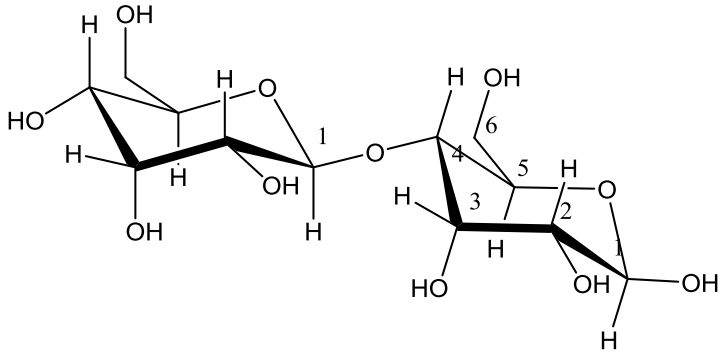

Fig.1 (a): α-1, 4-glycosidic linkage

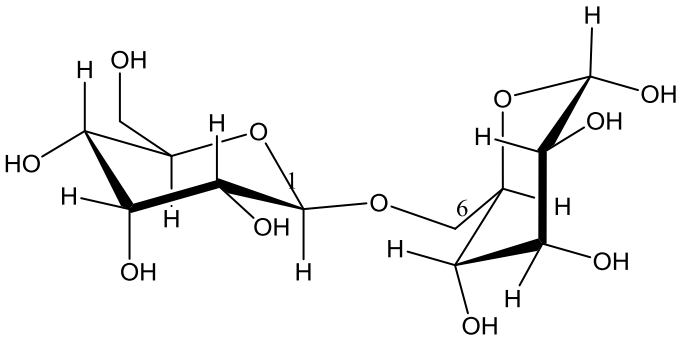

Fig 1(b) α-1, 6-glycosidic

Figure 1: Structure of Glycoside

2.2.3 Brush-border hydrolases

The final stage of digestion of dietary carbohydrates is performed by brush border hydrolase enzymes on the face of small intestinal enterocytes (Vaughan, 2002). Brush border enzymes, tethered to the plasma membrane. They vary in density and distribution depending on animals age and small intestine segments or may vary due to food type the animals was fed on. After digestion monosaccharides are absorbed into epithelial cells (Ross *et al*., 2016).

The brush border membrane contains two enzymes, sucrase-isomaltase and maltase-glucoamylase, (together are referred to as α-glucosidase). They perform the final stages of carbohydrate digestion (Simpson *et al*, 2015). Maltase-glyco-amylase has multiple active sites, converting maltose or maltotriose residues into α-D-glucose and releasing β-D-glucose. Similarly, sucrase-isomaltase has

two active sites with distinct specificities, catalyzing the breakdown of sucrose into fructose and glucose (Mhlongo, 2014). Controlling these enzymes may require general α-glucosidases inhibitors to prevent excessive glucose release into the bloodstream.

2.2.4 Enzyme Inhibition Modes

Enzyme structure studies can aid in understanding inhibitory mechanisms, although structural data may be unavailable, consequently limiting determination of enzyme-inhibitor binding affinity. Nevertheless, kinetic investigation using Michaelis-Menten (equation 1), has often been used to establish the inhibition modes of enzymes by different inhibitors (Kumar, 1985),

$$V_0 = \frac{V_{max}\,[S]}{K_m + [S]} \qquad \text{Equation } \mathbf{1}$$

where enzymatic activities is described in terms of; Michaelis constant, K_m and maximum velocity, V_{max} (Michaelis, 1913). Equation 1 can be modified to the double reciprocal rate equation known as Lineweaver – Burk equation (equation 2) in order to obtain linear plots for enzyme inhibition reactions (Tong and Jingyan, 1999). From this equation, Km and V_{max} can be obtained.

$$\frac{1}{v} = \frac{Km}{Vmax\left(1+\frac{[1]}{Ki}\right)} \cdot \frac{1}{[S]} + \frac{1}{Vmax} \quad or \quad \frac{1}{v} = \frac{K'm}{Vmax} \cdot \frac{1}{[S]} + \frac{}{V} \qquad \text{Equation}$$

An inhibitor may bind to an enzyme's active site (isosterically) and then fail to release the enzyme, preventing the formation of an enzyme-substrate complex and irreversibly inhibiting the conversion of the substrate into the product (Whitely, 2000). Conversely, inhibitors may also isosterically bind with an enzyme or allosterically bind but release the enzyme (reversible inhibition) (Punekar, 2018).

Reversible inhibitions can be classified as competitive, noncompetitive, or uncompetitive (Brandt *et al*., 1987). In the case of competitive inhibition, the inhibitor binds to the enzyme's active site to form the enzyme-inhibitor complex (scheme 1), which reduces the enzyme's affinity for the substrate and is indicated by an increase in the Michaelis constant (V_{max}, K_m apparent) (Fig 2(a)). When the substrate concentration increases, the excess substrate overcomes the inhibitor and the reaction proceeds to acquire the maximum rate of reaction (V_{max}). Therefore, in competitive inhibition, V_{max} is the same as that of the control while the turn over number (K_{cat}) remains constant (Cheng and Prusoff, 1973) as illustrated in figure 2(b).

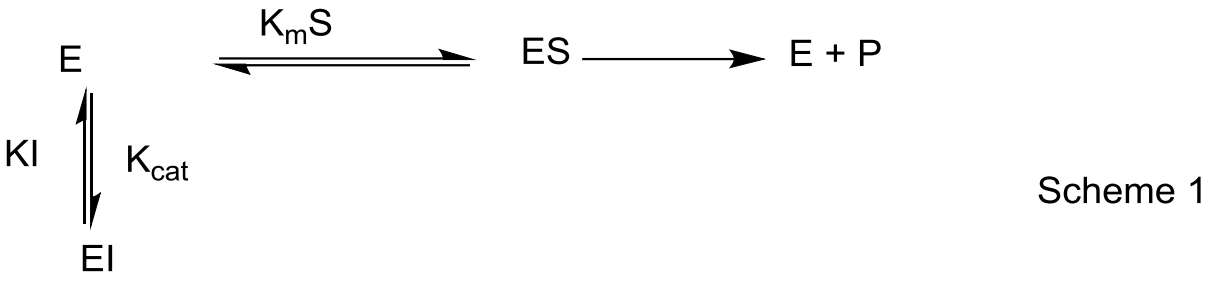

Scheme 1

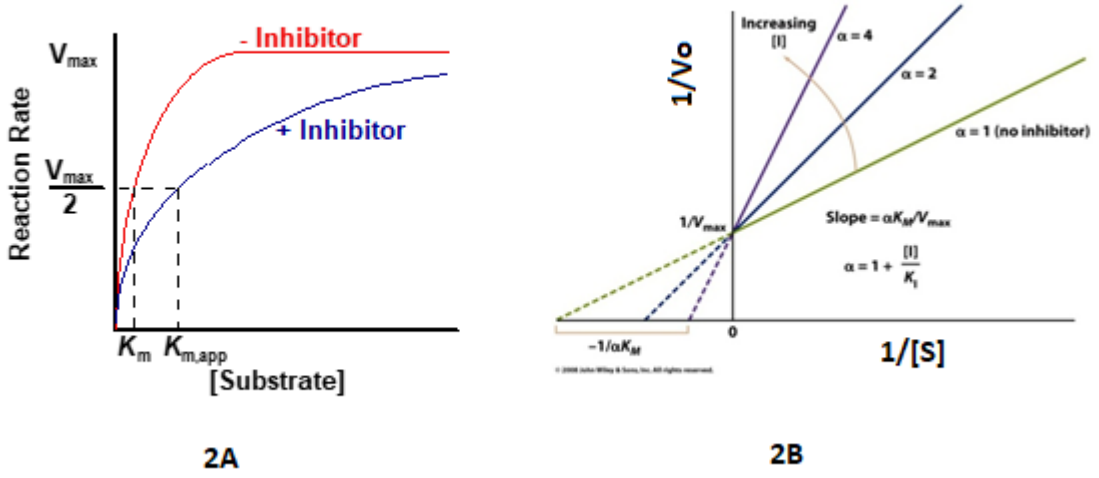

Figure 2: Competitive Inhibition curves: 2A) Michaelis-Menten plot reaction velocity vs substrate concentrations; 2B) Lineweaver-Burk plot of 1/initial velocity vs 1/[Substrate].

Inhibitor binds with both the free enzyme and the enzyme-substrate complex, resulting in noncompetitive inhibition. A tertiary complex (ESI) is created when the inhibitor attaches to the enzyme-substrate complex as well as when it binds to the free enzyme. This prevents the enzyme from converting the substrate into the product (scheme 2). The increase in substrate concentration does not overcome inhibition. The V_{max} decreases due to decrease in the number of functional enzymes since there is decrease in the number of active sites whereas K_m remains constant (Fig 3(a)). The turn over number is lowered because as the enzyme binds with the inhibitor, the inhibitor changes the shape of the enzyme making it non complementary to the substrate (Fig 3(b)) (Brandt *et al*, 1987).

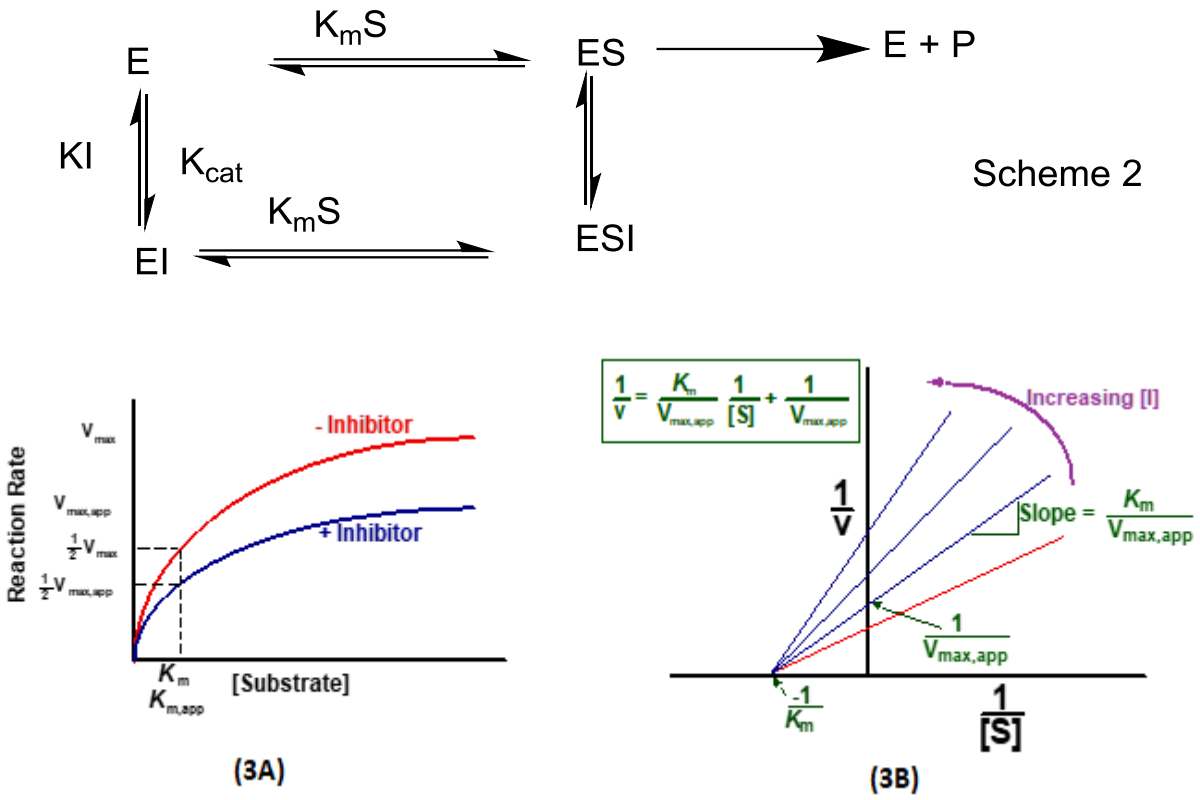

Figure 3: Non-Competitive Inhibition curves: (3A) Michaelis-Menten plot of reaction velocity vs substrate concentration; (3B) Lineweaver-Burk plot of reciprocal of initial velocity vs reciprocal of substrate concentrations

Enzyme-substrate-inhibitor complexes are formed through uncompetitive inhibition, wherein the inhibitor binds exclusively to the enzyme-substrate complex (scheme 3). Since the substrate is then firmly contained within the complex, no product is produced. Increase in the substrate concentration favors inhibition since more ES complexes are availed by increasing substrate concentration. The V_{max} is decreased (Figure 4(a)) since the number of functional enzymes is decreased because most of the ES are converted to ESI complex which does not dissociate to be converted to products (Tayyab, 1990). The K_m value decreases because when the ES combines with the inhibitor, the substrate is not released from the ESI complex hence affinity of the substrate to enzyme thus decreasing the K_m value (Cornish-Bowden, 1986).

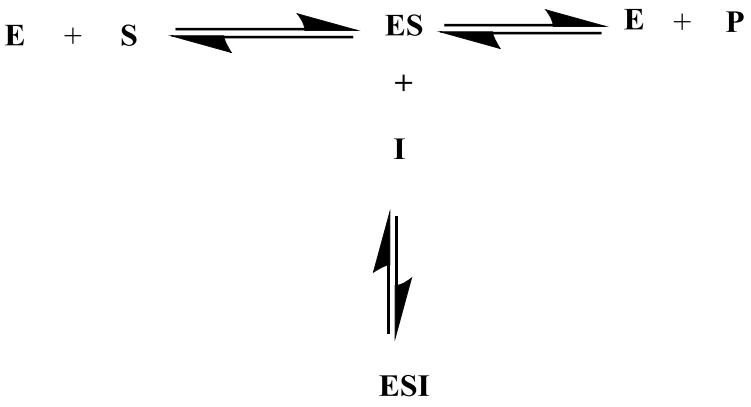

Scheme 3

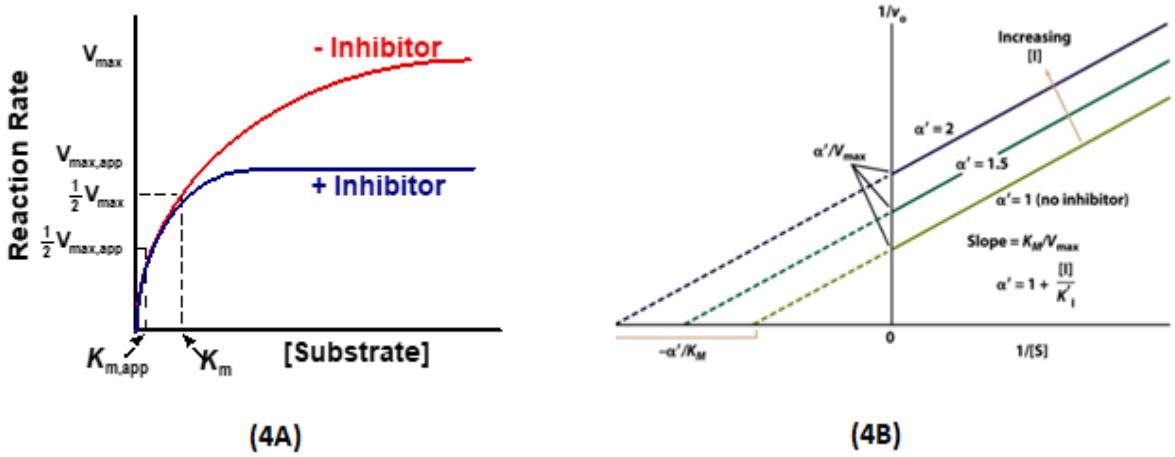

Figure 4: Uncompetitive Inhibition curves: (4A) Michaelis-Menten plots of reaction velocity vs substrate concentration; (4B) Lineweaver-Burk plot of reciprocal of initial velocities vs reciprocal of substrate concentration.

Enzyme-inhibitor (EI) and enzyme-substrate-inhibitor (ESI) complexes are formed when an inhibitor binds to both enzyme (E) and enzyme-substrate (ES) complexes. These complexes dissociate in distinct ways because the EI and ESI constants have different dissociation constants. Both V_{max} and K_m are lowered (Figure 4).

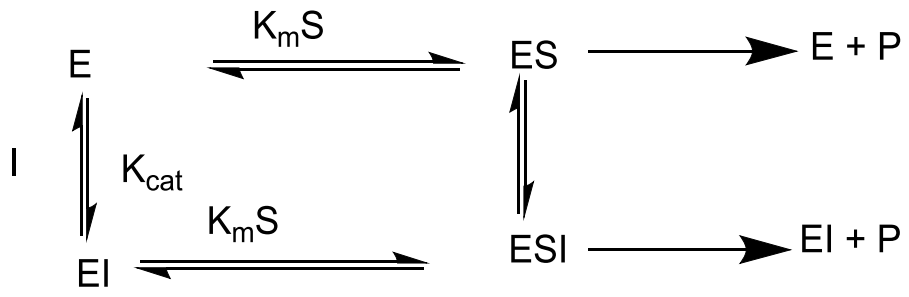

Scheme 4

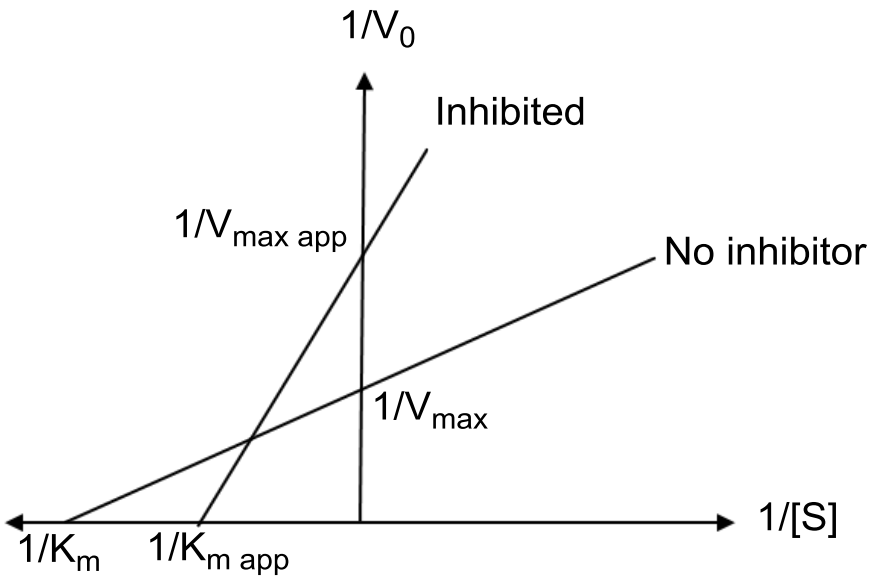

Figure 5: Lineweaver-Burk plot for Mixed Inhibition

2.3 Starch- Digesting Enzymes inhibitors

Enzyme-inhibitor (EI) and enzyme-substrate-inhibitor (ESI) complexes form when an inhibitor binds to both, obstructing the small intestine's process of converting disaccharide to monosaccharide. Such inhibitors thus slow glucose entry and can be used for management of postprandial hyperglycemia (Shimabukuro *et al*, 2006).

2.3.1 Acarbose and Miglitol

Acarbose (**1**) is an anti-hyperglycemic drug used to manage type-2 diabetes mellitus which until recently was believed to be effective, and safe and for treatment of type 2 diabetes (Zhang, 2013). Nevertheless, it has been noted as ineffective in patients on a relatively high carbohydrate diet (Zhu et al, 2011). Moreover, side effects associated with poor absorption leading to abdominal discomfort from the gastrointestinal tract have been reported on patients who use the drug (Putter *et al*, 19).

Conversely, miglitol (**6**) is an oral medication that lowers blood sugar levels by preventing the body from converting complex carbohydrates into glucose (Guntram, 2013) The amount of non-monosaccharide carbohydrates in an individual's diet determines how much miglitol (**6**) and other structurally related iminosugars inhibit α-amylase enzymes by slowing the digestion of carbs and decreasing postprandial hyperglycemia (Rebecca, 2013). Unlike acarbose (**1**), miglitol (**6**) is well

absorbed with a 100% systemic bioavailability. It is not metabolized and is eliminated by the kidneys in its unaltered form because of its strong structural similarity to glucose (Joubert *et al.,* 1990). As mentioned earlier, these two medications along with other plant-based inhibitors are used for treatment of postprandial hyperglycemia, as they have been demonstrated to have a strong inhibition activity against α-glucosidase and a little inhibitory impact on the activity of α-amylase (Afonne, 2002).

In recent times, herbal medicines have gain relevance in the management of diabetes mellitus since they are less costly and have less adverse effects than synthetic anti-hyperglycemic medications (Mukherjee *et al*, 2006). However, the specificity of the inhibition modes remains unknown since many herbal plants that have been cited to act against diabetes mellitus and not much has been documented such inhibitors.

2.4 Compounds from *Zanthoxylum* Plants and their biological activities

There have been reports of notable anti-hyperglycemic effects from a number of plants in the genus Zanthoxylum (Aloke *et al,* 2012). For example, root bark, stem bark and leaves of *Z. zanthoxyloides* is used medicinally for treating diabetes mellitus (Wagman, 2001).

In addition, stem bark of *Z. armatum* stem bark has been reported to have anti-hyperglycemic potential by lowering blood glucose levels in rats with diabetes caused by streptozotocin. This effect was related to the presence of alkaloids and phenolic compounds (Karki *et al*, 2014). When *Z. chalybeum* stem bark extract was given to streptozotocin-induced diabetic rats, blood glucose levels significantly decreased. This study finding partially supported the plant's traditional use in the treatment of diabetes (Kimani, 2015). The genus *Zanthoxylum* is a rich source of alkaloids, lignans, steroids, coumarins, benzonoids, terpenes, coumarines, flavonoids, fatty acids and amides (Fang *et al,* 2014). Alkaloids and coumarins are the primary elements of the genus, according to a review by Negi *et al*. (2011).

A number of species in the genus *Zanthoxylum* have been identified through phytochemical characterization as containing alkaloids, including chelerythrine (**20**), skimmianine (**21**) and arnottianamide (**22**), nitidine (**23**), N-methyl flindersine (**24**) (Krane *et al*., 1984), zanthomuurolanines (**25**) and dihydrochelerythrine (**26**) (Matu, 2011), rutaecarpine (**27**) and lignans (**28**) (Sheen *et al.,* 1994). *Z. nitidine* produced nitidine **(23**), which was isolated (Gakunju *et al*, 1995). Seven compounds were isolated from *Zanthoxylum holtszianum* during a phytochemical investigation for antimicrobial principles. Of these, three were benzophenanthridine alkaloids [dihydrochelerythrine (**26**), 6-acetonyldihydrochelerythrine (**27**) and 8-oxochelerythrine

(**28**)], along with a phenol canthine-6-one (**29**) and fatty acids, flavanones, and amides.Strong anti-diabetic effects were reported for flavonoids, chelerythrine (20), berberine (30), and phenol canthine-6-one (**29**) that were extracted from the methanol extract of *Z. zanthoxyloides* root bark (Odebiyi and Sofowora, 1979; Tsuchiya, 1996), supporting the activity described on *Z. chalybeum*.

Similarly, skimmianine (**21**) isolated from seed extract of *Z. chalybeum* showed both anti-hypeglycemic and anti-lipidemic properties (Olila *et al*, 2001). Muganga *et al*., (2014) in a bio-guided methanol root bark extract of Z. chalybeum fractionation identified nitidine **(23)** as the main antimalarial compound alongside chelerythrine (**20)** and methyl canadine (**31).** Adia *et al*, (2016) reported the isolation of fagaramide (**32**) from Uganda's *Z. chalybeum* stem bark that was associated with management of diabetes. Anza *et al*, (2014) reported that *Z. chalybeum* root extract (CH_2Cl_2/CH_3OH 1:1) underwent phytochemical screening, which identified the presence of anthraquinones, alkaloids, flavonoids, terpenoids, and tannins, but no pure molecule was ever extracted. A coniferyl alcohol derivative, 2,3-epoxy-6,7-methylenedioxy coniferyl (10) and a known alkaloid, dihydrochelerythrine (**26**), which had been previously isolated from *Z. nitidum*, were obtained from the extract by column chromatographic separation (Yang *et al,* 2014; Krane *et al*, 1984).

The aqueous root extract of *Z. chalybeum* showed good anti-hyperglycemic and anti-hyperlipidemic capabilities in an inquiry on the impact of the plant on diabetes-induced cardiac dysfunction in alloxan-induced type-1 diabetic rat. The study concluded that the plant possesses wide therapeutic benefits including anti-diabetic and anti-oxidant activities (Agwaya *et al*, 2016. A single phenolic 2,3-epoxy-6,7-methylenedioxy coniferyl alcohol (**10**) and two benzophenanthridines, 6-hydroxy-N-methyl decarine (**8**) and norchelerythrine (**9**) were isolated from the stem bark of *Z. chalybeum* and shown to exhibit antidiabetic activity by inhibiting carbohydrate hydrolytic activities (Wasiali, 2019). Compounds **8, 9** and **10** had comparable inhibitory activity ($p > 0.05$) against both α-amylase and α-glucosidase (IC_{50} = 64.54, 58.91 and 54.81; and 66.77, 62.53 and 58.03 µM) in comparison to the positive control acarbose (IC_{50} = 54.66 and 51.54 µM) (Wasiali, 2019).

In contrast, the triterpenoids that were extracted from the same extract and identified as lupeol (**11**), 3α,20-dihydroxy-28-lupanoic acid (**12**), 20-hydroxy-3-oxo-28-lupanoic acid (13) and 3α,20,28-trihydroxylupane (**14**) had minimal inhibitory effects on the two enzymes when compared to the same control (Wasiali, 2019). The work of Wasiali 2019, thus attributed the potential of *Z. chalybeum* to benzophenanthridine and possible phenolics, however for comprehensive structure

activity validation of active compounds the number of compounds used in the study could not provide a clear picture.

With extremely similar morphological characteristics to *Z. chalybeum*, and *Z. gilletii* is an indigenous deciduous tree that can reach heights of 10 to 35 meters. Even though it is found in Africa, it is also widely spread in nations like Zimbabwe, Zambia, Kenya, Sudan, Angola, and Malawi. Commonly reported traditional applications include treatment of stomachache by chewing the bark; against urinogenital infections, rheumatism and other pain related ailments (Kokwaro, 2009). In addition to its claimed anti-leukemic (Nakanishi et al., 1998), antibacterial, anti-inflammatory, analgesic, and anti-HIV effects, the plant was also found to possess strong anticancer properties (Tan et al., 1991). In identification of secondary metabolites, *Z. gilletti* has so far been able to establish benzophenanthridine alkaloids such as nitidine (**23**), dihydrochelerythrine (**26**) and chelerythrine (**20**) as well as furoquinoline alkaloids such as skimmianine (**21**), cinnamic acid amide, and fagaramide (**32**).

Z. gilletii serves as a better reservoir for alkaloids and phenolics some of which could be active compounds. However, these compounds have not been evaluated for anti-hyperglycemic potential. With the exception of pentacyclic triterpene acetate, 3β-acetoxy-16β-hydroxybetulinic acid (**7**), which was described as having modest α-glucosidase inhibitory activities. (Mbaze *et al.,* 2007).

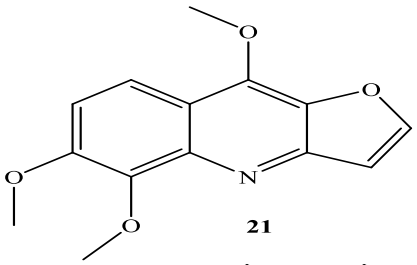

21

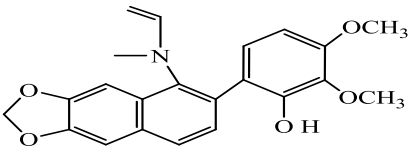

22

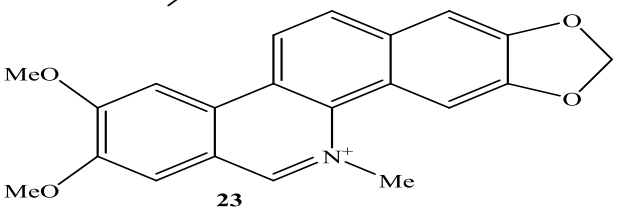

23

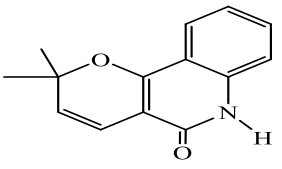

24

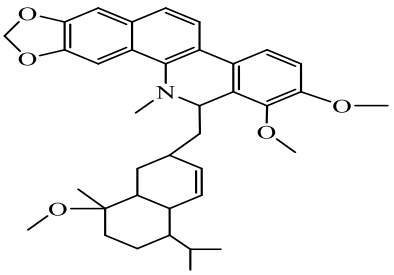

25

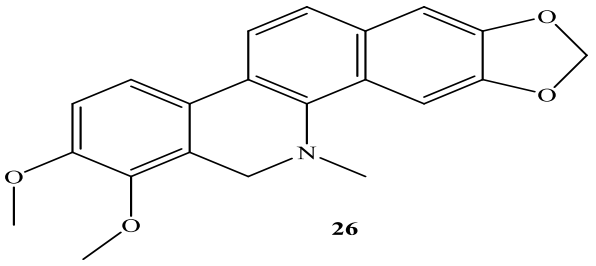

26

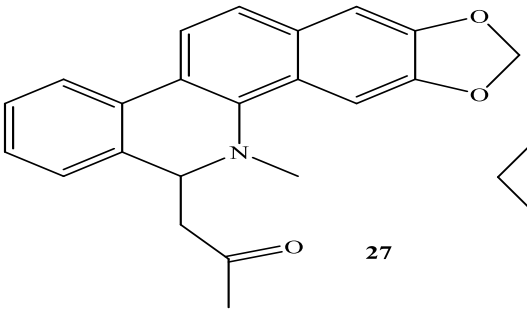

27

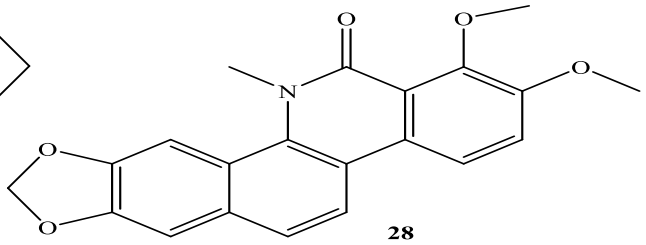

28

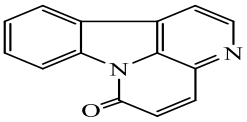

29

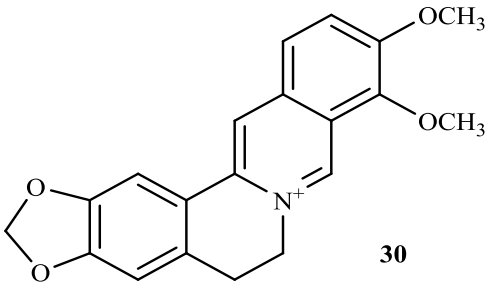

30

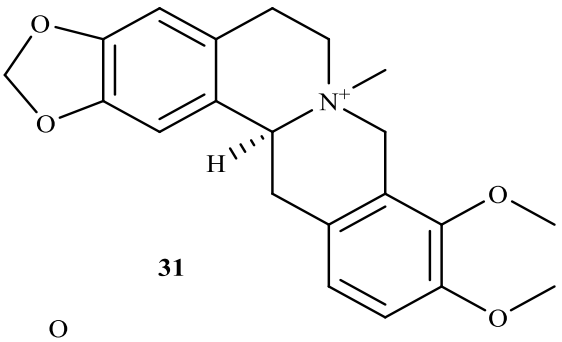

31

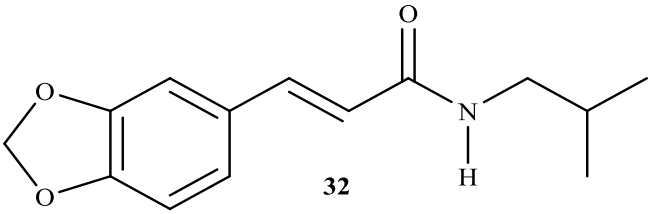

32

2.4.1 Structure Activity Relationship of Benzophenanthridine Alkaloids

Benzophenanthridine alkaloids belong to the benzyl isoquinoline alkaloid family and are primarily found in the Rutaceae and Papaveraceae families (Krane *et al*., 1984). More than 100 have been documented using various separation and identification procedures. They are divided into three types namely quaternary benzo[c]phenanthridine (QBP) type, dihydrobenzo[c]phenanthridine (DBP) type, and hexahydrobenzo[c]phenanthridine (HBP) type (Krane *et al*, 1984). HBP type consists of two aromatic rings, two cylcoalkanes and *N*-Me group: DBP type consist of three aromatic rings, one cycloalkane and *N*-Me group with an open ring B as *N*-acetonyl or methoxy group. Furthermore, Dihydrobenzo[c]phenanthridine alkaloids can be categorized further depending on the linkage between C-7 and C-8 and a polymerized type at C-8. QBP type takes the shape of a quaternary ammonium salt. (Figure 6).

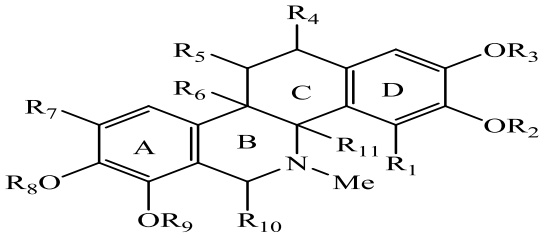

Hexahydrobenzo[c]phenanthridine type

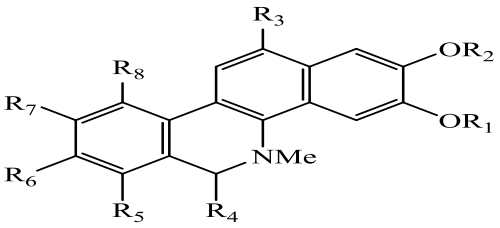

Dihydrobenzo[c]phenanthridine type

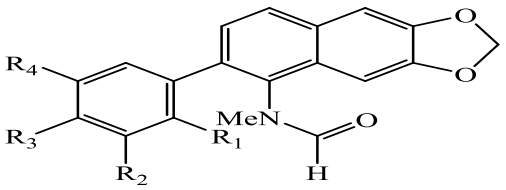

Dihydrobenzo[c]phenanthridine type I

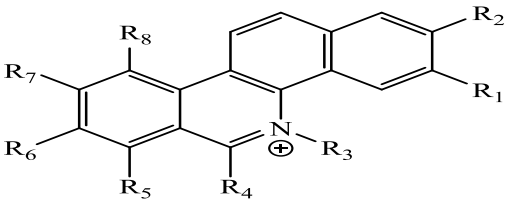

Quaternary benzo[c]phenathridine

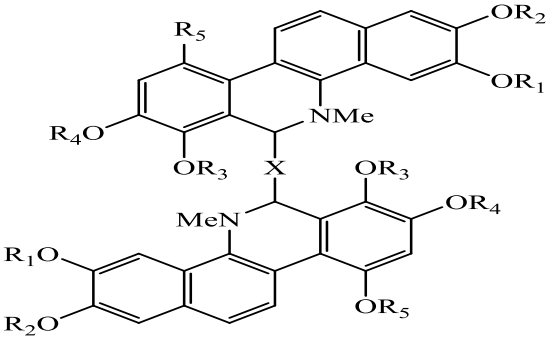

Dihydrobenzo[c]phenanthridine type II

Figure 6: The structures of different types of Benzophenanthridine alkaloids

The class DBP includes decarine (8), norchelerynthrine (9), dihydrochelerynthrine (26), avicine (33), dihydroavicine (34) among others whereas the QBP include nitidine (23), faragonine (35) and quaternary benzophenanthridine include faragamide (32) which are ubiquitous in the *Zanthoxylum* spp.

Benzophenanthridine alkaloids isolated from *Zanthoxylum spp* have been shown with as anti-inflammatory, anti-tumor, and anti-microbial qualities (Chen *et al*, 2005) and it has been demonstrated through modeling studies that the majority of them are protein kinase C inhibitors that preserve erythrocyte deformability (Yang *et al,* 2008) Some have been suggested to produces more reactive oxygen species, which can then exhibit bacteriolytic effects (Tane *et al.,* 2005). Both antibacterial and antifungal activities have been predicted to be dependent on a B/C ring fusion and the existence of an N-methyl group (Ma *et al,* 1999).

Higher antimicrobial activities has been reported for chelerythrine (20) and avicine (33), dihydrochelerythrine (26) and dihydroavicine (34). The corresponding hydrogenated alkaloids, suggest that the kind and location of substitution on ring D affects this kind of activity (Tavares *et al,* 2014). Comparably, it has been observed that molecules with a methylenedioxy group, like avicine (34) are more active than those having two methoxyl groups at positions C-8 and C-9, like nitidine (23) (Tavares *et al,* 2014).

Furthermore, the methoxyl groups' position is a relevant structural feature for antimicrobial activities of these alkaloids, since ortho coupled methoxyl groups at C-7 and C-8 as observed in chelerythrine (20) tend to enhances the antimicrobial activities better than dimethoxyl groups at C-8 and C-9 as in nitidine (23) (Tavares *et al*, 2014). The study by Tavares *et al*, (2014) (Figure 7) concluded the following moieties as important pharmacophores in benzophenanthridine alkaloids.

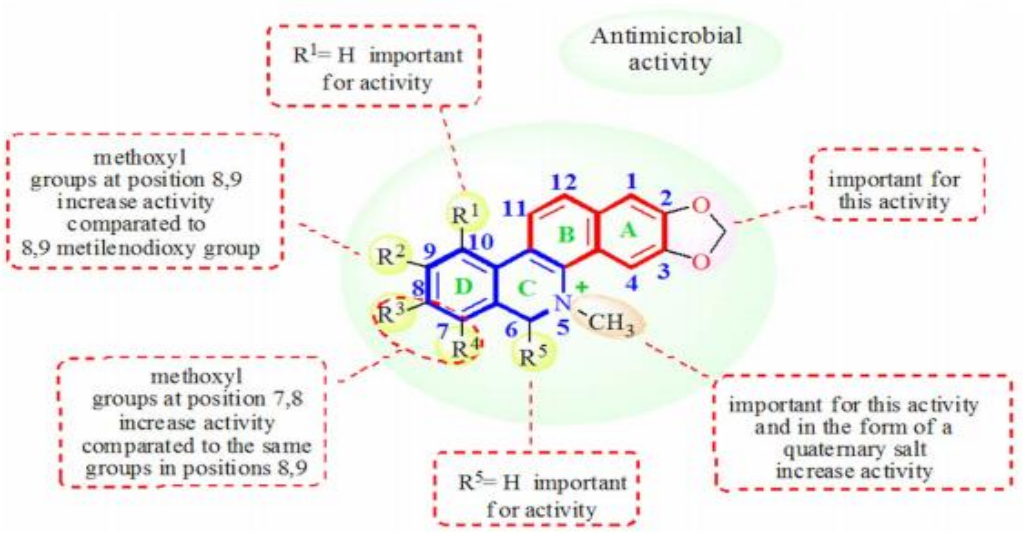

Figure 7: The structure-activity connection for the benzophenanthridine alkaloids' antibacterial activity (Tavares *et al*., 2014)

There have been reports that quaternary benzo[c]phenathridine, sanguinarine (35) and nitidine (23), block HIV-1 reverse transcriptase by thus considering benzophenanthridine alkaloids as potential anti-HIV compounds (Tan *et al*, 1991). Even non QBP molecules such as decarine (36) have been proved to have inhibitory potential against HIV-1 replication in H9 lymphocytes (Cheng *et al*, 2005) thus further validating activities of benzophenanthridine alkaloids (Cheng *et al*, 2005).

Based on the structure-activity relationship (SAR), which anticipated a C=N between positions 7 and 8 as a significant functionality, seven benzophenanthridine alkaloids with varying degrees of analgesic and anti-inflammatory properties were extracted from Zanthoxylum nitidum (Roxb.) DC (Hu et al, 2006). Conversely, replacement on C-8 reduced the anti-inflammatory activity, but the 9-OH and 10-OMe groups had greater anti-inflammatory activity (Hu *et al*, 2006).

According to research by Jursky and Balioya (2011), the two most potent compounds, chelerythrine (**20**) and sanguinarine (**37**), were found to selectively inhibit the glycine transport proteins GlyT 1 rather than GlyT, hence suppressing pain. Studies on anticancer agents similarly predicted C=N bond of benzophenanthridine alkaloids following a possible reaction between

C=N group on the B ring and -SH nucleophilic sites on the protein residues consequently exhibiting actions against proliferation and angiogenesis (Wolf and Knipling, 1993). Furthermore, the chemicals have the potential to impact DNA Topoisomerase I and II enzymatic activities through insertion into DNA molecules, hence impeding the rapid growth of tumor cells (Philchenkov et al., 2008). These mechanisms were reported based on study using chelidonine (**38**), sanguinarine (**37**) and chelerythrine (**20**) which are known for anti-microtubular effects (Wolf and Knipling, 1993). However, chelidonine (**38**) relies more on spatial steric hindrance brought on by the non-planar structures of the B and C rings, whereas sanguinarine (**37**) and chelerythrine (**20**) have similarly analogous mechanisms of action that depend on the C=N group on the B ring (Wolf and Knipling, 1993).

Structure-activity relationships on a set of 19 alkaloid molecules including benzophenanthridine alkaloids using ischemia-hypoxia H9C2 cells discovered that hexahydrobenzo[c]phenanthridine and dihydrobenzo[c]phenanthridine showed better activity more than proberberine and aporphine (Yang *et al*, 2014). The activities were noted to be reducing upon acetylation 6-OH or substitution of 8-H with OH, methyl group hydroxylation at positions C-2, 3, and 11, as well as the lack of N-Me (Yang *et al.*, 2014).

Benzophenanthridine alkaloids have also been noted for very good antioxidant activities against DPPH and ABTS better than known positive antioxidants. For instance, Proberberine is more potent clearance free radical than the alkaloids due to the phenolic hydroxyl group's location on the HBP skeleton (Han *et al*, 2016). Benzophenanthridine alkaloids are consequently acknowledged to exhibit promising possibilities for the creation of novel pharmacological substances.

Nevertheless, because only a small number of benzophenanthridine alkaloids have been isolated, research into these compounds is still ongoing. New analysis methods must be developed in order

to find more compounds, and their activities must be carefully screened in order to find novel treatments for a range of illnesses.

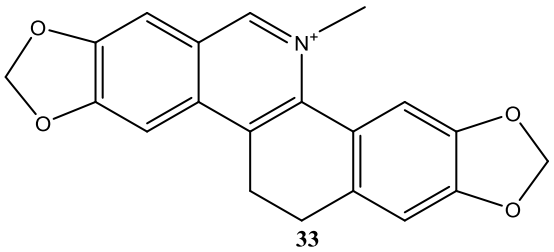

33

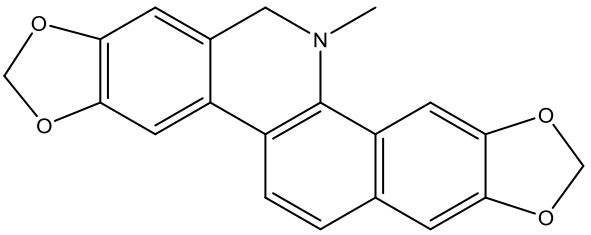

34

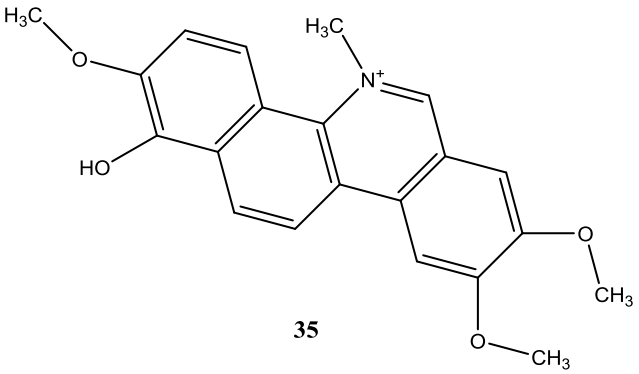

35

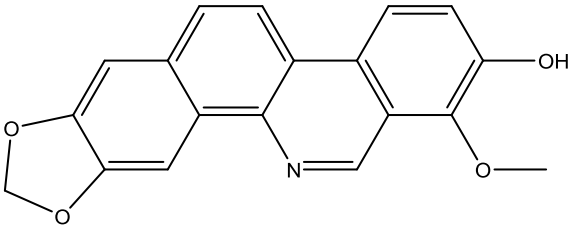

36

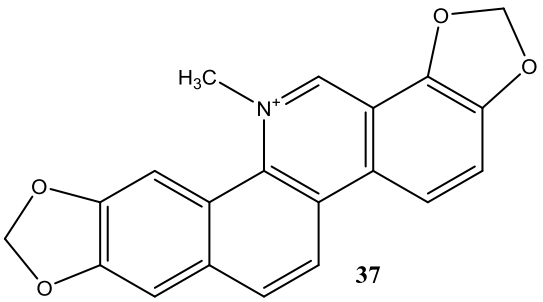

37

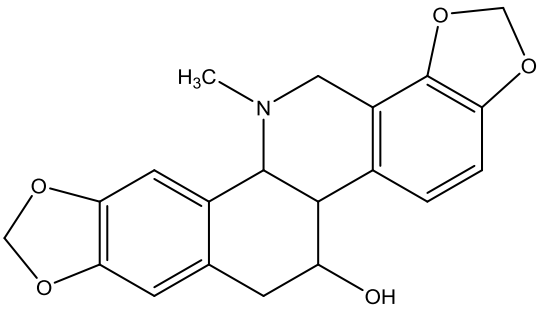

38

CHAPTER THREE
MATERIALS AND METHODS

3.1 Materials

3.1.1 General Instrumentation

The stem bark was ground into a powder using an electric pulverizer (Kika, M20), and the powdered materials samples were weighed using a top-loading analytical balance (Shimadzu, UX). Samples were concentrated using a rotary evaporator (EYELA, N-1000) that evaporated the liquids at low pressure. Gallen Kamp was used to record melting points with uncorrected capillary tubes. Kieselgel F_{254} aluminum silica gel plates were utilized in thin layer chromatography, and column chromatography was performed over silica gel (Merck 60G, 70-230 mesh) and sephadex LH-20 (Kobian, Kenya and Sigma Chemical Company, St. Louis, USA).

The TLC plates were viewed under UV lamp then heated using heat gun for two minutes. Detection and visualization were done by UV-Visible light spectrophotometer (molecular device Sunnyvale, USA) at the instrument room, Department of Chemistry, Maseno University. Bruker or Varian-Mercury spectrometers were used to record the 1 D (^{1}H-NMR (500 MHz) and ^{13}C-NMR (125 MHz)) and 2 D (COSY, NOESY, HSQC, and HMBC) using DMSO, $CDCl_3$, CD_2Cl_2, or CD_3OD as solvents with tetramethylsilane (TMS) serving as the internal standard. Chemical shifts were determined in ppm in □ values and coupling constants (*J*) in Hz compared to deuterated solvents and TMS. ESIMS spectra were obtained using a Finnigan MAT mass spectrometer with a direct input at 70 eV on SSq 710.

Using a SpectraMax GeminiXS Spectrofluorometer (Molecular Devices, Sunnyvale, CA), the α-amylase enzymatic activity (fluorescence) was measured. α-glucosidase enzyme activity (absorbance) was determined using a SpectraMax 190 Spectrophotometer (Molecular Devices, Sunnyvale, CA).

3.1.2 Chemicals and Reagents

The organic solvents and reagents used in the study were obtained from Sigma-Aldrich Chemical Company, St. Louis, USA, and Kobian, Kenya. These included ammonia solution, n-hexane, dichloromethane, ethyl acetate, glacial acetic acid, p-anisaldehyde, and Dragendorff's crystals. Organic solvents were distilled, Dimethylsulfoxide (DMSO) was analar grade from Kobian, Kenya, and α-glucosidase, bovine serum, p-nitrophenyl-α, D-glucopyranoside, and acarbose were purchased from Sigma-Aldrich Chemical Company.

3.1.3 Chromatographic conditions

TLC was performed on pre-coated aluminum silica gel plates (Merck 60, F254). Chromatographic zones on TLC plates were spotted by spraying *p*-anisaldehyde-sulphuric acid, iodine vapor, or ammonia vapor, and burned at 100 °C. For alkaloid tests, Dragendorff's reagent was sprayed on TLC plates. The *p*-anisaldehyde-sulphuric acid visualizing stain was prepared from a mixture of 0.5 ml of *p*-anisaldehyde, 85 ml of ethanol, 5 ml concentrated sulphuric acid, and 10 ml glacial acetic acid (Krishnaswamy, 2003). Column chromatography was carried out using silica gel (Merck 60G, 70-230 mesh) in glass columns measuring 3.0 × 60 cm and 2.0 × 50 cm. Solvents including n-hexane, dichloromethane (DCM), ethyl acetate (EtOAc), and 95% methanol were used in the study.

3.1.4 Plant Materials Collection and Preparation

Plants were identified from its natural habitat by assistance of a plant taxonomist and the samples collected were conserved at University Herbarium after authentication. The stem bark of *Zanthoxylum chalybeum* was sampled from Homa Hills, (0º, 23'S, 34º30'E) and *Zanthoxylum gilletii* stem bark was gathered in Kakamega Forest, (0º17'30''N, 34º51'22''E) in January, 2019. Samples were identified and authenticated by a taxonomist at Maseno University, Department of Botany where a voucher specimen (KYC/MSN/2019) for *Z. chalybeum* sample and (KYG/MSN/2019) for *Z. gilletii* were deposited at Maseno University herbarium. The plants materials were sliced into small pieces then allowed to dry by air under the shade. ZC stem bark dried after 21 days and ZG after 25 days. The dried materials were then pulverized differently into fine powder using an electric grinder at Maseno University Research Laboratory.

3.2 Methods

3.2.1 Extraction and isolation of compounds from *Z. chalybeum*

Using an electric pulverizer, the *Z. chalybeum* stem bark was ground into a fine powder after being sliced into small pieces and allowed to dry by air for 21 days in a shade. The 0.8 kg of powdered stem bark was extracted using 4 × 1.5 L of 95% aqueous methanol, and filtered through Whatman No. 1 using a Buchner filter funnel. Using a rotary evaporator, the consecutive filtrates were combined and concentrated in vacuum chamber to produce (45 g) of 5.625% crude extract at a temperature of 45ºC.

Total alkaloid extraction: total alkaloid was isolated 28 g of the crude extracts were suspended in 200 mL of 0.1 M H_2SO_4 in ethyl acetate and agitated for 30 minutes. The extracts were then

combined and the non-polar compounds were extracted three times using 300 mL of n-hexane in a separating funnel.

A 0.1 M ammonia hydroxide solution was used to neutralize the acidic polar fractions. 200 mL of dichloromethane (CH_2Cl_2) was then used to extract the material further until a negative Dragendorff's test result was obtained. Anhydrous sodium sulphate was used to dry the organic fraction (CH_2Cl_2 extracts), and then further concentration in a vacuum produced 10 g (1.25%). The alkaloid extract (9 g) was subjected to column chromatography on a normal phase silica gel 60 column using gradient polarity (v/v) of CH_2Cl_2: CH_3OH 10:0, 9:1, 8:2, 7:3, 3:2 1:1, (500 ml in each case) and finally 100% MeOH.

Following the use of Dragendorff's reagent spray on TLC plates, 34 fractions generated by this procedure were recombined into 10 fractions, which were then vacuum-concentrated using a rotary evaporator. Following their elution with 1% CH_3OH in CH_2Cl_2, fractions 2 (35 mg) and 3 (72 mg) were combined and further separated using preparative thin-layer chromatography (PTLC) developed with 8% CH_3OH in CH_2Cl_2. Two UV-active compounds, compound (**9**) and compound (**43**), were obtained by scrapping the bands associated with each isolated component, dissolving it in DCM, and filtering the mixture.

Based on their TLC profiles, fractions 4 and 5 were eluted with CH_2Cl_2: CH_3OH 8:2 v/v were combined and then subjected to a column (60 cm × 3.0 cm, SiO_2) chromatography eluting with CH_2Cl_2: CH_3OH gradient polarity of 9:1, 8:2, and 7:3 yielding 8 fractions (30mL). These fractions were then recombined into three fractions.

Compounds **21** (30 mg), **9** (50 mg), and **42** (80 mg) were produced through recrystallization using CH_2Cl_2: n-hexane from sub-fractions one, two, and three of Fractions 4 and 5. Fractions 6 (410 mg) and 7 (296 mg) were eluted with 7:3 v/v CH_2Cl_2:CH_3OH mixtures. Based on their TLC profiles, these fractions were combined and subjected to column (60 cm × 4.0 cm, SiO_2) chromatography. Twelve fractions (25 ml each) were obtained, which were then combined into four fractions in accordance with their TLC profiles.

Sub-fraction one of fraction 6 and 7 yielded crystalline compound **39** (86 mg) from CH_2Cl_2: n-hexane mixture. Third portion of fraction combined 6 and 7 yielded compound **40** (77 mg) as white crystalline solids from CH_2Cl_2: n- hexane mixture. Lastly, fractions 8, 9 and 10 (158, 214 and 176 mg, respectively) eluted with 1:1 v/v CH_2Cl_2: CH_3OH were combined and re-chromatographed on CC (60 cm and 4.0 cm, SiO_2), gradient elution with CH_2Cl_2: CH_3OH (7:3, 1:1 and 3:7 v/v). Four fractions were obtained, from which the second portion yielded compound **41** (30 mg) after

crystallization with CH_2Cl_2:CH_3OH. Third sub-fraction yielded compound **41** (45 mg) and yellow solids of compound **42** (61 mg), following fractional re-crystallizations in CH_2Cl_2: *n*-hexane.

Alkaloid-free extracts: The aqueous non-alkaloid fraction was concentrated *in vacuo* to dryness and afforded 10.9 g (1.36% of crude extracts) which was then suspended in 200 mL distilled water followed by sequential solvent extractions beginning with 3 × 300 mL n-hexane, followed by 3 × 300 mL ethyl acetate, and finally 3 × 300 mL n-butanol (C_4H_9OH) using a separatory funnel. The combined decanted organic layer extracts, were evaporated in vacuo to yield 2.05 g (0.13%), 5.01 g (0.63%) and 3.1 g (0.39%), respectively.

Dry *n*-hexane non-alkaloid extract (2 g) was loaded on silica gel in column (60 × 3 cm, SiO_2) and eluted stepwise with n-hexane adjusting the polarity with ethyl acetate as (1:0, 99:1, 95:5, 9:1, 4:1, 3:1, 2:1). Out of the 35 eluent fraction (25 mL each), five fractions were obtained after pooling the fractions with similar TLC profiles and monitored using p-anisaldehyde-sulphuric acid reagent. 80 mg of Compound **10** was obtained as white crystals from the third fraction after crystallizing it in methanol. Further purification of the fifth fraction using silica gel column (120 × 60 mm, SiO_2) eluting with n-hexane: ethyl acetate (9:1, 4:1) gave more of the white crystals of 25 mg with single spot on TLC which turned purple – blue after spraying the developed plate with *p*-anisaldehide-sulphururic acid, characteristics of a terpenoid A portion of *n*-C_4H_9OH fraction was (1.4 g) also chromatographed on reverse (C18 reverse phase SiO_2, 40–63 μm) flash chromatography, eluting with H_2O-CH_3OH (9.1); CH_3OH; CH_3OH - CH_2Cl_2 and finally CH_2Cl_2. A total of 30 fractions (each 50 ml) which were further combined to 3 fractions according to their TLC profiles were obtained. The first fraction yielded a white amorphous solid that was confirmed to be sesamine (**46**, 103 mg), the second fraction yielded few mixtures of compound (**46**) and compound (**44**) that crystalized in CH_2Cl_2; *n*-hexane as white crystalline solid (62 mg).

3.2.2 Extraction and Isolation of compounds from *Z. gilletii*

Z. gilletii stem bark were chopped into small pieces separately, air-dried at room temperature under shade for 25 days and pulverized into fine powder. The powdered stem bark material (1.05 kg) were extracted with 95% aqueous methanol (3 x 2.5 L) for 72 hours and filtered. The filtrates were combined and concentrated in *vacuo* using rotary evaporator to yield 53.74 g (5.21 %).

Total alkaloid extraction: The crude extracts suspended in 200 mL of 2% 0.1 M H_2SO_4 in dichloromethane under agitation for 40 min, replicated four times and the extracts were combined, followed by three times extraction of the non-polar compounds using 300 mL

n-hexane using a separatory funnel. The acidic polar fractions was neutralized using 0.25 M ammonia hydroxide solution, followed by further extraction using 200 mL dichloromethane (CH_2Cl_2), until a negative Dragendorff's test was observed. The organic fraction (CH_2Cl_2 extracts) was dried with anhydrous sodium sulphate, followed by further concentration in vacuo *to* yield 15.5 g (1.48 % of the crude extract).

The alkaloid crude extract (12.4 g) was subjected to a silica gel CC (8 × 120 cm, 1.7 kg SiO_2) and eluted n-hexane:CH_2Cl_2 mixture (1 : 0 to 9 : 1, 10% gradient, 500mL of each eluent; 9:1, 4:1, 7:3 to 3 : 2, 10% gradient, 500 mL of each eluent; 1:0 to 0 :1, 10% gradient, 500 mL of each eluent) and CH_2Cl_2-MeOH (1 : 0 to 9 : 1, 10% gradient, 500mL of each eluent) to yield 40 crude fractions which were combined to 6 fractions (D1–D6). TLC profiles of the five fractions then monitored with p-anisaldehyde-sulphuric acid reagent. The first three fractions D1, D2 and D3 showed one spot each using the UV lamp. The single spots were confirmed by heating the TLC plates using Heat gun at 100^{o}C. The fractions were then vaporized in vacuo and produced two compounds; Compounds **9**, yellow solid, (40 mg), and **43**, (35 mg) were obtained from fractions D1, D2, and D3 respectively. 2.4g of fraction D4 subjected to silica gel CC (5 × 80 cm, 160 g SiO_2) using mixtures of n-hexane-CH_2Cl_2 (1:0 to 7: 3, 10% gradient, 500mL of each eluent; 7:3 to 0:1, 10% gradient, 500mL of each eluent) yielding compound **9** (110 mg) as yellow solid. Further Fraction D5 (1.7 g) was eluted over silica gel CC (3 × 30 cm, 85 g SiO_2) with n-hexane-CH_2Cl_2 (1:4 to 0:1, 10% gradient, 500 mL of each eluent) and CH_2Cl_2-MeOH (1:0 to 9:1, 10 gradients, 0.2 L of each eluent) to afford white crystals of compounds **43** (45.5 mg) and yellow crystals of compound **42** (56.8 mg).

Alkaloid-free extracts: Aqueous non-alkaloid portion was concentrated *in vacuo* to dryness obtaining 13.5 g (1.29 % of crude extracts) then suspended in 200 mL distilled water. Sequential solvent extractions was done beginning with 3 × 300 mL n-hexane, then, 3 × 300 mL ethyl acetate, lastly, 3 × 300 mL n-butanol (C_4H_9OH) in a separatory funnel. The combined decanted organic layer extracts, were evaporated in vacuo to yield 2.23 g (0.21%), 6.38 g (0.61%) and 4.1 g, respectively.

n-Hexane extract (2.2 g) subjected on silica gel in column (60 x 3 cm, SiO_2) and eluted with *n*-hexane-EtOAc (99:1, 95:5, 9:1, 4:1, 7:3, 3:2, 2:1 and 1:1) 200ml each eluent resulting into 40 fractions (50 ml each) the fractions were combined according their similar TLC profiles monitored using p-anisaldehyde-sulphuric acid reagent giving 3 fractions. The first fraction gave white precipitate which produce a blue sport on TLC under UV lamp n-hexane-EtOAc (9:1) which dried

yielding white amorphous solid (Rf= 0.36) confirmed to be compound **12**, (56.8 mg) using TLC profile in comparison to authentic sample. The second fraction showed two spots on TLC and was dried in vacuo using a rotatory removed evaporator and re-crystallized using 60 % CH_2Cl_2 in n-hexane to produce a white amorphous solid (**46**, 31.2 mg). The mother liquor was recrystallized from 80 % CH_2Cl_2 in *n*-hexane, filtered and dried yielding, compound **44** (14.25 mg).

Dry EtOAc extract was eluted using n-hexane - EtOAc (99:1, 9:1, 4:1, 3:1, and 1:1) on silica gel CC giving twenty fractions. The fractions were then pooled and combined according to their similar TLC profiles to produce five fractions (E1 (1-7), E2 (8-19), E3 (20-26), E4 (27-36) and E5 (37-40). E1 showed a single blue spot on TLC. The portion was dried producing white amorphous solid (63.7 mg) producing a purple-blue spot when sprayed with *p*-anisaldehyde-sulphuric acid mixture and heated at 110ºC, characteristic of a terpenoid. Fraction E4 was dried *in vacuo* on a rotatory evaporator and loaded on a Sephadex LH 20 column leading to isolation of a white amorphous solid of compound **(44)** (15.15 mg).

3.2.3 Physical and spectroscopic data pure isolates from *Z. Chalybeum* and *Z. gilletti*

Compound (9) : yellow crystals; UV active with blue fluorescence; melting point of 210-212°C; ^1H and ^{13}C NMR data (Table 9);ESIMS $[M+H]^+$ *m/z* = 334 (cald for $C_{20}H_{15}NO_4$).

Compound (10): white crystals; melting point of 124 – 125 °C; ^1H and ^{13}C NMR ($CDCl_3$) data (Table 8); cald for $C_{10}H_{10}O_4$.

Compound 21: yellow powder; UV active; melting point of 180 ºC; 1H and 13C NMR data (Table 13; ESIMS: $[M+1]^+$ m/z 260 (cald. For $C_{14}H_{13}NO_4$).

Compound 39: white powder; UV ($CHCl_3$) λ_{max} (log ε): 305 (0.2),265 (0.47) nm; IR (KBr) ν_{max}: 3457, 3316, 2943,1625, 1551, 1505,1466, 1257 cm^{-1}; ^1H and ^{13}C NMR data (Table 1); HREIMS: *m/z* 287.1317 $[M]^+$ (calcd. for $C_{17}H_{21}NO_3$, 287.1312).

Compound 40: white crystalline; UV ($CHCl_3$) λ_{max} (log ε): 284 (0.76), 218 (0.48), 204 (0.24) nm; IR (KBr) ν_{max}: 3424, 1736, 1649,1560, 1431,1398, 1255, 1202, 1070 cm^{-1}; ^1H and ^{13}C NMR data (Table 2); HREIMS: *m/z* 219.1103 $[M]^+$ (calcd. for $C_{13}H_{17}NO_2$, 219.1105.

Compound 41: white crystalline; UV ($CHCl_3$) λ_{max} (log ε): 284 (0.76), 218 (0.48), 204 (0.24) nm; IR (KBr) ν_{max}: 3424, 1736, 1649,1560, 1431, 1398, 1255, 1202, 1070 cm^{-1};

^{1}H and ^{13}C NMR data (Table 3); HREIMS: *m/z* 285.11373 $[M]^{+}$ (calcd. for $C_{17}H_{19}NO_3$, 285.1365).

Compound 42: yellow crystals; melting point range 199-200ºC**;** 1H NMR ((DMSO-d_6)) and ^{13}C NMR (DMSO-d_6) (Table 4); Rf value 0.64 (CH_2Cl_2: MeOH (4:1)); ESIMS: $[M+H]^{+}$ m/z 349.1057(calcd for $C_{21}H_{18}NO_4^{+}$).

Compound 43: white crystals (DCM:MeOH extract); yield (45.5mg); Rf of 0.54 (40% DCM in hexane); Mp of 141-142 ºC; ^{1}H and ^{13}C NMR data (Table 5); HREIMS: *m/z* 497.1839 $[M]^{+}$ (calcd. for $C_{30}H_{27}NO_6$, 497.1838).

Compound 44 : white solid (n-hexane: EtOAc extract); yield (15.15 mg) Rf of 0.47 (80% EtOAc in *n*-hexane); Mp of 191-192ºC; ^{1}H and ^{13}C NMR data (Table 6); HREIMS: *m/z* 324.0996 $[M]^{+}$ (cald. for $C_{19}H_{16}O_5$, 324.0998).

Compound 45: white crystal; Rf of 0.57 (80% DCM in MeOH); ^{1}H and ^{13}C NMR data (Table 7); HREIMS: *m/z* 268.1322 (calcd. for $C_{12}H_{23}NO_4$, 268.1324).

Compound 46: white solid; UV active; melting point of 121-122ºC; HREIMS; *m/z* 354.35 cald for $C_{20}H_{18}O_6$.

3.2.4 α-Amylase inhibition assay

The anti-hyperglycemic activities of the pure isolated compounds were assayed against human salivary α-amylase using assay as described in the Worthington Enzyme Manual (Worthington, 1993; Kwon *et al*, 2006). Pre-incubation was carried out for 10 minutes at 25ºC in 500 µL of 0.02M sodium phosphate buffer (pH 6.9 with 0.006 M NaCl) containing 0.5 mg/mL of α-amylase. 500 µL of a 1% starch solution in 0.02M sodium phosphate buffer (pH 6.9 with 0.006M NaCl) was added to each tube containing pure isolates (0.05mM, 0.1mM, 0.2mM, 0.5mM, 1.0mM) at timed intervals. 1.0 mL of dinitrosalicylic (DNS) acid color reagent was used to stop the reaction. A boiling water bath was used to incubate the test tubes for five minutes, after which they were allowed to cool to room temperature. The reaction mixture was diluted by adding 5 to 15 mL of distilled water. Fluorescence measured using a SpectraMax GeminiXS Spectrofluorometer (Molecular Devices, Sunnyvale, CA) with excitation and emission wavelengths of 540 nm. The absorbance readings were compared with the controls that contain buffer instead of sample extract. The percentage α-amylase inhibitory activity was calculated using the equation;

$$\%\text{inhibition} = \frac{\text{Absorbance (control) - Absorbance (Extract)}}{\text{Absorbance (Control)}} \times 100$$

The percentage inhibitions were expressed as probit units then regressed against concentrations of the samples to obtain the 50% inhibitory concentration of each sample (IC_{50}).

3.2.5 α-Glucosidase inhibition assay

The anti-hyperglycemic activity of the pure isolated compounds were assayed against α-glucosidase (Omosa *et al*, 2019) pure compounds prepared as described in α-amylase assay above. The test compound and 2 mU of α-glucosidase was diluted to 97 µL in 0.1 M potassium phosphate buffer (pH 6.5) and pre-incubated in 96-well plates at 37 °C for 15 min. The reaction was initiated by adding 3 µL of 3 mM *p*-nitrophenyl-*α*-*D*-glucopyranoside (*p*-NPG) as substrate and incubated for an additional 15 min at 37 °C, followed by addition of 100 µL of 1 M Na_2CO_3 to stop the reaction. All test compounds were prepared in 5% DMSO in distilled water. The final concentrations of the compounds were between 5 and 200 µM while the final concentration of α-Glucosidase was 20 mU/mL. The enzyme activity was then determined by measuring the release of *p*-nitrophenol from the *p*-NPG substrate and the reaction monitored by change of absorbance at 410 nm using a SpectraMax 190 Spectrophotometer.

The α-Glucosidase inhibition rate was calculated relative to control as follows:

$$\%\text{inhibition} = \frac{\text{Absorbance (control) - Absorbance (Extract)}}{\text{Absorbance (Control)}} \times 100$$

3.2.6 Kinetic Analyses

Mode of inhibition of compounds against porcine pancreas α-amylase and yeast α-glucosidase activity were measured with increasing concentrations of *p*NPG (0.25, 0.5, 1, 2 and 5 mM) as a substrate, in the absence and presence of the pure compounds and acarbose at 0, 0.5, 1, 2.5, 10 and 20 mM. The mode of inhibition was determined by the Lineweaver-Burk plots, followed by secondary plots (Dixon plots) depending on the established mode of inhibition. The inhibition constants (K_i) were calculated using the following equation (Segel, 1993):

$$v = V_{\max} \times S/K_m(1 + [I]/K_i) + S(1 + [I]/\alpha K_i)$$

where v is the initial velocity in the absence and presence of inhibitor; S and I are the concentration of substrate and inhibitor, respectively; V_{max} is the maximum velocity; K_m is the Michaelis-Menten constant; K_i is the competitive inhibition constant and αK_i is the uncompetitive inhibition constant.

3.3 Statistical Analysis

Lineweaver-Burk and Dixon secondary linear regression analysis used for establishing the inhibitory constants were developed on MS Excel 2019. Variance analysis was performed using Tukey HSD/Tukey Kramer post-analysis (Segel, 1993).

CHAPTER FOUR
RESULTS AND DISCUSSION

4.1 Structure Elucidations

4.1.1 Chalybemide A {6-benzo[1,3]dioxol-5-yl-hexa-2,5-dienoic acid isobutylamide} (39)

Compound 39 was isolated as white powder with molecular mass determined by HREIMS, m/z =287.1317[M] $^{+}$ (calcd for $C_{17}H_{21}NO_3$ 287.1312) giving its formula as $C_{17}H_{21}NO_3$ indicating eight degrees of unsaturation. The IR spectrum showed an amide functionality, aromatic and/or alkene based on 3457 cm^{-1}, 1505-1447 cm^{-1} absorptions, respectively.

From ^{1}H and ^{13}C spectra (Table 1), characteristic signal for a benzo[1,3]dioxol unit was predicted based on the protons δ_H 5.92 (br, s, 2H, OCH_2O) attached to δ_C 99.39, δ_H 6.89 (d, *J* = 1.2 Hz, H-8) attached to δ_C 107.87, 6.73 (d, J=8.0 Hz, H-11) attached to δ_C 109.14 and δ_H 6.75 (dd, *J* = 8.0, 1.2 Hz, H-12) attached to 120.15 and δ_C 132.30, 147.87 and δ_C 148.56 carbon signals closely related to the data reported by Li et al., (2019). The HMBC correlations supported the benzo[1,3]dioxol as observed from δ_H 5.92 (OCH_2O) displaying contours to δ_C 147.9 (C-9), 148.6 (C-10); while proton at δ_H 6.87 (H-8) correlating to δ_C 148.6 (C-10) and δ_C 120.2 (C-12); proton at δ_H 6.73 (H-11) correlating to δ_C 132.5 (C-7) and δ_C 147.9 (C-9) and proton at δ_H 6.83 (H-12) to δ_C 107.8 (C-8) and δ_C 148.6 (Figure 8a).

Another characteristic signal indicated the sets of *trans* oriented olefinic protons at δ_H 5.74 (d, *J* = 15.2 Hz, H-2), 6.05 (dd, *J* =15.2, 7.0 Hz, H-), δ_H 6.77(d, *J* = 15.2Hz, H-6) attached to two pairs of olefinic carbon signals at δ_C 123.8, 146.8, 129.9 and 129.5 as supported by DEPT and HSQC (Table 1). ^{1}H-^{1}H COSY showed correlation between δ_H 2.39 (m, 2H) with two of the olefinic protons; δ_H 5.74 (d, J=15.2, H-2) and δ_H 6.24 (dd, J =15.2, 7.0, H-5) together with HMBC correlations to carbon signals at δ_C 123.8 and δ_C 129.5 indicated a methylene link between the C=C showing the presence of penta-1,3-diene moiety. The ^{1}H NMR further displayed a signal at δ_H 3.13 (t, *J* = 6.0 Hz, 2H) attached to δ_C 49.5 (HSQC) which showed COSY coupling with N-H and another proton at δ_H 1.78 (m, 1H) attached to δ_C 29.3, which coupled δ_H 0.98 (d, *J* = 6.0 Hz, 2-CH_3) indicating the presence of isobutylamide moiety (Mansoor *et al*, 2013). Furthermore, HMBC correlations between δ_H 3.13 (CH_2 to δ_C 169 (^{3}J, C=O) and δ_C 29.3 (^{2}J, C-2'); ^{2}J correlations between the methane proton δ_H 1.78 and methylene carbon (δ_C 49.5) and methyl carbons (δ_C 19.4) (Figure 8A) confirmed (C=O)$NHCH_2CH(CH_3)_2$ moiety, a common structural features of *Zanthoxylum* amide alkaloids. These NMR spectra established a

typical amide alkaloid except the presence of penta-1,3-diene moiety, from which one of the alkene proton at δ_H 6.77 (H-6) and δ_C 129.2 showed a mutual correlation to benzo[1,3]dioxol signal at δ_H 6.24 and δ_C 107.9 (C-8), while another olefinic proton δ_H 5.74 (H-2) correlation to the carbonyl carbon (δ_C 169.3, C-1) and the methylene carbon (δ_C35.3) (Figure 8a) confirming penta-1,3-diene as the moiety joining the isobutylamide and the benzo[1,3]dioxol. These spectral evidences characterized compound **39** as 6-benzo[1,3]dioxol-5-yl-hexa-2,5-dienoic acid isobutylamide obtained as new natural product from *Z. chalybeum* and named as chalybemide A.

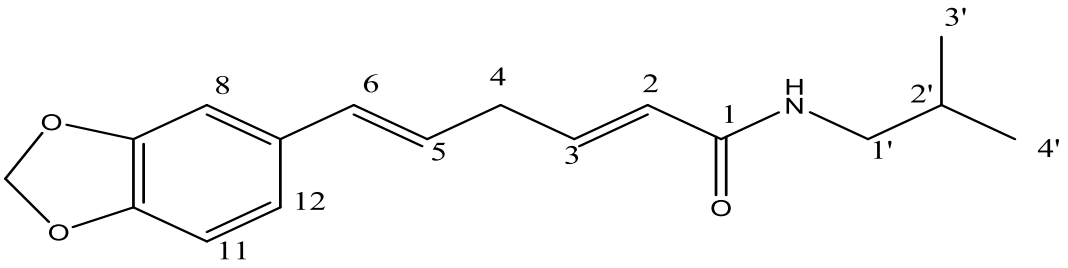

39

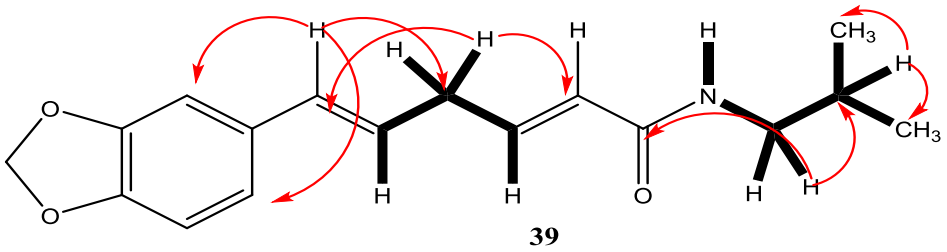

39

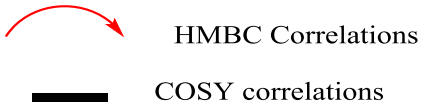

8(a)

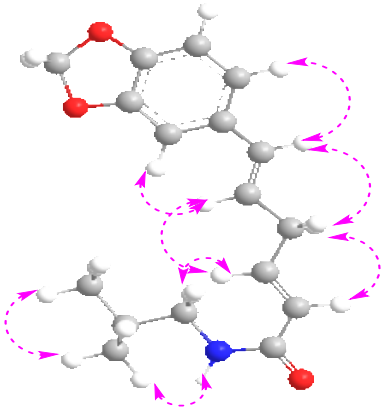

8(b)

Figure 8: (a) is HMBC, COSY significant correlations and 8(b) is ROESY correlations of compound 39

Table 1: 1H (600MHz) and 13 NMR (150 MHz) (CDCl3) spectral data for Chalybemide A

C-Position	δ_H, multi	δ_C	HMBC	COSY
1		169.3(C=O)		
2	5.74, d,(*J* = 15.2)	123.8 (CH)		
3	6.05 dd (*J* = 15.2, 7)	146.8 (CH)		H_3-H_4
4	2.39 m	35.3 (CH_2)		H_4-H_5
5	6.24 dd (*J* = 15.2, 7)	129.2 (CH)		
6	6.77 d (*J* = 15.2)	129.5 (CH)		
7		132.5 (C)		
8	6.89 d (*J* =1.2)	107.9 (CH)	C-10,12	
9		147.9 (C-O)		
10		148.6 (C-O)		
11	6.73 d (*J* =1.2)	109.1 (CH)	C-7,9	
12	6.83 dd (*J*=8, 1.2)	120.2 (CH)	C-8,10	
1'	3.13 t (*J* = 15.2)	49.5 (CH_2)	C-1,2'	$H_{1'}$-$H_{2'}$
2'	1.78 m	29.3 (CH)		$H_{2'}$-$H_{3'}$,$H_{2'}$-$H_{4'}$
3'	0.91 d (*J* = 15.2)	19.3 (CH_3)		
4'	0.94 d (*J* = 15.2)	19.3 (CH_3)		
OCH_2O	5.92 br s	99.4 (CH_2)	C-9,10	

4.1.2 Chalybemide B {4-Methoxy-*N*-(2-methoxy-phenyl)-*N*-methyl-benzamide}

Compound **40** was obtained as white crystalline solids with molecular formula $C_{13}H_{15}NO_2$ deduced from its HREIMS at m/z 219.1103 $[M]^+$ (calculated for $C_{13}H_{15}NO_2$, 219.1103)

predicted for seven degrees of unsaturation. ^{13}C NMR (Table 2) supported the mass spectrometry data by exposing thirteen carbon atoms characterized by DEPT-135 spectra as seven methines, one methylene and three quaternary carbons including one hydroxylated and one carbonyl carbon.

^{1}H NMR displayed two aromatic signals as two broad doublets integrated for two protons at δ_H 7.36 (d, J = 7.2 Hz H-6 (2H)) and δ_H 7.53(d, *J* = 7.2 Hz) and multiplet at δ_H 7.47 (1H) attributed to a monosubstituted aromatic ring. The presence of *trans* configured alkene moiety was noted based on the signals δ_H 6.64 (d, *J* = 15.5) and δ_H 7.73 (d, *J* = 15.5), which showed HMBC correlations with carbonyl carbon at δ_C 166.5 (C=O) and quaternary aromatic carbon at δ_C 134.9 (C-4) predictive of a phenylethylene skeleton attached to carbonyl carbon. Moreover, HSQC shows that proton signal at δ_H 3.47 (-CH_2, s) attached to δ_C 58.8 having a COSY correlations with N-H and HMBC correlations to δ_C 70.1 (C-2') and to carbonyl δ_C 166.5 suggesting a methylene amide group. HMBC further shows two mutually coupled methyl groups (δ_H 1.19) to carbon at δ_C 70.1 (C-2') and to δ_C 57.1 (C-H_2) (Figure 9(a) confirming the moiety as a 2-isobutylamide (Djeukeu et al, 2019). Following HMBC correlations of the ethylene protons and methylene protons to a carbonyl carbon and the ROESY correlations (Figure 9(b)) which confirmed compound **40** as *N*-(2-hydroxy-2-methylpropyl)-3-phenylacrylamide, isolated and characterized from *Zanthoxylum chalybeum* for the first time and named as Chalybemide B.

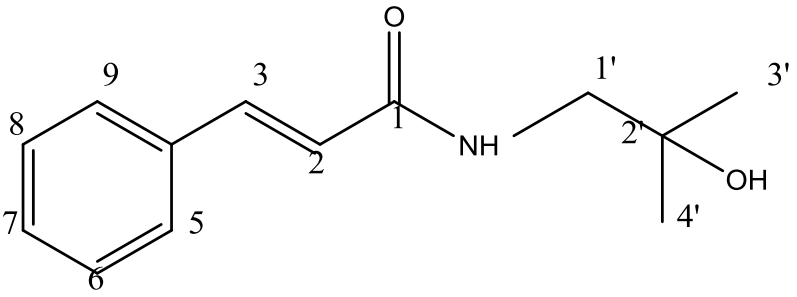

40

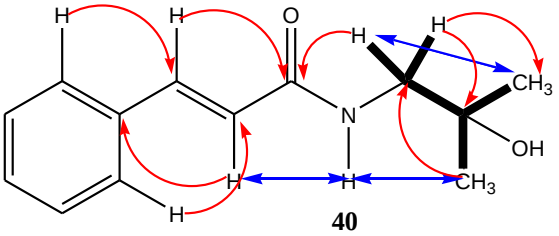

40

HMBC Correlations

ROESY correlations

COSY colations

Figure 9 (a): HMBC, ROESY and COSY for compound 40

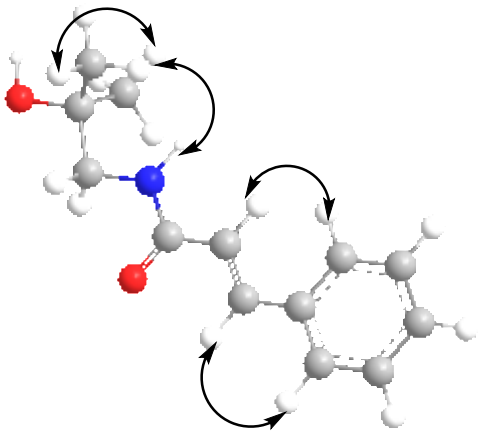

9(b)

Figure 9 (b): 3D and ROESY correlations for 40

Table 2: 1H (600MHz) and 13 CNMR (150 MHz) (CDCl3) spectral data for Chalybemide B

C-Position	δH, mult (J, Hz)	δC	HMBC	COSY
1		166.5(C=O)		
2	6.64 (d, *J* =15.5)	119.8(CH)	C-4	
3	7.73 (d, *J* = 15.5)	141.6 (CH)	C-1	
4		134.9 (C)		
5	7.53 (d, *J* = 7.2)	126.2 (CH)	C-2	
6	7.36 (d, *J* =7.2)	128.4 (CH)		
7	7.47 m	127.7 (CH)		
8	7.36 m	128.4 (CH)		
9	7.53 m	126.2 (CH)	C-3	
1'	3.47 br s	58.8 (CH_2)	C-1, 2', 3'	$H_{1'}$-$H_{2'}$
2'	–	70.1 (C-O)		
3′	1.19 br s	27.2 (CH_3)		$H_{3'}$-$H_{4'}$
4'	1.19 br s	27.2 (CH_3)		

4.1.3 Chalybemide C {*N*-(2-Hydroxy-2-methyl-propyl)-3-phenyl-acrylamide} (41)

Compound 41 was isolated as white crystals with molecular formula of $C_{17}H_{19}NO_3$ determined by HREIMS at m/z 285.1373$[M]^+$ (cald. for. $C_{17}H_{19}NO_3$, 285.1373), indicating nine degrees of unsaturation. ^{1}H NMR spectrum displayed a pair of protons which were mutually coupled with aromatic signals at δH 6.86 (d, *J* = 8.5 Hz, 2H) and δ_H 7.15 (d, *J* = 8.5 Hz, 2H) typical of *para* disubstituted ring. Another ortho disubstituted benzene ring signaled by δ_H 6.89 (1H, d, *J* = 8.5 Hz, H-3), δ_H 7.52 (1H, m, H-4), δ_H 7.05 (1H, t, *J* = 7.7 Hz, H-5) and δ_H 7.86 (1H, dd, *J* = 7.7, 1.8 Hz, H-6). ^{13}C NMR (Table 3) spectra predicted the presence of one aliphatic methylene (δ_C 57.1), an *N*-methyl (δ_C 34.9), three oxygenated carbons: two methoxyls (δ_C 54.4 and 56.6) and a carbonyl (δ_C 168.1) and twelve aromatic carbons as classified by DEPT.

The data was comparable to that of tessmamide previously isolated from *Zanthoxylum tessmanii* (Kimani, 2015) except for the presence of methylene group and absence of methylenedioxy group on the compound.

HMBC and COSY correlations (Figure 10A) confirmed the overall connectivity and the planar structure of compound 41. A proton at δ_H 3.73 (OCH_3) showed a ^3J correlations to δ_C 113.2 (C-3′/C-5′) and δ_H 6.86 (H-3′/H-5′) to δ_C 56.4 (OCH_3) placing it at C-4’ in ring B and the other methoxy group δ_H 3.72 correlated to δ_C 112.2 (C-1) and δ_C 122.2 (C-4)In addition, a proton δ_H 6.89 (H-3) correlated to δ_C 56.6 (OCH_3) placing it at C-3 in ring A. Moreover, a proton for *N*-CH3 showed a ^3J correlation to a methylene carbon δ_C 57.1 (C-7’) and to carbonyl carbon δ_C 168.1 (C-1) corroborated by COSY off diagonal peaks between δ_H 3.19 (N-CH3) and δ_H 3.91 (CH_2) which in turn coupled with δ_H 7.15 (H-2’/H-6’) and confirmed *N,N*-methylenemethyl amide moiety. From the data mentioned above, compound 41 was as characterized 4-methyl-*N*-(2-methoxyphenyl)-*N*-methylbenzamide, isolated and characterized for the first time from *Z, chalybeum* and named as chalybemide C

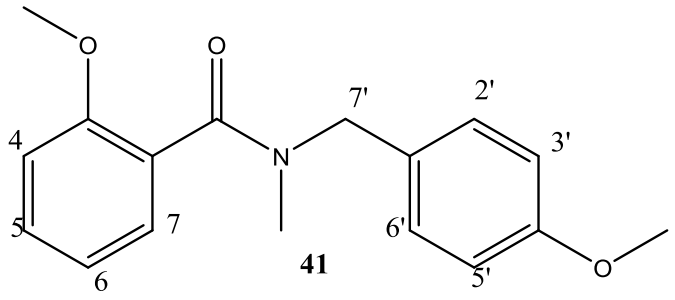

41

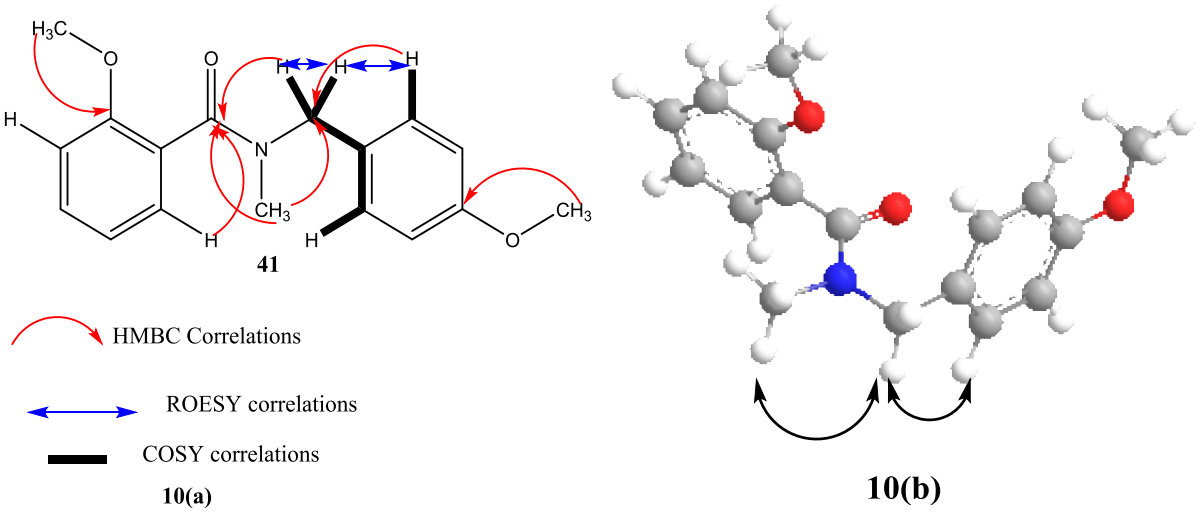

Figure 10:(a) HMBC, ROESY and COSY correlations on 2D structure while 10(b) is 3D ROESY correlations for compound 41

Table 3: 1H (600MHz) and 13 CNMR (150 MHz) (CDCl3) spectral data for Chalybemide C

Position	δH, mult (*J*, Hz)	δC	HMBC	COSY
1		168.1(C)		
2		122.2(C)		
3		159.8(C)		
4	6.89 dd (*J* = 8.3, 1.2)	112.2(CH)		
5	7.52 m	132.4(CH)		
6	7.05 t (*J*= 7.7)	122.5(CH)		
7	7.86 dd (*J* = 8.3, 1.8)	132.1(CH)	C-1	
1'		131.6(C)		
2′	7.15 d (*J* = 7.2)	127.1(CH)	C-7'	$H_{2'}$-$H_{7'}$
3'	6.86 d (*J* = 7.2)	113.2(C)		
4′		158.2(C-O)		
5′	6.86 d (*J* = 7.2)	113.2(CH)		
6′	7.15 d (*J* = 7.2)	127.1(CH)		$H_{6'}$-$H_{7'}$
7'	3.91 br s	57.1(CH2)	C-1	
5-OCH_3	3.73 br s	56.4 (CH3)	C-5	
4'-OCH_3	3.72 br s	56.6 (CH3)	C-4'	
NCH_3	3.19 s	56.6 (CH3)	C-1,7'	

4.1.4{1,3-dimethoxy-12-methyl-9H-[1,3]benzodioxolo[5,6-c]phenanthridin-12-ium}

Phenanthridine A

Compound **(42)** was obtained as yellow needle crystals. Its ESI–MS (positive mode) displayed a molecular ion peak at m/z 349.2795 corresponding to a molecular formula $C_{21}H_{18}NO_4^+$, ascribed to thirteen degrees of unsaturation. According to ^{1}H NMR spectrum, an o*rtho* coupled protons at δ_H 8.28 (1H, d, *J*=7.2 Hz, H-11) and δ_H 8.28 (1H, d, *J* = 7.2 Hz, H-12), *meta* coupled protons at δ_H 8.828 (1H, d, *J* = 2 Hz, H-8) and δ_H 8.844 (1H, d, *J* = 2.0 Hz, H-10), singlets at δ_H 7.781 (1H, s H-1), δ_H 8.322 (1H, s, H-4) and 10.10 (1H, s) indicated the presence of seven aromatic protons characteristics of a benzophenathridine alkaloid skeleton. A methylene singlet at δ_H 6.357 (2H, s, 2, 3-OCH_2O) characteristic of a methylenedioxy, two methoxy singlets with δ_H 4.12 (s, 7-OCH_3), δ_H 3.86 (s, 9-OCH_3) and a downfield signal (5.77 s, 3H) commonly associated with NCH_3 group.

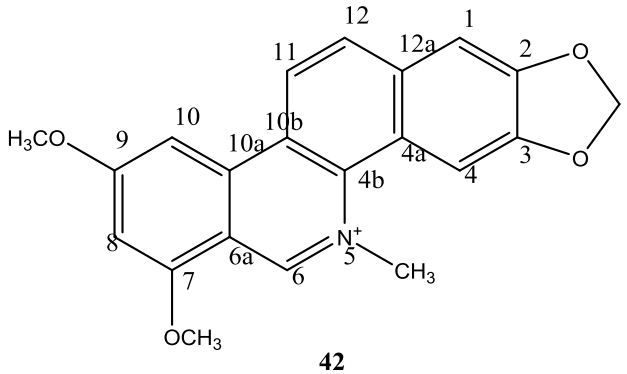

42

^{13}C NMR (Table 4) spectrum showed twenty one carbon signals which were classified as three oxygenated carbons (one methylenedioxy, δ_C 102.8 (OCH_2O) and methoxy groups, δ_C 61.93 (9-OCH_3) and δ_C 58.68 (7-OCH_3), ten quaternary carbons in the aromatic region methyl amine and seven aromatic methines. The ^{1}H and ^{13}C NMR data were then reconciled by the HMQC proton-carbon attachment observed between: δ_H 7.781 (1H, s) and δ_C 106.1; δ_H 8.322 (1H, s) and δ_C 131.7; δ_H 10.10 (1H, s) and δ_C 151.3; δ_H 8.828 (1H, d, *J*=1.6) and δ_C 119.3; δ_H 8.844 (1H, d, *J*=2.0) and 119.5; δ_H 8.28 (1H, d, *J*=7.2) and δ_C 105.4; δ_H 8.28 (1H, d, *J*=7.2) and δ_C 126.3. These 1D data would closely predict four aromatic skeleton of a benzophenanthridine with N-CH_3, a methylenedioxy and two methoxy groups (Miao *et al*, 2010) except for the position of the methoxy groups. The difference was noted with presence of a *meta* coupled protons at δ_H 8.83 (1H, d, *J*=1.6, H-8) and δ_H 8.84 (1H, d, *J*=2.0, H-10) instead of a pair of *ortho* coupled protons as observed with chelerythrine. This was supported by HMBC correlation between methoxy protons 4.12 to 142 C-7 and 3.89 to 145 (C-9), which were noted to have ^2J correlation with (H-10) and (H-8),

respectively as shown in Figure 10 (appendix 4.4). Additional HMBC (^{2}J and ^{3}J) correlations between δ_H 5.077 (s) and these two carbon signals {δ_C 130.8 (C-4b), δ_C 151.3 (C-6)} predicted the presence of a methyl amine with nitrogen at position 5. The spectra also confirmed the presence of two methoxy groups at carbon position 7 and 9 based on HMBC correlations between δ_H 8.828 (1H, d, J=1.6, H-8) and δ_C 58.68 (9-OCH_3) and δ_C 61(7-OCH_3), respectively (Figure11B). These chemical shifts characterized chelerythrine derivative 1,3-dimethoxy-12-methyl-9H-[1,3]benzodioxolo[5,6-c]phenanthridin-12-ium named as phenanthridine A.

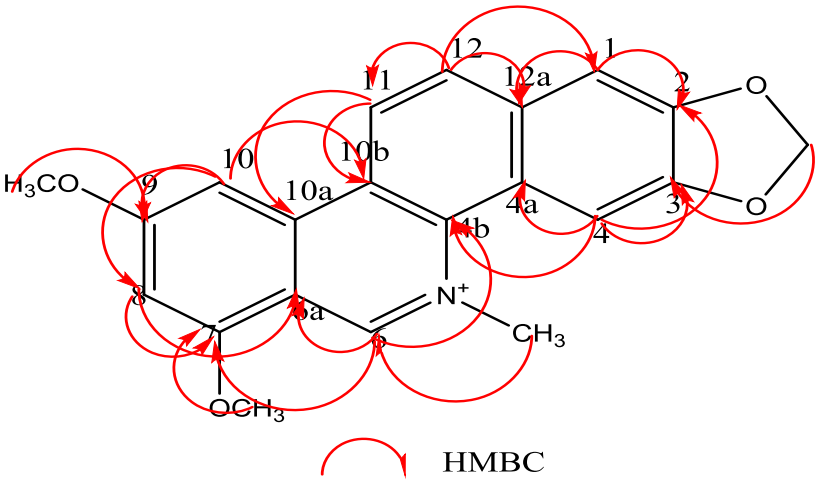

Figure 11(b): Compound 42 and its HMBC

Table 4: 1H and 13CNMR (DMSO-d6) spectral data for Phenanthridine A.

C-Position	δ_H, multi	δ_C	HMBC (^3J)
1	7.781 (1H, s)	106.1	C-2, C-12a, C-6a
2	-	147.2	-
3	-	147.0	-
4	8.322 (1H, s)	131.7	C-2, C-4a, C-6a, C-10b
4a	-	125.3	-
4b	-	130.6	-
6	10.10 (1H, s)	151.3	NCH_3, C-2, C-4, C-12a, C-4b
6a	-	120.7	-
7		151.2	-
8	8.828 (1H, d, *J* = 1.6)	119.3	9-OCH_3, 7-OCH_3
9	-	144.3	-
10a	-	128.5	-
10	8.844 (1H, d, *J* = 2.0)	119.5	C-6, C-7, C-4, C-10a, C-12, C-12a
10b	-	118.8	-
11	8.28 (1H, d, *J*=7.2)	105.4	C-10b, C-10a, C-10b, C-4a,C-4b
12a	-	130.8	-
12	8.28 (1H, d, *J* = 7.2)	126.3	C-10a, C-10b, C-4a, C-4b
2,3-OCH_2O	6.357 (2H, s)	102.8	C-3
7-OCH_3	4.117 (s)	61.93	C-7
9-OCH_3	3.86 (s)	58.68	C-9
NCH_3	5.077 (s)	52.24	C-4b, C-6

4.1.5 Zanthocapensine (43) {(R) (1′E)-5′-methoxy-6′-hydroxy-cinnamyl-(1′ → 6)-dihydrochelerythrine

Compound (**43**), named zanthocapensine, was isolated as a white crystal with melting point of 141-142˚C. Its HREIMS indicated a molecular ion at *m/z* 497.1839, which was in showing molecular formula $C_{30}H_{27}NO_6$ (cald for $C_{30}H_{27}NO_6$, 497.1838), with eighteen degrees of unsaturation. Analysis of the ^{1}H NMR spectral data (Table 5) showed three sets of aromatic protons alongside other protons including: two pairs of *ortho*-coupled protons signals at δ_H 7.80 (1H, d, *J* = 8.4 Hz, H-11) and 7.51 (1H, d, *J* = 8.4 Hz, H-12);7.68 (1H, d, *J* = 8.4 Hz, H-10) and7.13 (1H, d, *J* = 8.4 Hz, H-9), corresponding to two 1,2,3,4-tetrasubstituted benzene rings; a second set of aromatic protons signals at δ_H 6.53 (1H, d, *J* = 8.0 Hz, H-7′), 6.43 (1H, br d, *J* = 8.0 Hz, H-8′), and 6.67 (1H, br s, H-4′) predicted a 1,3,4-trisubstituted benzene ring supported by the COSY correlation between the *ortho* coupled protons; a third aromatic moiety was predicted by the presence of two singlets at δ_H 7.62 (1H, s, H-4) and δ_H 7.29 (1H, s, H-1), indicating a 1,2,4,5-tetrasubstituted aromatic ring.

Other protons signals noted on compound **43** included δ_H 6.13 (2H, d, *J* = 3.2 Hz) for methylenedioxy H-atoms; δ_H 5.15 (1H, d, *J* = 4.0 Hz, H-6) for methine adjacent to quaternary nitrogen; two aromatic methoxyl groups signals at δ_H 3.89 (3H, s) and 3.82 (3H, s) and an *N*-methyl group signal at δ_H 2.60 (3H, s). Simultaneously, evaluation of the ^{13}C NMR, DEPT (Table 5) and HSQC spectra (appendix 5.4), thirty carbon signals were categorized as one *N*-methyl, one methylenedioxyl, three methoxyl, twelve methines (one sp^3 and eleven sp^2), and thirteen sp^2 quaternary carbons (including six oxygenated carbons atoms). These data suggested a 6-substituted dihydrochelerythrine skeleton, with exception of the signal for *trans*-oriented protons at δ_H 5.99 (1H, d, *J* = 16.0 Hz, H-2′) and 5.92 (1H, dd, *J* = 16.0, 4.0 Hz, H-1′) which showed HMQC contours to δ_C 129.72 and 127.04, respectively.

The appearance of the *trans*-oriented olefinic moiety was further confirmed to have mutual HMBC correlation with carbon signals at δ_C 127.75 and 146.26 for C-3'and C-6' on the 1,3,4-trisubstituted benzene ring which was in turn confirmed by HMBC (appendix 5.5) to hold one -OH at C-4'and OCH_3 at C-5' thus pointing to the presence of a cinnamonyl unit in compound **43**. Unambiguous confirmation of 5′-methoxy-6′-hydroxy-cinnamenyl moiety was based on a NOE cross-peak between the aromatic proton H-4′ and a methoxyl singlet at δ_H 3.64. HMBC between the proton signal at δ_H 5.15 (6-H) to both olefinic carbons (δ_C 127.04 and 129.7) which in turn correlated to 6a (126.46) and 4b (140.06), provided the basis for asserting the 5′-methoxy-6′-hydroxy-cinnamonyl was attached at the C-6 of the dihydrochelerythrine skeleton.

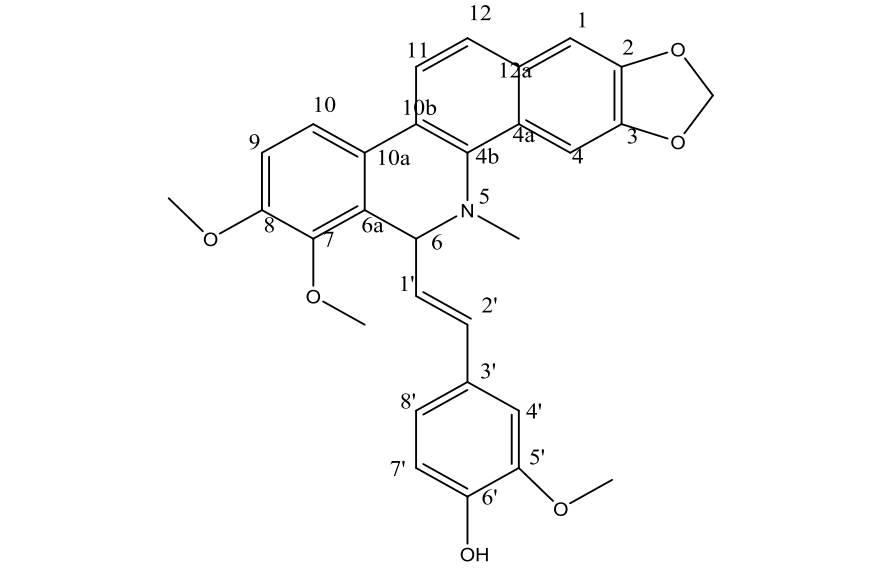

43

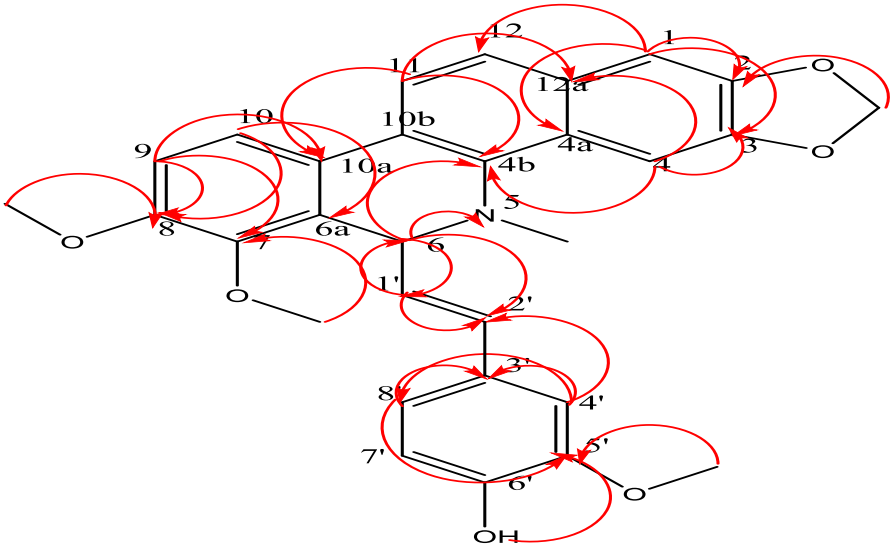

12(a)

Figure 12B: Structure of compound 43 and its HMBC correlations

Table 5: 1H and 13CNMR (DMSO-d6) spectral data for Zanthocapensine (43)

			Spectral data for 43	Literature data (Luo et al.,, 2012)	
Position	**δ_H (*J* in Hz) mult**	**δ_C**	**HMBC**	**δH (*J* in Hz) mult**	**δC**
1	**7.29 (1H, s)**	**104.3**	**2,3,4a,12**	**7.29 (s)**	**104.3**
2		**147.24**			**147.2**
3		**147.91**			**147.9**
4	**7.62 (1H, s)**	**99.76**	**2,3,4b,12a**	**7.62 (s)**	**99.8**
4a		**126.89**			**126.9**
4b		**140.06**			**140.1**
6	**5.15 (1H, d, *J* = 4.0)**	**58.44**	**4b,6a,1',2', N-Me**	**5.15 (d, 4.0)**	**58.4**
6a		**126.46**			**126.5**
7		**145.71**			**145.7**
8		**151.97**			**152**
9	**7.13 (1H, d, *J* = 8.4)**	**111.97**	**7,8,10a**	**7.13 (d, 8.4)**	**112**
10	**7.68 (1H, d, *J* = 8.4)**	**119.14**	**8,6a,10b**	**7.68 (d, 8.4)**	**119.1**
10a		**124.21**			**124.2**
10b		**123.44**			**123.4**
11	**7.80(1H, d, *J* = 8.4)**	**119.96**	**4b,10a,12a**	**7.80 (d, 8.4)**	**120**
12	**7.51 (1H, d, *J* = 8.4)**	**123.66**	**1,4a,10b**	**7.51 (d, 8.4)**	**123.7**
12a		**130.5**			**130.5**
1,	**5.92 (1H, dd, J=16.0,4.0)**	**127.04**	**6,2',3'**	**5.92 (dd, 16.0, 4.0)**	**127**
2'	**5.99 (1H, d, *J* = 16.0)**	**129.72**	**6,1',3',4',8'**	**5.99 (d, 16.0)**	**129.7**
3'		**127.75**			**127.8**
4'	**6.67 (br s)**	**109.42**	**2',3',6',8**	**6.67 (br s)**	**109.4**
5'		**147.6**			**147.6**
6'		**146.26**			**146.3**
7'	**6.53(1H, d, *J* =8.0)**	**115.3**		**6.53 (d, 8.0)**	**115.3**
8'	**6.43(1H, d, *J* = 8.0)**	**119.46**	**3',5'**	**6.43 (br d, 8.0)**	**119.5**
OCH_2O	**6.13 (2H,s)**	**101.24**	**2',4',6'**	**6.13 (s, 3.2)**	**101.2**
NCH_3	**2.60 (3H, s)**	**42.26**	**2,3**	**2.60 (s)**	**42.3**
7-OCH_3	**3.82 (3H, s)**	**60.48**	**6,4b**	**3.82 (s)**	**60.5**
8-OCH_3	**3.89 (3H, s)**	**55.7**	**7**	**3.89 (s)**	**55.7**
5'-OCH_3	**3.64 (3H, s)**	**55.49**	**8**	**3.64 (s)**	**55.5**
6'-OH	**8.97 (br s)**		**5'**	**8.97 (br s)**	

Further analysis of HMBC spectrum showed the following correlation: contours intersection 6.13 signal for the methylenedioxy protons and carbons signal at δ_C 147.24 and 147.91 for C-2 and C-

3, respectively which in turn correlated to proton signal at δ_H 7.62 (1H, s, H-4) and δ_H 7.29 (1H, s, H-1), thus confirming the 1,2,4,5-tetrasubstituted benzene ring (Figure 12B). Following the comparable spectroscopy of compound **43** and that of previously isolated phenyl substituted dihydrobenzophenanthridine alkaloid from *Zathoxylum capens* (Fotie et al., 2007) hence characterized as zanthocapensine.

4.1.6 Zanthocapensol (44) {2-(3′,4′-methylenedioxyphenyl)-5-[(*E*)-3′′-hydroxy-1′′-propenyl]-7-methoxybenzofuran}

Zanthocapensol (**44**) was obtained as a pale yellow amorphous solid with the melting point 191-192˚C with a molecular formula $C_{19}H_{16}O_5$ predicted by both 1D and 2D NMR data and HREIMS at a molecular ion of m/z 324.099 (calculated. for $C_{19}H_{16}O_5$, 324.0998) predictive of twelve degrees of unsaturation.

The ^{13}C NMR spectrum of compound **44** indicated nineteen carbon signals, showing two oxygenated methylenes (one methylenedioxyl, δ_C 101.51), one methoxyl group (δ_C 55.84), eight sp^2 quaternary carbons (five oxygenated) and eight sp^2 methines (Table 6). According to ^1H NMR (DMSO-d_6) spectrum (Table 6), two broad singlets in the aromatic region at δ_H 7.18 (^1H, br s) and 7.04 (1H, br s), signified a tetra substituted benzene ring moiety); and a tri-substituted aromatic ring moiety displaying an ABX spin systems constituted by a *meta*-coupling and *ortho* coupling {δ_H 7.40 (1H, br d, J = 8.0, 1.5Hz,);7.05 (1H, d, J = 8.0 Hz) and δ_H 7.44 (1H, dd, J = 1.5Hz)}). Presence of a singlet at δ_H 7.25 (1H, s) attached to carbon signal at 101.38 with ^3J HMBC correlation to aromatic carbon signal δ_C 111.18 holding a singlet proton (δ_H 7.18) and another quaternary aromatic carbon δ_C 142.61 indicated an ethenyl unit as one of the substituents of the tetrasubstituted benzene ring.

Moreover, the presence of a *trans*-3-hydroxy-1-propenyl group was noted based on the signals for *trans* coupled alkene protons {δ_H 6.61 (1H, d, J = 16.0 Hz), 6.38 (1H, dt, J = 16.0, 4.8 Hz)} which showed HMBC correlation to an oxymethylene carbon holding two hydroxymethelene protons at δ_H 4.14 (2H, dd, J = 5.0, 4.8 Hz) which in turn showed ^3J correlation to alkene carbon δ_C 129.8. The attachment of the *trans*-3-hydroxy-1-propenyl to the tetrasubstituted aromatic rings was justified based on HMBC correlation between the proton signal at δ_H 6.61 and carbon signals at δ_C 111.18 and 104.78 (carbon atoms holding the singlet protons). The other two substituents were noted as a methoxyl group and phenyl ether linkage. The methoxy group was based on the HMBC correlation between the methoxy signals at δ_H 3.98 and carbon signal at δ_C 144.77 which in turn correlated with singlet protons at δ_H 6.03. Whereas the phenyl ether linkage was noted as

cyclization point with the ethene substituent to a furan group following the HMBC correlation of the alkene proton (δ_H 7.255) to both *O*-substituted aromatic carbon (δ_C 142.61) and *O*-substituted alkene carbon (δ_C 155.50). A benzofuran skeleton with *trans*-3-hydroxy-1-propenyl and methoxyl group was thus noted with a clear indication of substitution at carbon 2.

Considering the ABX substitution pattern of the other aromatic ring that would attach at carbon 2, a methylenedioxy group {δ_H 6.101 (2H, s)} on carbon 3' and 4' automatically fitted the structure. It was thus concluded that the compound **44** named 2-(3′,4′-methylenedioxyphenyl)-5-[(E)-3″-hydroxy-1″-propenyl]-7-methoxybenzofuran was a derivative of 2-arylbenzofuran neolignan, class of *Zanthoxylum* metabolite previously reported from *Zanthoxylum capense* (Luo *et al*., 2013

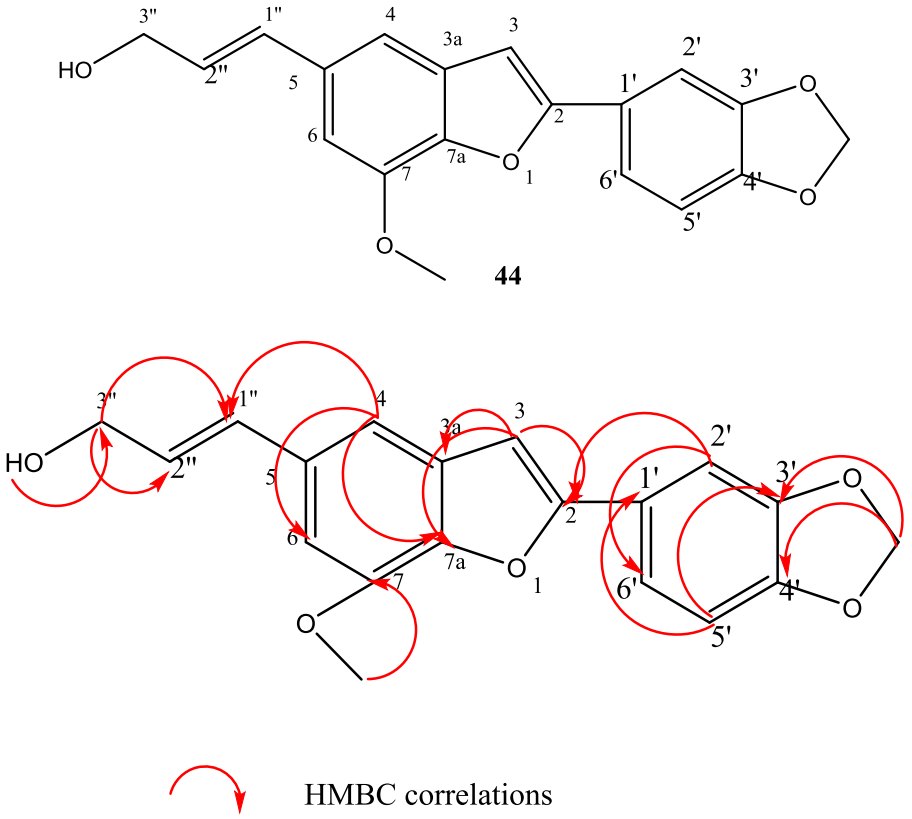

Figure 13: Structure of Compound 44 and its HMBC correlations

Table 6: 1H and 13 CNMR (DMSO-d6) spectral data for Zanthocapensol (44)

Spectral data for Zanthocapensol (44)				**Literature data (Luo X et al,2012)**	
Position	**δ_H, multi**	δ_C	**HMBC**	**δ_H, multi**	δ_C
2		155.5			155.5
3	7.255 (1H, s)	101.38	2,3a.7a	7.25 (s)	101.3
3a		130.66			130.7
4	7.181 (1H, br s)	111.18	3,6,7a,1''	7.18 (br s)	111.2
5		133.45			133.5
6	6.035 (1H, br s)	104.78	4,7,7a,1''	7.03 (br s)	104.8
7	7.442 (1H, br s)	144.72			144.7
7a		142.61			142.6
1'		123.85			123.8
2'	7.053 (1H, d, *J* = 8.0)	105.04	2,3',4',6'	7.44 (br s)	105
3'	7.403 (1H, d, *J* = 8.0)	148			148
4'	6.612 (1H, d, *J* = 16.0)	147.94			147.9
5'	6.376(1H, dt, *J* = 16.0, 4.8)	108.88	1',3',4'	7.05 (d, 8.0)	108.9
6'	4.149 (2H, dd, *J* =5.0, 4.8)	118.84	2,2',4'	7.41 (br d, 8.0)	118.8
1"	6.101 (2H, s)	129.01	4,6,2'',3''	6.61 (d, 16.0)	129
2"	3.980 (3H, s)	129.81	5,1'',3''	6.39 (dt, 16.0, 4.8)	129.8
3"	4.884 (1H, s)	61.62	1'',2''	4.13 (dd, 5.0, 4.8)	61.6
OCH_2O		101.51	3',4'	6.10 (s)	101.5
7-OMe		55.84	7	3.98 (s)	55.8
3''-OH			3''	4.88 (t, 5.0)	

4.1.7 Zanthoamide D (45) {*(E)-N*-(2-Hydroxy-2-methylpropyl)-6, 6-dimethoxyhex-2-enamide}

Compound **45** was isolated as white crystals from the alkaloid fraction of the crude extract portion using hexane: DCM 1:9 solvent system for crystallization and showed a blue spot when sprayed with with p-anisaldehyde. The ^{1}H NMR (Table 7) showed two protons signals characteristic of alkene protons at δ_H 6.85 (1H, d, *J* = 15.0) and δ_H 6.08 (1H, d, *J* = 15.0) with *trans* orientation, three methylene protons δ_H 1.80 (2H, m), δ_H 2.24 (2H, t), δ_H 3.15 (2H, s), one methine proton δ_H

4.47 (1H, t), two methyl signals integrating to 6H (δ_H 1.17, 3H, s) and proton signals characteristic of methoxy groups δ_H 4.47 (1H, s). The ^{13}C NMR (Table 7) revealed a total of twelve carbons; two quaternary carbons at δ_C 169.5 and 71.6, two sp^2 methine carbons at δ_C 125.0 and 147.2, three methylene carbons at δ_C 33.6, 29.0 and 53.6, one methine carbon at δ_C 107.2, two symmetric methyl carbons at δ_C 28.0 and two symmetric methoxy carbons at δ_C 55.5. The ^{13}C NMR thus, supported the ^{1}H NMR data based on the attached proton analysis (HMQC spectrum), with exception of a broad proton signal at δ_H 6.96 suggested being for *N*-H from an amide moiety.

HMBC correlation showed ^{2}J and ^{3}J correlations between the methine proton signal at δ_H 4.47 with the methylene carbon signal at δ_C 33.6; methylene proton at δ_H 1.80 with methylene carbon at δ_C 29.0; methylene proton at δ_H 2.24 with olefinic methine carbon at δ_C 125.0. Moreover, ^{3}J correlation between methine proton signal at δ_H 6.85 and the quaternary carbon at δ_C 169.4 and methine carbon at δ_C 125.0 revealed the connectivity between C-1 to C-6 with acetal moiety at C-6 O=C-C=C-CH_2-CH_2-C$(OCH_3)_2$. On the other hand, methylene proton at δ_H 3.15 showed a correlation with carbon signal at δ_C 28.0 and 71.6 which confirmed connectivity from C-1' to C-3' as -H*N*-CH_2-C{(OH)$(CH_3)_2$}. The data was confirmed by ESIMS a molecular peak at m/z 268.1322, thus characterizing compound **45** as a derivative of 6,6-dimethoxy hex-2-enamide isolated for the first time from *Z. gilletii* named as Zanthoamide D

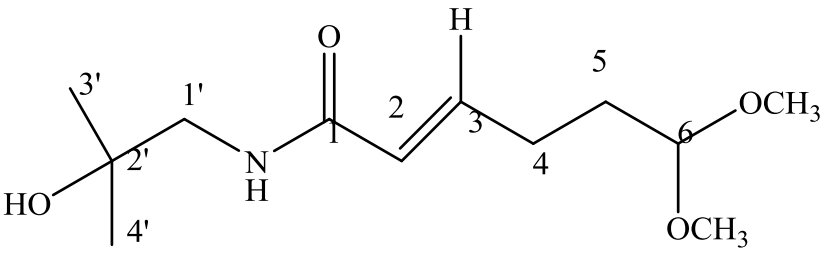

45

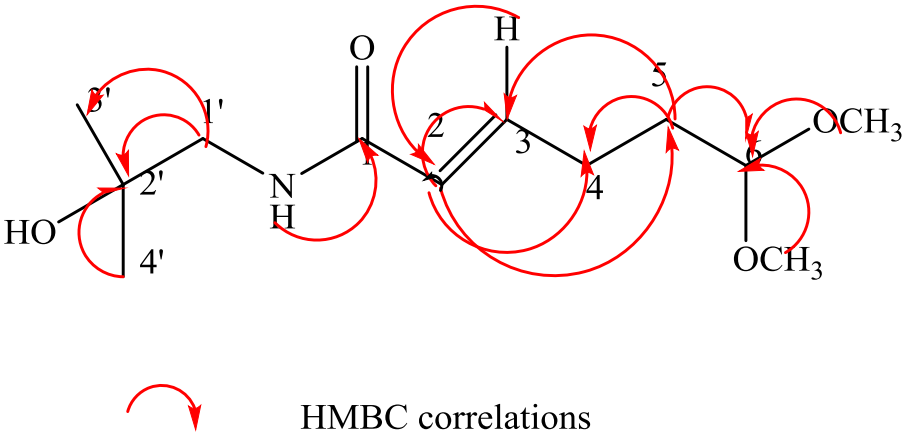

HMBC correlations

Figure 14: Structure of compound 45 and its HMBC correlations

Table 7: 1H and 13C NMR (DMSO-d6) spectral data for Zanthoamide D

C. position	δ_H, Multiplicity	δ_C	^1H-^1H	HMBC
1	-	169.5	-	-
2	6.08, 1H dt, (J=15.0)	125.0	6.85, 2.24	C-5, C-3, C-1
3	6.85, 1H, dt (J=15.0)	147.2	6.08	C-1, C-2, C-4
4	2.24, 2H td	29.0	1.80, 6.85	C-6, C-5
5	1.80, 2H m	33.6	2.24, 4.47	107.2, 29.0
6	4.47, 1H t	107.2	1.80	C-5
1'	3.15, 2H s	53.6	-	C-3', C-2'
2'	-	71.6	-	-
3'/4'	1.17, 3H s	28.08	-	C-1', C-2'
2 x OCH_3	3.25, 3H	55.5	-	-

4.1.8 2,3-epoxy-6,7-methylenedioxy coniferyl alcohol (10)

Compound 10 was isolated as a white crystal (melting point: 124-125°C) with a molecular formula of $C_{10}H_{10}O_4$ as predicted by both 1D and 2D NMR and The 1 H NMR spectrum ($CDCl_3$, Table 8) corresponded to that of 2,3-epoxy-6,7-methylenedioxy coniferyl alcohol isolated from *Z. chalybeum by* Wasiali (2019).

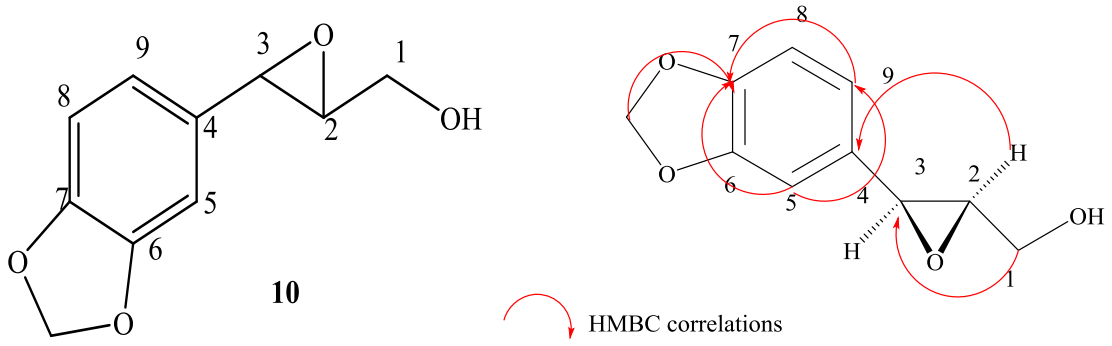

Figure 15: Compound 10 and its HMBC

Table 8: 1H and 13CNMR (CDCl3) spectral data for 2,3-epoxy-6,7-methylenedioxy coniferyl alcohol

C-Position	δ_C	δ_H, Multiplicity	COSY (^1H-^1H)	HMBC	**Literature data (Anza *et al*, 2014)** δ_H, Multiplicity	δ_C
1	71.7	3.89 (1H, d, *J* = 16.0, 7.2) 4.25 (1H, dd, *J* = 16.0, 13.0)	$H_{1,1'}$-H_2	C-2,3	4.25 dd(1H, d, *J* = 16.0, 7.2) 3.89 dd(1H, dd, *J* = 16.0, 13.0)	71.7
2	54.3	3.05(m)	H_2-$H_{1,3}$	C-1, 3, 4	3.10 m	54.3
3	85.7	4.73(1H, d, *J* = 4.4)	H_3- H_2	C-1,2,4,5,9	4.74 d(1H, d, *J* = 4.4)	85.9
4	135.0	-	-			135.1
5	119.3	6.82 (1H, dd, *J* = 0.8,1.2)	-	C-3,4,6,9	6.82 dd(1H, dd, *J* = 0.8,1.2	119.4
6	147.8	-	-	-		147.9
7	147.1	-	-	-		147.1
8	108.1	6.86 (1H, dd, *J* = 8.0,0.8)	H_8-H_9	C-4,6,7	6.86 dd	108.2
9	106.5	6.80 (1H, *J* = 8.0, 1.2)	H_9-H_8	C-3,4,5,7	6.80 dd(1H, *J* = 8.0, 1.2)	106.5
OCH_2O	101.3	5.95 (2H, s)	-	C-6,7	6.02 1H,s	101.1

4.1.9 1,2-dimethoxy-[1,3]benzodioxolo[5,6-c]benzophenanthridine (Norchelerythrine) (9)

Compound **9** was isolated as yellow crystals, UV active with blue fluorescence with melting point of 210-212°C. Its molecular mass determined by ESIMS $[M+H]^+$, *m/z* = 334 giving molecular formula as $C_{20}H_{15}NO_4$ indicating thirteen degrees of unsaturation. ^1H NMR spectrum showed two pairs of *ortho* coupled proton signals at δ_H 8.20 (d, *J* = 8.7), δ_H 8.59 (d, *J* = 8.7) and δ_H 8.62 (d, *J* = 9.7), δ_H 8.65 (d, *J* = 9.7) supported by COSY spectrum together with a deshielded proton peak predictive of an imine proton (HC=N) at δ_H 9.95 (Table 9).

^{13}C spectrum revealed the presence of 17 sp^2 carbons, ten quaternary carbon atoms including four oxygenated carbons; methylenedioxy group at δ_C 104.5 and two methoxy groups at δ_C 57.7 and δ_C 63.0, typical of benzophenanthridine structure. These data and the literature were similar to that of norchelerythrine previously isolated from roots of *Z. gilletii* (Wafula, 2014) and from roots of *Z. chalybeum* (Wasiali, 2019).

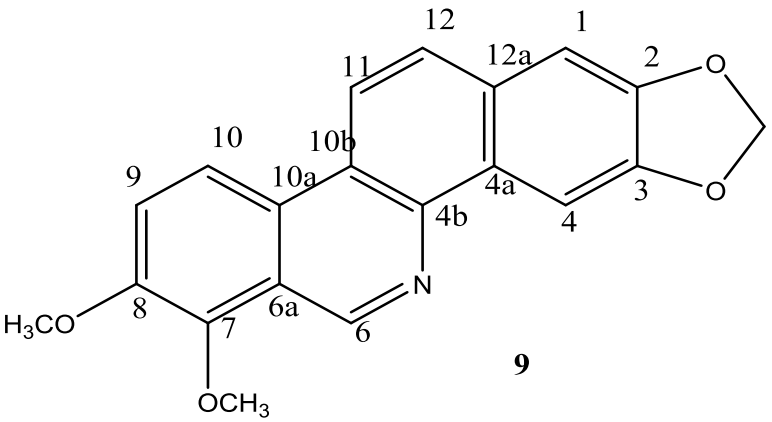

9

Table 9: 1H and 13CNMR (CDCl3) spectral data for Norchelerythrine (9)

C-Position	Compound **9** δ_H, Multiplicity	δ_C	HMBC	**Literature data (Maliwat *et al*, 1997)** δ_H, Multiplicity	δ_C
1	7.52 (1H, s)	107.2	C- 3, C-12	7.52 (1H, s)	104.4
2		152.2			149.4
3		151.9			148.5
4	8.18 (1H, s)	105.2	C-2, C- 4b	8.72(1H, s)	102.0
4a		133.5			129.7
4b		134.3			129.7
6	9.95 (1H, s)	151.9	C-6a, C- 10a	9.75 (1H, s)	140.0
6a		127.2			128.1
7		150.9			148.3
8		147.6			146.6
9	8.65 (1H, d, *J* = 9.7 Hz)	132.7	C- 6a, 8-OCH_3	8.36 (1H, d, *J*=9.09 Hz)	129.2
10	8.62 (1H, d, (*J* = 9.7 Hz)	120.0	C- 6a, 7-OCH_3, 8-OCH_3	7.59 (1H, d, *J*=9.09 Hz	120.0
10a		121.8			121.9
10b		130.1			129.7
11	8.59 (1H, d, *J* = 8.7 Hz)	119.6	C-4b, 10a, C-10b	8.35 (1H, d, *J*=8.74 Hz)	118.7
12	8.20 (1H, d, *J* = 8.7 Hz)	127.5	C-1, C-12a	7.86 (1H, d, *J*=8.74 Hz)	127.1
12a		120.0			120.0
OCH_2O	5.95 (2H, s)	101.3	C-6, C-7	6.13 (2H, s)	101.3
7-OCH_3	4.28 (3H, s)	150.9	C-7	4.08 (3H,s)	61.9
8-OCH_3	4.13 (3H, s)	147.6	C-8	4.13 (3H, s)	56.8

4.1.10 Sesamine (46)

Compound 46 was isolated as white amorphous solid which is UV active with molecular mass of 121 - 122°C. Its molecular formula is $C_{20}H_{18}O_6$ predicted by both 1D and 2D NMR data and HREIMS at a molecular ion of m/z = 354 (calculated. for $C_{20}H_{18}O_6$, 354.35) giving twelve degrees of unsaturation. Its ^{1}H NMR and ^{13}C NMR spectral and its TLC spots together physical

properties was similar to those of a lignan, sesamine which previously isolated from *Z. budrunga* by Mukhlensur (2005) and from *Z. gilletii* by Wafula (2014).

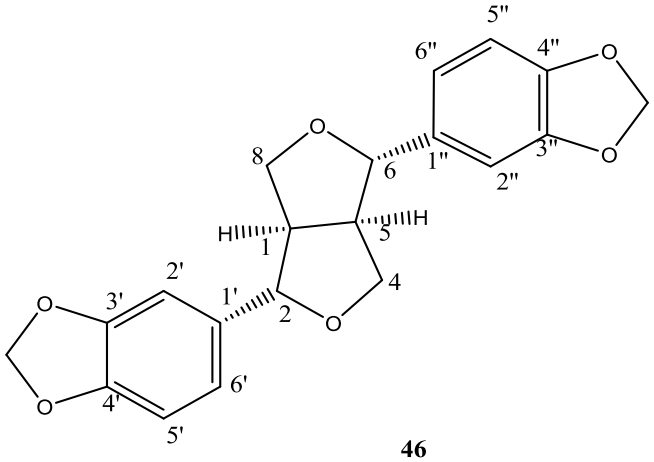

46

Table 10: 1H and 13CNMR (CDCl3) spectral data for sesamine(46)

C-Position	δ_H, Multiplicity	δ_C	Literature data (Ali *et al*, 2007) δ_H, Multiplicity	δ_C
1	3.11 (1H, m)	55.1	3.11 (1H, m)	55.3
2	4.65 (1H, d, *J* = 4.8)	87.1	4.65 (1H, d, *J* = 4.8)	87.1
4	3.82 (1H, m) 4.20 (1H, m)	72.4	3.82 (1H, m) 4.20 (1H, m)	72.3
5	3.09 (1H, m)	55.1	3.09 (1H, m)	55.0
6	4.70 d, *J* = 5.1	87.1	4.70 d, *J* = 5.1	87.1
8	3.83 m 4.23 m	72.4	3.83 m 4.23 m	72.3
1'		133.5		133.4
2'	6.80 d, *J* = 8.1	114.2	6.80 d, *J* = 8.1	114.1
3'		146.4		146.4
4'		145.7		145.6
5'	6.70 d, *J* = 8.1	116.2	6.70 d, *J* = 8.1	116.2
6'	6.69 dd, *J* = 1.8, 8.1	118.5	6.69 dd, *J* = 1.8, 8.1	118.5
1''		136.2		136.1
2''	6.87 d, *J* = 1.5	107.3	6.87 d, *J* = 1.5	107.2
3''		148.7		148.7
4''		148.7		148.7
5''	6.77 d, *J* = 8.1	108.7	6.77 d, *J* = 8.1	108.7
6''	6.84 dd, *J* = 8.1, 1.5	120.1	6.84 dd, *J* = 8.1, 1.5	120.1
OCH_2O	5.91 (2H, s)	101.8	5.91 (2H, s)	102.0
OCH_2O	5.90 (2H, s)	102.0	5.90 (2H, s)	102.0

4.1.11 Skimmianine (21)

Compound 21 was isolated as yellow coloured powder with the melting point of 179-180ºC with molecular ion peak at m/z 260 $[M+H]^+$ corresponding $C_{14}H_{13}NO_4$ supported by ^1H and ^{13}C NMR data (Table 11). The data was compared to the literature and marched exactly with that of skimmianine as was isolated from *Glycosmis pentaphylla* by Natarajan *et al*, 2020.

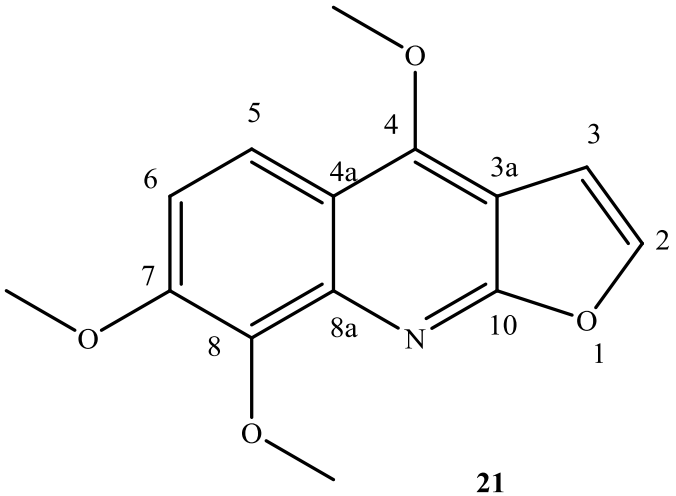

21

Table 11: 1H and 13CNMR (CDCl3) spectral data for Skimmianine (21)

C-Position			Literature data (Ali et al, 2007)	
	δ_H, Multiplicity	**δ_C**	**δ_H, Multiplicity**	**δ_C**
2	7.54, d, J=7.84	142.8	7.56, d, (*J*=8.0)	142.8
3	7.01, d, J=7.84	101.9	7.02, d, (*J*=8.0)	101.9
3a		104.3		104.4
4		152.0		152.1
4a		114.8		114.6
5	7.96, d (J= 8.0)	117.9	7.99, d, (*J*=8.0)	117.8
6	7.23, d J= 8.0)	112.2	7.23, d, (*J*=8.0)	112.2
7		157.0		157.0
8		164.2		164.4
8a		114.4		114.8
10		142.1		142.1
4-OCH_3	4.03, s	56.7	4.03, s	56.7
7-OCH_3	4.11,s	58.8	4.11, s	58.8
8-OCH_3	4.41,s	61.5	4.41, s	61.4

4.2. α-Amylase and α-Glucosidase inhibition of pure isolates from *Z. chalybeum* and *Z. gilletti*

The dose dependent α-amylase and α-glucosidase inhibitory activities of the isolated

compounds were processed on long probit analysis (regression analysis) to establish IC_{50} values (Table 12). There was no significant difference in the activities ($P > 0.05$) between the eight alkaloids compared to activity of acarbose (standard drug) with IC_{50} = 42.67 μM against α-amylase. Two phenolic compounds; 2,3-epoxy-6,7-methylenedioxy coniferyl alcohol (**10**) and zanthocapensol (**44**) showed no significant difference ($p > 0.05$) in the activity (IC_{50} of 48.34 and 48.21 respectively) with acarbose while sesamine (**46**) displayed significantly low activity (IC_{50} = 54.67 μM) against α-amylase enzyme relative to acarbose.

Table 12: In vitro IC50 values of compounds from Z. chalybeum and Z. gilletii against α-amylase and α- glucosidase inhibition compared to standard control inhibitor (acarbose)

Compounds	**α-amylase**	**α-glucosidase**
	(μM)	(μM)
Acarbose	42.67	44.88
Chaylbemide A ***(39)***	45.76	43.54
Chaylbemide B ***(40)***	43.22	44.32
Chaylbemide C ***(41)***	46.76	47.43
Zanthoamide D ***(45)***	47.36	47.23
Skimmianine ***(21)***	47.72	47.63
Norchelerythrine ***(9)***	46.49	48.7
Zanthocapensine ***(43)***	48.36	47.27
Phenanthridine A ***(42)***	48.91	49.20
*Zanthocapensol****(44)***	48.21	47.11
2,3-Epoxy-6,7-methylenedioxy coniferyl ***(10)***	48.34	47.45
Sesamine ***(46)***	54.67	54.77
LSD (P < 0.05)	8.11	8.6
CV%	40	34

IC_{50} values, calculated from regression using five different concentrations (10.0, 20.0, 50.0, 100.0, and 150.0 μM) are expressed as mean of replicated experiments with percentage coefficient of variation (CV %) indicated, LSD ($p < 0.05$): Least Significant

difference considered significant at $p \leqslant 0.05$.

The isolates showed a similar activity against α-glucosidase enzyme as was (Table 12) indicating that all the isolated alkaloids and two phenolics (zanthocapensol (**44**) and 2,3-epoxy-6,7-methylenedioxy coniferyl alcohol (**10**)) from the stem barks of the two plants had no significant difference in the inhibitory activity ($p > 0.05$) compared to control acarbose but sesamine showed significantly ($p < 0.05$) different compared to the control which implied that sesamine among phenolics displayed moderately lower activity against α-glucosidase activities. The results from the assay deduced that inhibitory activity of the isolated alkaloids and slightly to the phenolic compounds from the plant *Z. chalybeum* and *Z. gilletii* thus agreeing with the previously established anti-hyperglycemic activities of *Z. chalybeum* stem and root extracts (Agwaya,2016). Hydrogen bonding interaction between inhibitor and the enzyme had previously been cited as a possible inhibition mode involving active sites of α-amylase and α -glucosidase and the hydroxyl groups of compounds with phenolic entities (Bahadoran *et al*, 2013).

4.3 *In-vitro* modes of α-amylase and α-glucosidase inhibition of active compounds from *Z. chalybeum* and *Z. gilletii*

Different inhibitors show varied modes of inhibition against enzymes. The modes of inhibition are predicted by considering Lineweaver-Burk plot, from which kinetic parameters are obtained such as maximum velocities (V_{max}) and K_m (Menten constant; substrate concentration at which V_{max} is ½) are obtained to predict the modes of inhibition.

The modes of inhibition and the enzymes-inhibitor inhibition constants were deduced using kinetic analysis based on both Dixon plots (Appendix 12.0) and Lineweaver-Burk plots (Table 13). The results revealed that compounds showed mixed inhibitory modes. These compounds were Skimmianine (**21**), Norchelerythrine (**9**), Zanthocapensine (**43**), and Phenanthridine A (1,3-dimethoxy-12-methyl-9H-[1,3]benzodioxolo[5,6-c]phenanthridin-12-ium) (**42**) showing comparable inhibitor constant, K_i of to acarbose ($p > 0.05$) which are lower indicating that it's difficult to dissociate enzyme-inhibitor complex hence better inhibitor against α-amylase enzyme while the other six compounds which showed significantly ($p < 0.05$) low activity compared to acarbose due their higher K_i values indicating enzyme-inhibitor complex bond easily dissociate as displayed by either noncompetitive or uncompetitive modes against α-amylase actions on starch.

The compounds that exhibited mixed inhibition on amylase also exhibited comparable modes on α-glucosidase activities. These compounds had considerably ($p < 0.05$) higher K_i values than acarbose, indicating a better potential for inhibition against glucosidase than amylase.

On the other hand, the other compounds that exhibited uncompetitive and non-competitive inhibitions against α-glucosidase activities had similar K_i values ($p < 0.05$) in comparison to acarbose. One compound 2,3-Epoxy-6,7-methylenedioxy coniferyl (**10**) showed a competitive mode of inhibition both on amylase and glucosidase with K_i of 5.54 ± 0.58 ($R^2 = 0.985$) and 17.21 ± 0.15 ($R^2 = 0.8692$), respectively which were statistically comparable ($p < 0.05$) to that of acarbose thus indicative of the most active inhibitors from the *Z. chalybeum* and *Z. gilletti* extracts. The most potent inhibitors of α-amylase and α-glucosidase were reported to be compound **10** and the alkaloids **45**, **21**, **9**, and **43**, which exhibit competitive and mixed inhibitions, respectively.

Conversely, the compounds **45, 39, 40, 41, 43**, and **46** exhibited different mechanisms of inhibition and corresponding dissociation constants in relation to the two enzymes, indicating moderate inhibitory activities. Alkaloids exhibit superior inhibitory activities against α-amylase and α-glucosidase possible due to H-bond interactions, while phenolics' effectiveness could due to OH groups.

Table 13: Inhibition modes and inhibition constant (Ki) values for compounds from Z. chalybeum and Z. gilletii against α-amylase and α-glucosidase inhibition relative to acarbose inhibitions, as determined by Lineweaver-Burk plots and Dixon Plots, respectively

Compound	α-amylase				α-glucosidase			
	Inhibition Mode	K_m	V_{max}	K_i (mM)	Inhibition mode	K_m	V_{max}	K_i (mM)
Chaylbemide A (39)	Non-competitive	2.55	0.041	13.36±2.43**	Non-competitive	8.47	0.044	20.95±2.14
Chaylbemide B (40)	Non-competitive	5.87	0.035	11.05±0.58**	uncompetitive	6.03	0.048	44.58±1.65
Chaylbemide C (41)	Non-competitive	6.35	0.034	14.83±0.50**	Non-competitive	6.86	0.044	17.56±0.24
Zanthoamide D (45)	Non-competitive	4.28	0.036	26.69±2.13**	Non-competitive	14.18	0.047	34.73±0.79**
Skimmianine (21)	Mixed	5.51	0.034	2.74±0.06	Mixed	9.58	0.044	7.64±0.02**
Norchelerythrine (9)	Mixed	8.14	0.044	7.57±0.59	Mixed	14.3	0.028	7.68±0.04**
Zanthopensine (43)	Mixed	12.11	0.033	3.34±0.03	Mixed	15.286	0.042	4.73±0.10**
Phenanthridine A (42)	Mixed	6.14	0.035	3.10±0.20	Mixed	11.92	0.044	9.17±0.10**
Zanthocapensol (44)	Uncompetitive	8.61	0.033	26.28±1.47**	uncompetitive	11.89	0.044	20.62±1.94
2,3-Epoxy-6,7-methylenedioxy coniferyl (10)	Competitive	3.77	0.04	5.54±1.02	competitive	3.76	0.05	17.21±0.16
Sesamine (11)	Uncompetitive	2.5	0.043	12.53±1.957**	Uncompetitive	5.17	0.05	24.33±1.93
Acarbose	Competitive	7.68	0.033	6.14±0.01	Competitive	4.59	0.043	22.40±1.23

** values are significantly different from the standard inhibitor (acarbose) Inhibition constant (K_i) based on Tukey HSD / Tukey Kramer post-analysis of one-way analysis of variance replicated K_i values. Least significant difference was considered at $p < 0.05$

CHAPTER FIVE

SUMMARY, CONCLUSION AND RECOMEDATION

The study was intended to establish the modes of inhibition of alkaloids and phenolics from *Z. chalybeum* and *Z. gilletii* against α-amylase and α-glucosidase and validation of the rationale behind the use of Z. *chalybeum* and *Z. gilletii* in managing diabetes mellitus**.**

5.1 Summary

Nine pure compounds were isolated from the stem bark of *Z. chalybeum.* Among them are seven alkaloids including two benzophenanthridine alkaloids; norchelerythrine **(9)** and phenanthridine A **(**1,3-dimethoxy-12-methyl-9H-[1,3]benzodioxolo[5,6-c]phenanthridin-12-ium) (**42**), four amides: chalybemide A (**39**), chalybemide B (**40**), chalybemide C (**41**) and one furoquinoline alkaloid: skimmianine (**21**), two phenolics: 2,3-epoxy-6,7-methylenedioxy coniferyl alcohol (**10**) and sesamine (**46**). Six compounds were isolated from *Z. gilletii* including four alkaloids among them are three benzophenanthridine alkaloids**:** Norchelerythrine **(9),** phenanthridine A (**42**) (chelerythrine derivative) and Zanthocapensine (**43**) and an amide alkaloid; zanthoamide D (**45**), and two phenolics zanthocapensol (**44**) and sesamine (**46**). This totals to thirteen pure compounds from the two plants; *Z. Chalybeum* and *Z. gilletii.*

All the eight alkaloids and three phenolics isolated from the two plants were assayed against the two enzymes: α-amylase and α-glucosidase. All the alkaloids, norchelerythrine **(9),** phenanthridine A (**42**), chalybemide A (**39**), chalybemide B (**40**), chalybemide C (**41**) zanthoamide D (**45**), skimmianine (**21**) and zanthocapensine (**43**) and two phenolics: 2,3-epoxy-6,7-methylenedioxy coniferyl alcohol (**10**) and zanthocapensol (**44**) showed no significant difference ($p > 0.05$) in the activity compared to acarbose the standard drug but sesamine showed a significant difference in the activity compared to acarbose against α-amylase. The same pattern was displayed in the activity against α-glucosidase where all alkaloids and phenolics assayed showed no significant difference ($p > 0.05$) in the inhibition compared to acarbose but sesamine showing relatively lower activity.

2,3-epoxy-6,7-methylenedioxy coniferyl (**10**) displayed competitive inhibition mode on both α-amylase and α-glucosidase with K_i of 5.54±0.58 (R^2 = 0.985) and 17.21±0.15 (R^2 = 0.8692), respectively. These were statistically comparable ($p < 0.05$) to that of acarbose indicating the most active inhibitor from the *Z. chalybeum* and *Z. gilletii* extracts. Compound **10** and the alkaloids **42, 21, 9**, and **43** display competitive and mixed inhibitions, respectively were noted as the most potent inhibitors of both α-amylase and α-glucosidase. The other compounds **45, 39, 40, 41, 43, and 46** showed varied modes of inhibition and associated dissociation constants towards the two enzymes (Table 11) which would be categorized as moderate inhibitory activities compared to acarbose.

5.2 Conclusion

i. Alkaloids and phenolics that were isolated from *Z. Chalybeum* and *Z. gilletii* were Norchelerythrine **(9),** phenanthridine A**,** (**42**), chalybemide A (**39**), chalybemide B (**40**), chalybemide C (**41**) and Zanthoamide D (**45**) skimmianine (**21**), 2,3-epoxy-6,7-methylenedioxy coniferyl alcohol (**10**) sesamine (**46**) and two triterpenes: zanthocapensine (**43**) and zanthocapensol (**44**) of which phenanthridine A (**42**), chalybemide A (**39**), chalybemide B (**40**), chalybemide C (**41**) are reported for the first time while zanthocapensine (**43**) and zanthocapensol (**44**) are reported from *Z. gilletii* for the first time.

ii. All isolated compounds showed no significant difference ($P<0.05$) in their inhibitory activities against α-amylase and α-glucosidase compared to acarbose (IC_{50}= 42.67 and 44.88, respectively) except sesamine (**46**) (IC_{50}= 54.67 and 54.77, respectively) which showed relatively lower activity.

iii. 2,3-Epoxy-6,7-methylenedioxy coniferyl (**10**) showed a competitive mode of inhibition against both α-amylase and α-glucosidase with lower K_i of 5.54±0.58 (R^2 = 0.985) and 17.21±0.15 (R^2 = 0.8692), respectively showing the most active inhibitor against α-amylase and α-glucosidase together with compounds **42**, **21**, **9**, and **43** showed mixed mode of inhibition with relatively lower K_i values showing stronger binding and better inhibition**.** Compounds **45, 39, 40, 41, 43,** and **46** showed both noncompetitive and uncompetitive modes of inhibition with relatively higher K_i values compared to acarbose ($p > 0.05$), indicating that they easily dissociate from inhibitor – enzyme complex due weak binding hence moderately lower inhibition against α-amylase and α-glucosidase activities.

5.3 Recommendation

i. *Z. chalybeum* and *Z. gilletti* contain bio active compounds such as amide, quinoline and benzophenanthridine alkaloids and phenolics. The plants are recommended for in vivo studies.

ii. The relatively active compounds recommended for further computational studies in order that their templates may be used for development of anti-hyperglycemic drugs.

iii. *Z. chalybeum* and *Z. gilletti* contain bio active compounds such as amide, quinoline and benzophenanthridine alkaloids and phenolics which can further be evaluated for potential application in diabetic drug discovery

5.4 Significance of study

The *in vitro* anti-hyperglycemic activities of the isolated compounds from the stem bark of Z. *chalybeum* and *Z. gilletii* showed the activity against α-amylase and α-glucosidase in controlling hyperglycemia. The plant should therefore be subjected to further analysis to check the efficiency on the use the plants and to create a variety of herbal products that can safely, less costly and efficiently manage diabetes mellitus. The active phenolics and alkaloids isolated from the two plants should be subjected to toxicological studies and to serve as templates for developing anti-hyperglycemic drugs if found safe.

5.5. Suggestions for further studies

i. From the kinetic results obtained, it would thus be better that molecular interaction studies based on *in silico* experiments to be done to confirm the conclusive information about the compounds and their activities.
ii. Toxicological and *in vivo* testing will be conducted to determine the effectiveness and toxicity of the separated chemicals.

REFERENCES

Adia, M. M.-K. (2016). Antiplasmodial activity and phytochemical analysis of extract from selected Ugandan medicinal plants. *Journal of ethnopharmacology, 186*, 14-19.

Afonne, J. O. (2002). Nephrotic actions of low dose mercury in mice. *Archives of Environmental Health, 57*(2), 98-102.

Agwaya M. S., A. N. (2016). Protective effects of Zanthoxylum chalybeum in diabetes induced myocadial dysfuction in rats. *European Journal of Medicinal Plants, 12*, 1-10.

Ali, A. B. (2006). *international Centre for Under utilized crops.* Southampton: Feedipedia.

Aloke, C. N. (2012). Effects of Zanthoxylum zanthoxyloides leaves on blood glucose, lipid profile and some liver enzymes in alloxan induced diabetic rats. *International Journal of Science, 3(3)*, 497-501.

Anza, M. T. (2014). A coniferyl alcohol derivative from roots of Zanthoxylum chalybeum. *Journal of Coastal Life Medicine*, 43-48.

Bahadoran Z., M. G. (2013). The association of dietary phytochemical index and cardiometabolic risk factors in adults: Tehran lipid and glucose study. *Journal of Human Nutrition and Dietics*, 145-153.

Brandt R. B., L. J. (1987). Calculation of inhibitor Ki and inhibitor type from the concentration of inhibitor for 50% inhibition for Michaelis-Menten enzymes. *Biochemistry of Medical Metabolites, 37*, 344–349.

Chen, J. J. (2005). New indolopyridoquinazoline, benzo[c]phenanthridines and cytotoxic constituents from Zanthoxylum integrifoliolum. *Planta Medica, 71*, 470-475.

Cheng Y-C, P. W. (1973). Relationship between the inhibition constant (Ki) and the concentration of inhibitor which causes 50 per cent inhibition (IC50) of an enzymatic reaction. *BiochemisryPharmacology, 22*, 3099–3108.

Cheng, M. J. (2005). Two new sesquiterpenoids and anti-HIV principles from the root bark of Zanthoxylum ailanthoides. *Bioorganic & Medicinal Chemistry, 13*, 5915-5920.

Cornish-Bowden, A. (1986). Why is uncompetitive inhibition so rare? A possible explanation, with implications for the design of drugs and pesticides. *FEBS Letter, 203*, 3–6.

Djeukeu C. K., A. K. (2019). A new aomatic amide from the roots of Zanthoxylum tessmannii (Rutaceae). *Chemistry of Biodiversity, 16*, e1800590.

Eckel, G. D. (2011). metabolic syndrome from insulin resistance to obesity and diabetes. *Medical clinic in North America, 95*(5), 855-873.

Fang, L. C. (2014). Protein tyrosine phosphatase 1B (PTP1B) and alpha glucosidase inhibitory activities of Schisandra chinensis (Turcz.)Bail. *Journal of Functional Foods, 9*, 264–270.

Fernandez-Mejıa, C. (2013). *Oxidative stress and chronic degenerative diseases and role for antioxidants.* . Mexico City, USA: InTechnology.

G., W. C. (2000). Mechanistic and kinetic studies of inhibition of enzymes. *Cell Biochemistry and Biophysical, 33*, 217–225.

Gakunju, D. M. (1995). Potent antimalarial activity of the alkaloid nitidine, isolated from a Kenyan herbal remedy. *Antimicrobial Agents Chemotherapy, 39*, 2606–2609.

Galand, G. (1989). Brush border membrane sucrase-isomaltase, maltase-glucoamylase and trehalase in mammals. Comparative development, effects of glucocorticoids, molecular

mechanisms ang phylogenetic implications. *Comparative Biochemistry and Physiology, 94*(1), 1-11.

Gardner, D. a. (2011). *Greenspan's basic and clinical endocrinology* (9th ed.). New York: McGraw-Hill Medical.

Gerich, J. M. (2006). Different mechanisms for impaired fasting glucose and impaired postprandial glucose tolerance in human beings. *Diabetes care*, 9-14.

Gough, S. N. (2010). *Insulin and Insulin Treatment.* New York: John Wiley & Sons Ltd.

Grant, P. J. (2003). Beneficial effects of metformin on haemostasis and vascular function in man. *Diabetes and Metabolism*, 6544-6552.

Guntram, S. C.-H. (2013). Do we still need poiglitazone for the treatment of type-2 diabetes? A risk benefit critique in 2013. *Diabetes care, 36*, 155-161.

Gupta, R. S. (2011). . Antidiabetic and antioxidant potential of β-sitosterol in streptozotocin-induced experimental hyperglycemia. *Journal of Diabetes, 3(1)*, 29-37.

Han, N. Y. (2016). Research Progress on Natural Benzophenanthridine Alkaloids and their Pharmacological Functions. *A Review Natural Product Report, 11 (8)* , 1181-1188.

Haque, M. T. (2017). Pain: A patient with a painful diabetic neuropathy and post herpetic neuralgia. *Nutrition and Metabolism, 1*(1), 1-9.

Henrissat, B. D. (1995). Structures and mechanisms of glycosyl hydrolases. *Curriculum opinion on structural Biology, 3*(9), 853-859.

Hooton, D. L. (2015). The secretion and action of brush border enzymes in the mammalian small intestine. *Reviews of physiology, biochemistry abd pharmacology, 59*, 118.

Horton, D. T. (2015). *Advances in Carbohydrate Chemistry and Biochemistry* (Vol. 68). Columbus,, Ohio, USA: Ohio State University.

Hu, J. Z. (2006). Benzophenanthridine alkaloids from Zanthoxylum nitidum (Roxb.) DC and their analgesic and anti-inflammatory activities. *Chemistry & Biodiversity, 3*, 990-995.

Islam, A. B. (2001). Antimicrobial activity and cytotoxicityof Zanthoxylum budrunga. *Fitoterapia, 72*, 428-430.

J.O., K. (2009). *Medicinal Plants of East Africa* (3rd ed.). Nairobi: University of Nairobi Press.

Johansen JS, H. A. (2005). Oxidative stress and the use of antioxidants in diabetes: Linking basic science to clinical practice. *Cardiovascular Diabetology*, 4-5.

Joubert, P. V. (1990). The keffect of miglitol and acarbose after an oral load: A novel hypoglycaemic mechanism. *Clinical Pharmacology, 30*, 391-396.

Jursky, F. B. (2011). Differential effect of the benzophenanthridine alkaloids sanguinarine and chelerythrine on glycine transporters. *Neurochemistry International, 58*, 641-647.

Karki, H. U. (2014). Antidiabetic potential of Zanthoxylum armatum bark extract on streptozotocin-induced diabetic rats. *International Journal of Green Pharmacy, 8*, 77-83.

Kimani, C. N. (2015). Antihyperglycemic activity of Zanthoxylum chalybeum stem bark extract in diabetic rats. *The Journal of Phytopharmacology, 4(3)*, 183-189.

Kokwaro, J. (2009). *Medicinal Plants of East Africa* (Vol. 3). Nairobi, Kenya: University of Nairobi Press.

Krane B. D., F. M. (1984). The benzophenanthridine alkaloids. *Journal of Natural Products, 47*, 1-43.

Krentz, A. J. (2005). Oral antidiabetic agents: Current role in type 2 diabetes mellitus. *Drugs, 65(3)*, 385–411.

Kumar, N. M. (1985). A lupenediol from Euonymus revolutus. *Phytochemistry, 24*, 1337-1340.

Kwon, Y. I. (2006). Evaluation of clonal herbs of Lamiaceae species for management of diabetes and hypertension. *The Journal of Clinical Nutrition, 15*(1), 107–118.

L.K. Omosa, G. M. (2019). Citotoxicity of faragamide derivate and cantin-6-one from Zathoxylum (Rutaceae) species against multidrug resistant leukemia cells. *Natural Products* , 1-8.

Lei Miao, L. L. (2019). Delivery of mRNA vaccines with heterocyclic lipids increases anti-tumor efficacy by STING-mediated immune cell activation. *Nature Biotechnology*, 37, 1174–1185.

Li Y.Q., Z. F. (2009). Comparative Evaluation of quercetin, isoquercetin and rutin as inhibitors of alpha-glucosidase. *Journal of Agriculture and Food chemistry, 57*, 11463-11468.

Lin Y, S. Z. (2010). Current views on type 2 diabetes. *Journal of Endocrinology*, 204:1–11.

Lombard, V. R. (2014). The carbohydrate-active enzymes database (CAZy) in 2013. *Nucleic Acids Research*, D490–D495.

Luna, B. F. (2001). Oral agents in the management of type 2 diabetes mellitus. *Am. Fam. Physician, 63*(9), 1747-1756.

Ma, W. F. (1999). Fungitoxic alkaloids from Hokkaido Corydalis species. *Fitoterapia*, 258-265.

Maliwat, L. P. (1997). An Alkaloid and Saponin from Argemone Mexicana. *Kimika*, 7-9.

Mansoor T.A., P. B. (2013). Apoptosis inducing activity of benzophenanthridine-type alkaloids and 2-arylbenzofuran neolignans in HCT116 colon carcinoma cells. *Phytomedicine, 20,* 923-929.

Mathers, C. D. (2006). Projections of global mortality and burden of disease from 2002 to 2030. *PLoS Medication, 3 (11), ,* 442.

Mbaze, L. M. (2007). α-Glucosidase inhibitory pentacyclic triterpenes from the stem bark of Fagara tessmannii (Rutaceae). *Phytochemistry, 68(5),* 591-595.

Mbaze, L. M. (2007). α-Glucosidase inhibitory pentacyclic triterpenes from the stem bark of Fagara tessmannii (Rutaceae). *Phytochemistry, 68(5),* 591-595.

Mhlongo, N. N. (2014). Critical survey of average distances between catalytic carboxyl groups in glycoside hydrolases. *Proteins, 82,* 1747–1755.

Michaelis, L. M. (1913). Die kinetic der invertinwirkung. *Biochemistry, 49,* 333–369.

Muganga, R. A. (2014). In vitro and in vivo antiplasmodial activity of three Rwandan medicinal plants and identification of their active compounds. *Planta Medica, 80,* 482–489.

Mukherjee, S. K. (2006). Mutational analysis of intramembranous H10 loopof yeast Nhx1 reveals a critical role in ion homoeostasis and vesicle trafficking. *Biochemistry, 398*(1), 97-105.

Nakanishi, T. S. (1998). Synthesis of NK 109, an anticancer Benzo[c]phenanthridine alkaloid. *Journal of Organic chemistry, 63,* 4235-4239.

Negi, J. S. (2011). Chemical constituents and biological activities of the genus Zanthoxylum; A review. *Journal of Pure and Applied Chemistry, 5(12),* 412-416.

Nelson D. L, Cox M. M. (2008). *Lehninger Principles of Biochemistry* (Vol. 5th edition). New York , NY, USA: W.H. Freeman.

Odebiyi, O. O. (1979). Antimicrobial alkaloids from Nigerian chewing stick (Fagara zanthoxyloides). *Planta Medica, 36*, 204-207.

Olila, D. O.-O.-A. (2001). Antibacterial and antifungal activities of extracts of Zanthoxylum chalybeum and Warburgia ugandensis; Ugandan medicinal plants. *African Health Sciences, 1 (2)*, 66-72.

Pareek, H. S. (2008). Evaluation of hypoglycemic and anti-hyperglycemic potential of Tridax procumbens. *Compliment alternative medicine, 9*, 48.

Philchenkov, A. K. (2008). Apoptogenic activity of two benzophenanthridine alkaloids from Chelidonium majus L. does not correlate with their DNA damaging effects. *Toxicology in Vitro, 22*, 287-295.

Playford, R. P. (2013). Use of the alpha-glucosidase inhibitor acarbose in patients with 'Middleton system': Normal gastric emptying causing postprandial reactive hypoglycemia and diarrhea. *Canadian Journal on Gastroenology, 27*, 403-404.

Punekar, N. (2018). *Enzymes: catalysis, kinetics and mechanisms.* Scotland: University of the West of Scotland.

Putter, G. P. (1985). Avermectins, MK-933 and MK-936, for mosquito control. *Transaction of Rooyal society of tropical medicine and Hygiene, 79*(6), 797-799.

Quezada C., C. C. (2007). Luminal Substrate "brake" on mucosal maltase-glucoaylase activity regulates total rate of starch digestion to glucose. *Pediatric and Gastroenterology Nutrition, 45*(1), 32-43.

Rajagopalan, G. a. (2008). α-amylase production from catabolite depressed Bacillus subtilis KCC103 utilizing sugarcane bagasse hydrolysate. *Bioresource Technology, 99*, 3044-3050.

Rebecca, B. M. (2013). Search strategies to identify diagnostic accuracy studies in MEDLINE and EMBASE. *Cochrane database System*, 11.

Ross, S. A. (2004). Syncaparmide, a New Antiplasmodial (+)-Norepinephrine Derivative from Zanthoxylum syncarpum. *Journal of Natural Products*(67), 88-90.

Ross, S. A. (2016). Syncaparmide, a New Antiplasmodial (+)-Norepinephrine Derivative from Zanthoxylum syncarpum. *Journal of Natural Products, 67*, 88-90.

S., W. (2004). Global prevalence of Diabetes Estimates for the 2003 and projection for 2030. *Diabetes care, 27*, 1047-1053.

Segel, I. (1993). *Enzyme Kinetics: Behavior and Analysis of Rapid Equilibrium and Steady-State Enzyme Systems.* New York, N.Y., U.S.A: John Wiley & Sons.

Shai, L. J. (2010). Yeast alpha-glucosidase inhibitory and antioxidant activities of six medicinal plants collected in Phalaborwa, South Africa. *South African Journal of Botany*, 465–470.

Sheen, W. S. (1994). Nor-neolignan and phenyl propanoid from Zanthoxylum ailanthoides. *Phytochemistry, 36*, 213-215.

Shimabukuro, M. H. (2006). Effects of a single a single administration acarbose on postprandial glucose excursion and edothelial dysfunction in type 2 diabetic patients: a randomized cross over study. *Journal of clinical Endocrinology, 91*, 837-842.

Simpson, S. S. (2015). Dietary protein to carbohydrate ratio and caloric restriction: comparing metab0lic otcomes in mice. *Cell report, 11*(10), 1501-1678.

T., N. T. (1969). Low potential from the epiphysis cerebri of fishes. *Vision Research, 9*, 621-623.

Tan, G. T. (1991). .Evaluation of natural products as inhibitors of human immunodeficiency virus type 1 (HIV1) reverse transcriptase. *Journal of Natural Products, 54*, 143–154.

Tane, P. W. (2005). A new benzophenanthridine alkaloid from Zanthoxylum buesgenii. *Fitoterapia, 76*, 656-660.

Tarling, C. A. (2008). The search for novel human pancreatic alpha amylase inhibitors: High throughput screening of terrestrial and marine natural products ectracts. *Biochemistry*, 433-438.

Tavares L.C., Z. G. (2014). Structure-Activity Relationship of Benzophenanthridine Alkaloids from Zanthoxylum rhoifolium Having Antimicrobial Activity. *Journal of natural products*, 50-62.

Tayyab, S. (1990). Biochemistry through cartoons – understanding enzymes. *Biochemistry Education, 18*, 42–43.

Trojan-Rodrigues M, A. T. (2012). Plants used as anti-diabetics in popular medicine in Rio Grande do Sul, southern Brazil. *Journal of Ethnopharmacology, 139*, 155–163.

Tsuchiya, H. S. (1996). Comparative study on the antimicrobial activity of phytocchemical flavones against methicillin resistant Staphylococcus aureus. *Journal of Ethnopharmacology, 50*, 27-34.

Ünal, D. K. (2012). Insulin hormone: Mechanism and effects on the body and relationship with central nervous system. *Dicle Medical Journal*, 310-315.

Ünal, D. K. (2012). Insulin hormone: Mechanism and effects on the body and relationship with central nervous system. *Dicle Medical Journal, 2*, 310-315.

Vaughan, R. P. (2002). The fine structure of regenerating epithelium in small intestine. *Cell pathology, 7*, 314-341.

Verspohl, E. (2012). Novel pharmacological approaches to the treatment of type2 diabetes. *Pharmacology Revised, 64*, 188–237.

Wagman, A. S. (2001). Current therapies and emerging targets for the treatment of diabetes. Current. *Pharmaceutical Research, VII*, 417–450.

Wasiali, D. (2019). Evaluation of α-amylase and α-glucosidase Inhibitory compounds from Zanthoxylum chalybeum stem and root barks. *Fitoterapia*, 64.

Whiting, D. R. (2011). IDF Diabetes Atlas: Global estimates of the prevalence of diabetes for 2011 and 2030. *Diabetes research and clinical practice, 94*, 311–321.

WHO. (1999). *Definition, diagnosis and classification of diabetes mellitus and its complications.Report of a WHO Consultation. Part 1: Diagnosis and classification of diabetes mellitus.* Geneva: World Health Organization.

WHO. (2016). *Global Report on Diabetes.* Geneva: World Health Organization.

WHO. (2020). *Global Report on Diabetes.* Geneva: World Health Organization,.

Wickham, M. S. (2015). Digestion of gluen proteins is reduced by baking and enhanced by starch digestion. *Molecular Nutrition and Food Research, 59*(10), 2034-2043.

Williams, J. J. (1979). Isolation and Partial Biochemical Charactrization of the brush boder Plasmamembrane from the Cestode, Hymenolepis diminuta. *Parasitology, 65*(5), 715-731.

Wolf, J. K. (1993). Antimicrotubule properties of benzophenanthridine alkaloids. *Biochemistry, 32*, 13334-13339.

Worthington, V. (1993). In worthington manual: Worthington Biochemical corporation. *Freehold*, 36-41.

Xuan Luo, D. P. (2013). Zanthoxylum capense constituents with antimycobacterial activity against Mycobacterium tuberculosis in vitro and ex vivo within human macrophages. *Journal of Ethnopharmacology*, 417-422.

Yang Z.Y., J. B. (2014). Ambiguanine A-G, hexahydrobenzophenanthridine alkaloids from Corydalis ambigua var. amurensis. *Phytochemistry, 105*, 158-163.

Yang, C. C. (2008). Dihydrobenzo[c]phenanthridine alkaloids from stem bark of Zanthoxylum nitidum. *Journal of Natural Products, 71*, 669-673.

Ye, T. e. (2008). The pathway by which the yeast protein Kinase Snf1p controls acquisition of sodium Tolerance. *Microbiology*, 2814-2826.

Yoshikawa, T. N. (1998). free radical-scavenging activityof Crassostera gigas extract. *Biomedical and Pharmacotherapy, 51*(8), 328-332.

Zeyana, S. A. (2013). Evaluation of T2DM related knowledge and practices of Omani patients. *Saudi Pharmaceuticals*, 48.

Zhang, C. H. (2013). Benzophenanthridine alkaloids from Zanthoxylum nitidum (Roxb.) DC and their analgesic and anti-inflammatory activities. *Chemistry & Biodiversity, 3*, 990-995.

Zhu, W., Chen, M., Shou, Q., Li, Y., & Hu, F. (2011). Biological Activities of Chinese Propolis and Brazilian Propolis on Streptozotocin-Induced Type 1 Diabetes Mellitus in Rats. *Evidence Based Complementary Alternatives for Medication, 11*, 1–8.

APPENDICES

1. Spectra for compound 39 Chalybemide A {6-Benzo[1,3]dioxol-5-yl-hexa-2,5-dienoic acid isobutylamide}

1.1 ^{1}H NMR of Compound 39

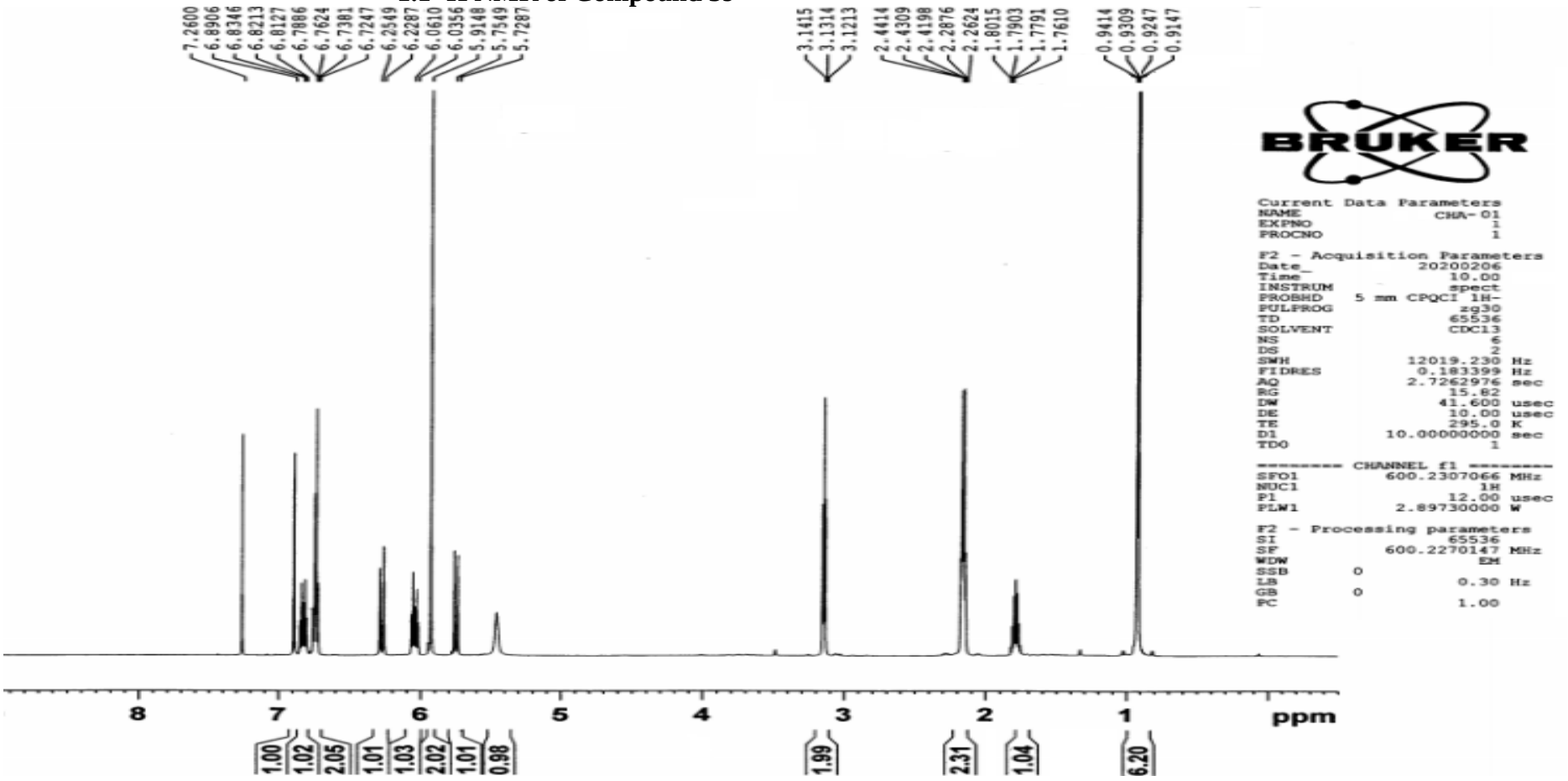

1.2 ^{13}C NMR (DEPT) of compound 39

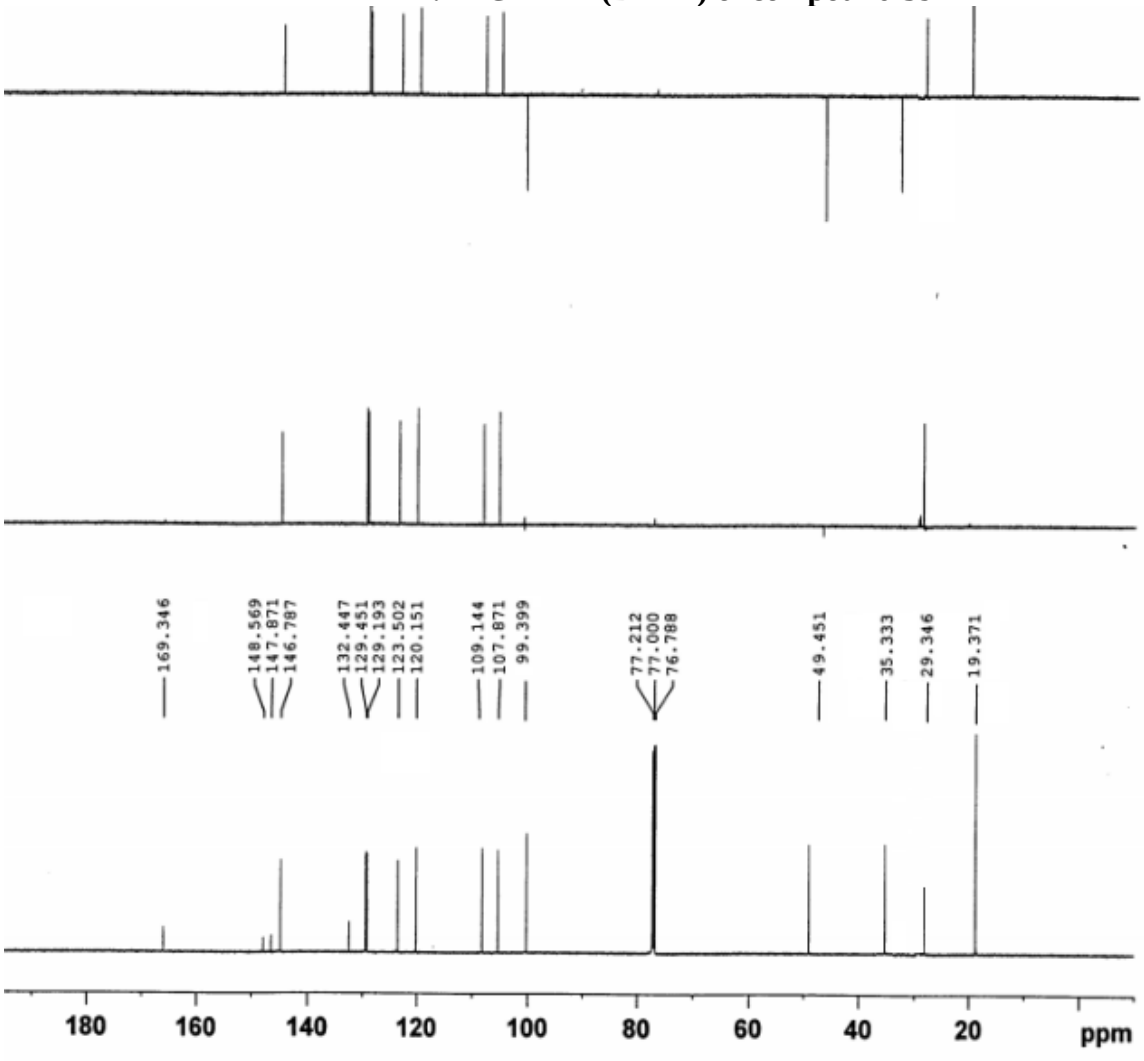

BRUKER

```
Current Data Parameters
NAME                  CHA-01
EXPNO                      4
PROCNO                     1

F2 - Acquisition Parameters
Date_              2020.0207
Time                   18.06
INSTRUM                spect
PROBHD   5 mm CPQCI 1H-
PULPROG                zgdc
TD                    65536
SOLVENT               CDCl3
NS                      320
DS                        4
SWH               36231.883 Hz
FIDRES             0.552855 Hz
AQ                 0.9043968 sec
RG                    199.06
DW                    13.800 usec
DE                    18.00 usec
TE                    295.0 K
D1                 2.00000000 sec
D11                0.03000000 sec
TD0                        1

======== CHANNEL f1 ========
SFO1          150.9438010 MHz
NUC1                    13C
P1                    11.20 usec
PLW1           94.00000000 W

======== CHANNEL f2 ========
SFO2          600.2294009 MHz
NUC2                    1H
CPDPRG[2             waltz16
PCPD2                 80.00 usec
PLW2           2.89730000 W
PLW12          0.06519000 W

F2 - Processing parameters
SI                     131072
SF            150.9272056 MHz
WDW                       EM
SSB       0
LB                     1.00 Hz
GB        0
PC                     1.40
```

1.3: HSQC spectrum of compound 39

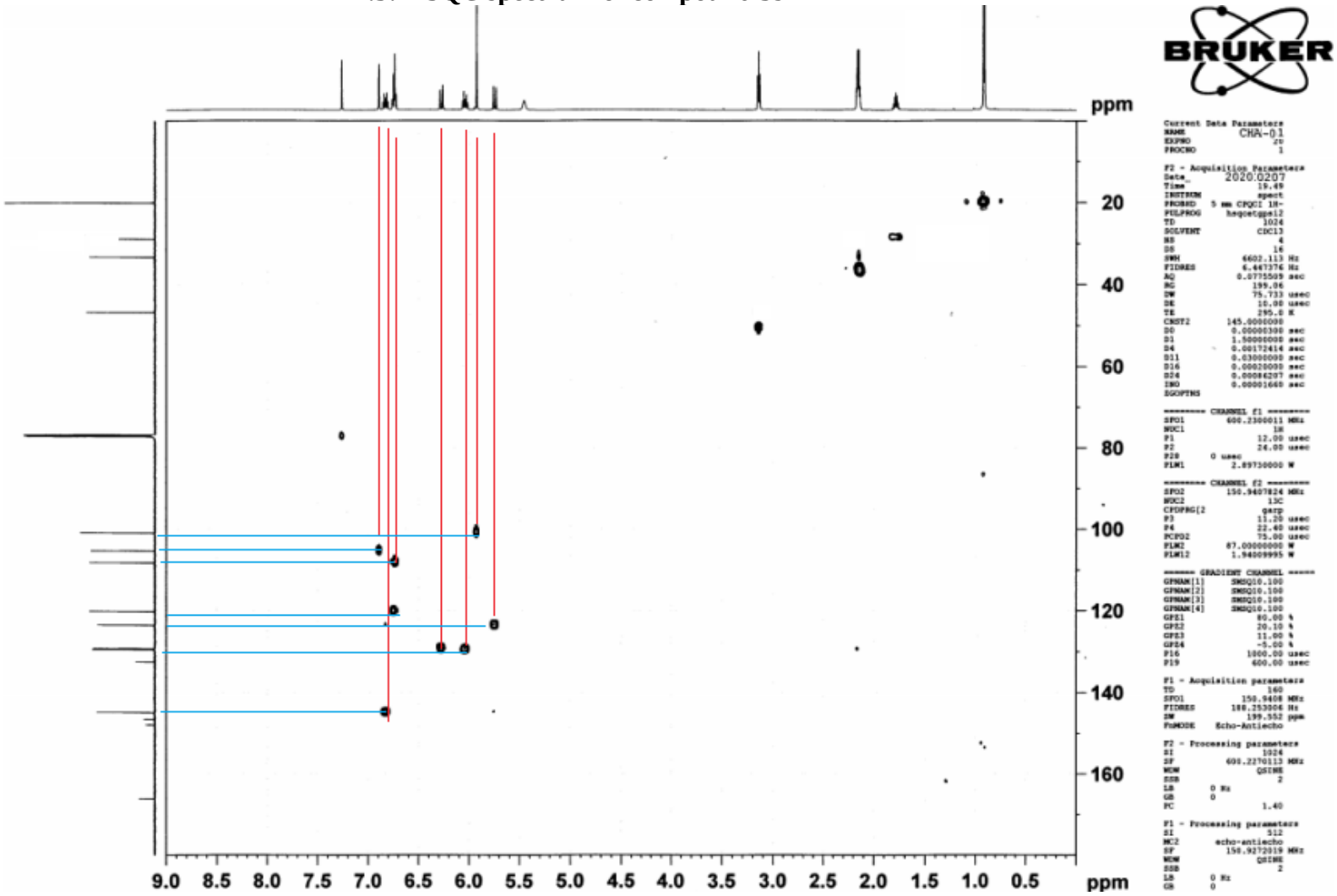

1.4 COSY spectrum of compound 39

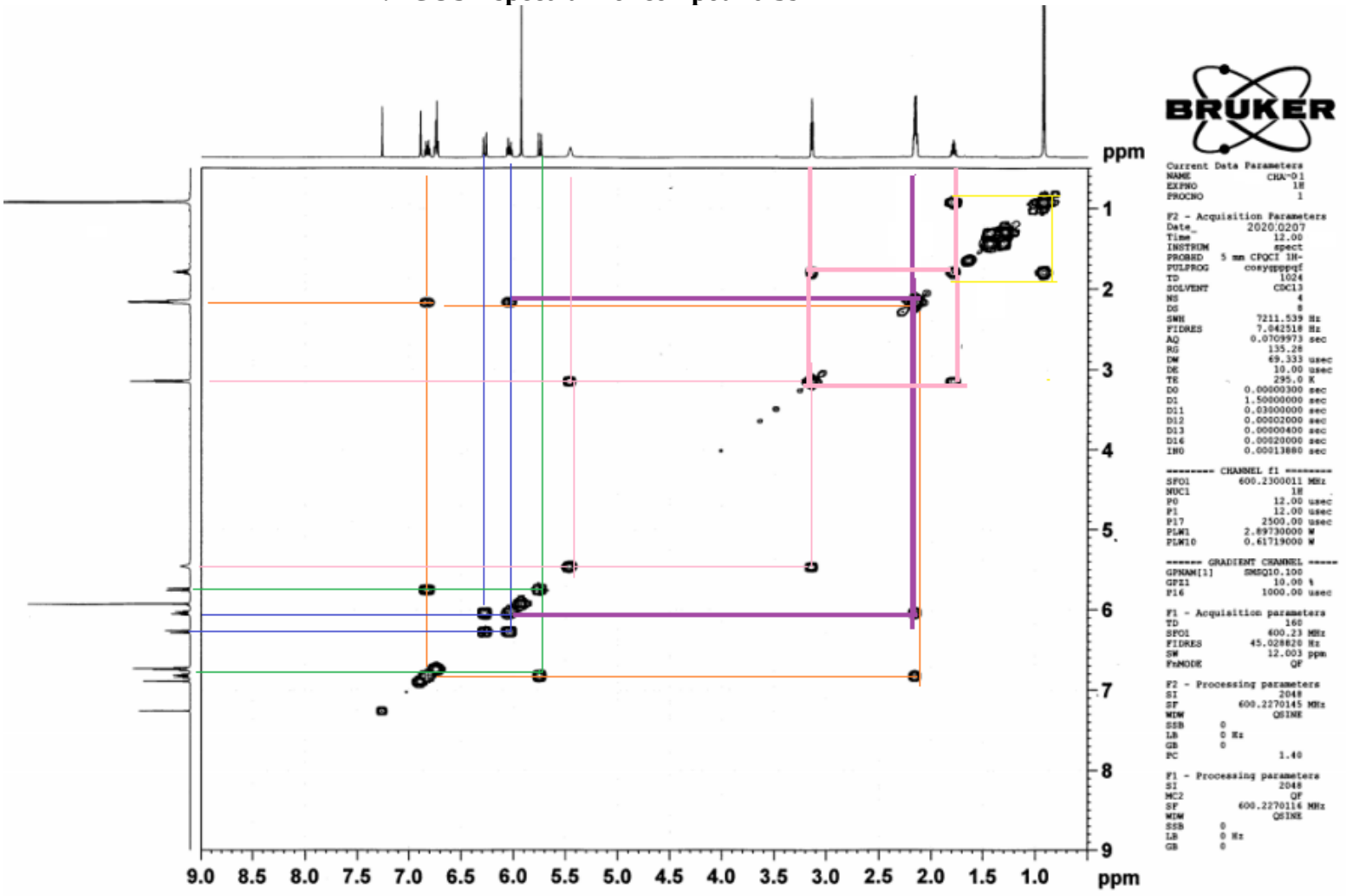

1.5: ROESY spectrum of compound 39

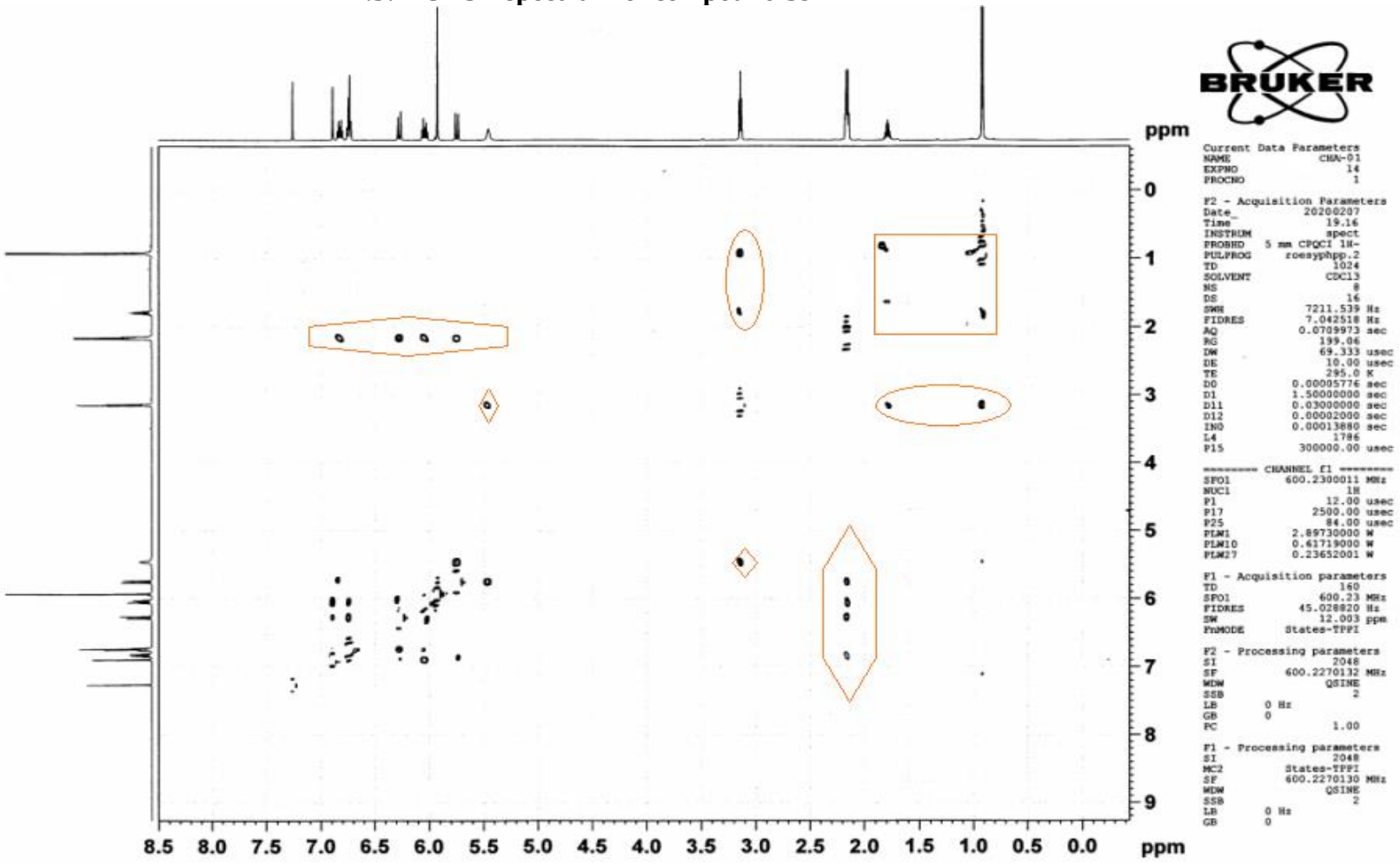

1.6:HMBC spectrum of compound 39

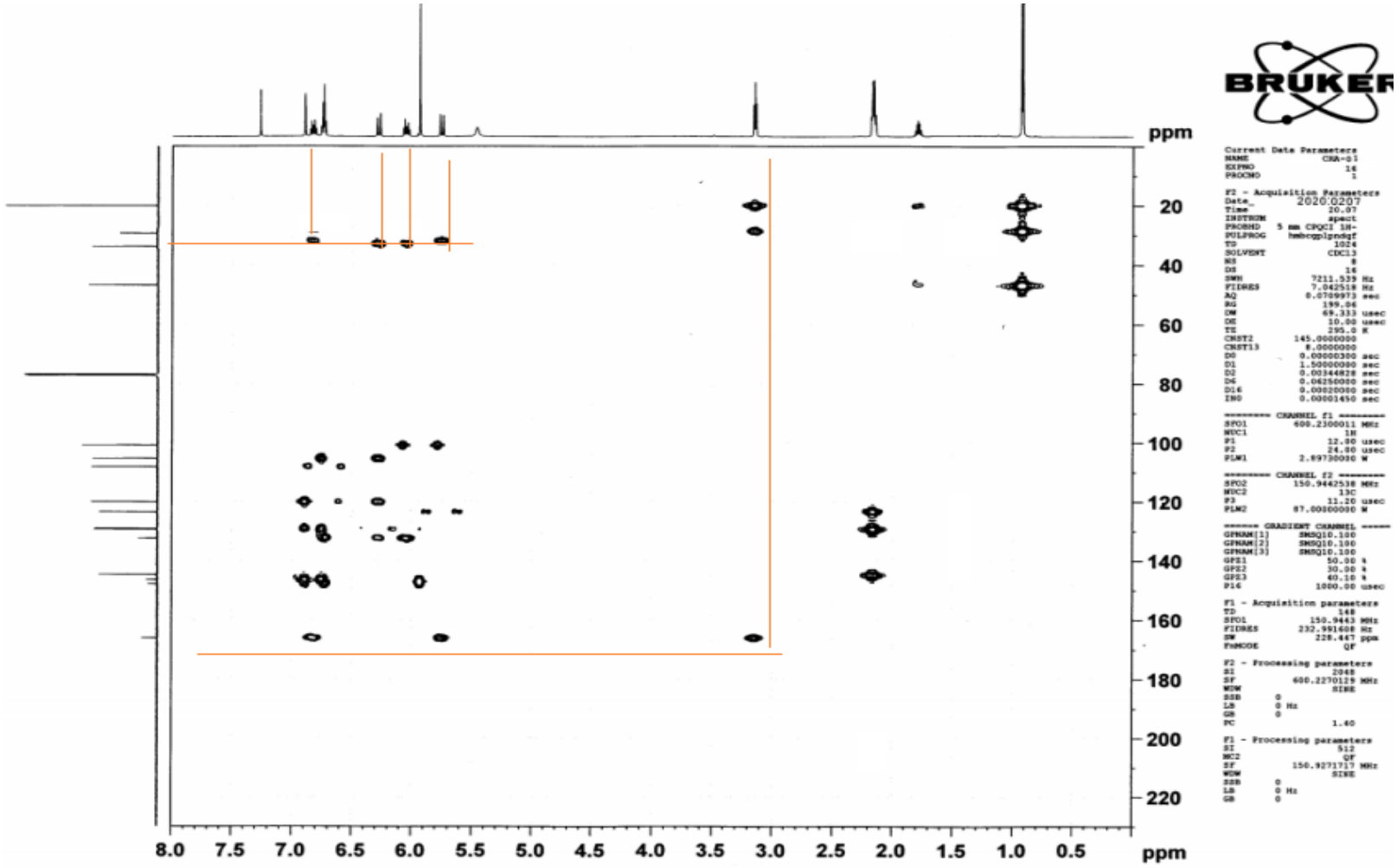

1.7: FTIR spectrum of compound 39

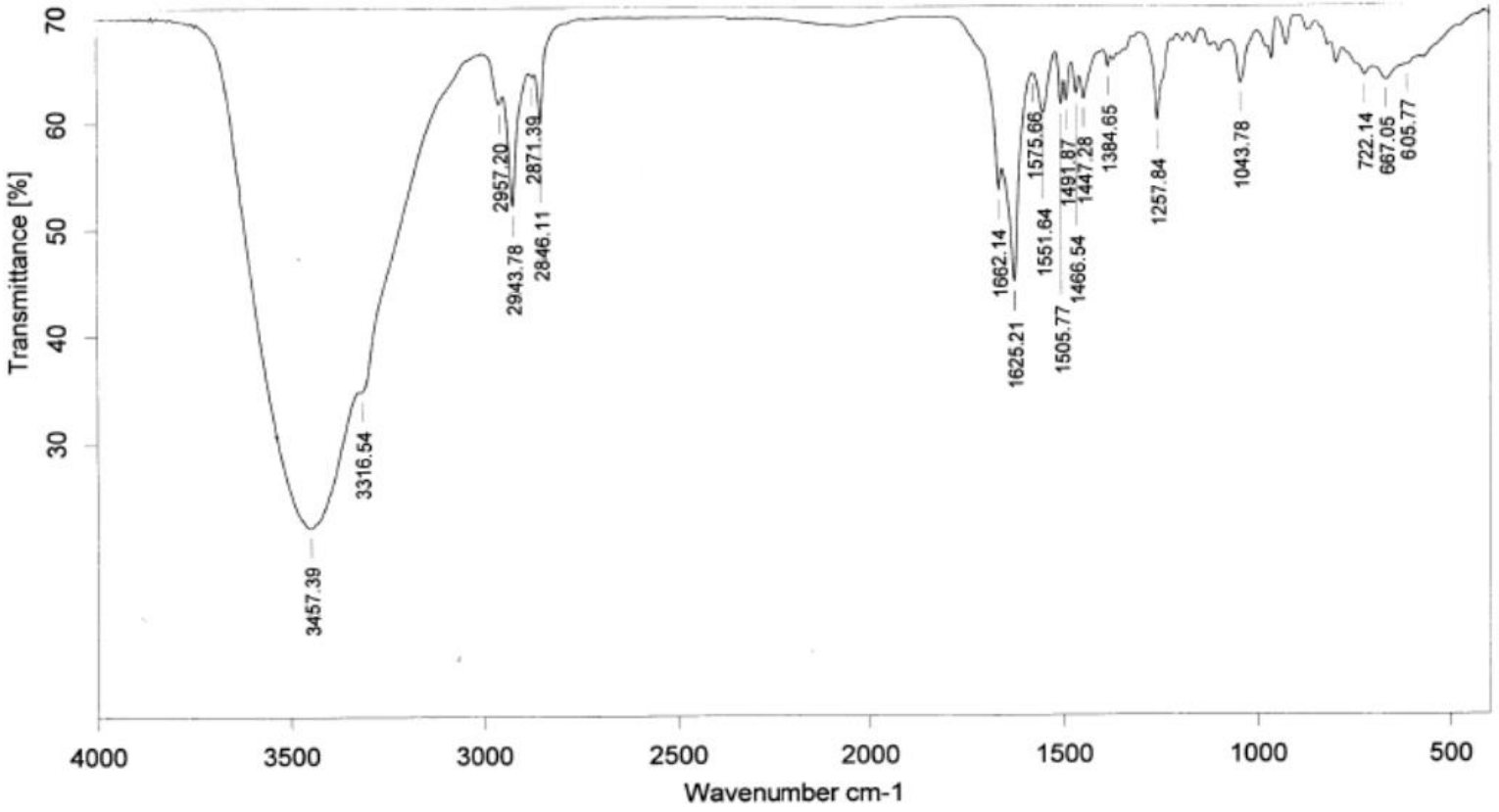

1.8: HREIMS spectrum of compound 39

Single Mass Analysis
Tolerance = 10.0 PPM / DBE: min = -10.0, max = 120.0
Selected filters: None

Monoisotopic Mass, Odd and Even Electron Ions
20 formula(e) evaluated with 2 results within limits (up to 52 closest results for each mass)
Elements Used:
C: 0-200 H: 0-400 N: 1-1 O: 2-4

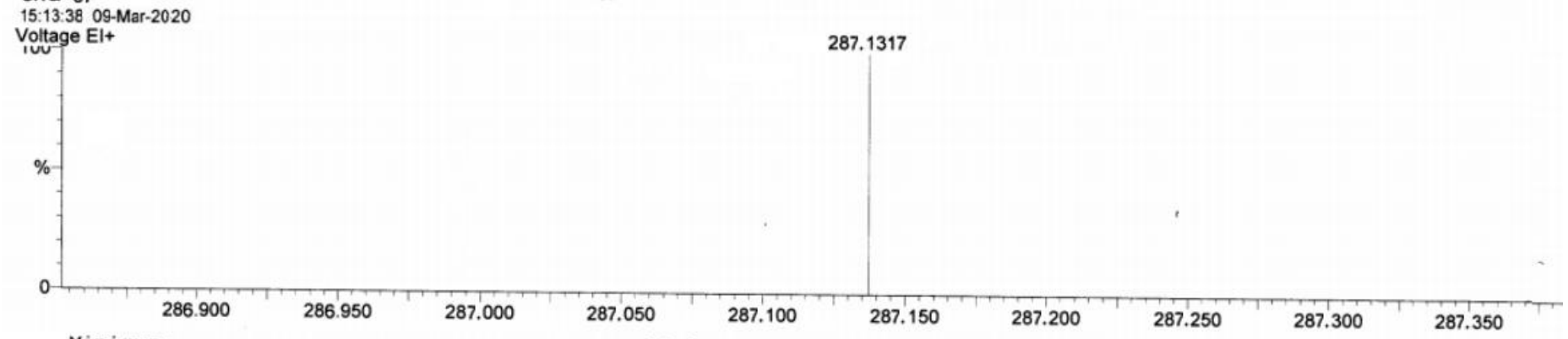

Minimum:				-10.0		
Maximum:		200.0	10.0	120.0		
Mass	Calc. Mass	mDa	PPM	DBE	i-FIT	Formula
287.1317	287.1312	0.8	2.8	9.0	5546027.5	C17 H21 N O3

2. Spectra for Compound 40 (Chalybemide B)

2.1: ^{1}H NMR spectrum of compound 40

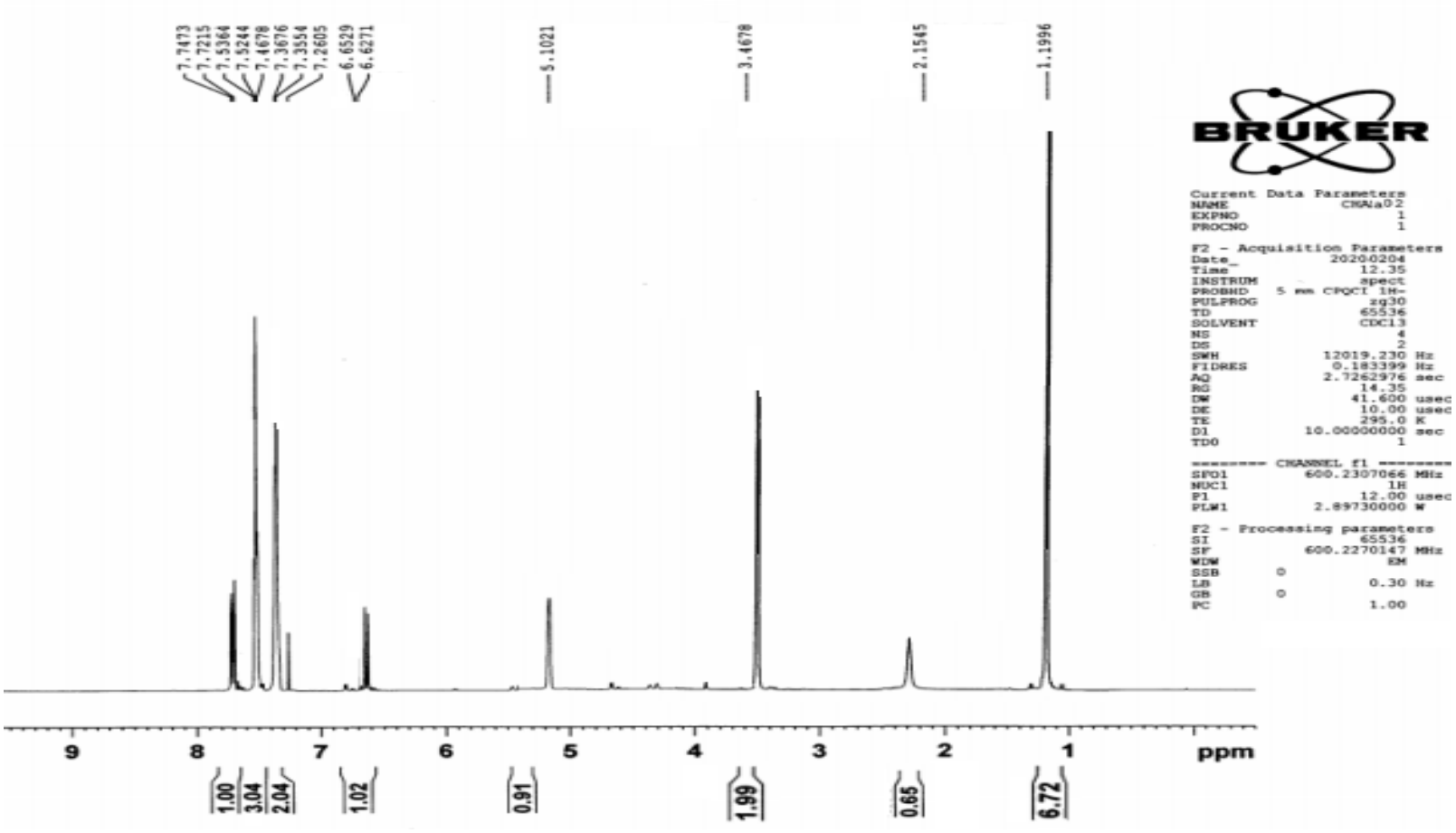

2.2 ^{13}C NMR (DEPT) spectrum of compound 40

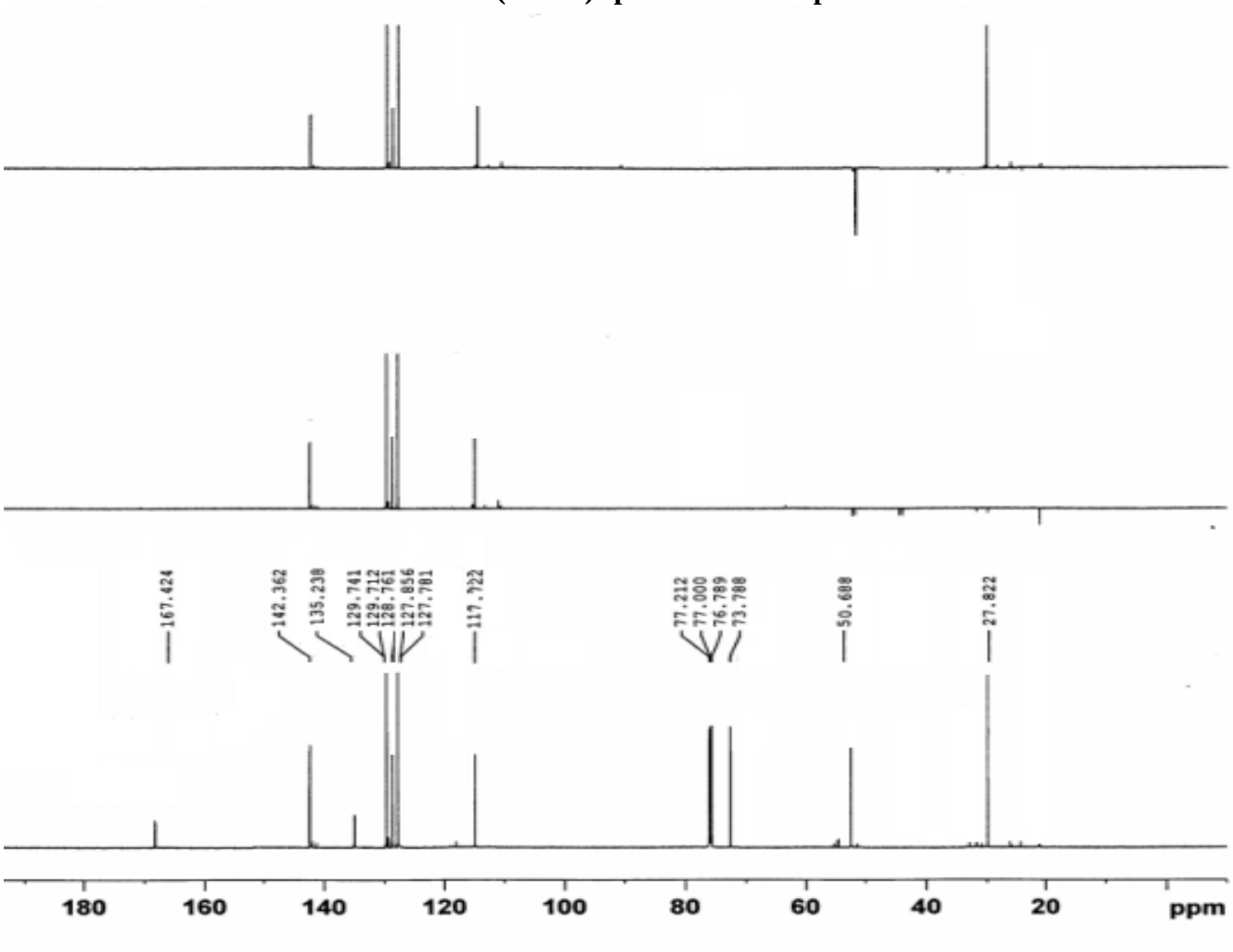

BRUKER

```
Current Data Parameters
NAME                  CHA-02
EXPNO                     13
PROCNO                     1

F2 - Acquisition Parameters
Date_              20200204
Time_                 13.06
INSTRUM               spect
PROBHD    5 mm CPQCI 1H-
PULPROG               zgdc
TD                   65536
SOLVENT              CDCl3
NS                     256
DS                       4
SWH               36231.883 Hz
FIDRES            0.552855 Hz
AQ                0.9043968 sec
RG                   199.06
DW                   13.800 usec
DE                   18.00 usec
TE                   295.0 K
D1                2.00000000 sec
D11               0.03000000 sec
TD0                        1

======== CHANNEL f1 ========
SFO1            150.9438010 MHz
NUC1                    13C
P1                    11.20 usec
PLW1           94.00000000 W

======== CHANNEL f2 ========
SFO2            600.2294009 MHz
NUC2                    1H
CPDPRG[2             waltz16
PCPD2                 80.00 usec
PLW2           2.89730000 W
PLW12          0.06519000 W

F2 - Processing parameters
SI                    131072
SF              150.9272109 MHz
WDW                     EM
SSB       0
LB                    1.00 Hz
GB        0
PC                    1.40
```

2.3 HSQC spectrum of compound 40

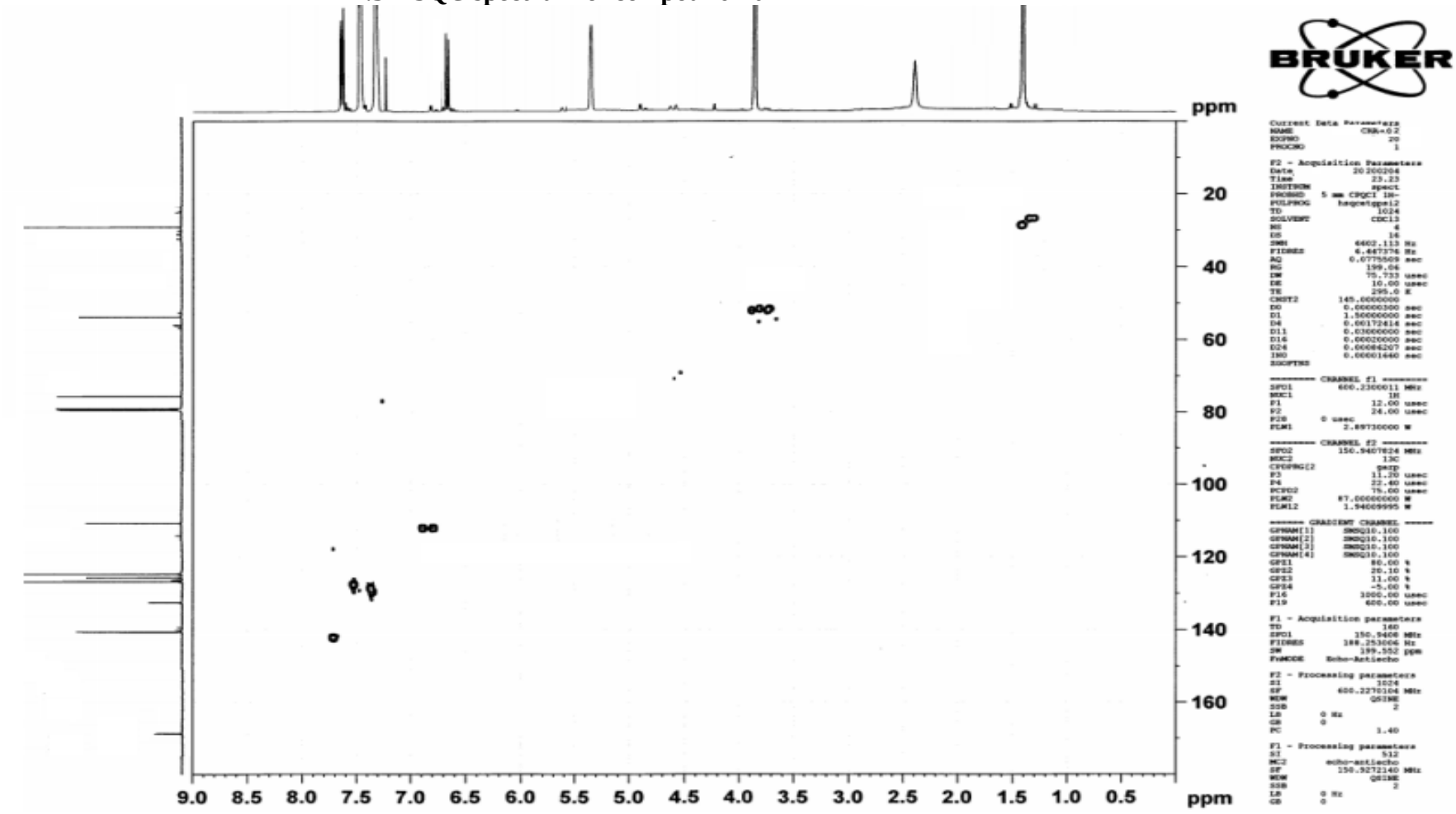

2.4: COSY spectrum of compound 40

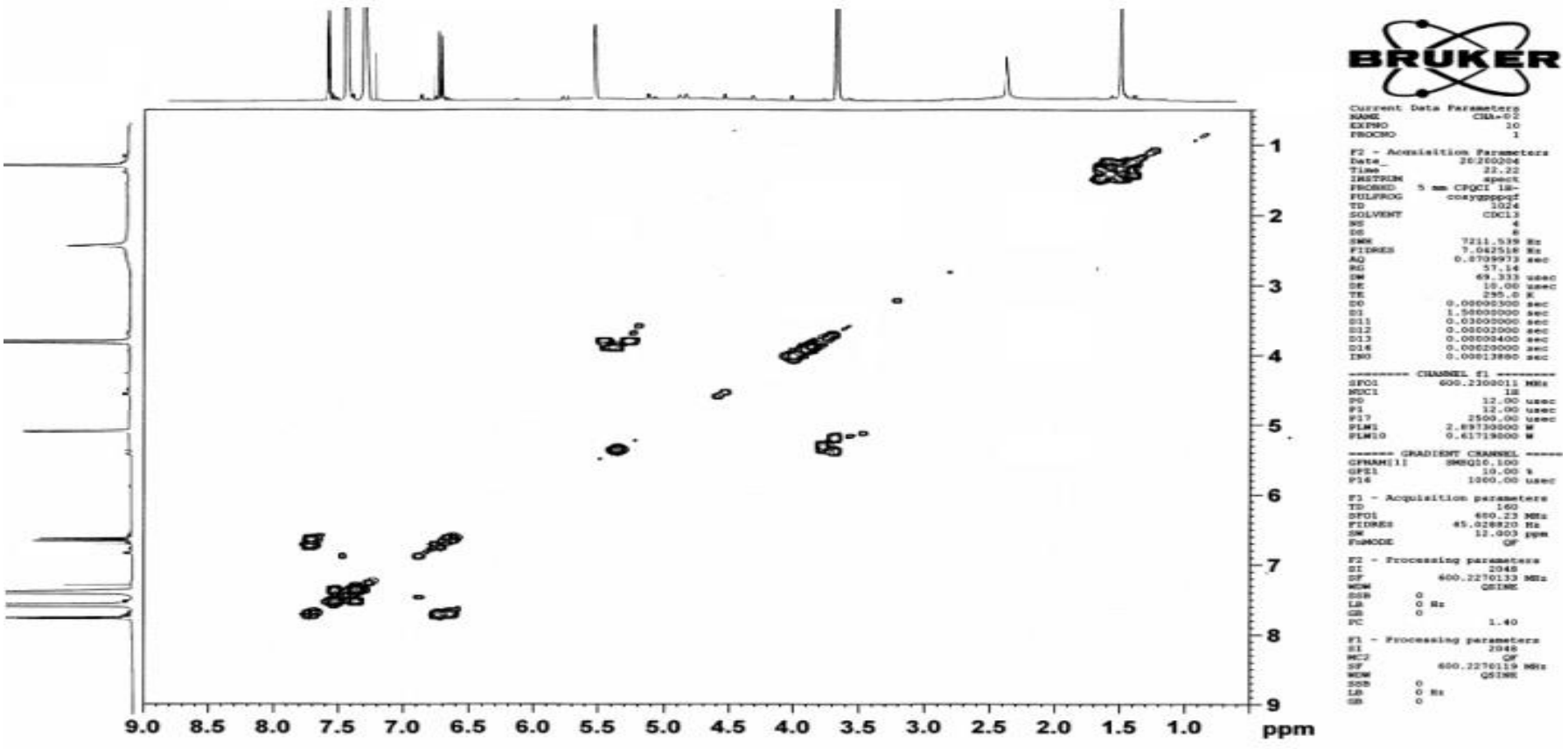

2.5: HMBC spectrum of compound 40

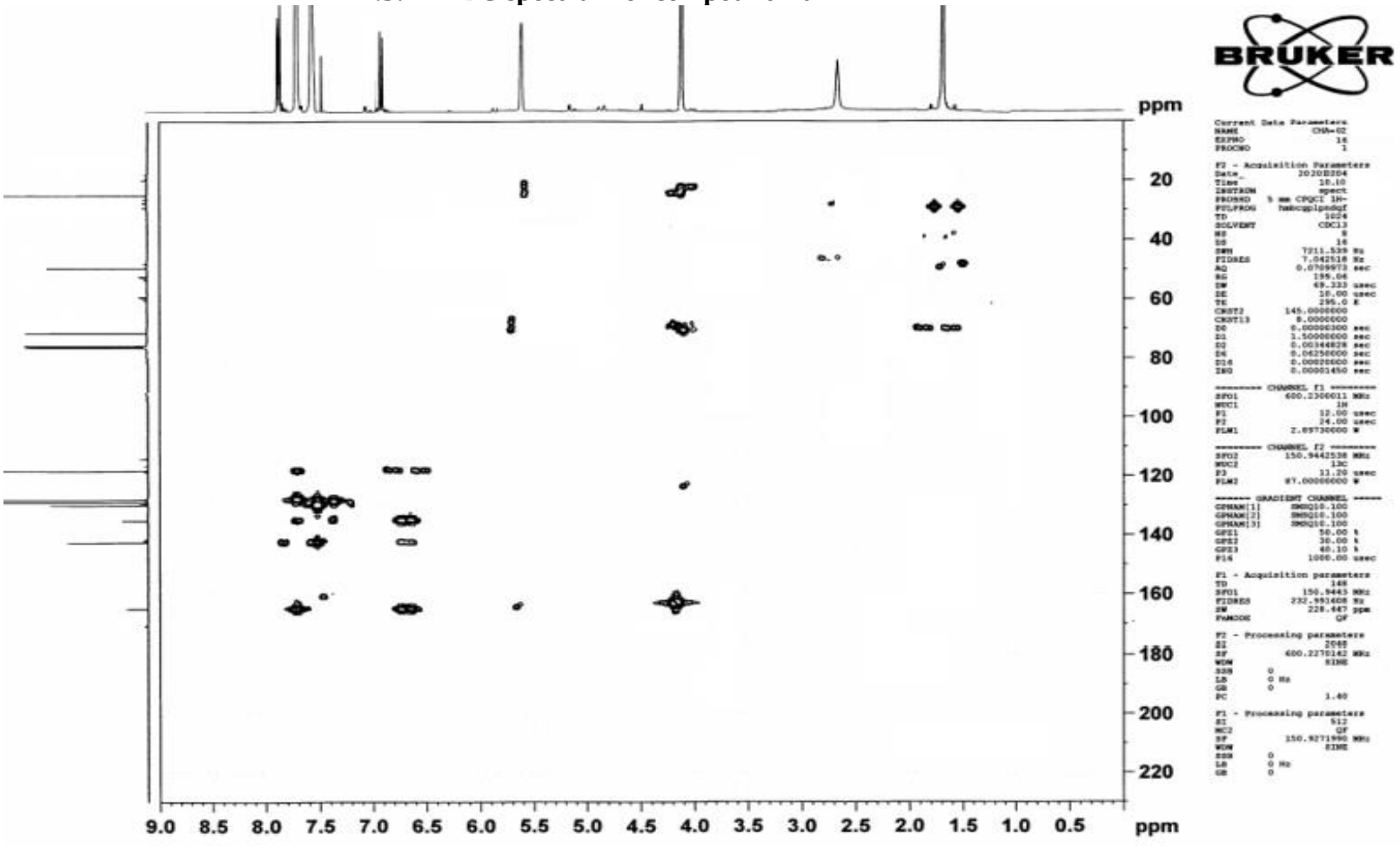

2.6: ROESY spectrum of compound 40

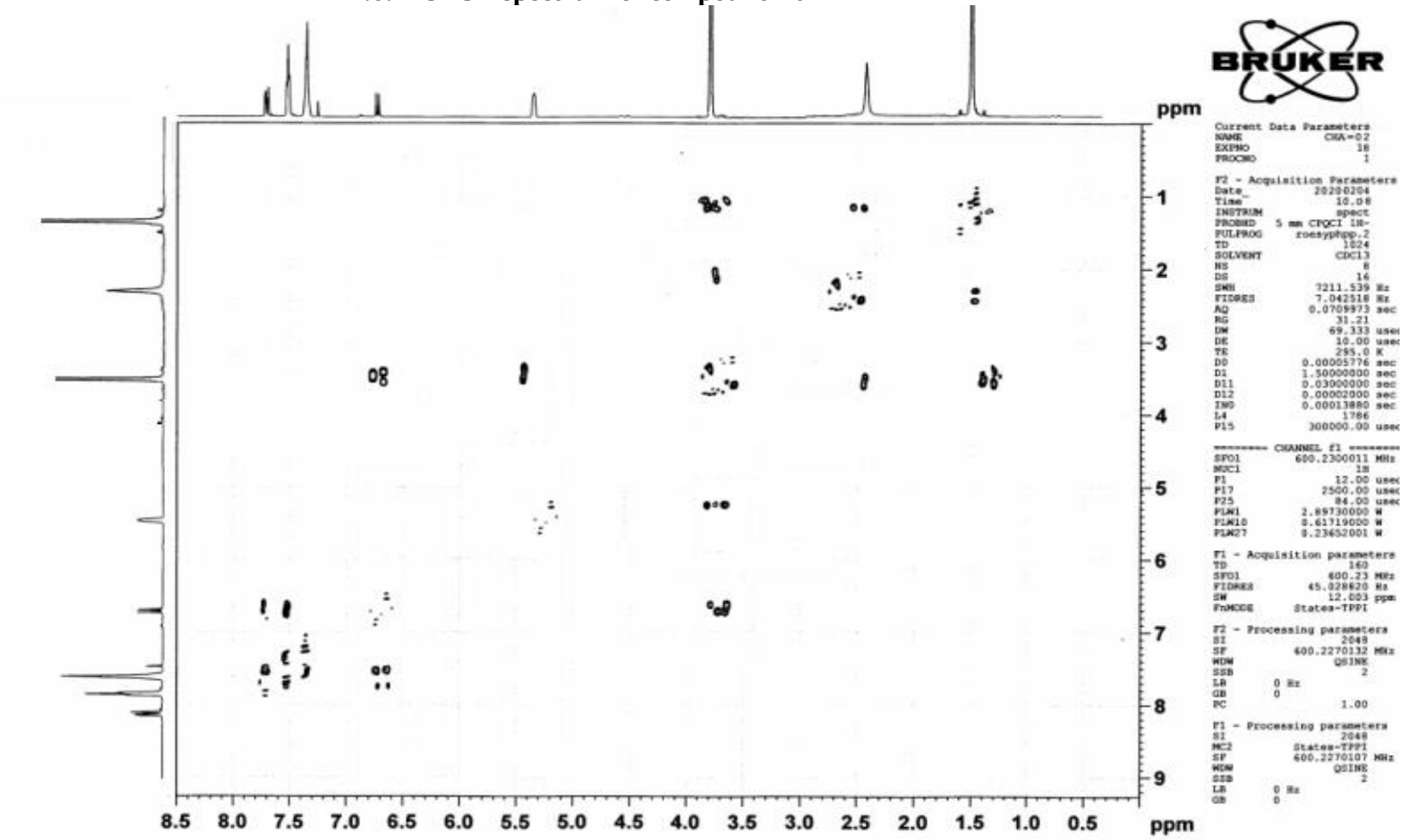

2.7 : HREIMS spectrum of compound 40

Single Mass Analysis
Tolerance = 10.0 PPM / DBE: min = -10.0, max = 120.0
Selected filters: None

Monoisotopic Mass, Odd and Even Electron Ions
11 formula(e) evaluated with 1 results within limits (up to 50 closest results for each mass)
Elements Used:
C: 0-200 H: 0-400 N: 1-1 O: 1-3
cha-02
02:22:20 02-Apr-2020
Voltage EI+

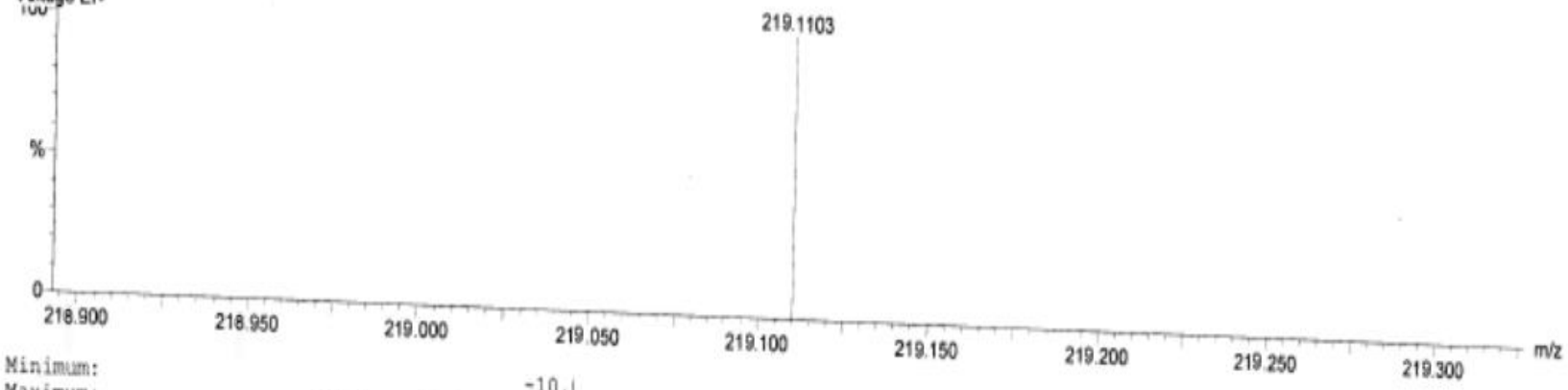

Minimum:				-10.0		
Maximum:		200.0	10.0	120.0		
Mass	Calc. Mass	mDa	PPM	DBE	i-FIT	Formula
219.1103	219.1103	0.0	0.0	7.0	5546025.5	C13 H17 N O2

2.8: FTIR spectrum of compound 40

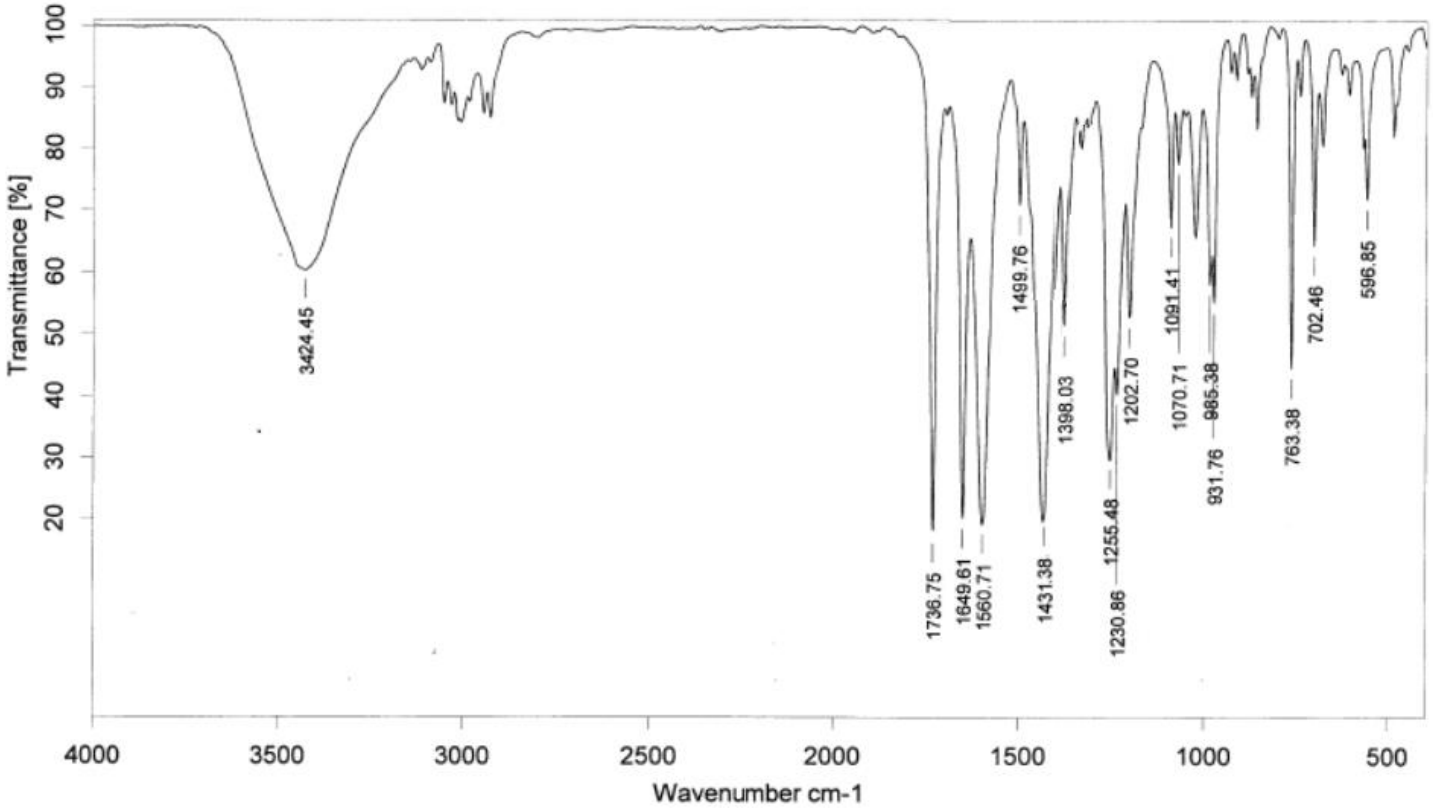

3. Spectra for Compound 41 (Chalybemide C)

3.1: ^{1}H NMR spectrum of compound 41

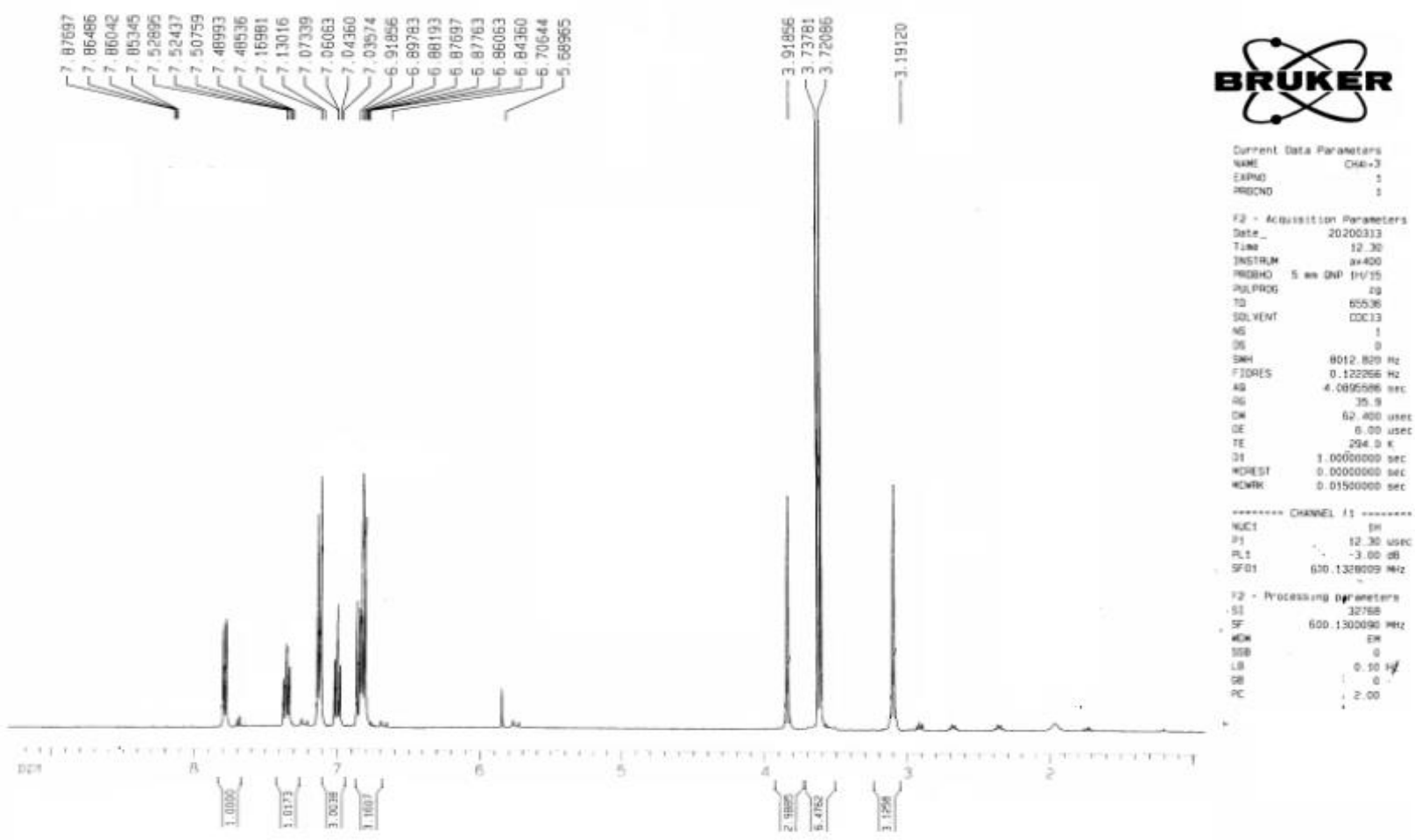

3.2: ^{13}C NMR spectrum of compound 41

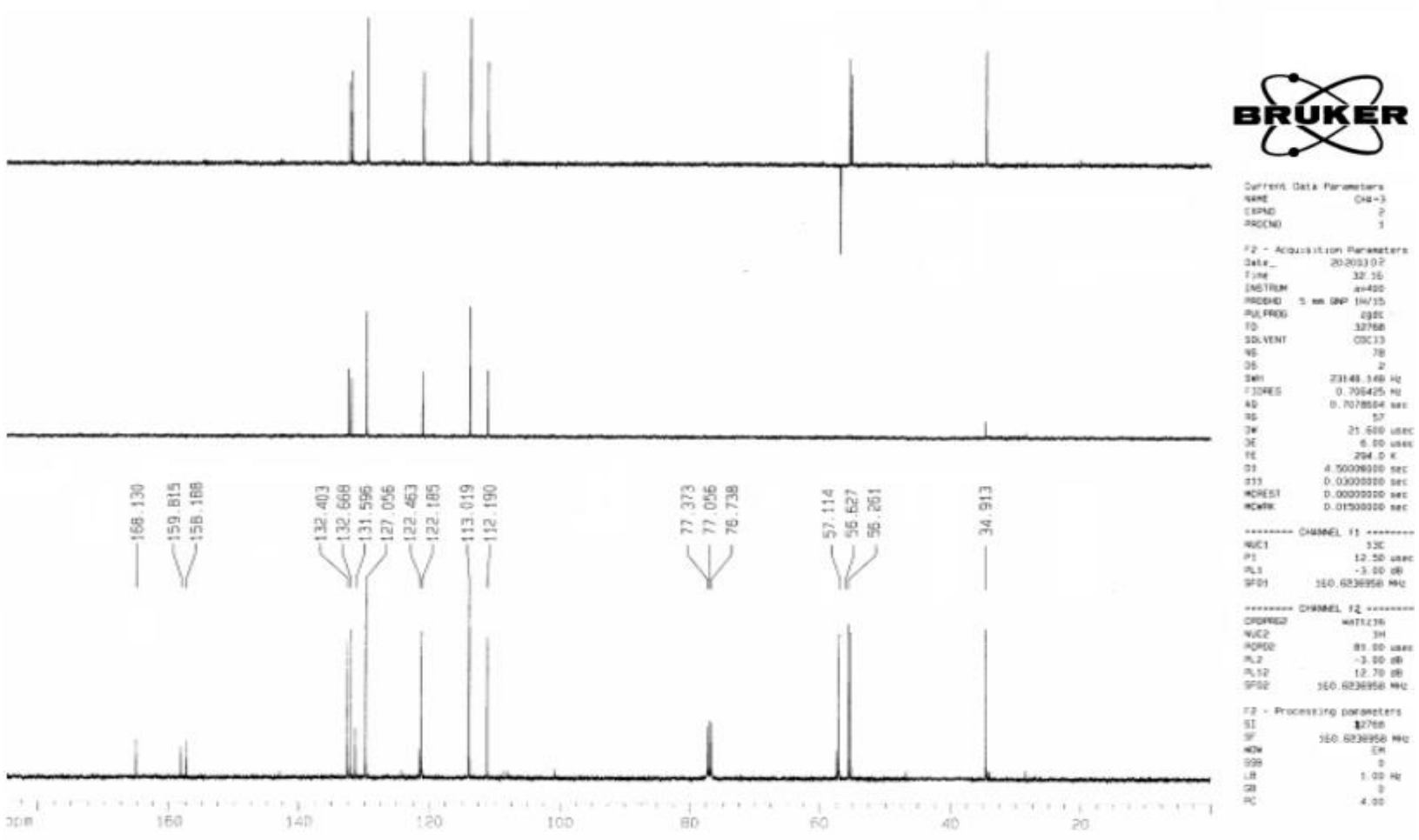

3.3: HSQC spectrum of compound 41

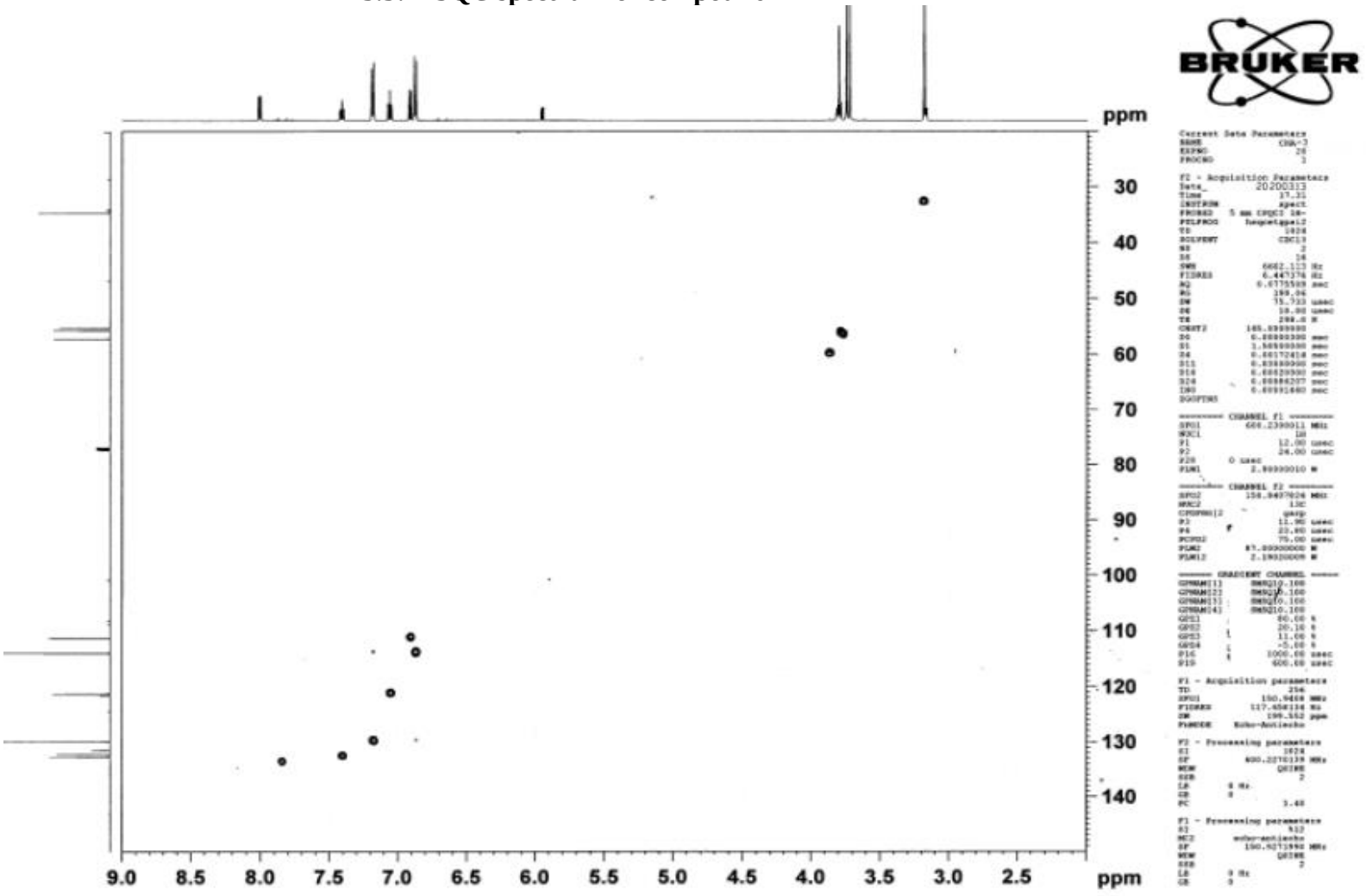

3.4: COSY spectrum of compound 41

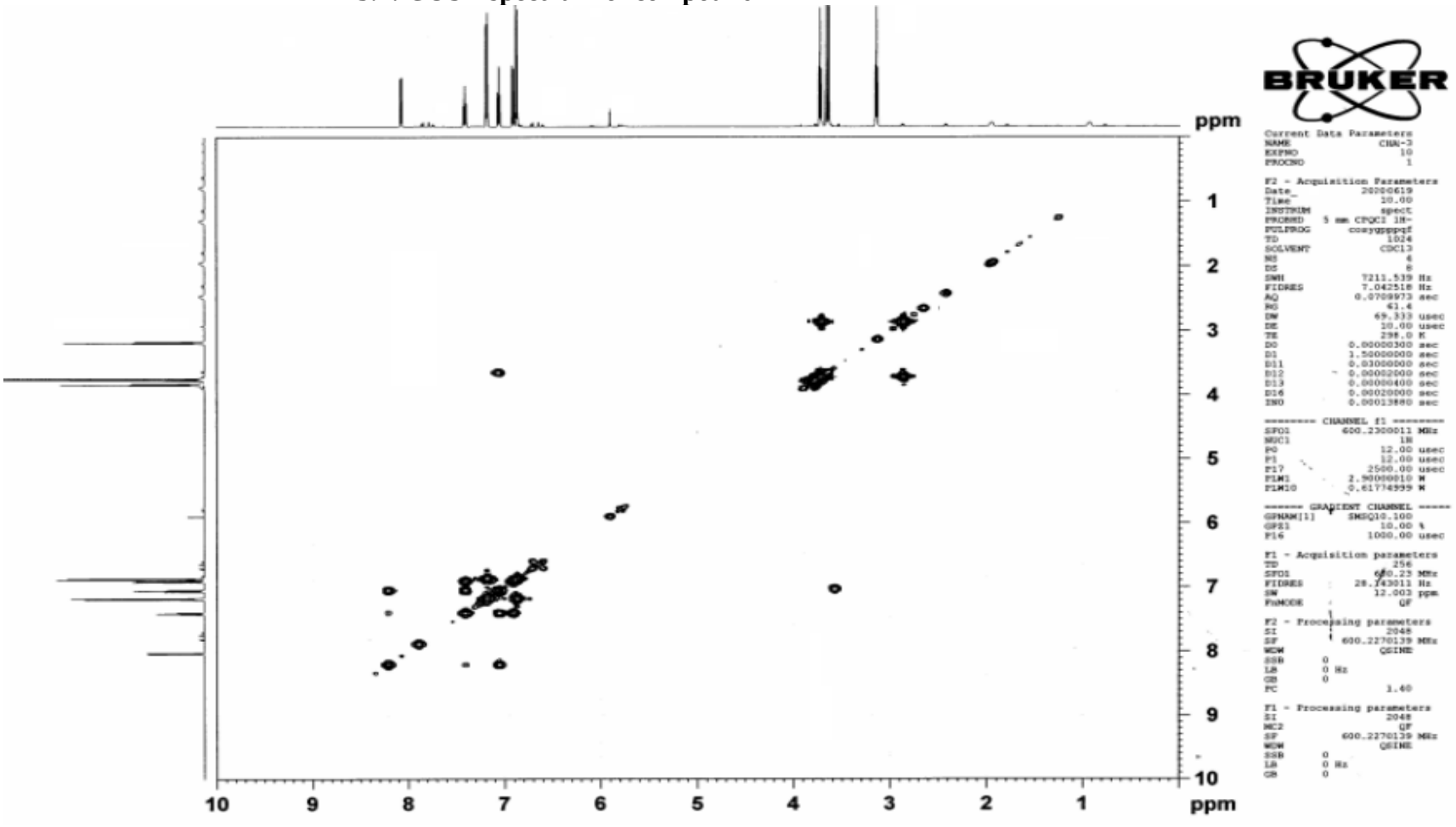

3.5: HMBC spectrum of compound 41

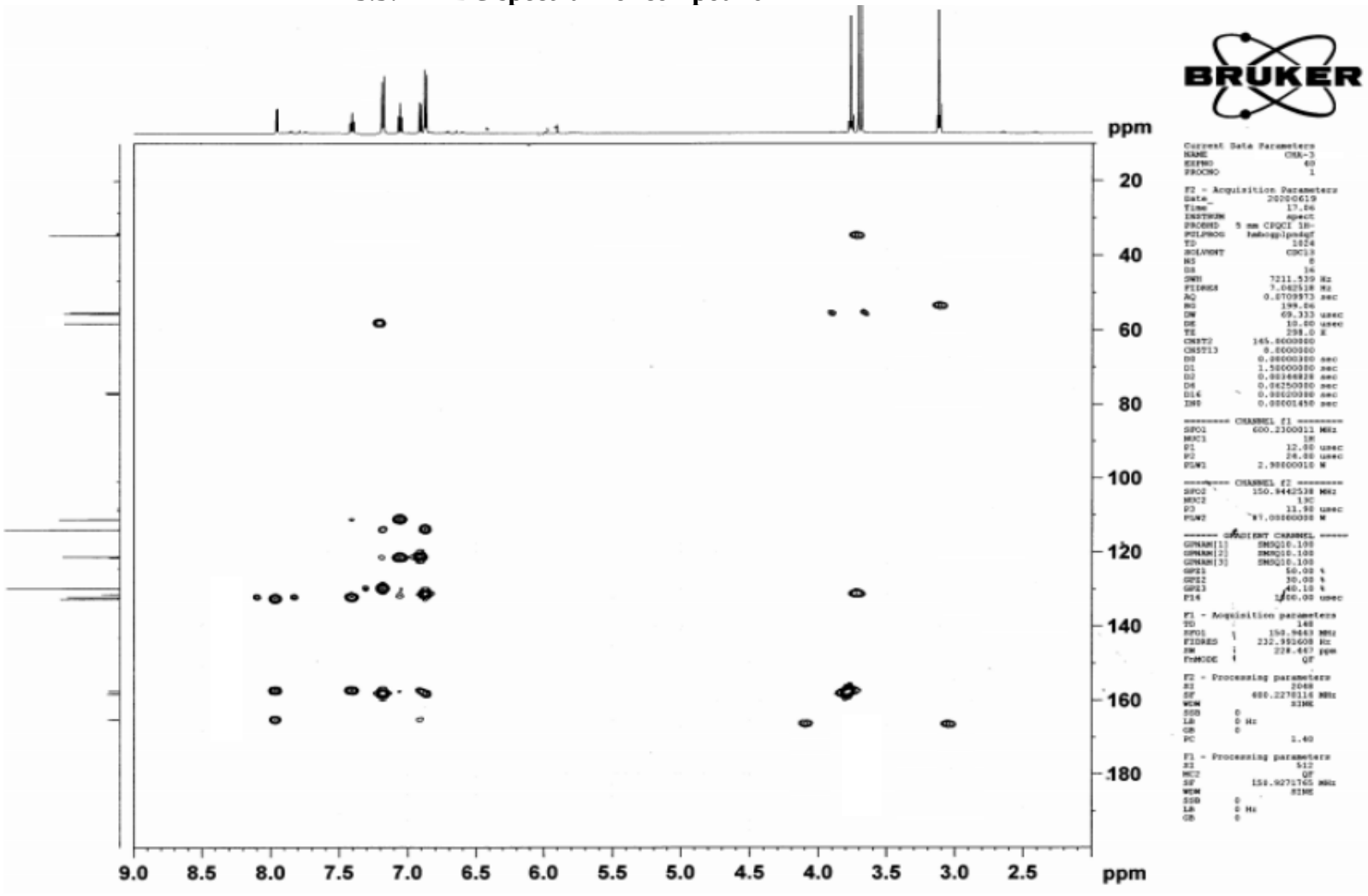

3.6: ROESY spectrum of compound 41

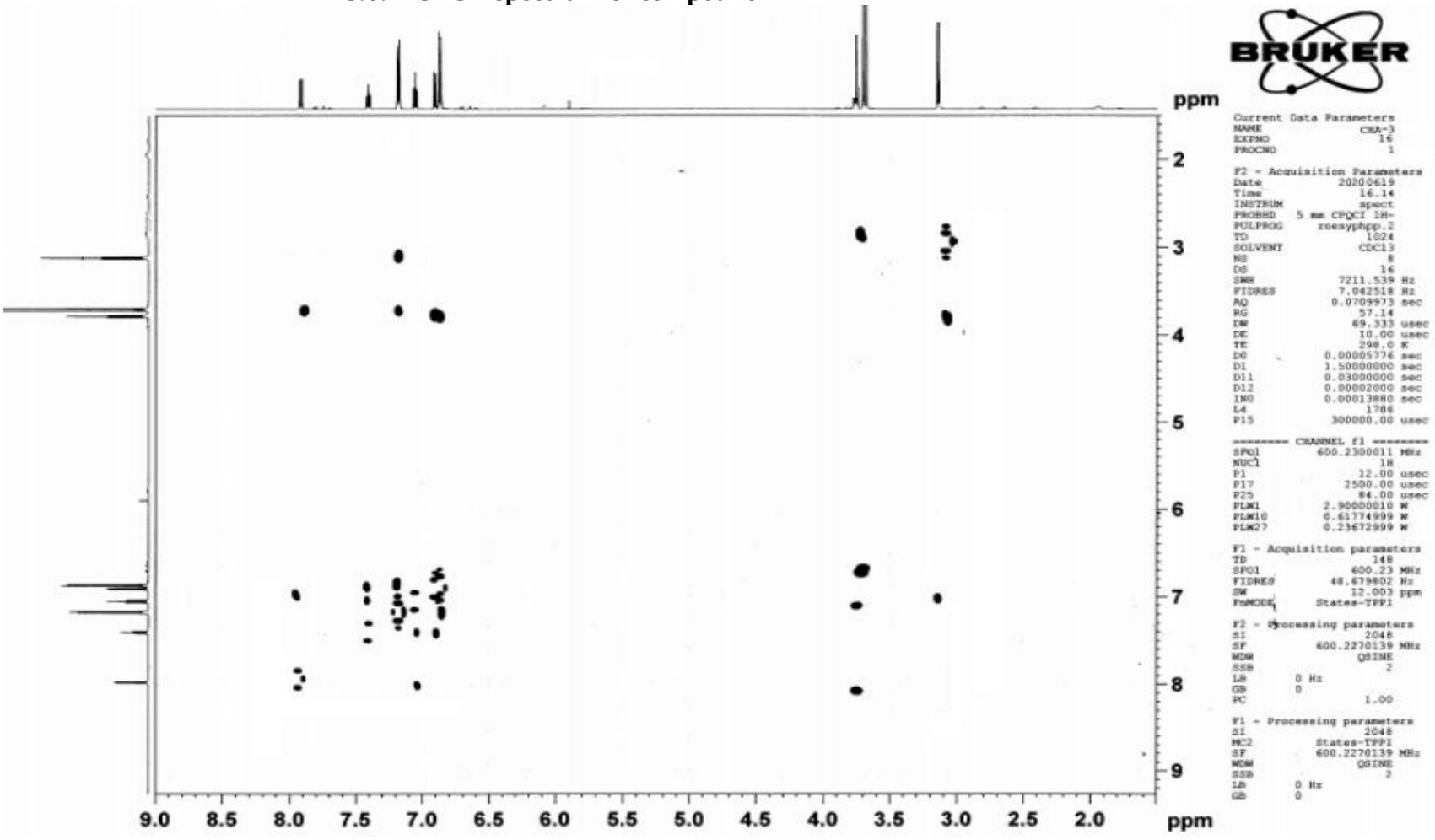

3.7: HREIMS spectrum of compound 41

Single Mass Analysis
Tolerance = 10.0 PPM / DBE: min = -10.0, max = 120.0
Selected filters: None

Monoisotopic Mass, Odd and Even Electron Ions
10 formula(e) evaluated with 1 results within limits (up to 21 closest results for each mass)
Elements Used:
C: 0-200 H: 0-400 N: 1-1 O: 2-4
cha-3
13:30:20 14-Jul-2020
Voltage EI+

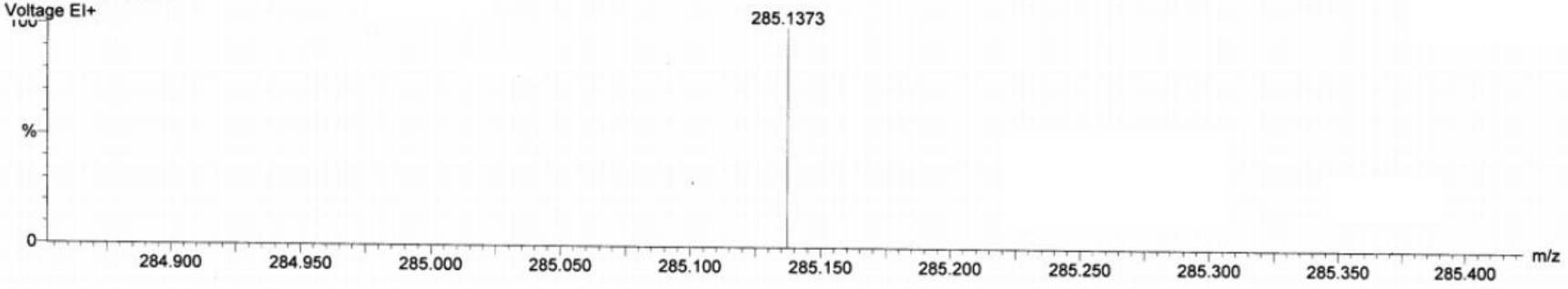

Minimum:				-10.0		
Maximum:		200.0	10.0	120.0		
Mass	Calc. Mass	mDa	PPM	DBE	i-FIT	Formula
285.1373	285.1365	0.8	2.8	9.0	5546027.5	C17 H19 N O3

3.8: FTIR spectrum of compound 41

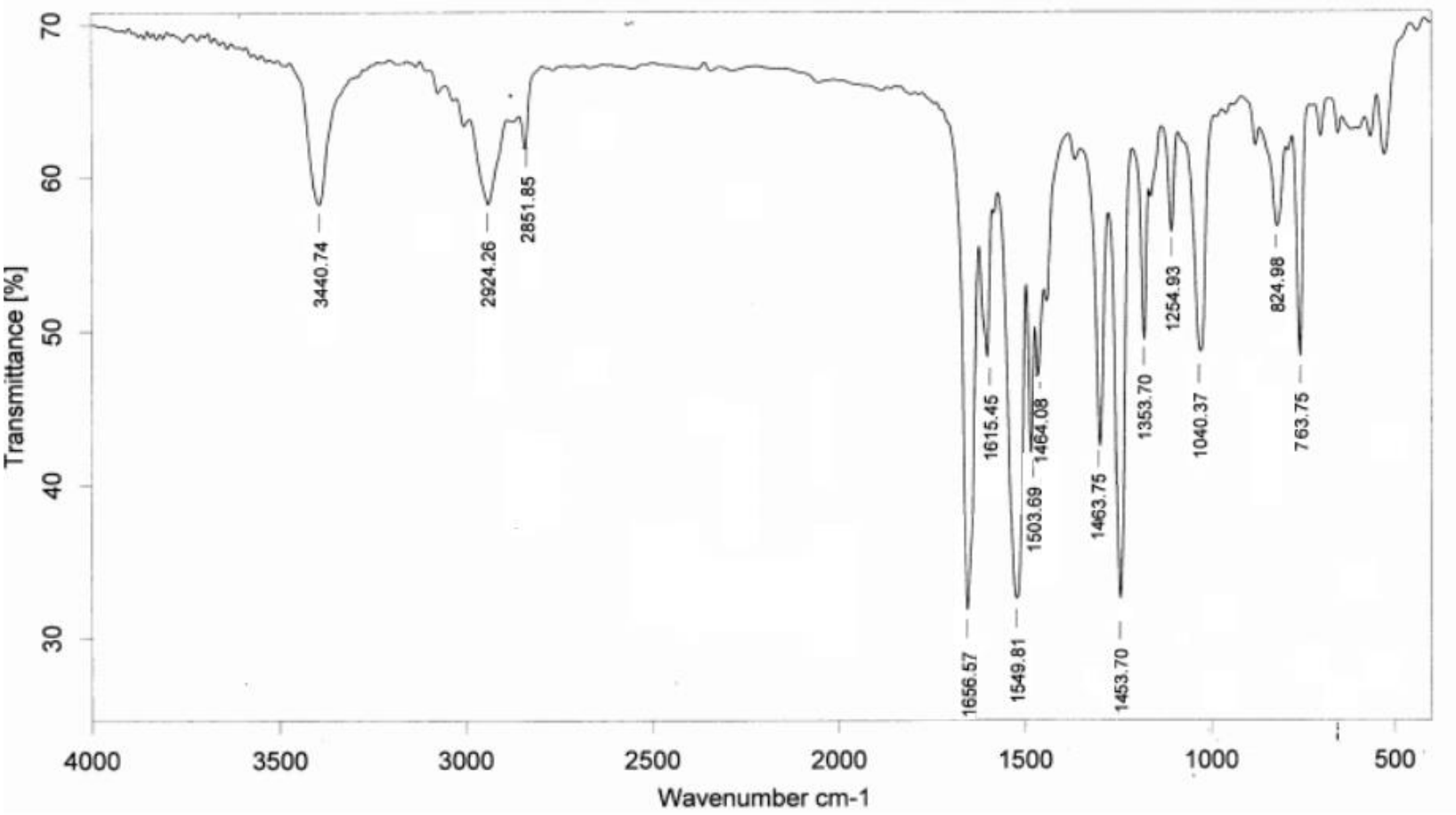

4. Spectra for Compound 42 (Phenanthridine A)

4.1: ^{1}H NMR spectrum of compound 42

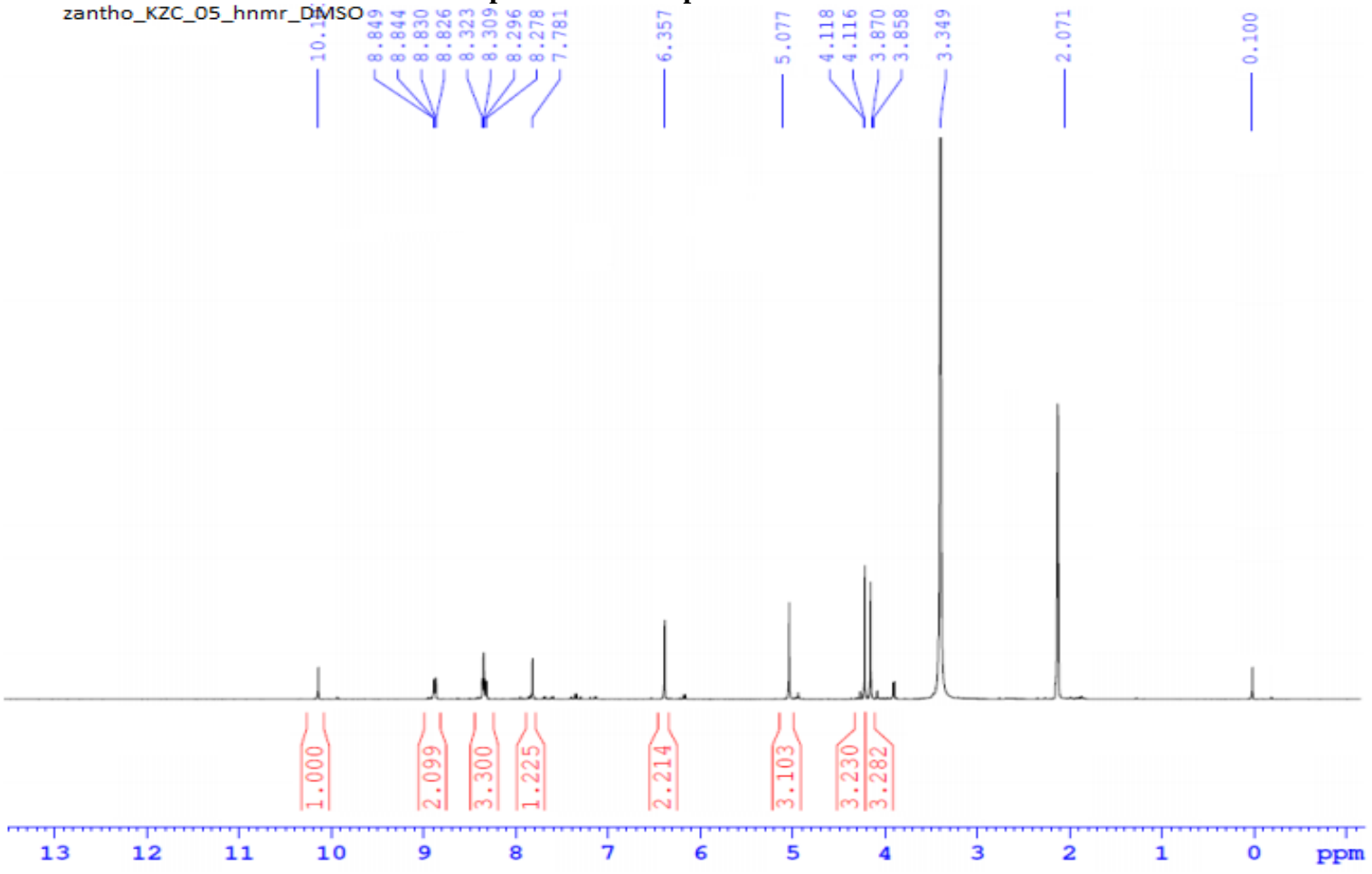

4.2: ^{13}C NMR spectrum of compound 42

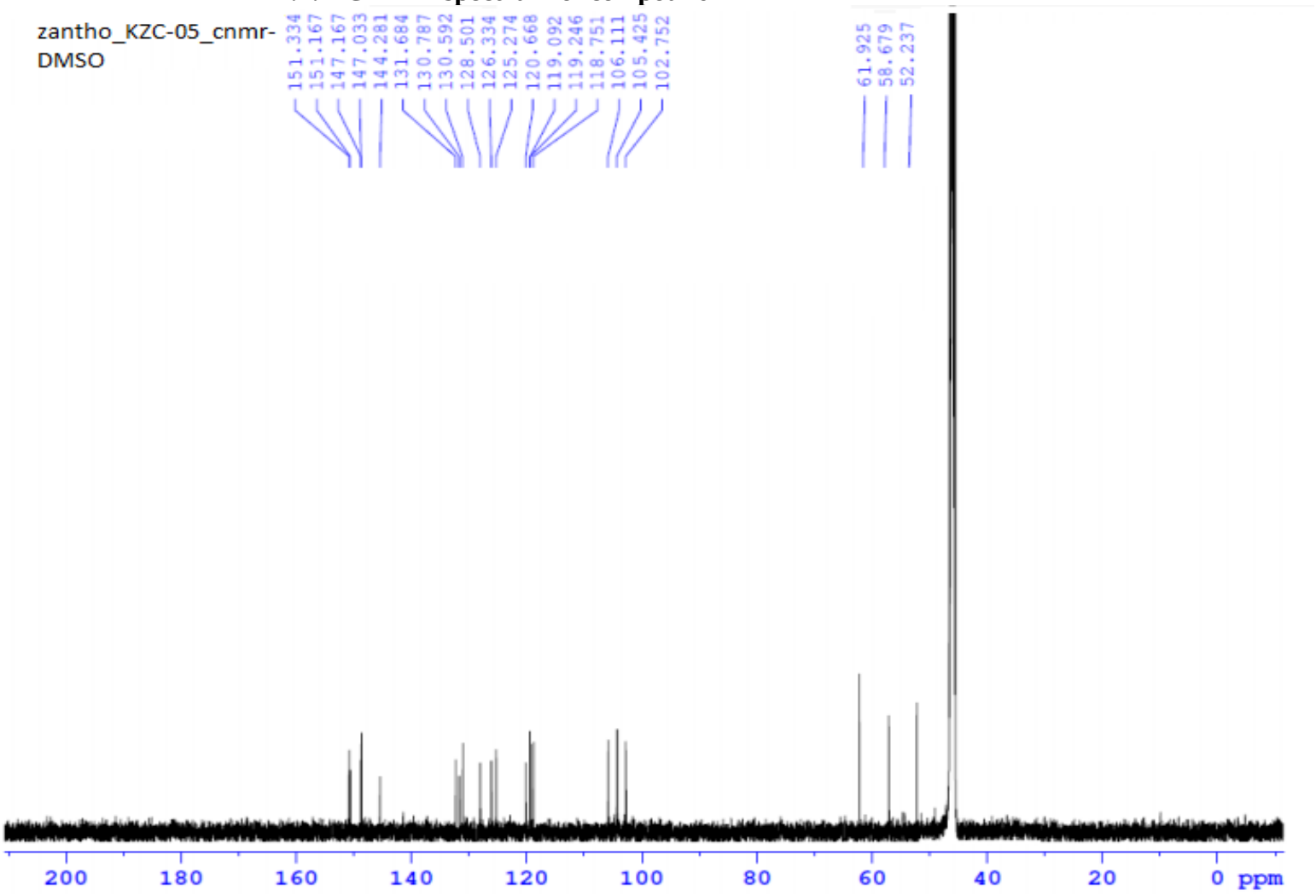

4.3: DEPT NMR spectrum of compound 42

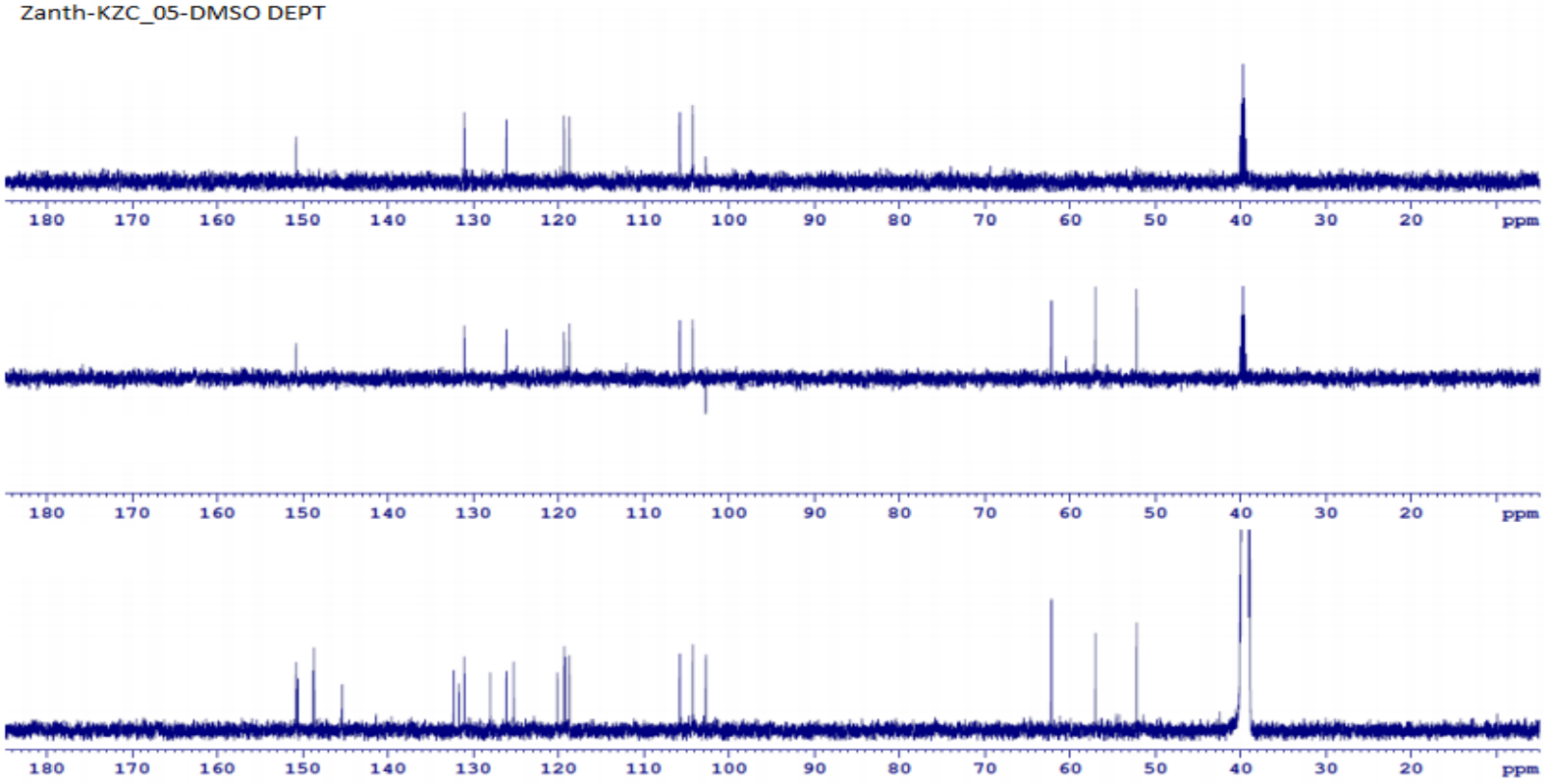

4.4: HSQC spectrum of compound 42

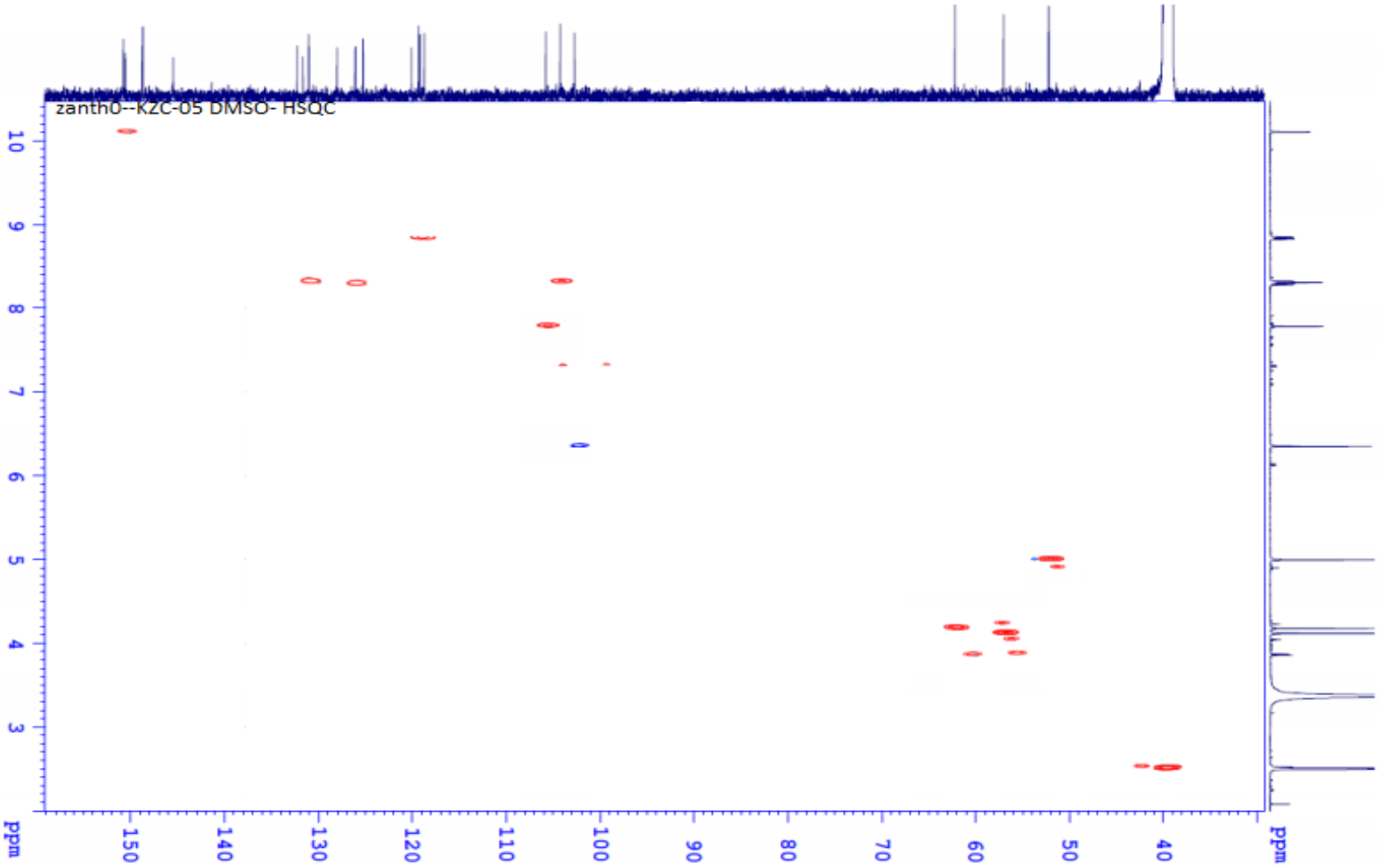

4.5: HMBC spectrum of compound 42

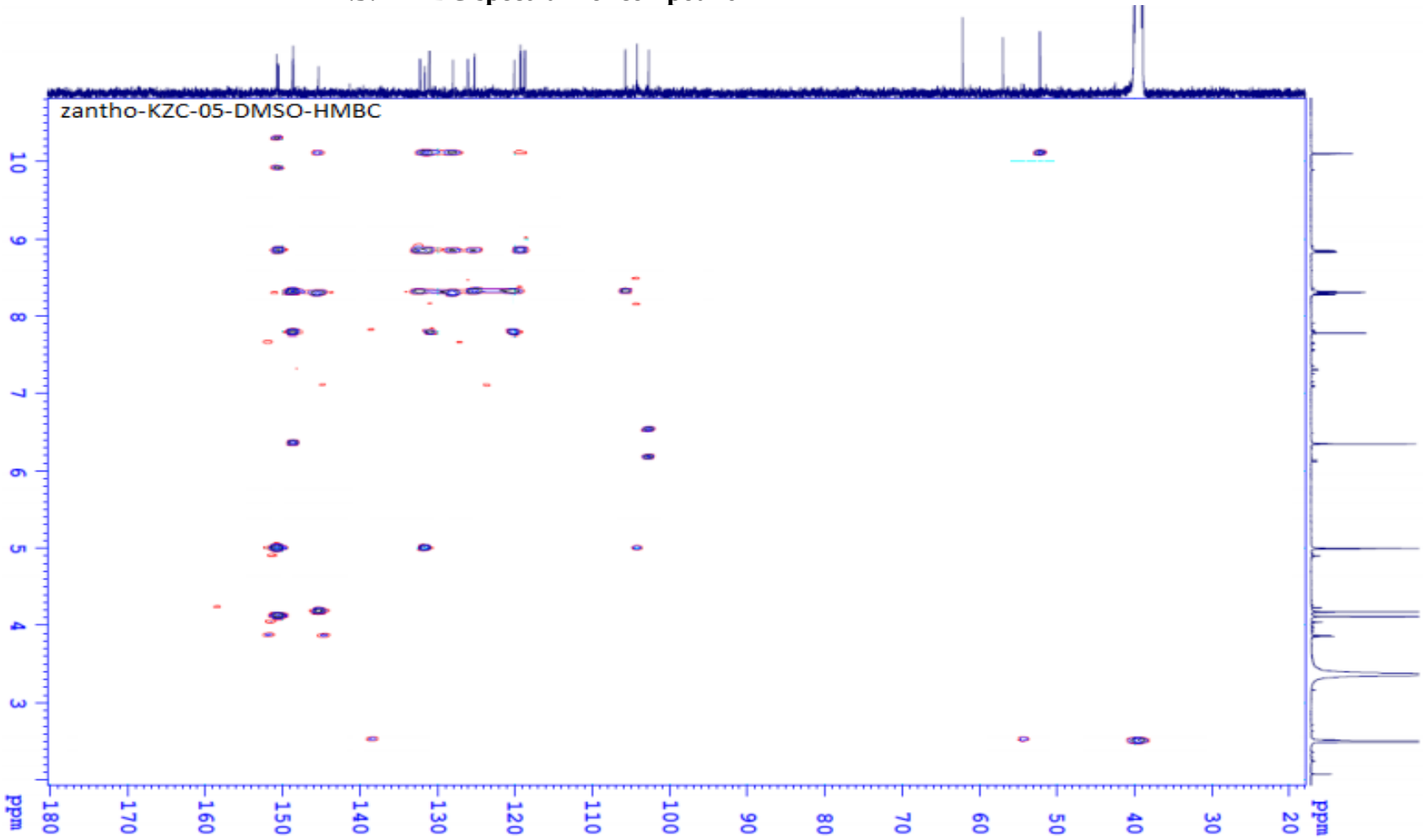

4.6: ESIMS spectrum of compound 42

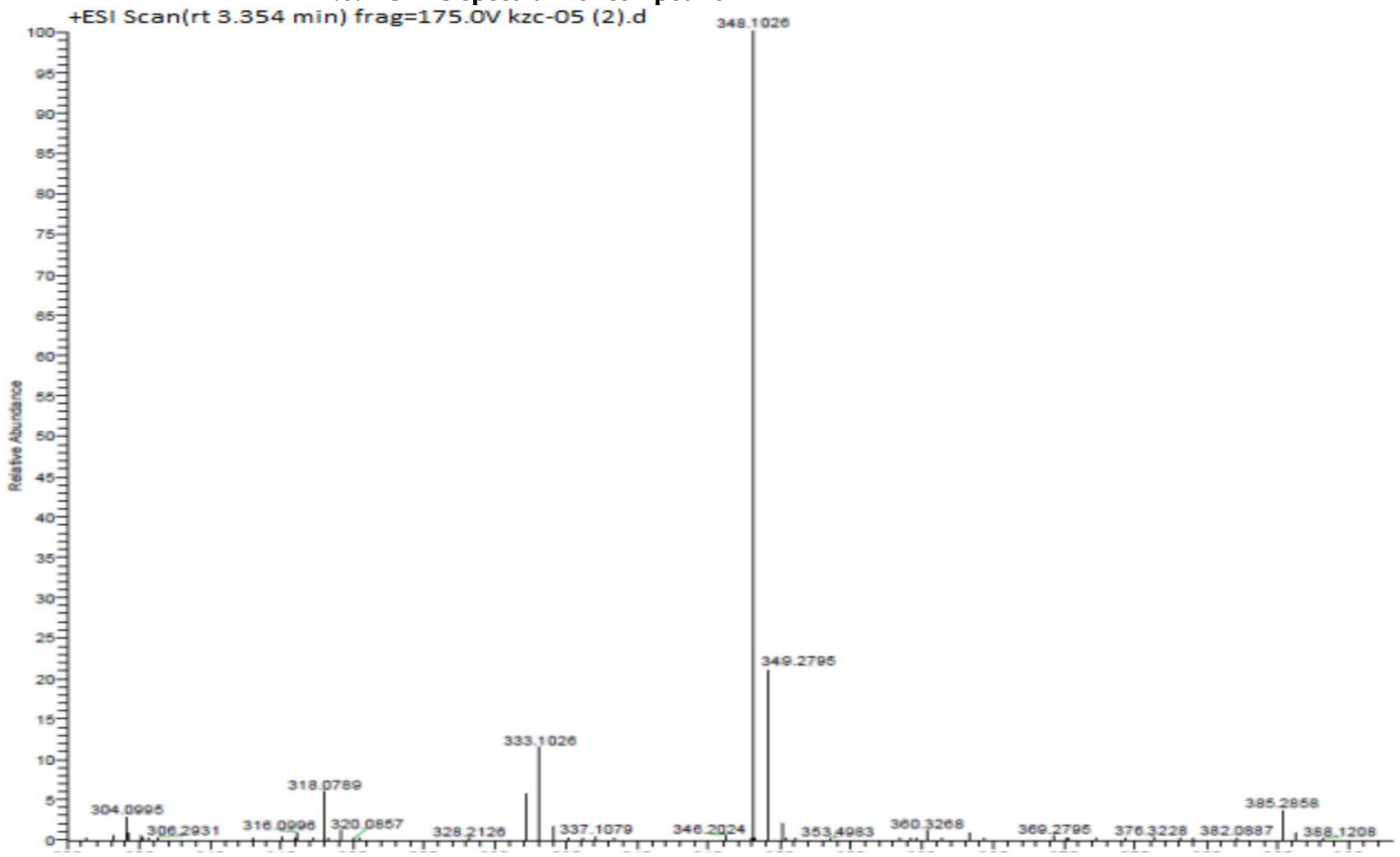

5. Spectra for Compound 43 (Zanthocapensine)

5.1: ^{1}H NMR spectrum of compound 43

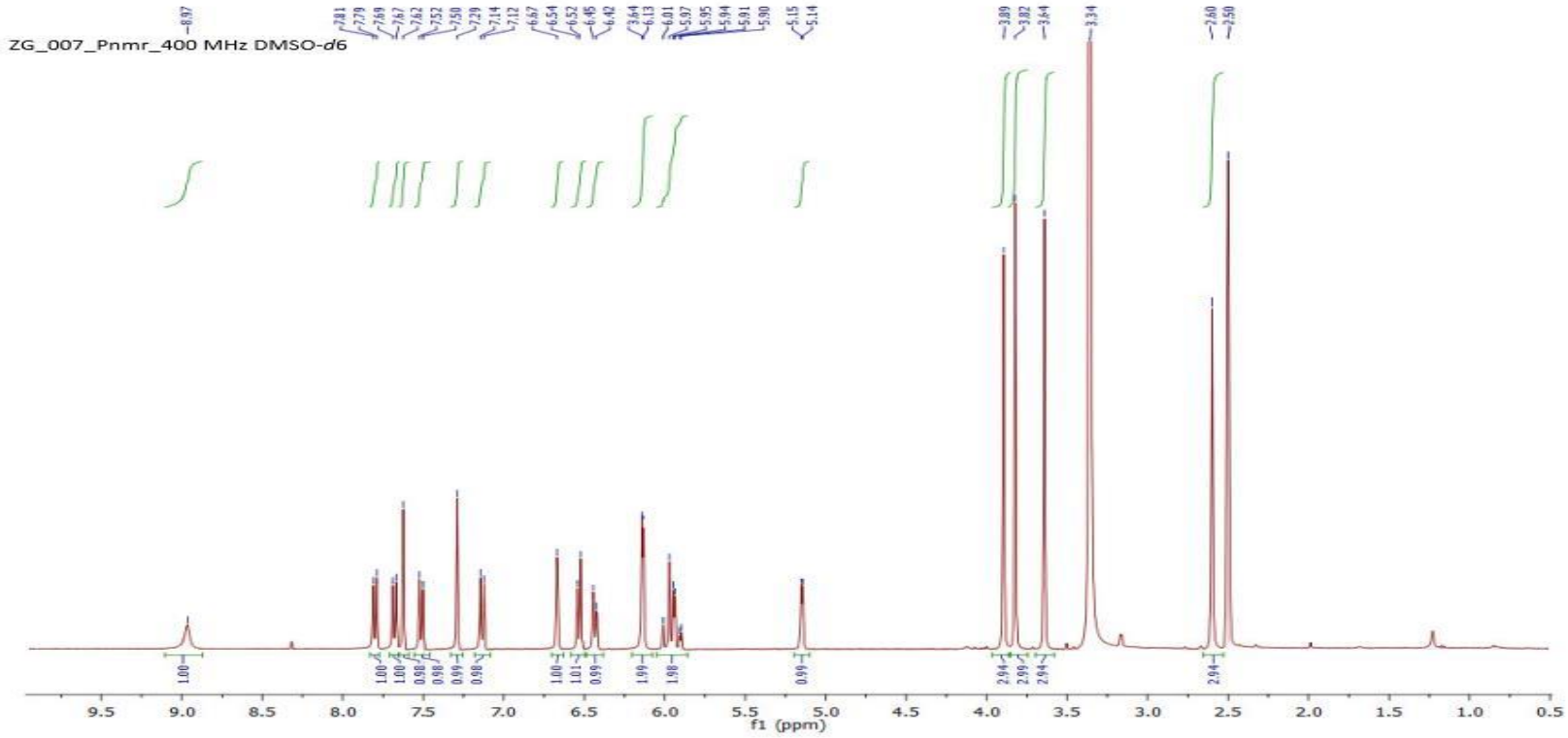

5.2: 13C NMR spectrum of compound 43

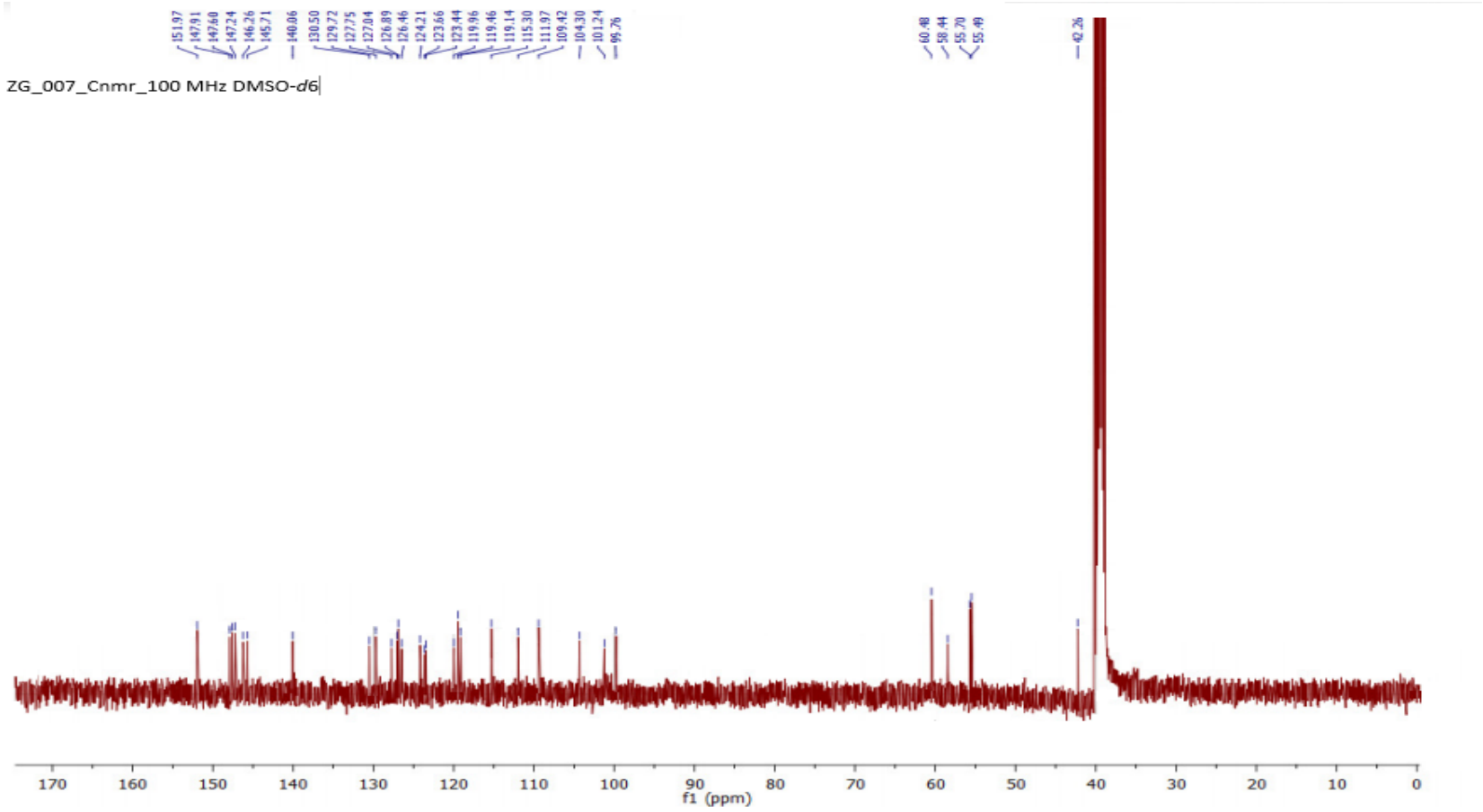

5.3: DEPT NMR spectrum of compound 43

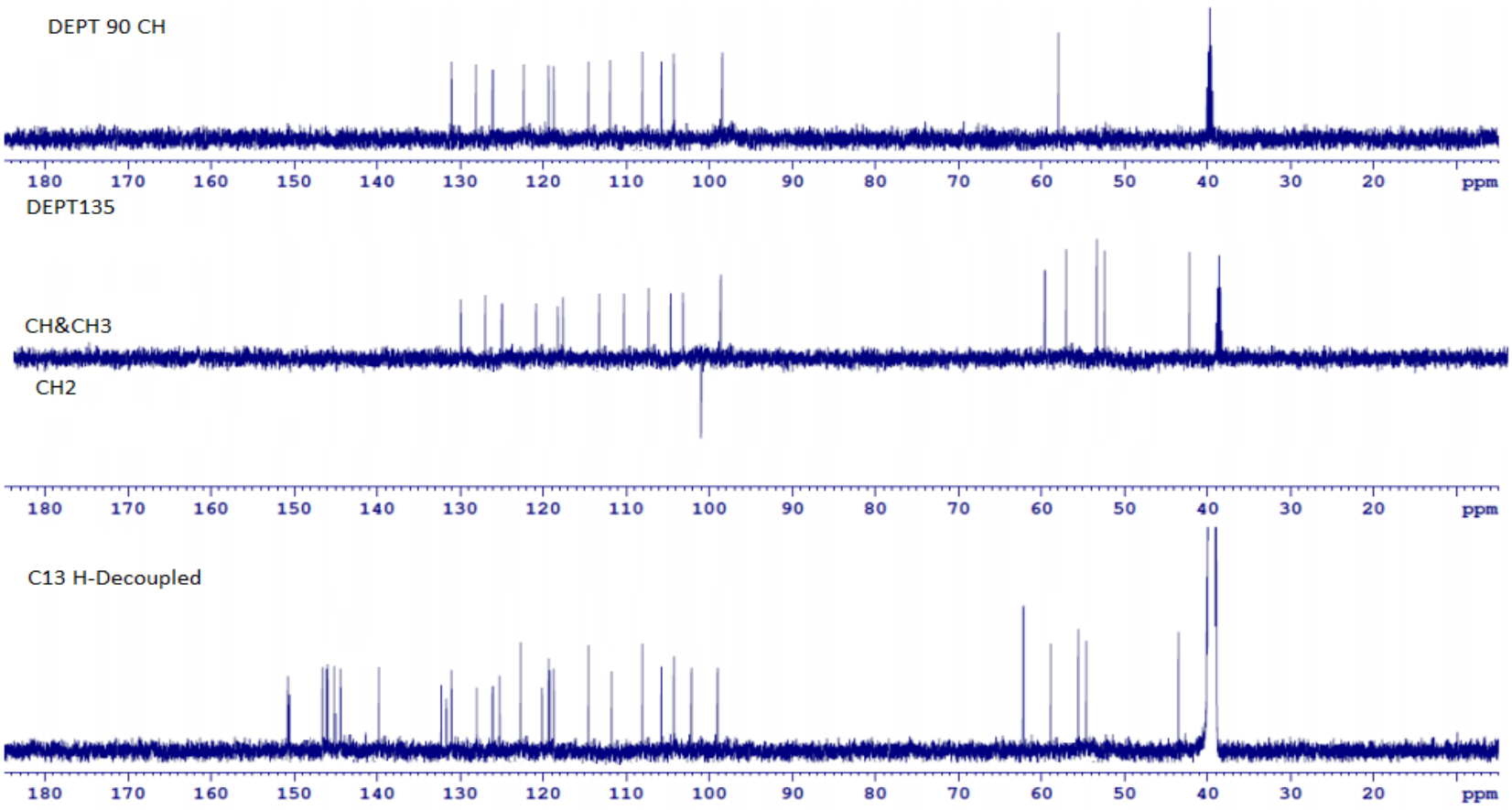

5.4: HSQC spectrum of compound 43

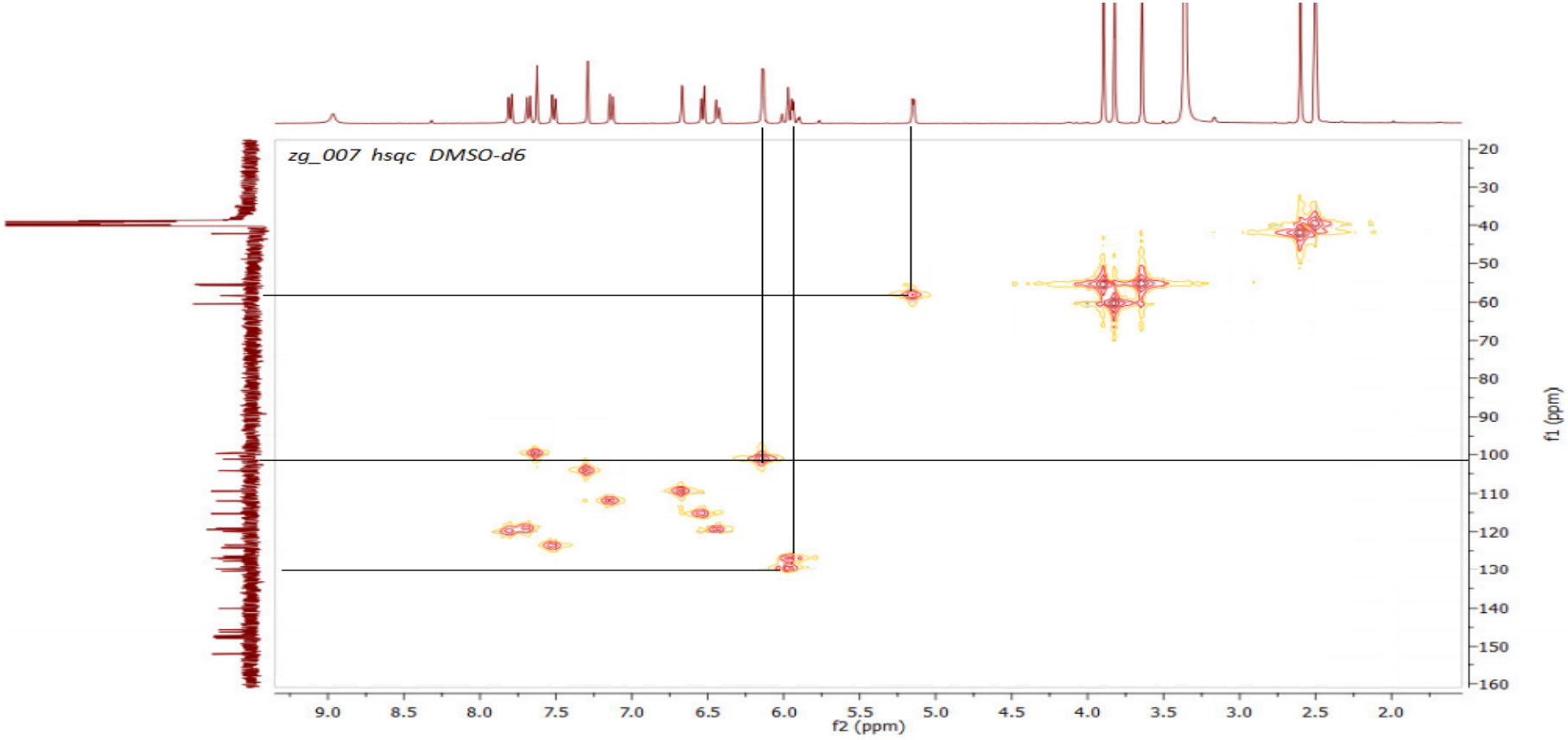

5.5: HMBC spectrum of compound 43

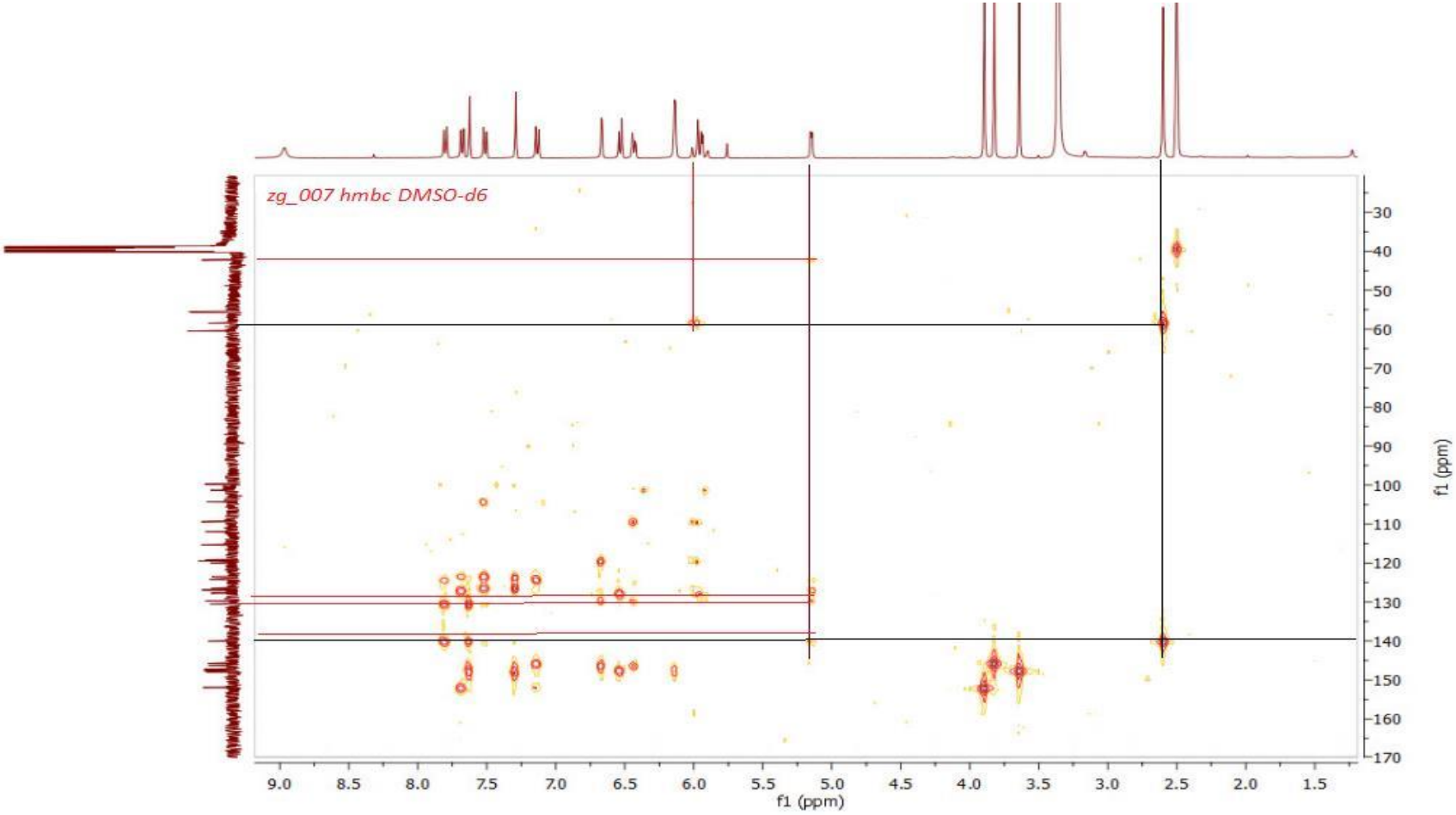

5.6: ESIMS spectrum of compound 43

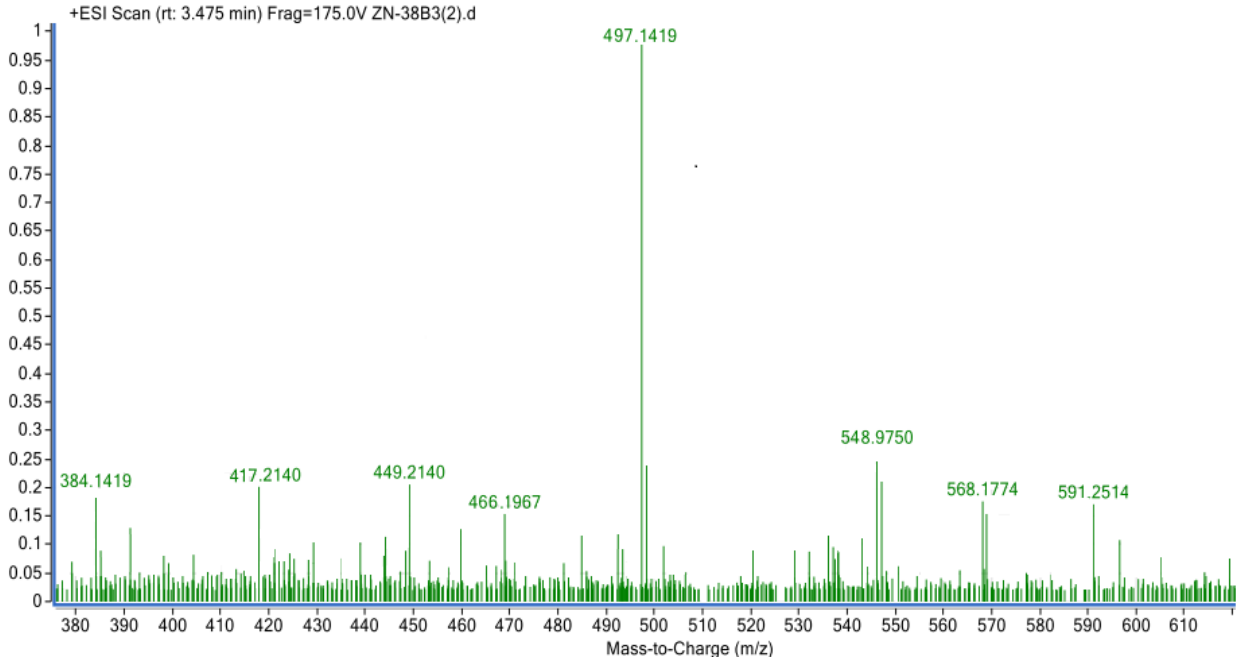

6. Spectra for Compound 44 (Zanthocapensol)

6.1: ^{1}H NMR spectrum of compound 44

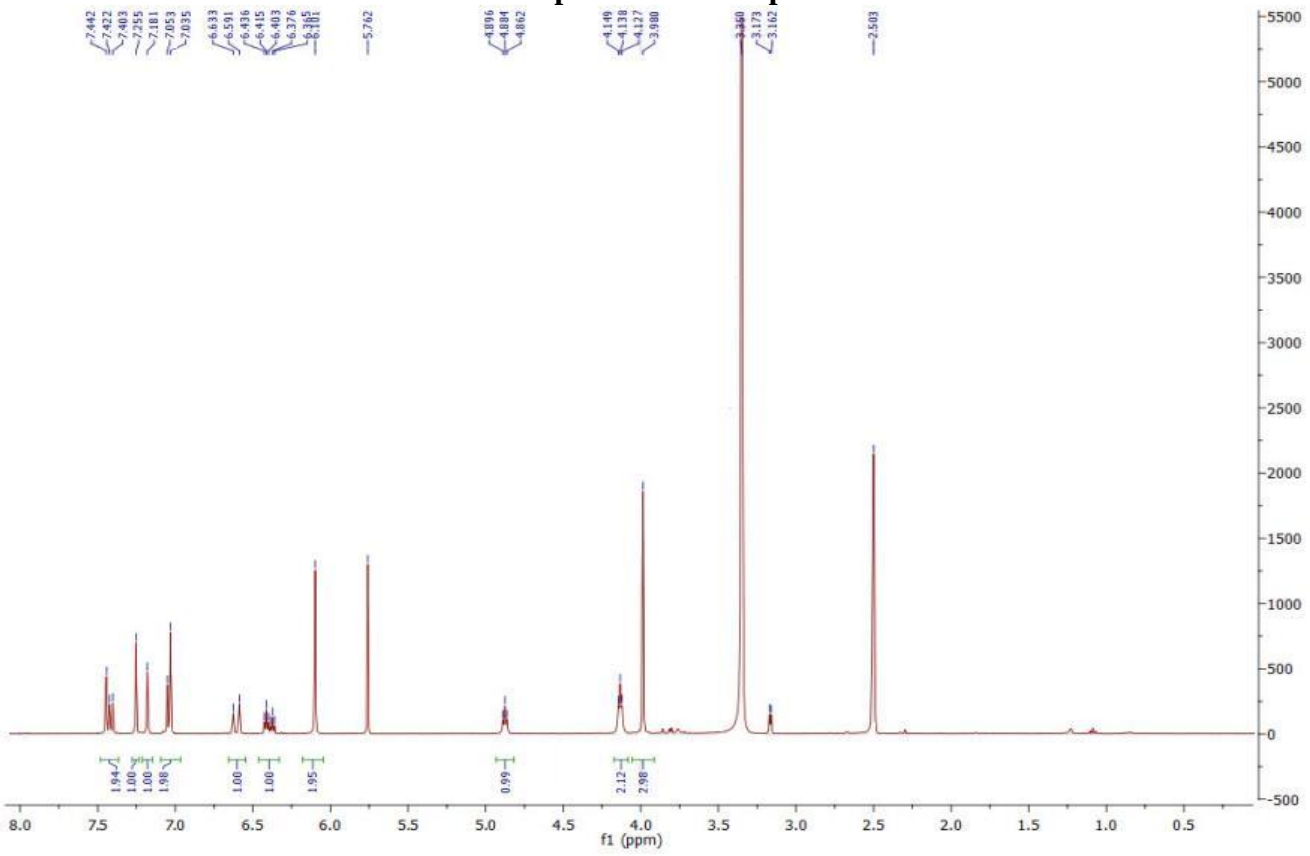

6.2: ^{13}C NMR spectrum of compound 44

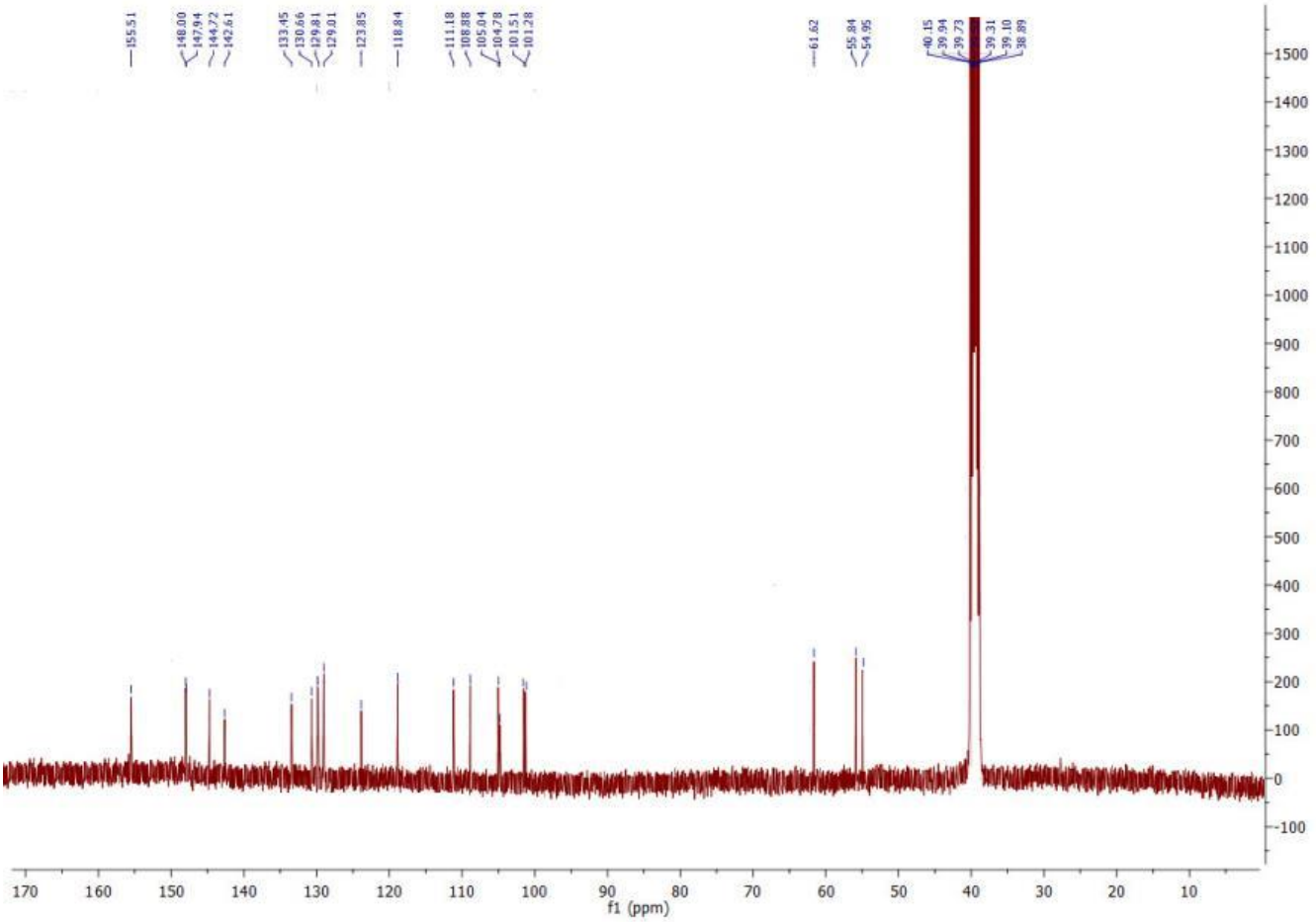

6.3: HSQC spectrum of compound 44

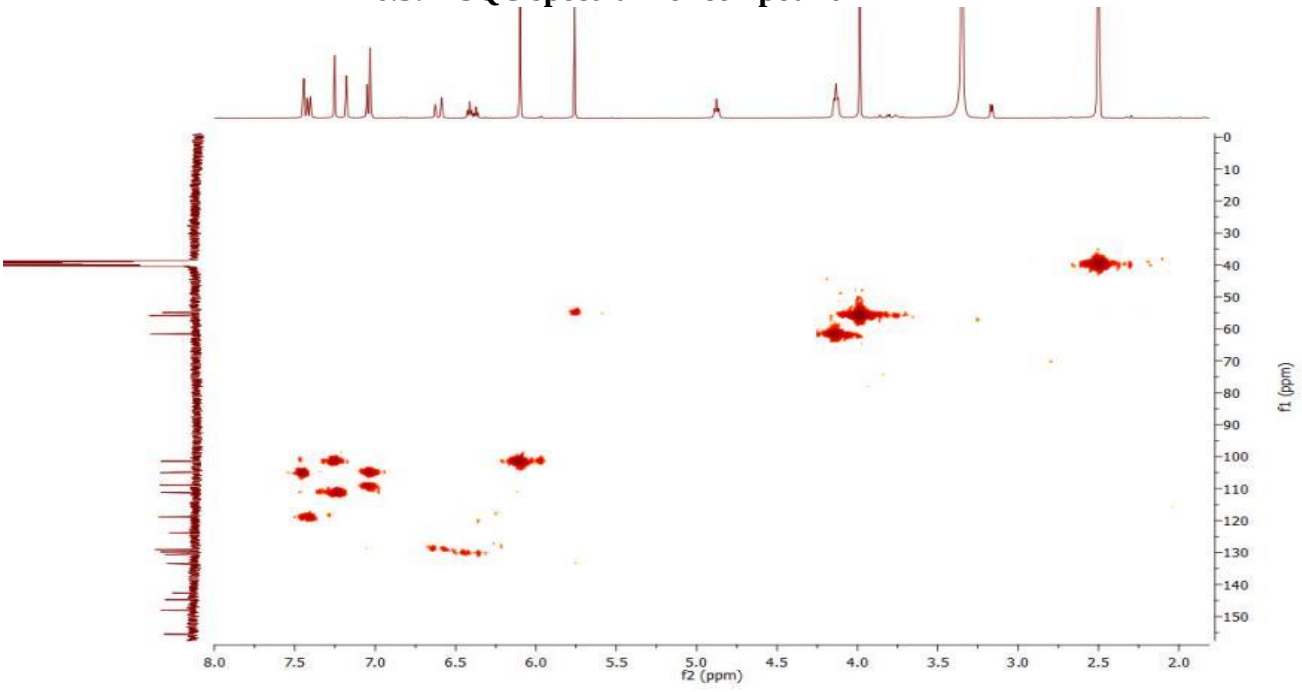

6.4: HMBC spectrum of compound 44

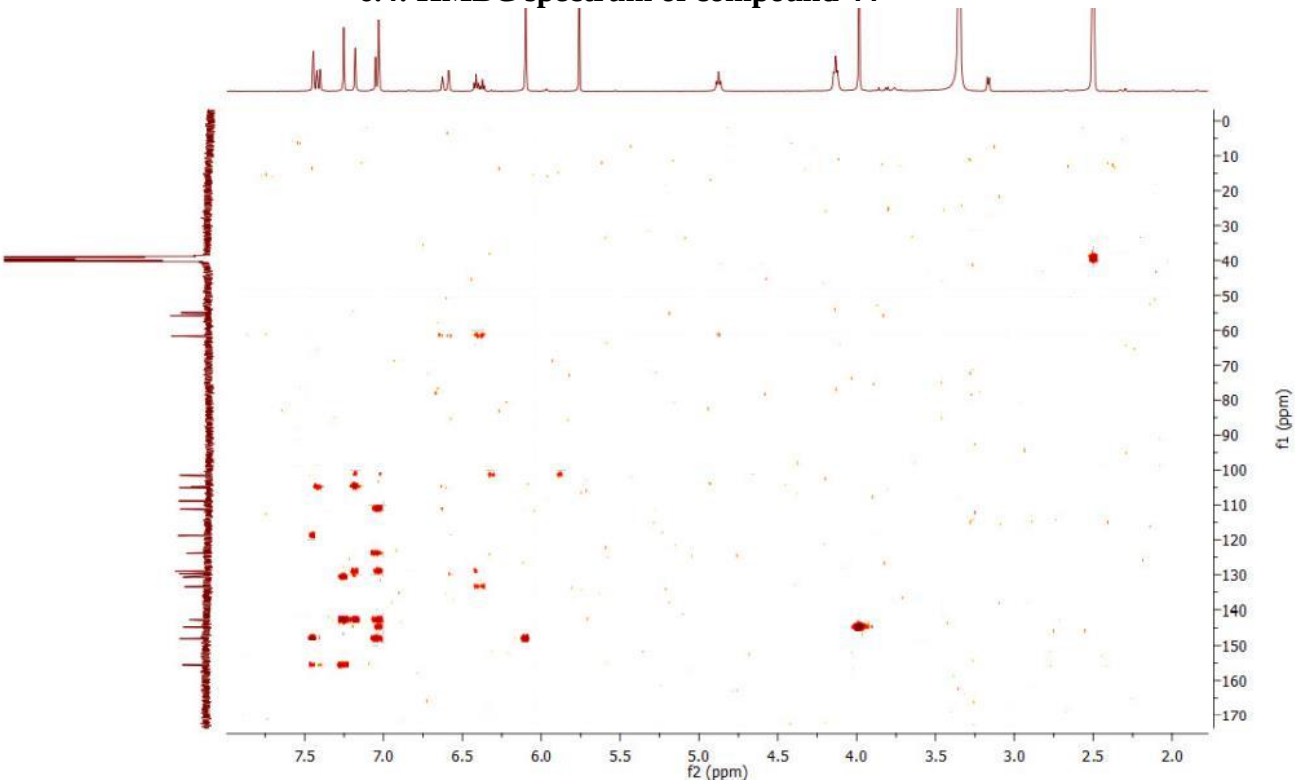

7. Spectra for Compound 45 (Zanthoamide D)

7.1: ^{1}H NMR spectrum of compound 45

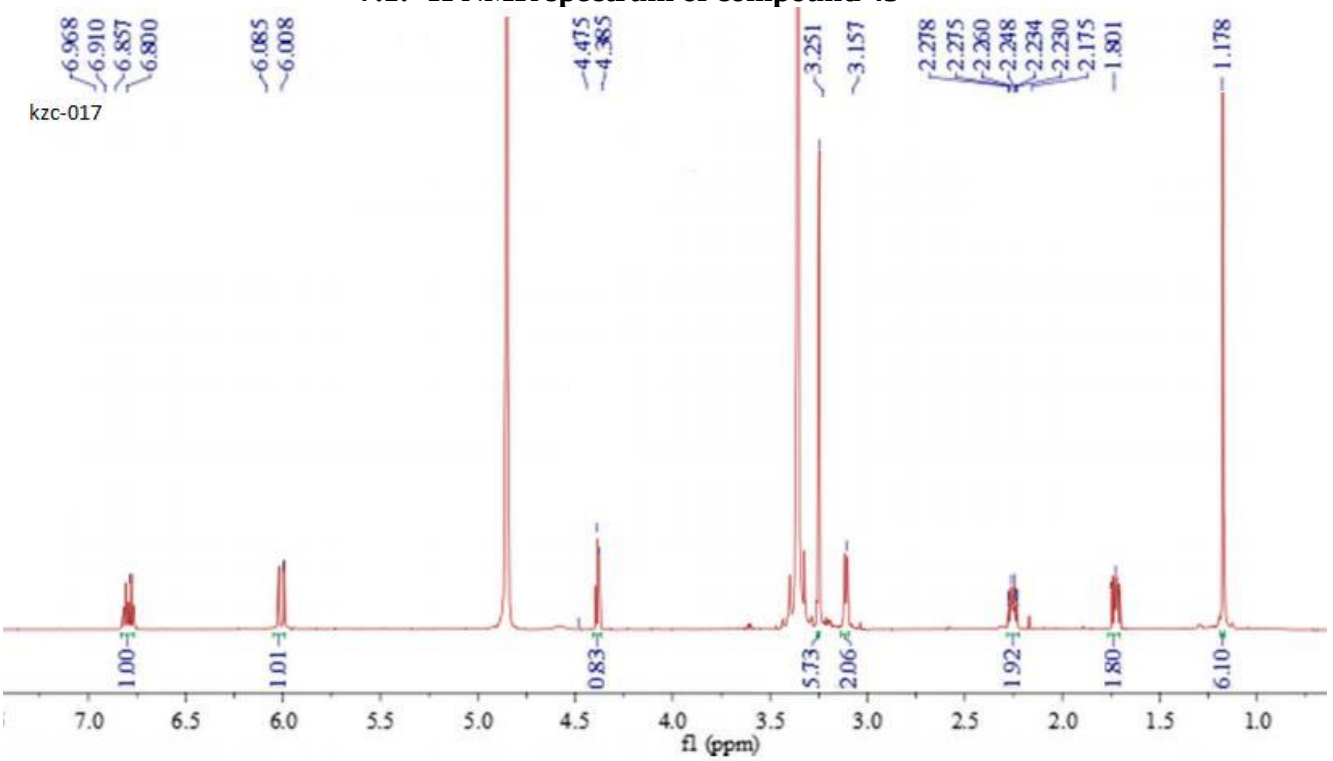

7.2: ^{13}C NMR spectrum of compound 45

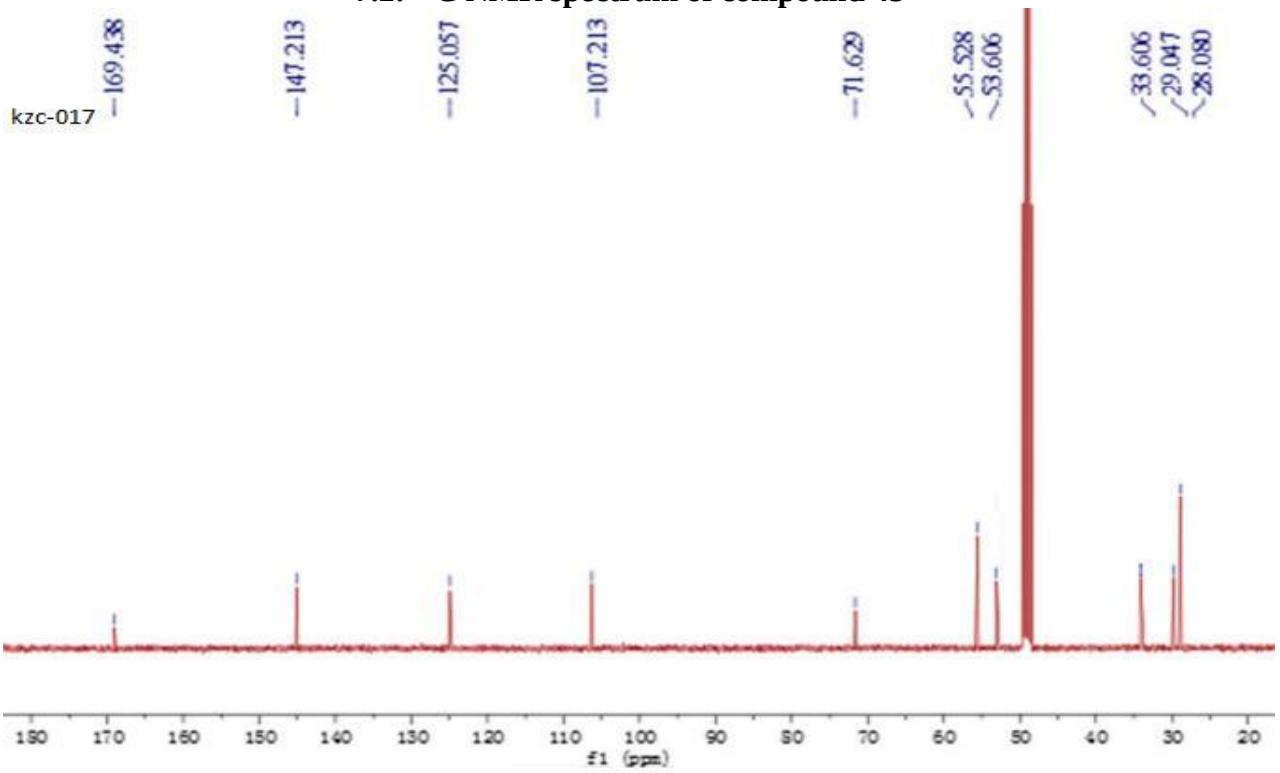

7.3: COSY spectrum of compound 45

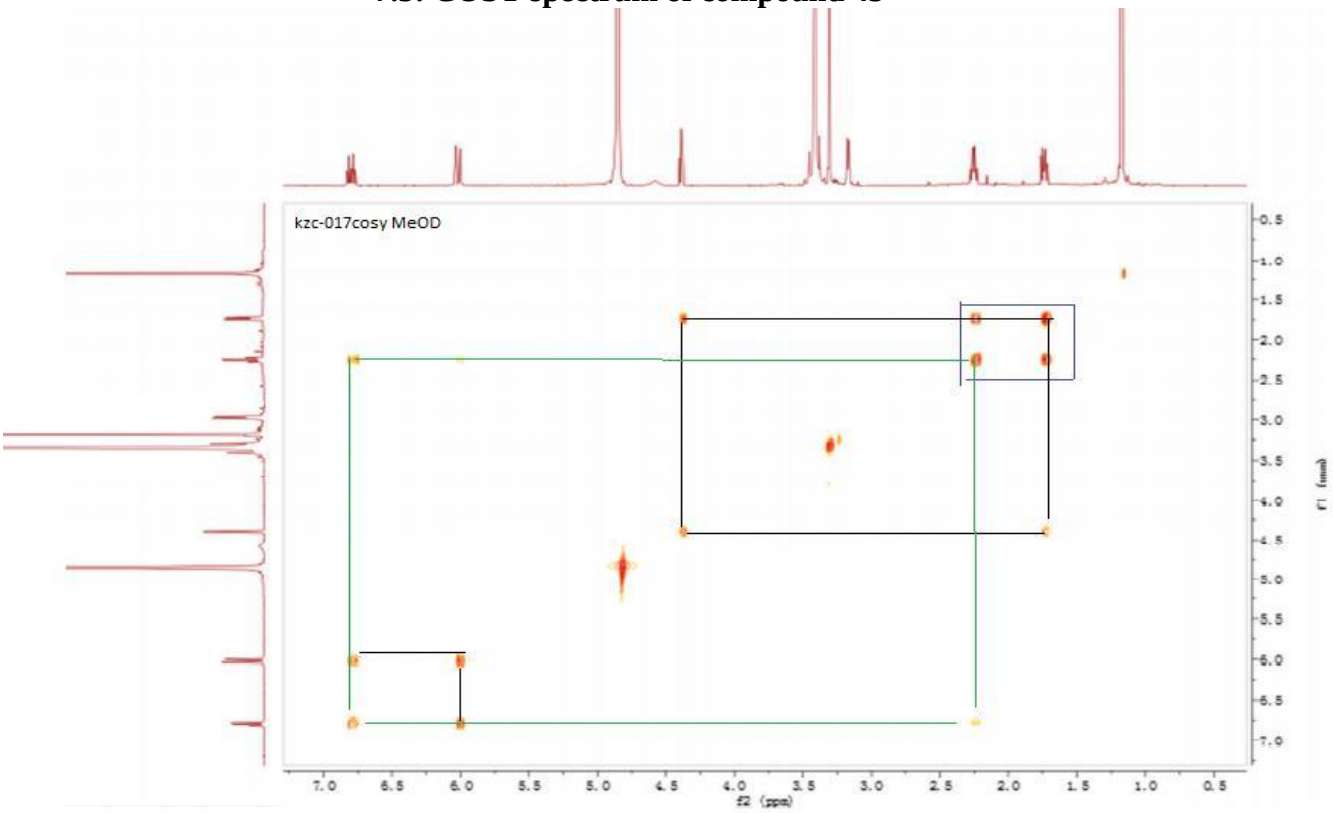

7.4: HSQC spectrum of compound 45

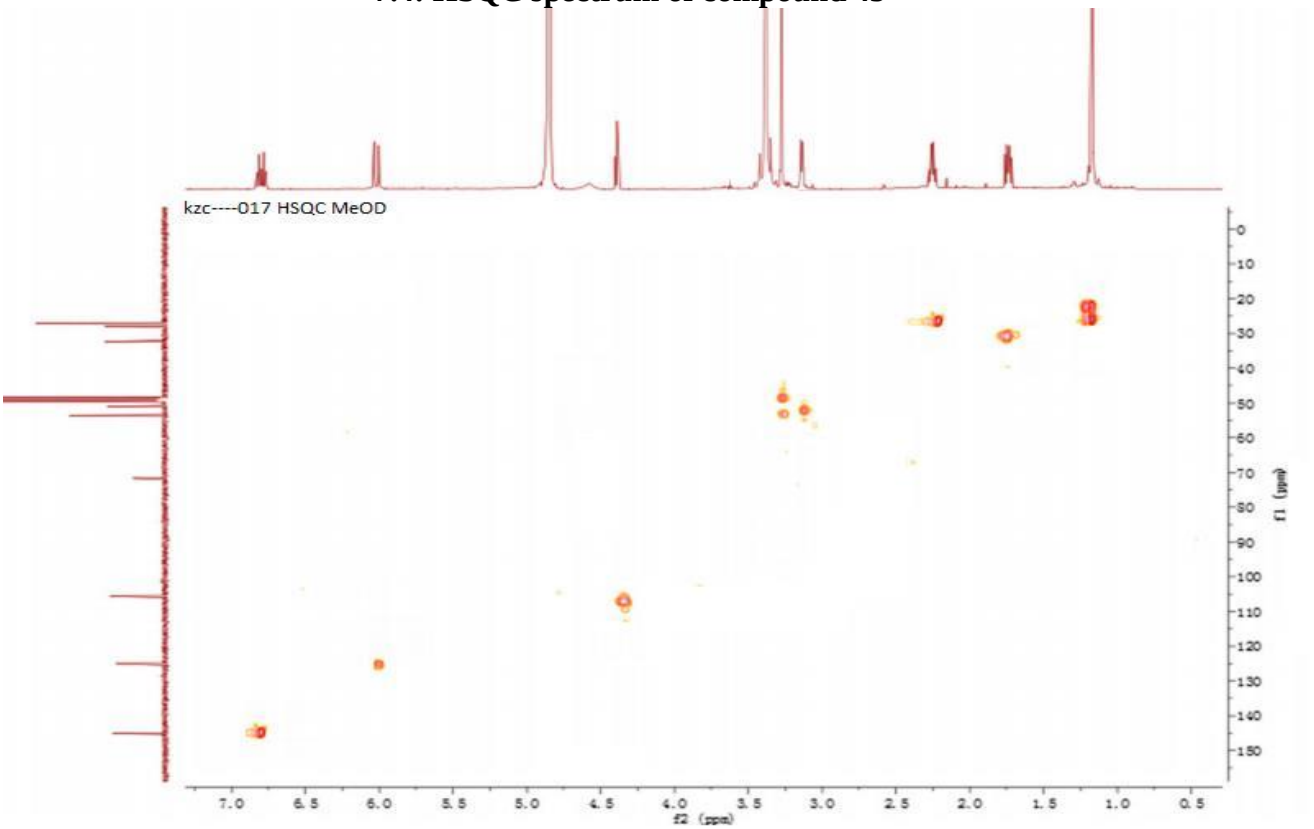

7.5: HMBC spectrum of compound 45

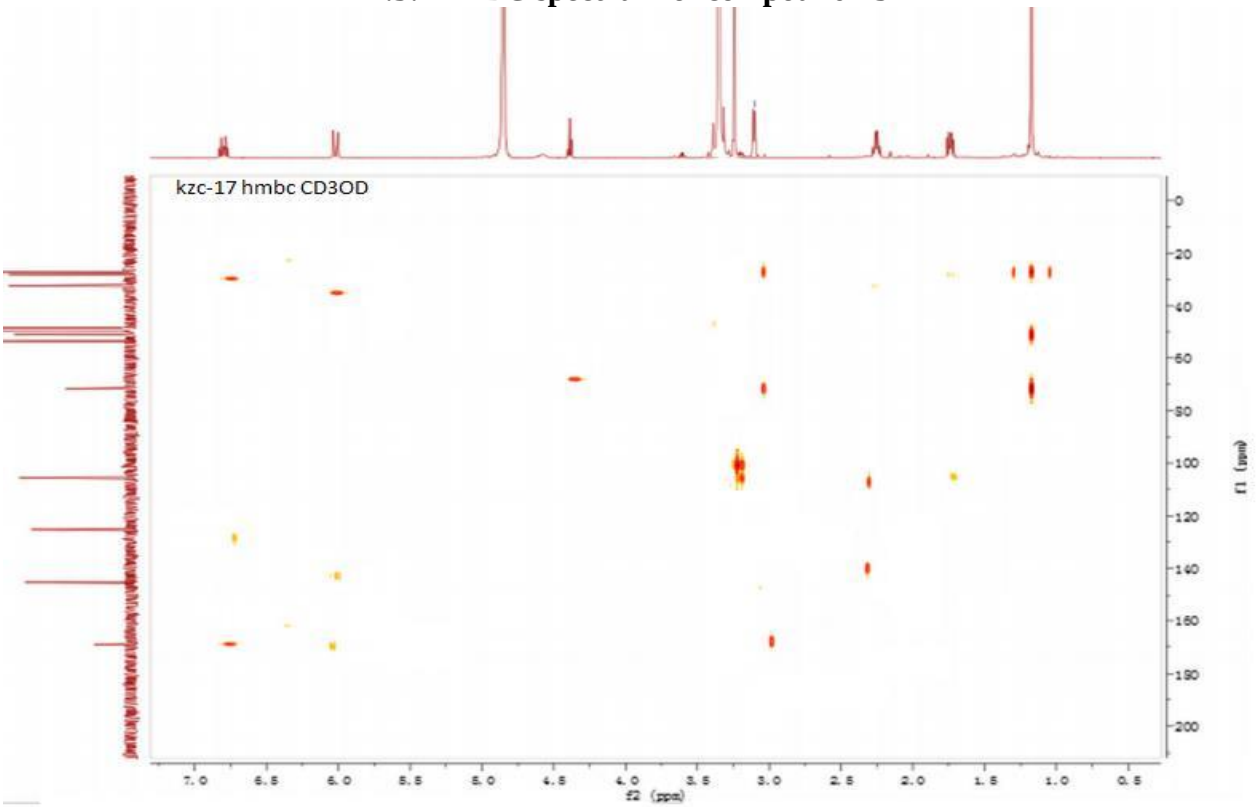

7.6: ESIMS spectrum of compound 45

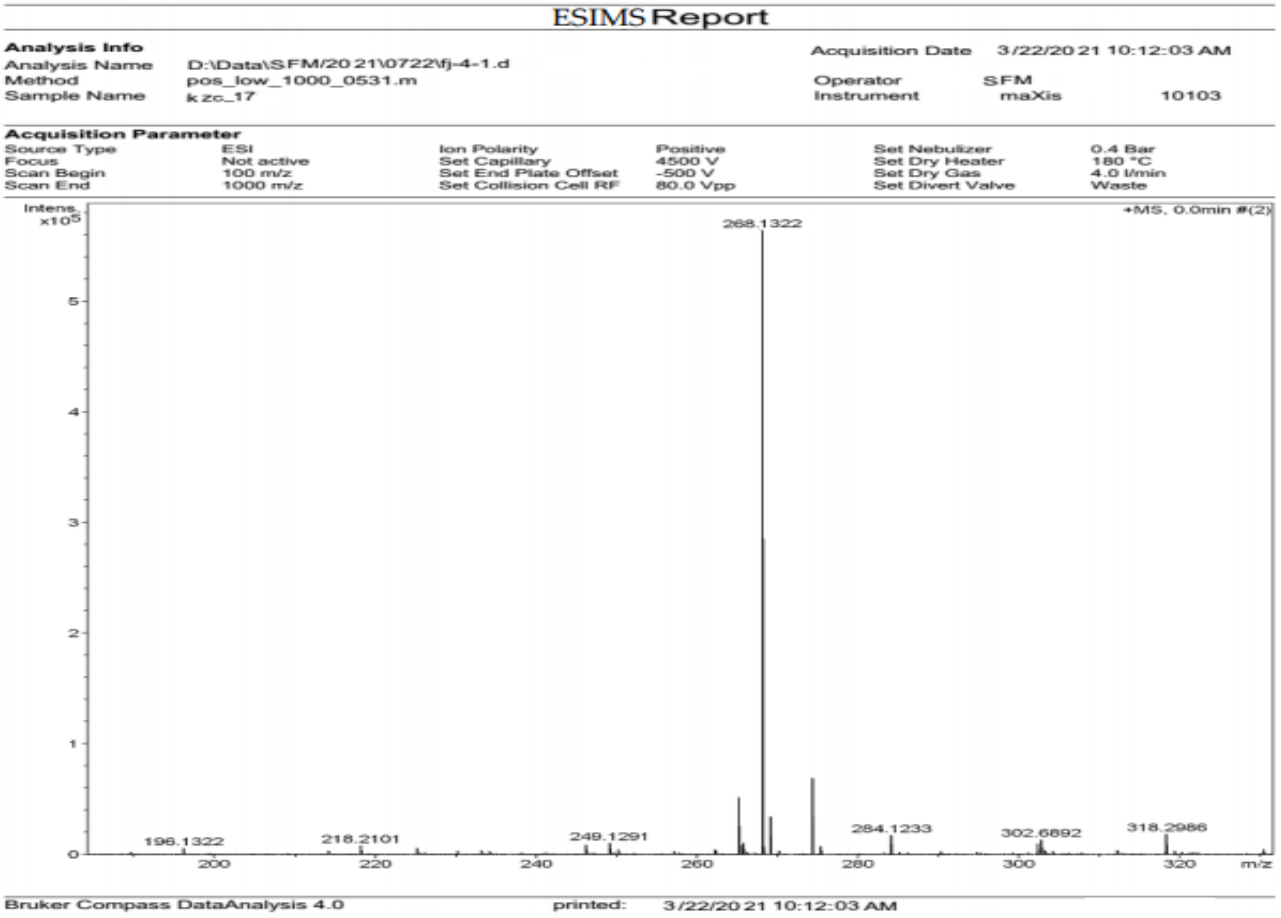

8. Spectra for Compound 9 (Norchelerythrine)

8.1: ^{1}H and ^{13}C NMR spectrum of compound 9

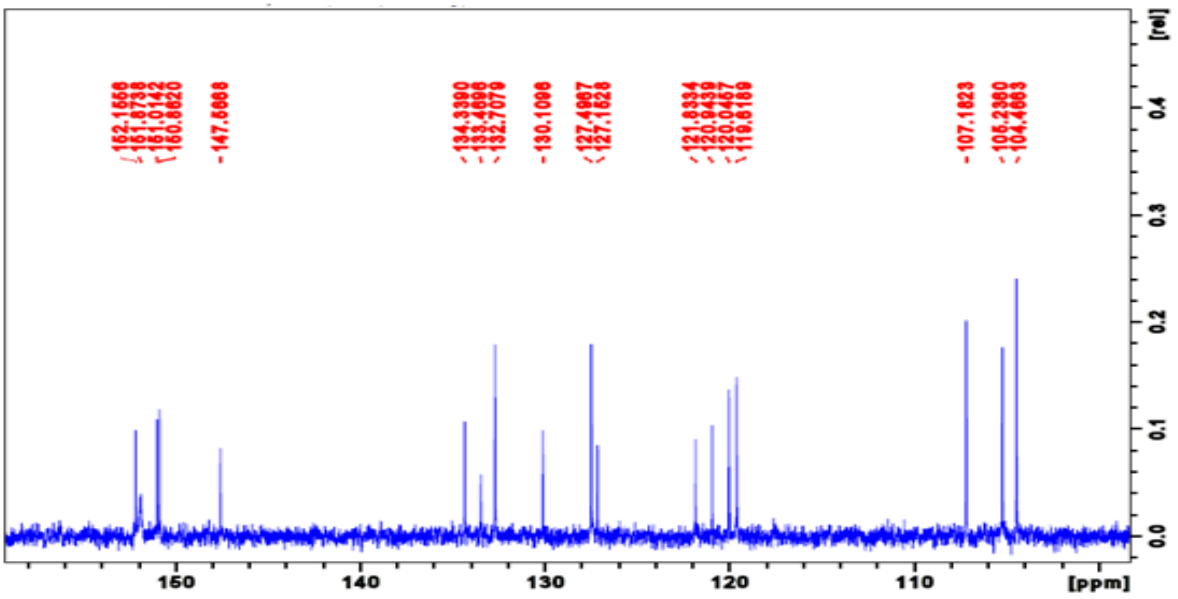

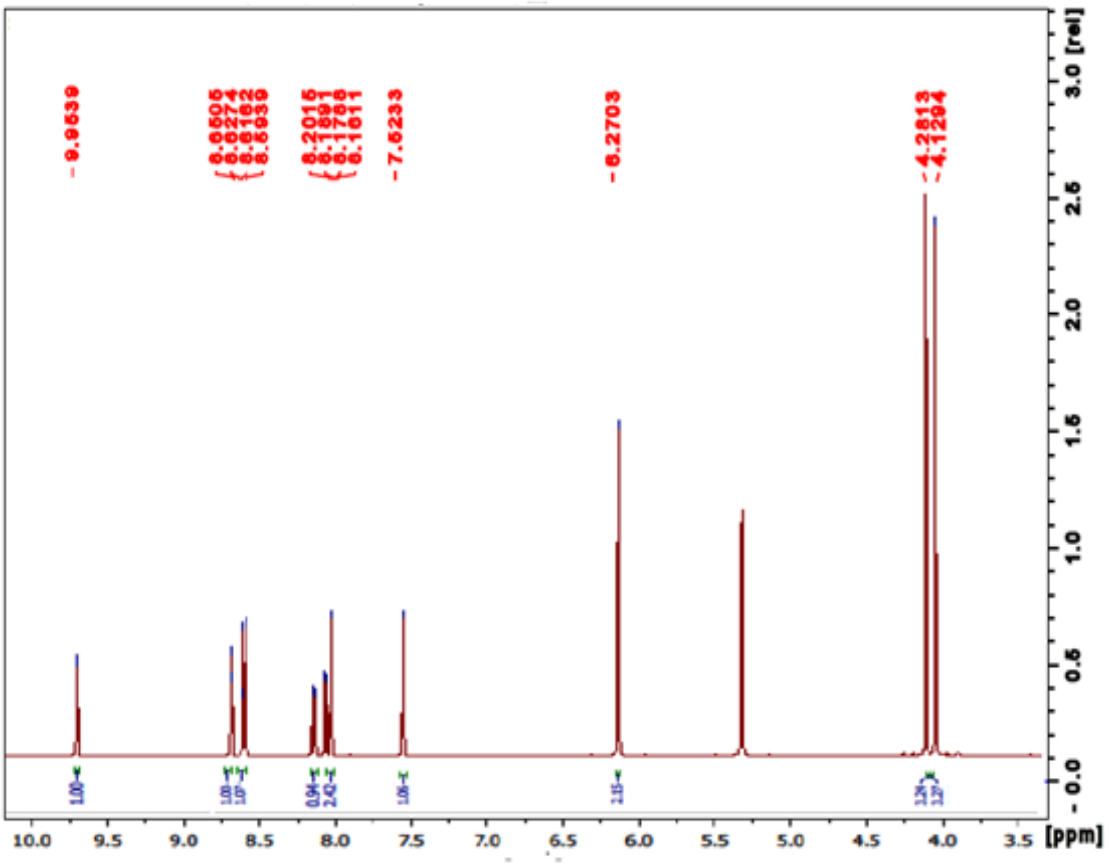

9. Spectra for Compound 10 (2,3-epoxy-6,7-methylenedioxy coniferyl alcohol)

9.1: ^{1}H and ^{13}C NMR spectrum of compound 10

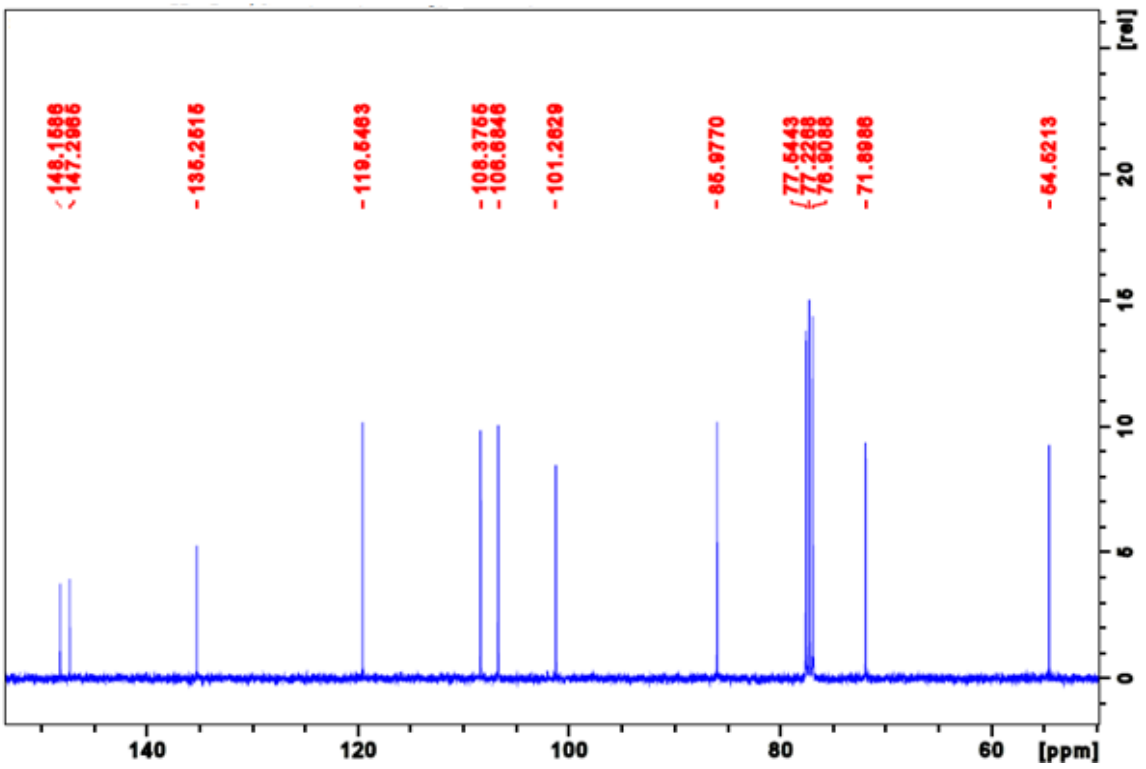

10. Spectra for Compound 46 (Sesamine)

10.1: ^{1}H and ^{13}C NMR spectrum of compound 46

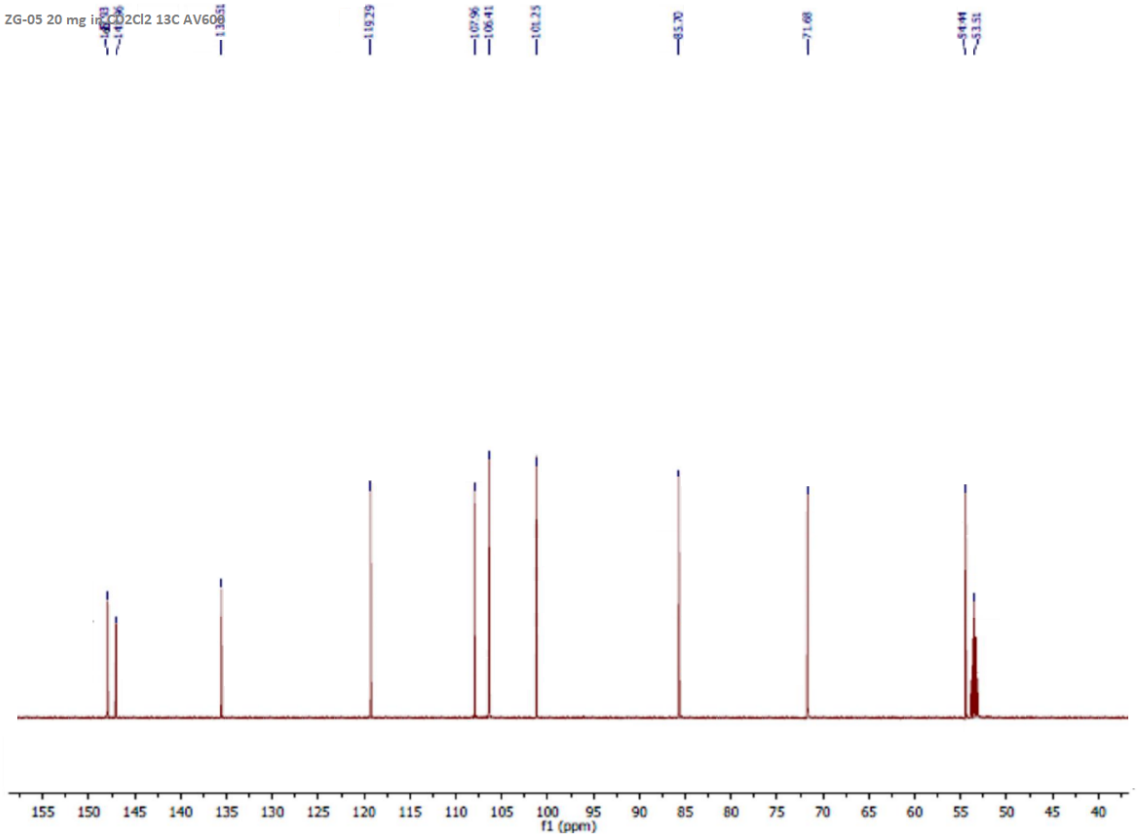

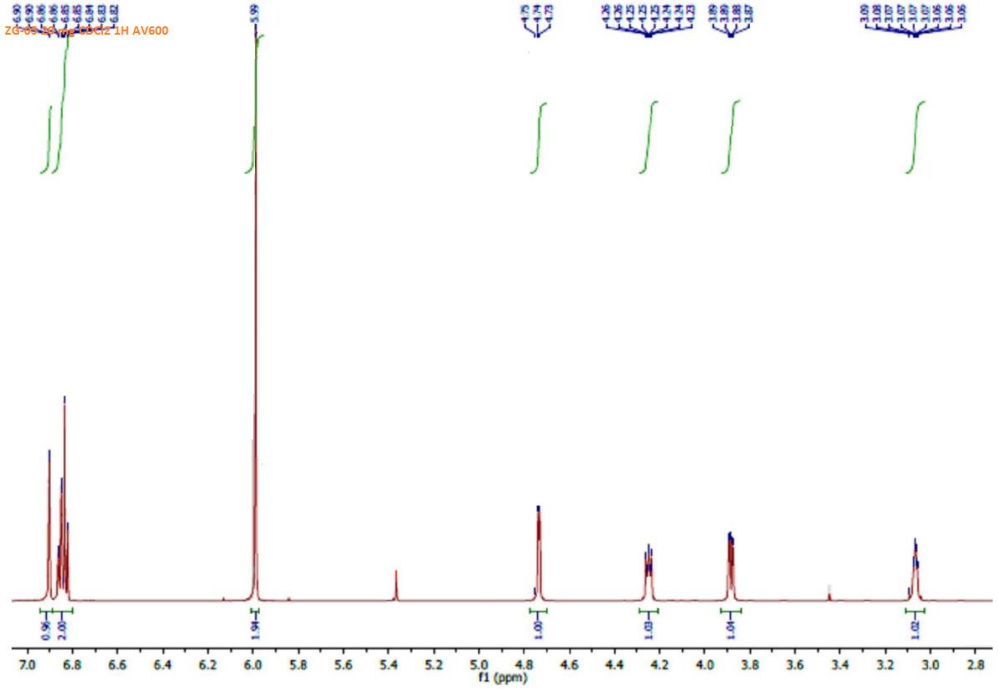

11. Spectra for Compound 21 (Skimmianine)

11.1: ^{1}H spectrum of compound 21

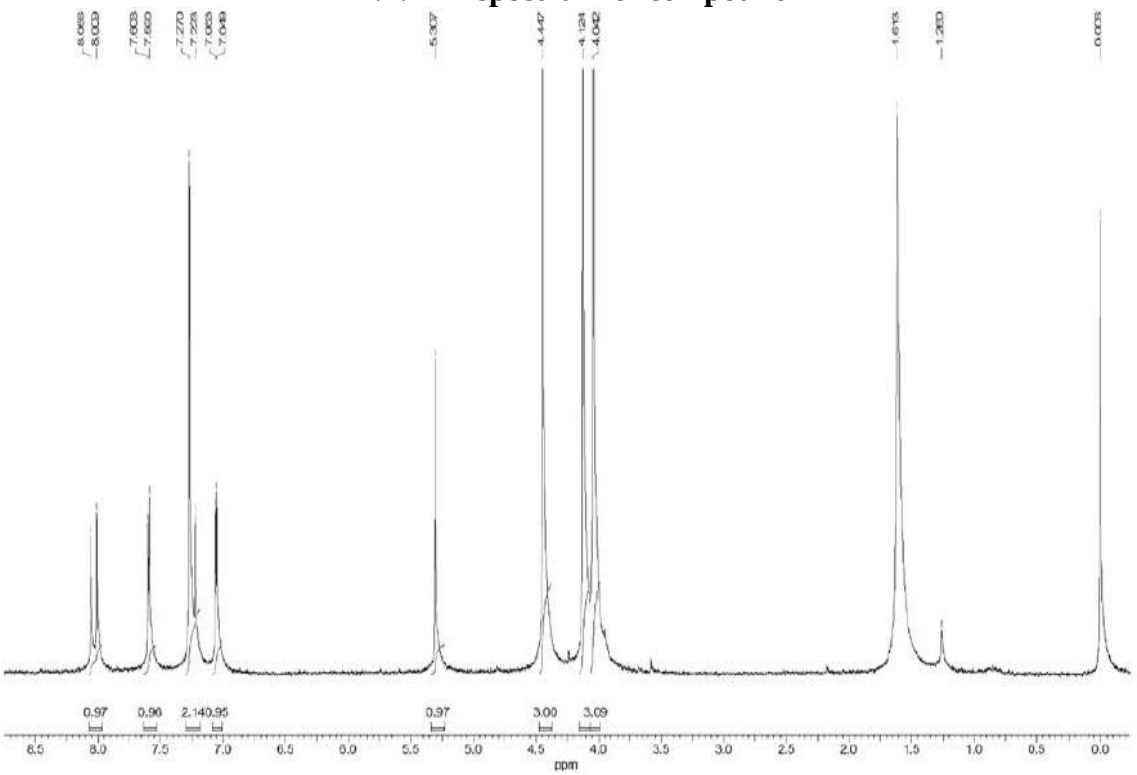

12. Lineweaver-Burk plots and Dixon secondary plots

12.1: Lineweaver-Burk plots and Dixon plots for Norchelerythrine (9)

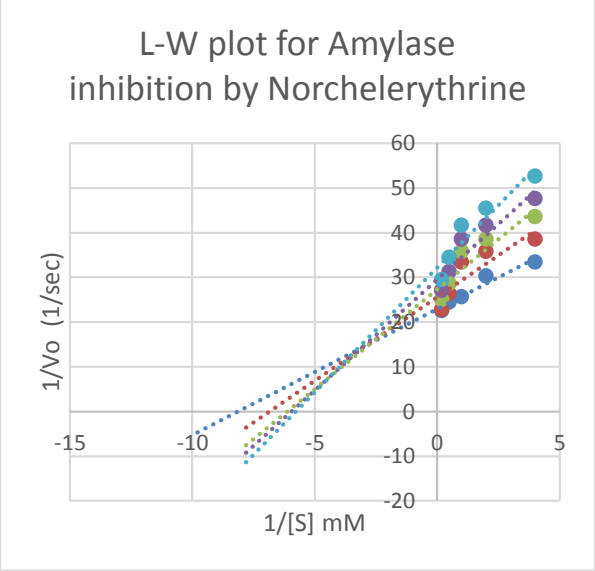

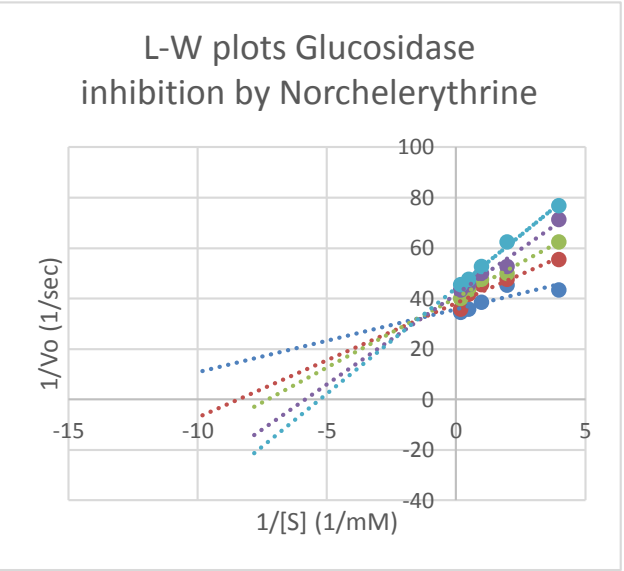

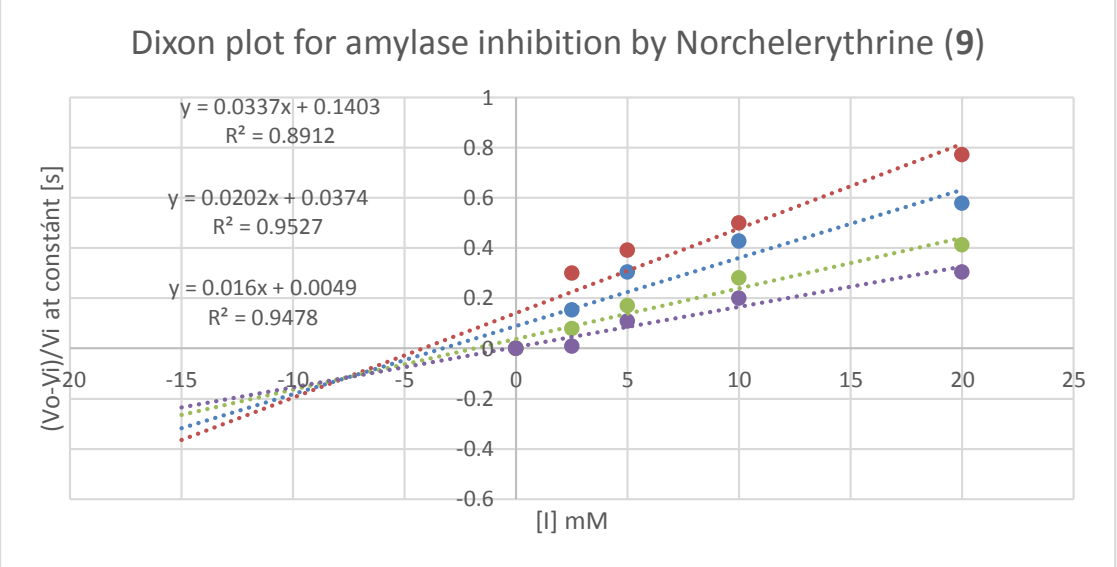

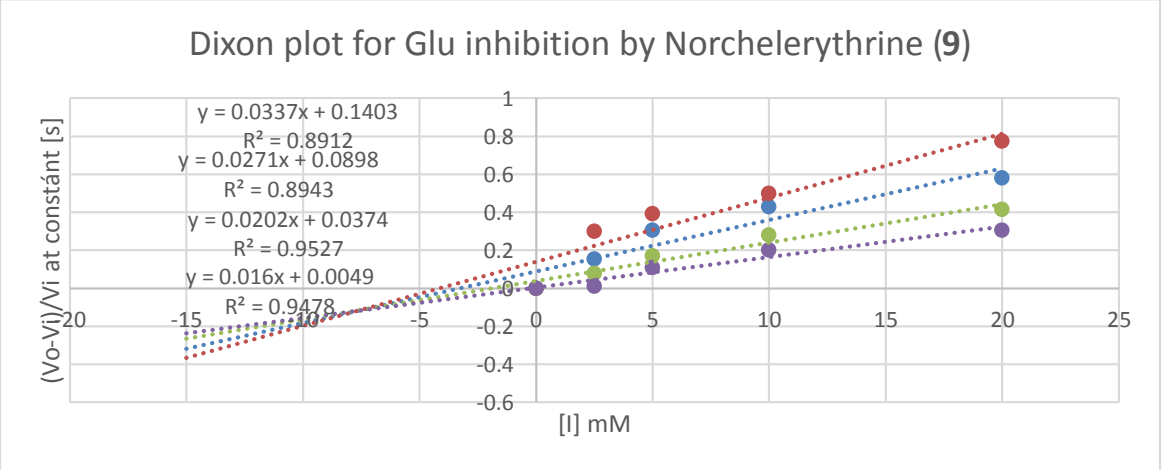

12.2: Lineweaver-Burk plots and Dixon plots for Skimmianine (21)

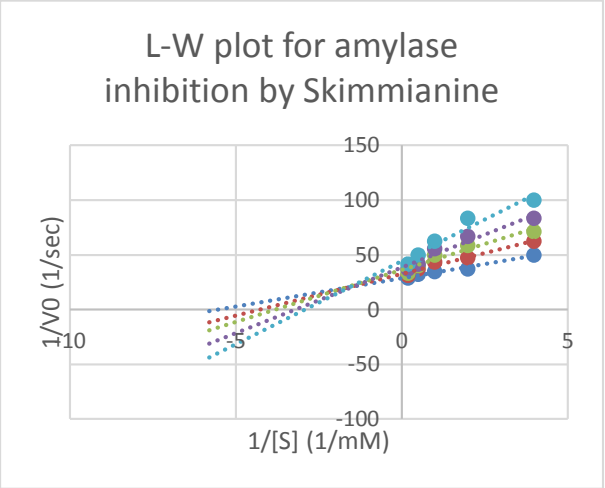

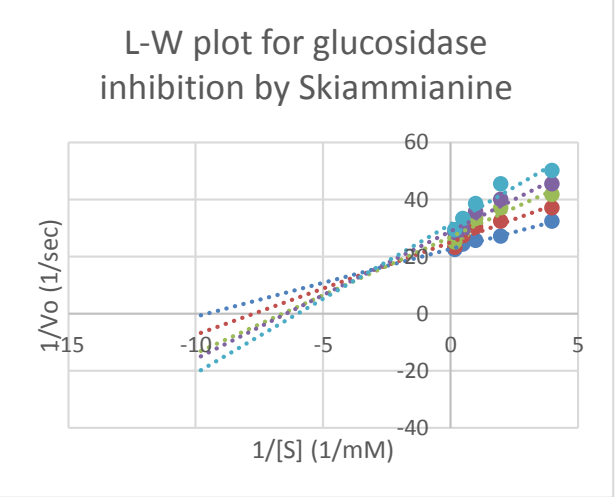

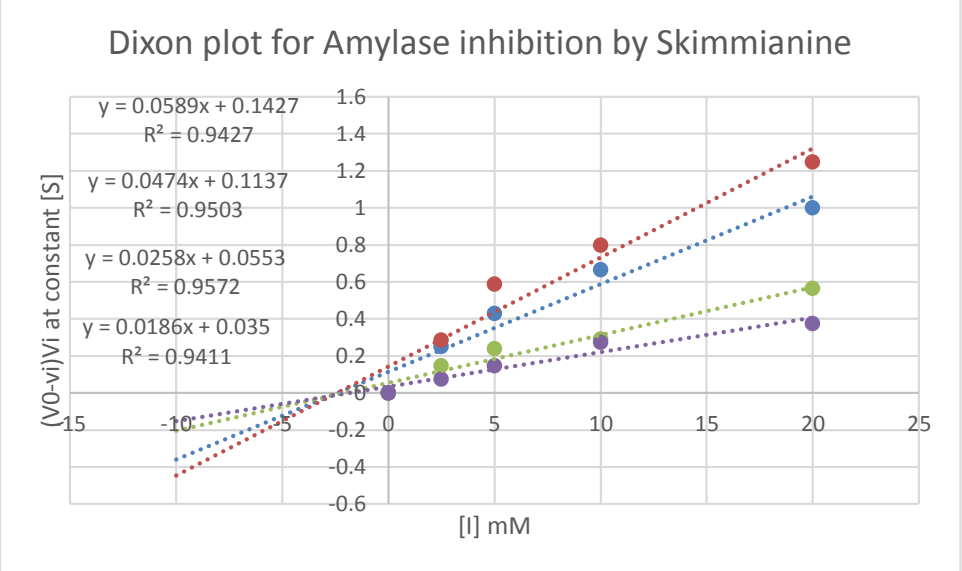

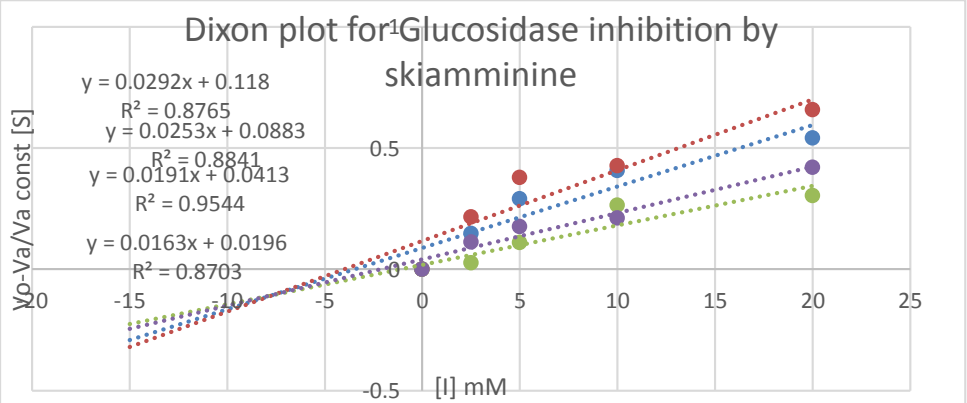

12.3: Lineweaver-Burk plots and Dixon plots for Zanthocapensine (43)

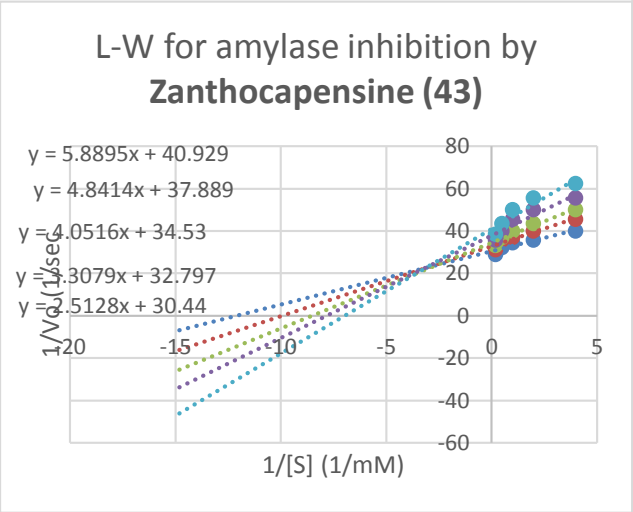

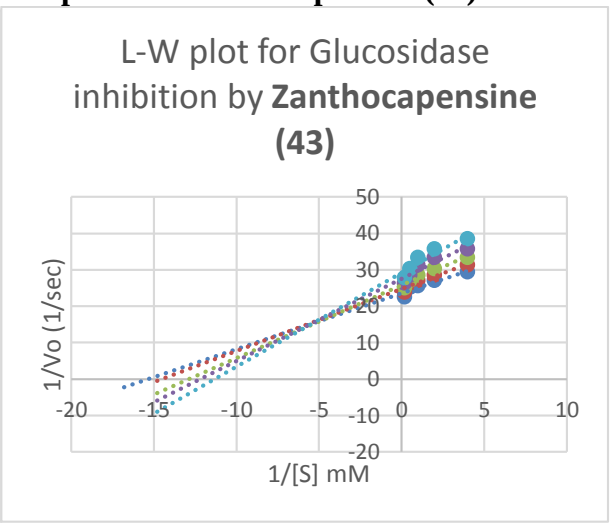

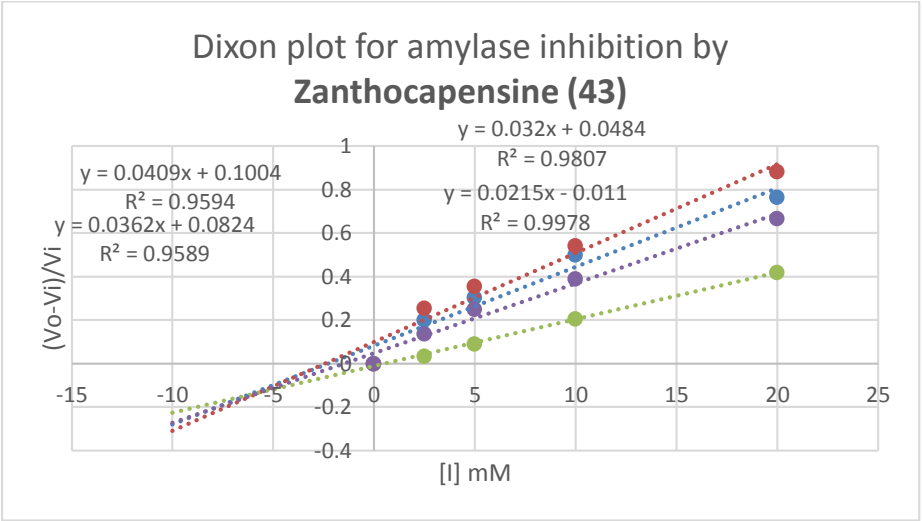

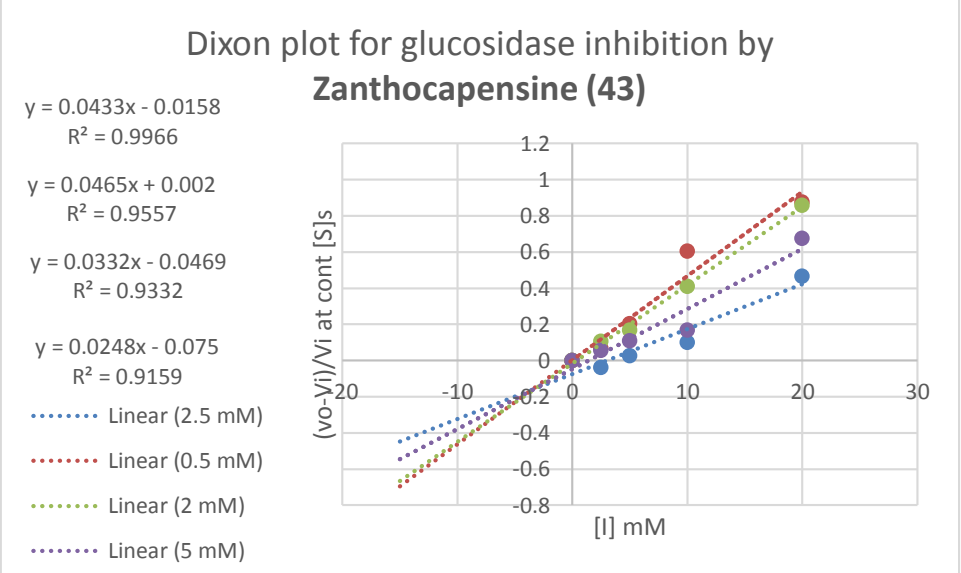

12.4: Lineweaver-Burk plots and Dixon plots for Zanthoamide D

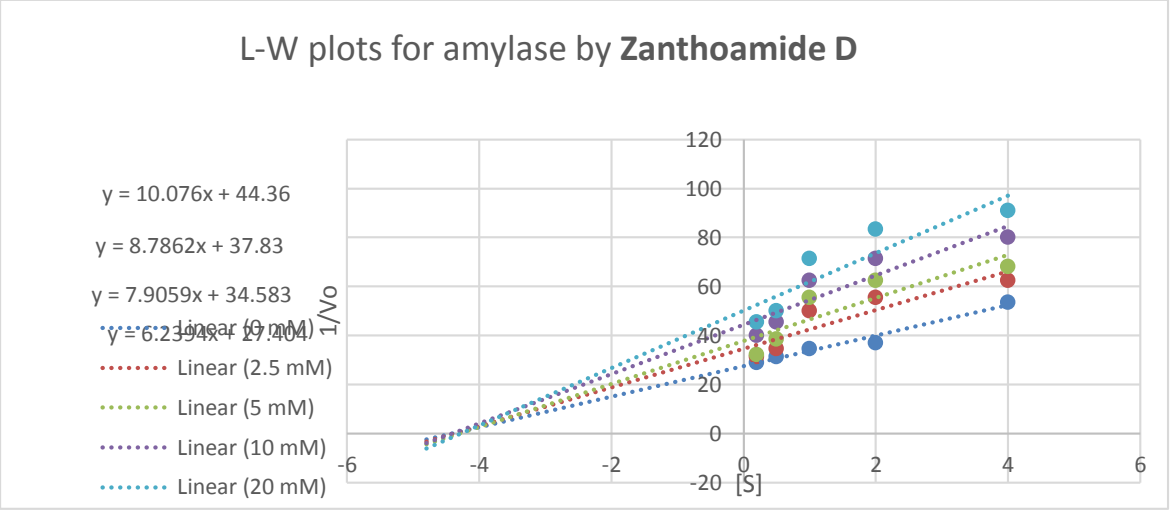

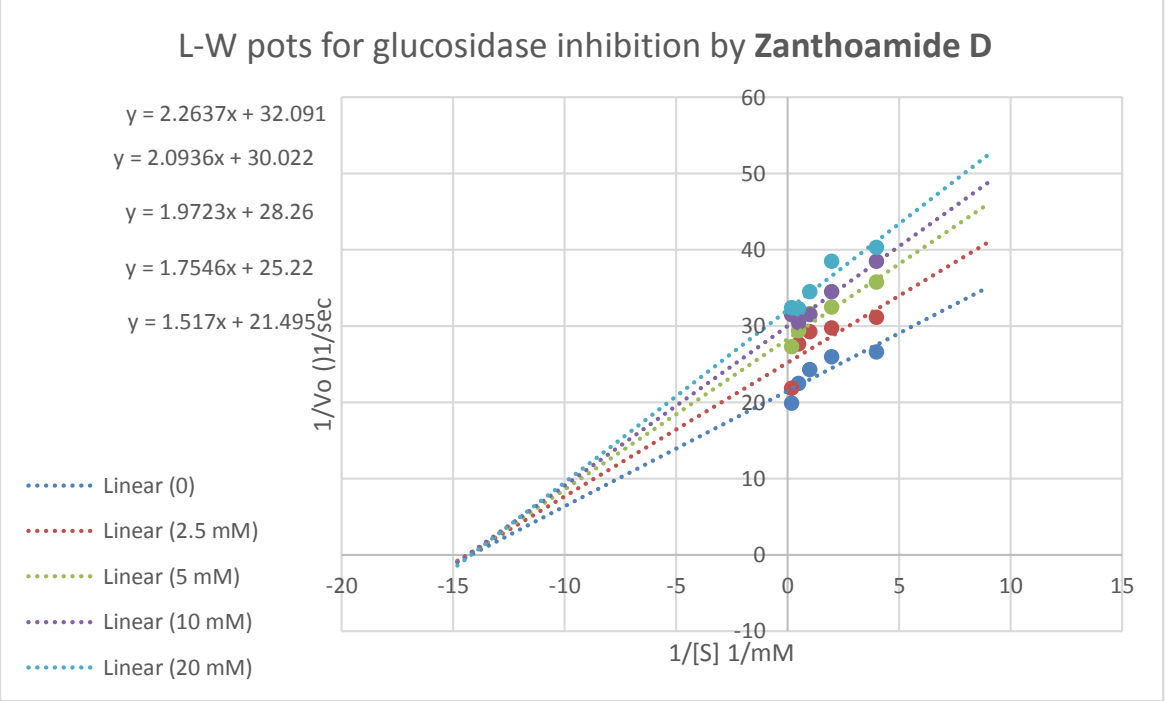

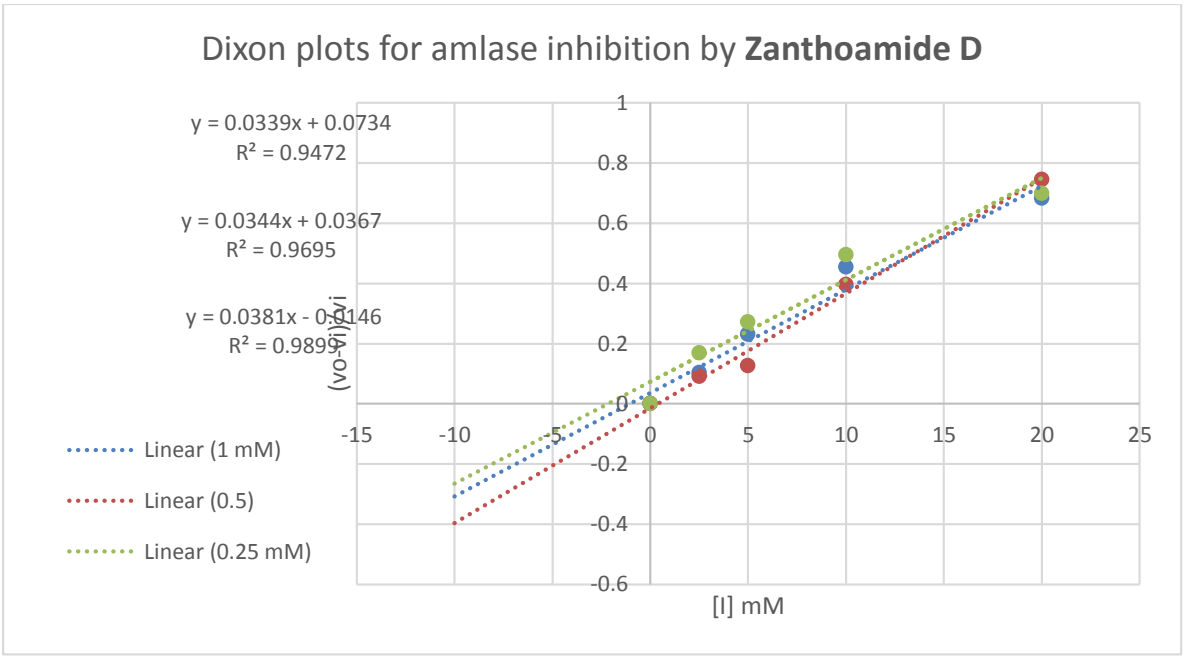
Dixon plots for amlase inhibition by **Zanthoamide D**
y = 0.0339x + 0.0734
R² = 0.9472
y = 0.0344x + 0.0367
R² = 0.9695
y = 0.0381x - 0.0146
R² = 0.9899
(vo-vi)/vi
[I] mM
Linear (1 mM)
Linear (0.5)
Linear (0.25 mM)

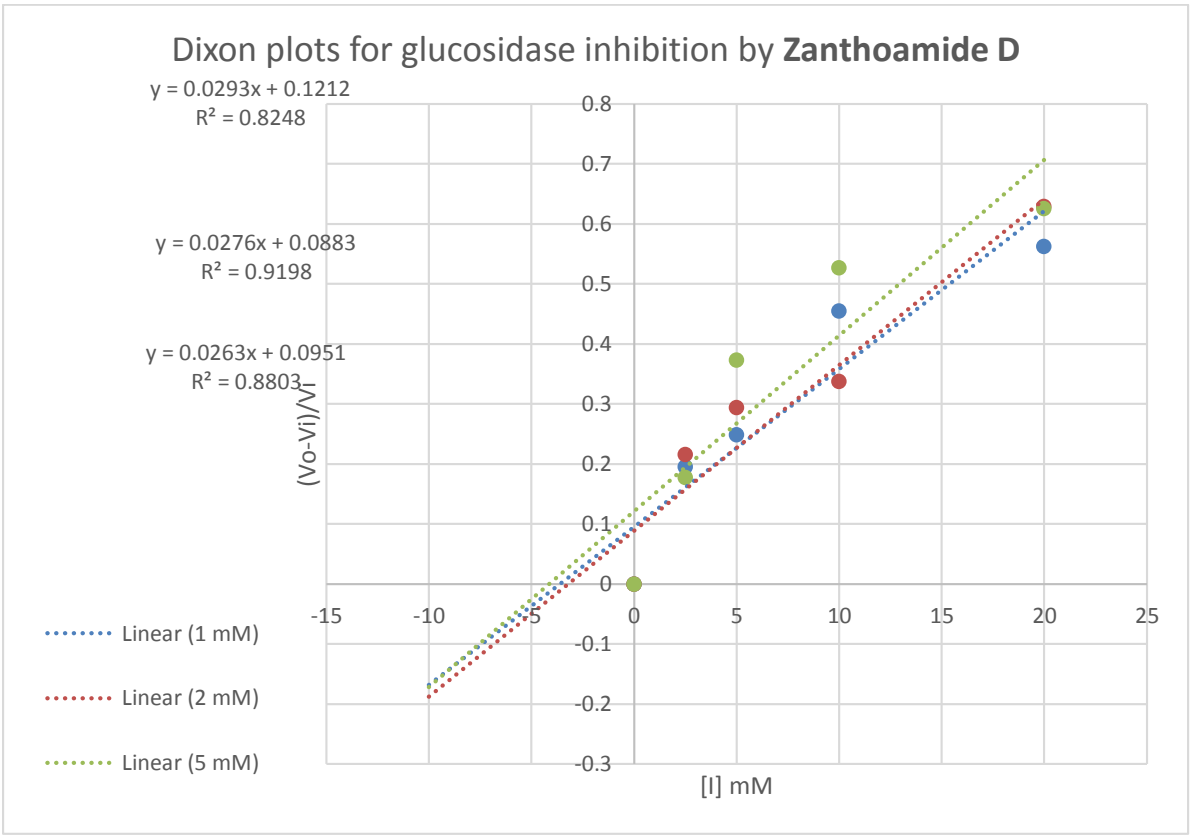
Dixon plots for glucosidase inhibition by **Zanthoamide D**
y = 0.0293x + 0.1212
R² = 0.8248
y = 0.0276x + 0.0883
R² = 0.9198
y = 0.0263x + 0.0951
R² = 0.8803
(Vo-Vi)/Vi
[I] mM
Linear (1 mM)
Linear (2 mM)
Linear (5 mM)

12.5: Lineweaver-Burk plots and Dixon plots for Sesamine (46)

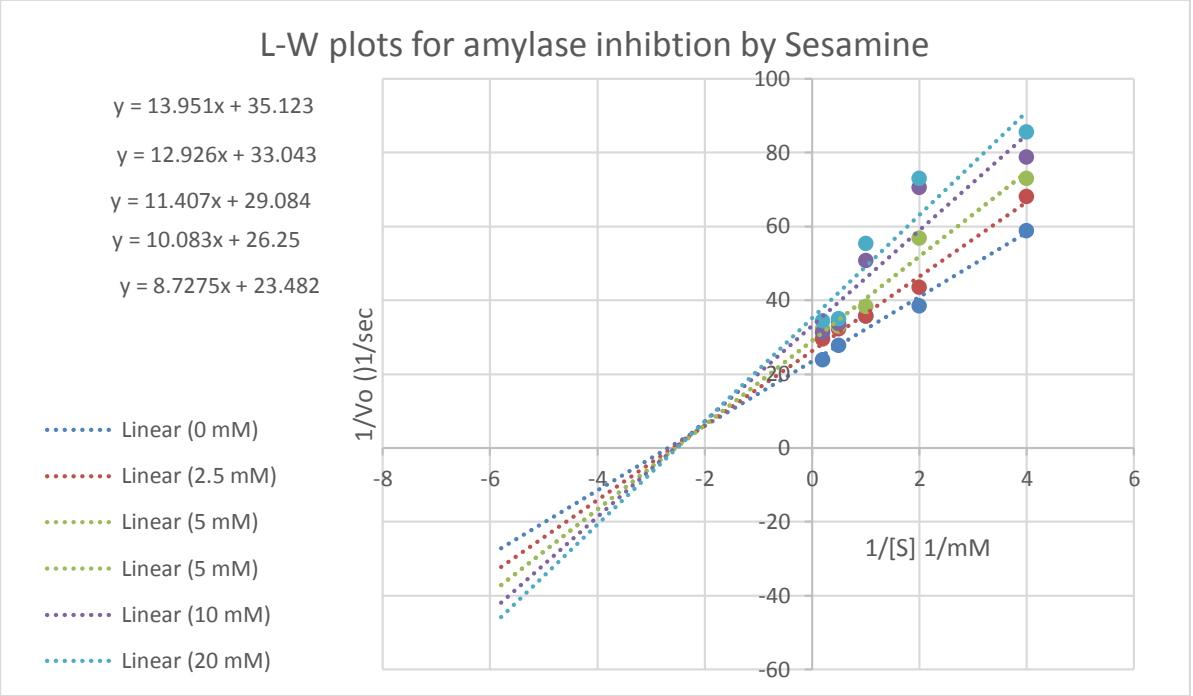

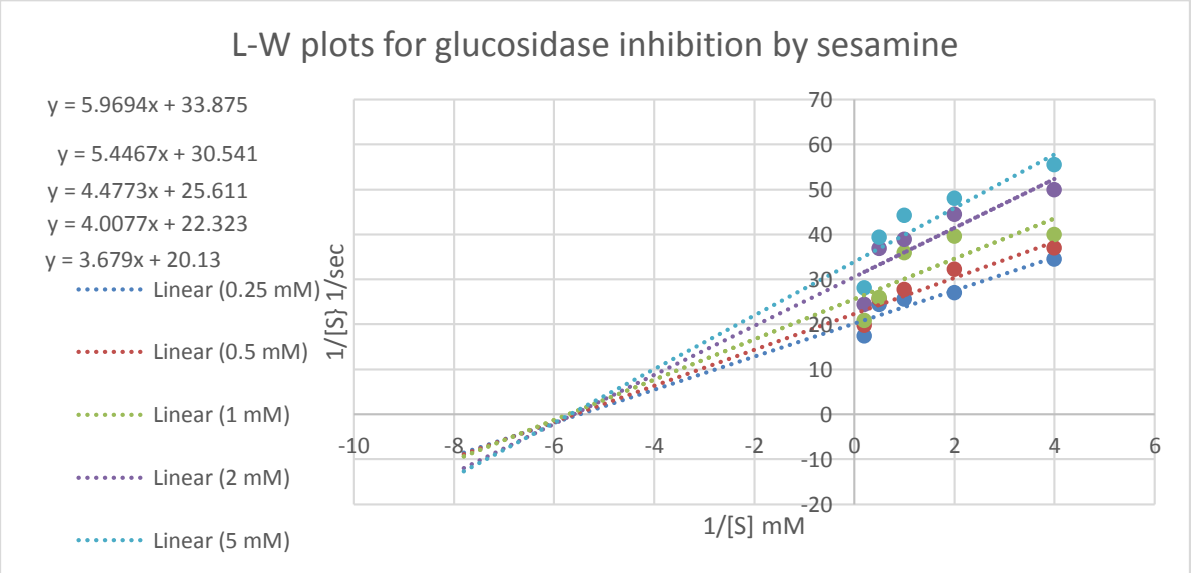

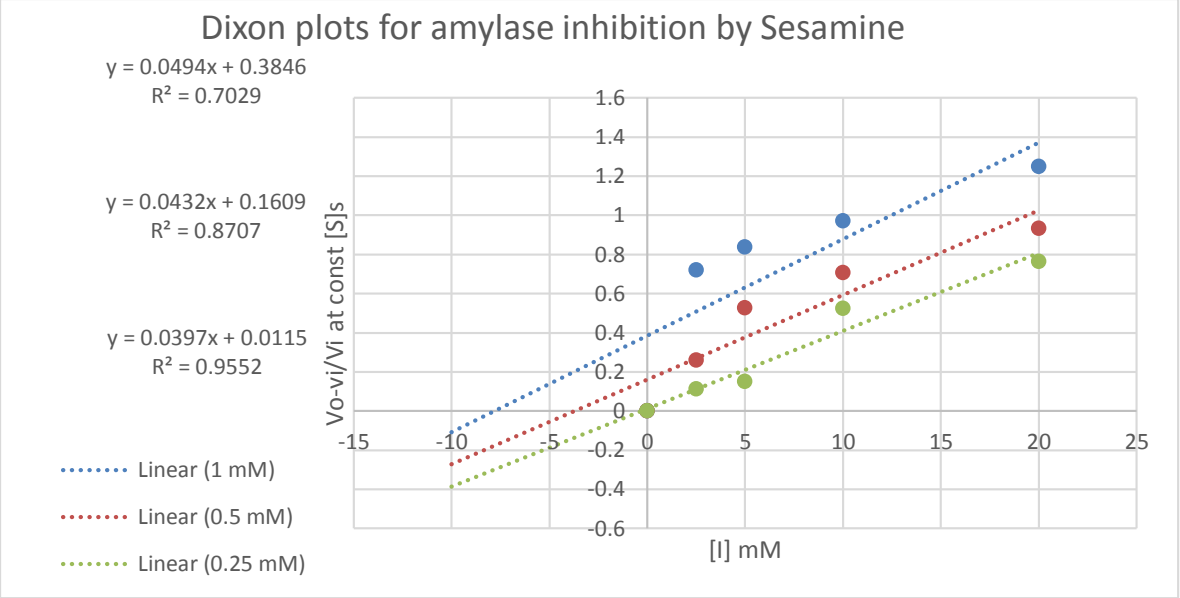
Dixon plots for amylase inhibition by Sesamine
y = 0.0494x + 0.3846
R² = 0.7029
y = 0.0432x + 0.1609
R² = 0.8707
y = 0.0397x + 0.0115
R² = 0.9552
Linear (1 mM)
Linear (0.5 mM)
Linear (0.25 mM)
Vo-vi/Vi at const [S]s
[I] mM
1.6
1.4
1.2
1
0.8
0.6
0.4
0.2
0
-0.2
-0.4
-0.6
-15
-10
-5
0
5
10
15
20
25

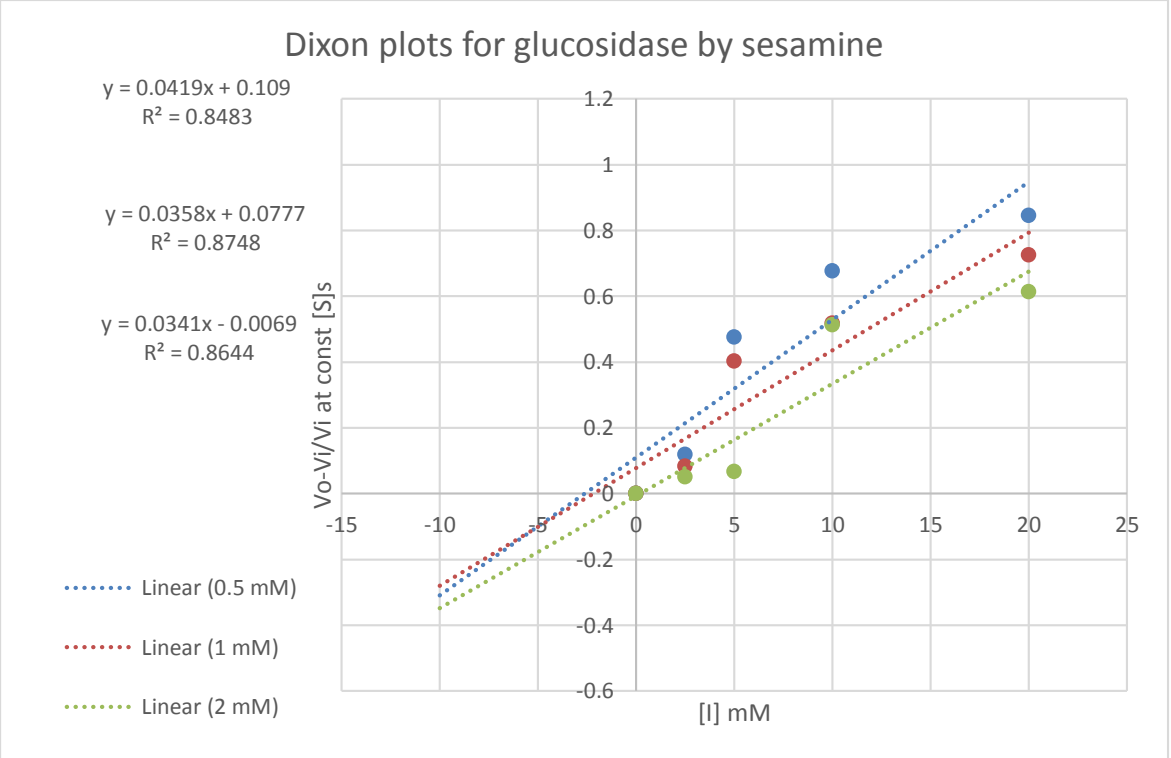
Dixon plots for glucosidase by sesamine
y = 0.0419x + 0.109
R² = 0.8483
y = 0.0358x + 0.0777
R² = 0.8748
y = 0.0341x - 0.0069
R² = 0.8644
Linear (0.5 mM)
Linear (1 mM)
Linear (2 mM)
Vo-Vi/Vi at const [S]s
[I] mM
1.2
1
0.8
0.6
0.4
0.2
0
-0.2
-0.4
-0.6
-15
-10
-5
0
5
10
15
20
25

12.6: Lineweaver-Burk plots and Dixon plots for Chalybemide A

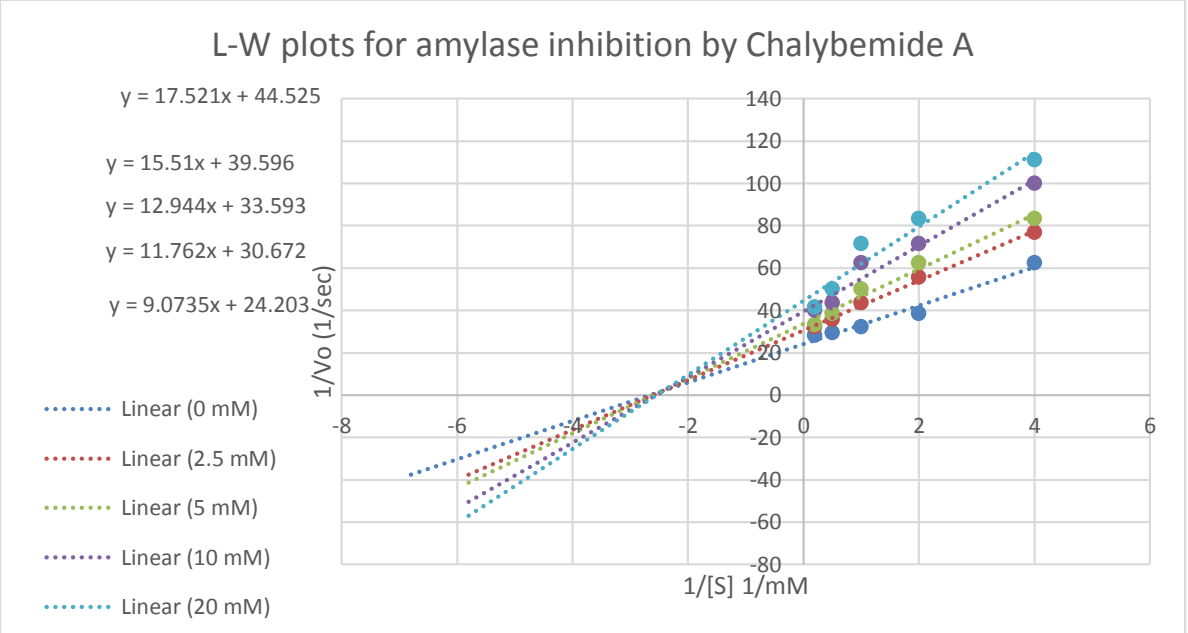

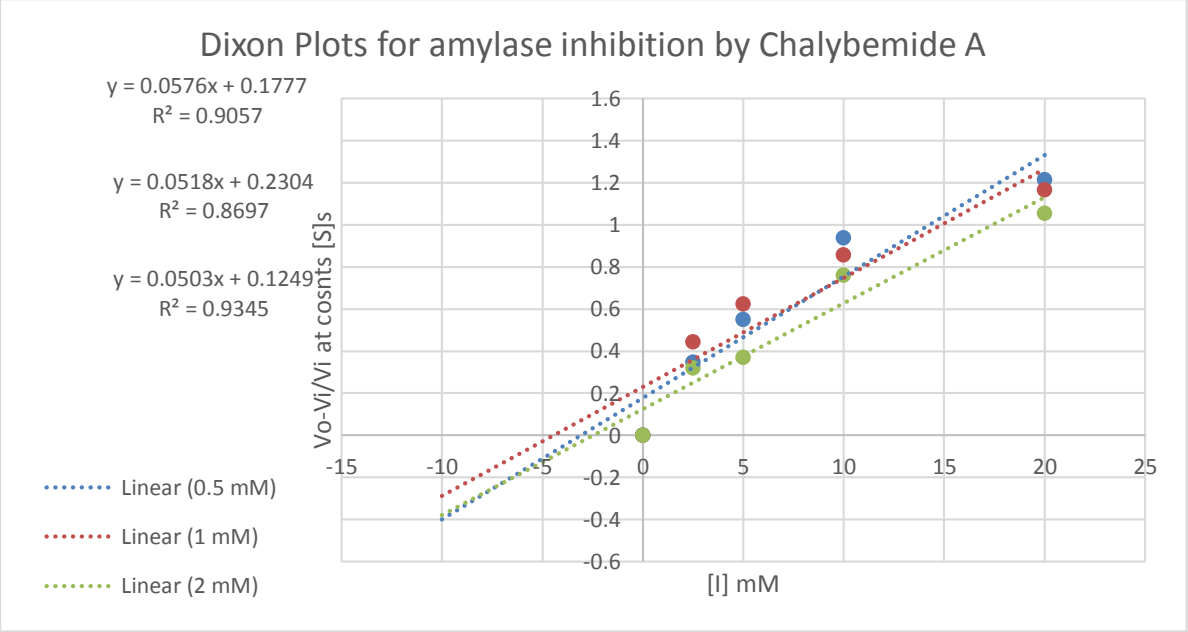

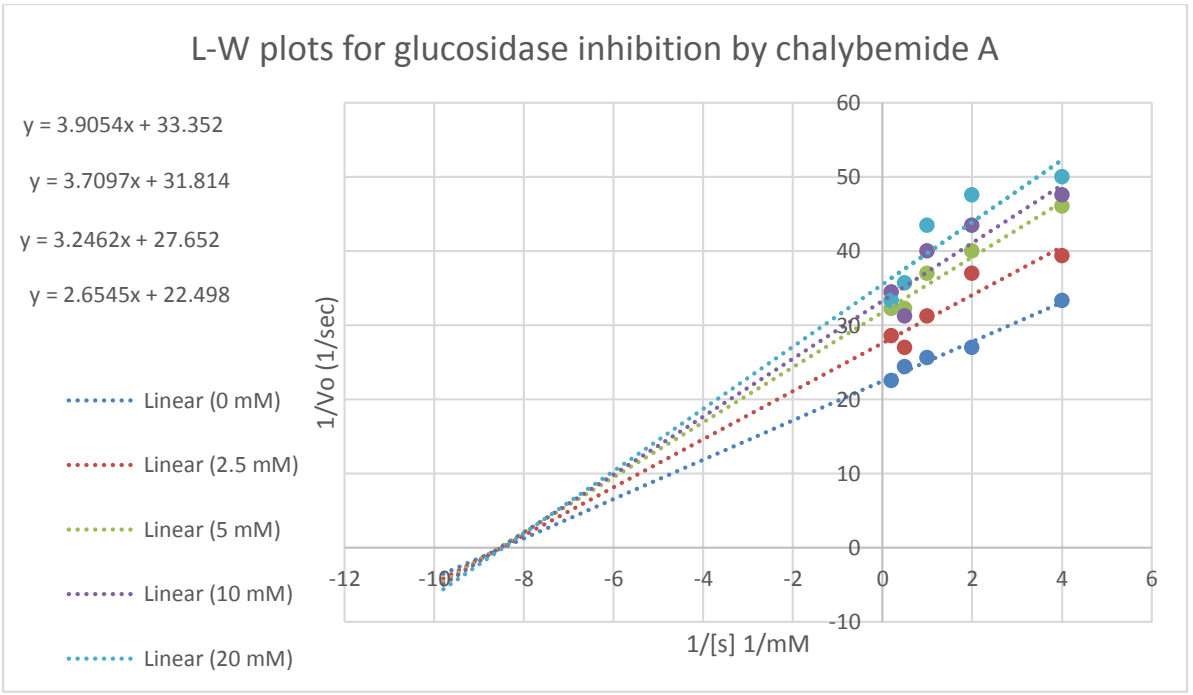
L-W plots for glucosidase inhibition by chalybemide A
y = 3.9054x + 33.352
y = 3.7097x + 31.814
y = 3.2462x + 27.652
y = 2.6545x + 22.498
Linear (0 mM)
Linear (2.5 mM)
Linear (5 mM)
Linear (10 mM)
Linear (20 mM)
1/Vo (1/sec)
1/[s] 1/mM
60
50
40
30
20
10
0
-10
-12
-10
-8
-6
-4
-2
0
2
4
6

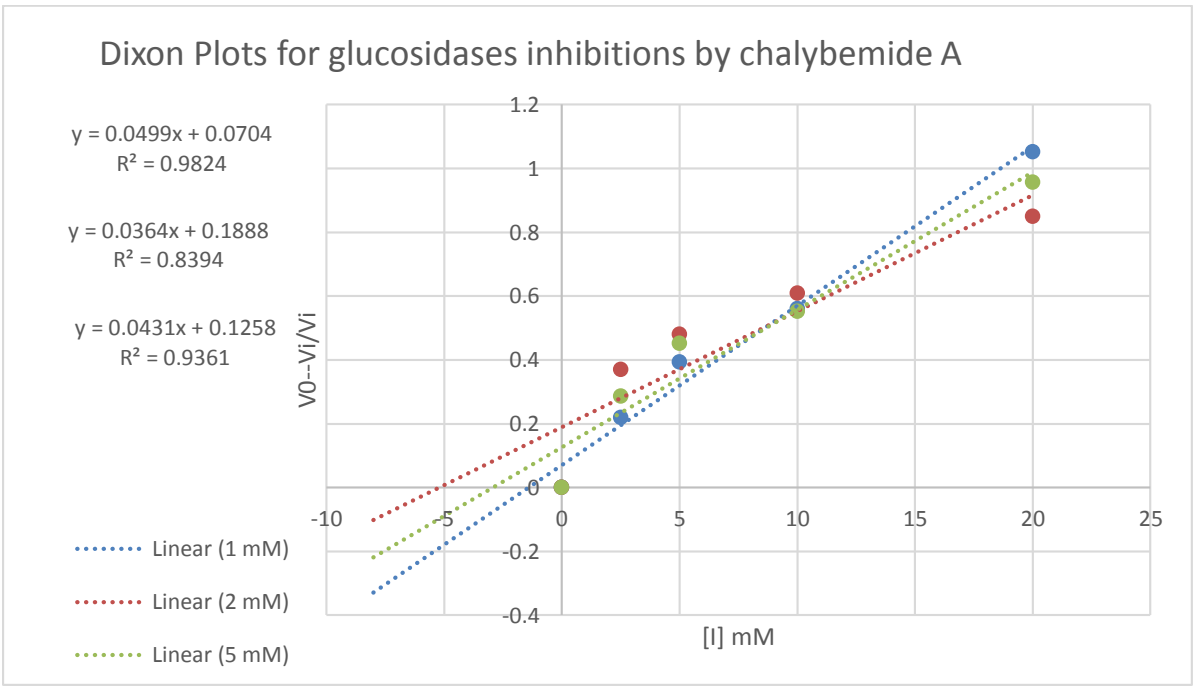
Dixon Plots for glucosidases inhibitions by chalybemide A
y = 0.0499x + 0.0704
R² = 0.9824
y = 0.0364x + 0.1888
R² = 0.8394
y = 0.0431x + 0.1258
R² = 0.9361
Linear (1 mM)
Linear (2 mM)
Linear (5 mM)
V0--Vi/Vi
[I] mM
1.2
1
0.8
0.6
0.4
0.2
0
-0.2
-0.4
-10
-5
0
5
10
15
20
25

12.7: Lineweaver-Burk plots and Dixon plots for Chalybemide B

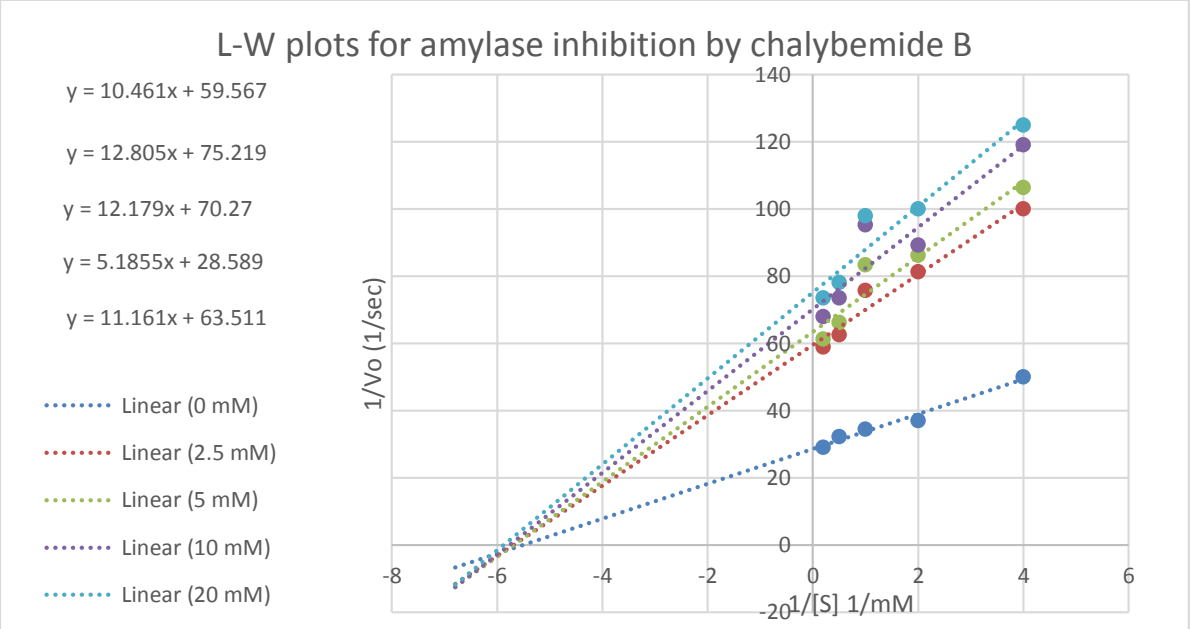

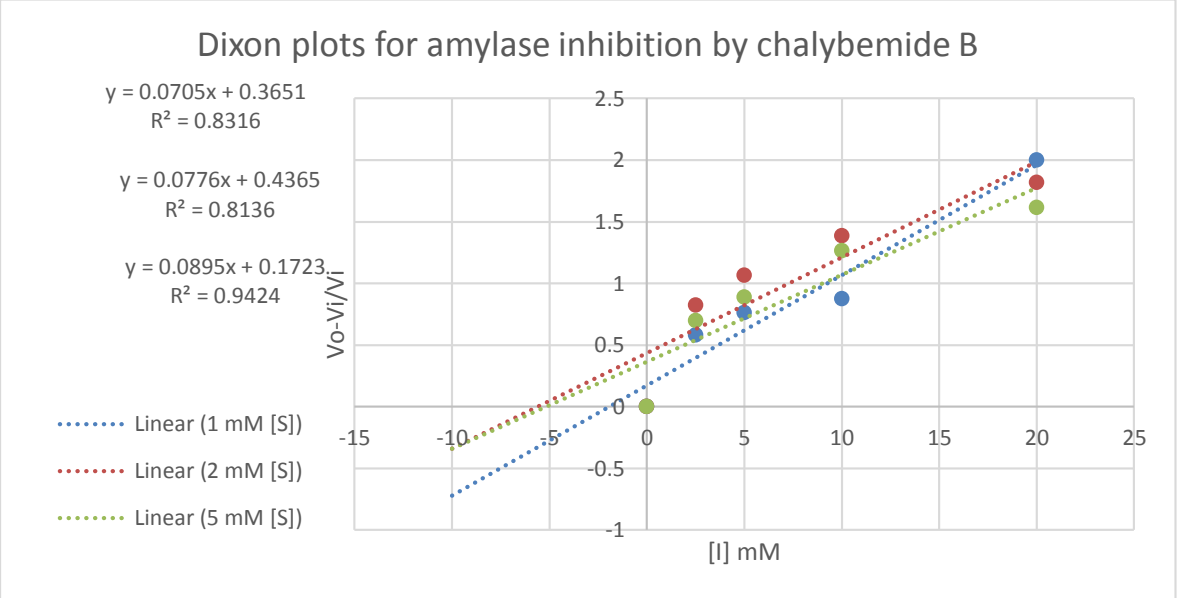

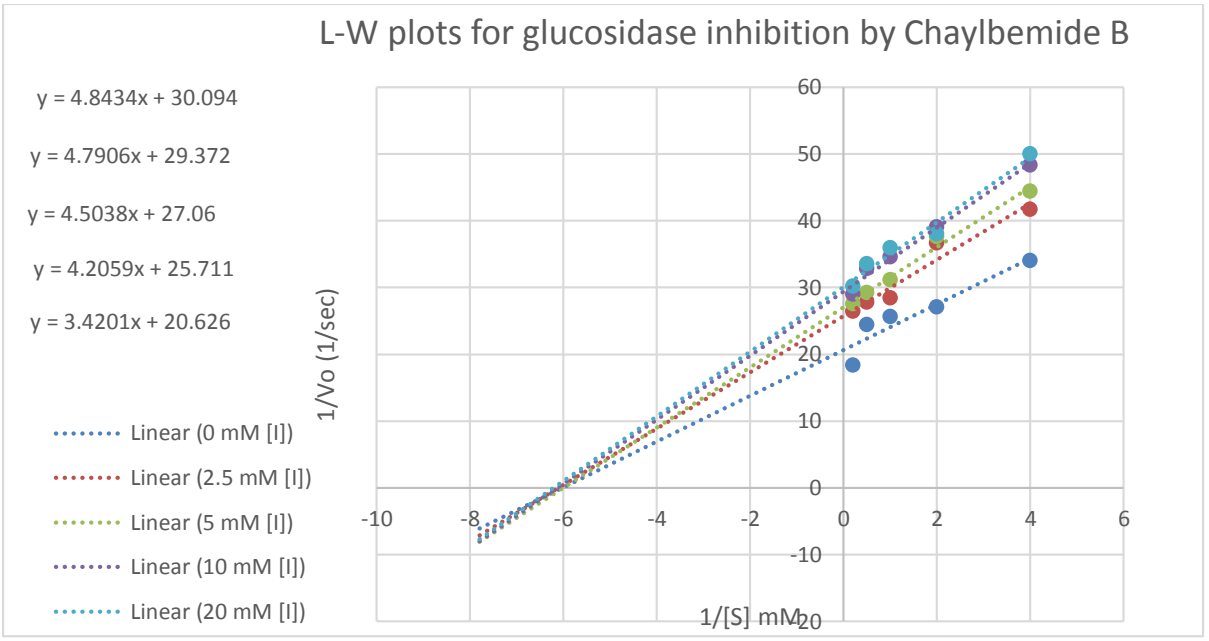
L-W plots for glucosidase inhibition by Chaylbemide B
y = 4.8434x + 30.094
y = 4.7906x + 29.372
y = 4.5038x + 27.06
y = 4.2059x + 25.711
y = 3.4201x + 20.626
Linear (0 mM [I])
Linear (2.5 mM [I])
Linear (5 mM [I])
Linear (10 mM [I])
Linear (20 mM [I])
1/Vo (1/sec)
1/[S] mM
60
50
40
30
20
10
0
-10
-20
-10
-8
-6
-4
-2
0
2
4
6

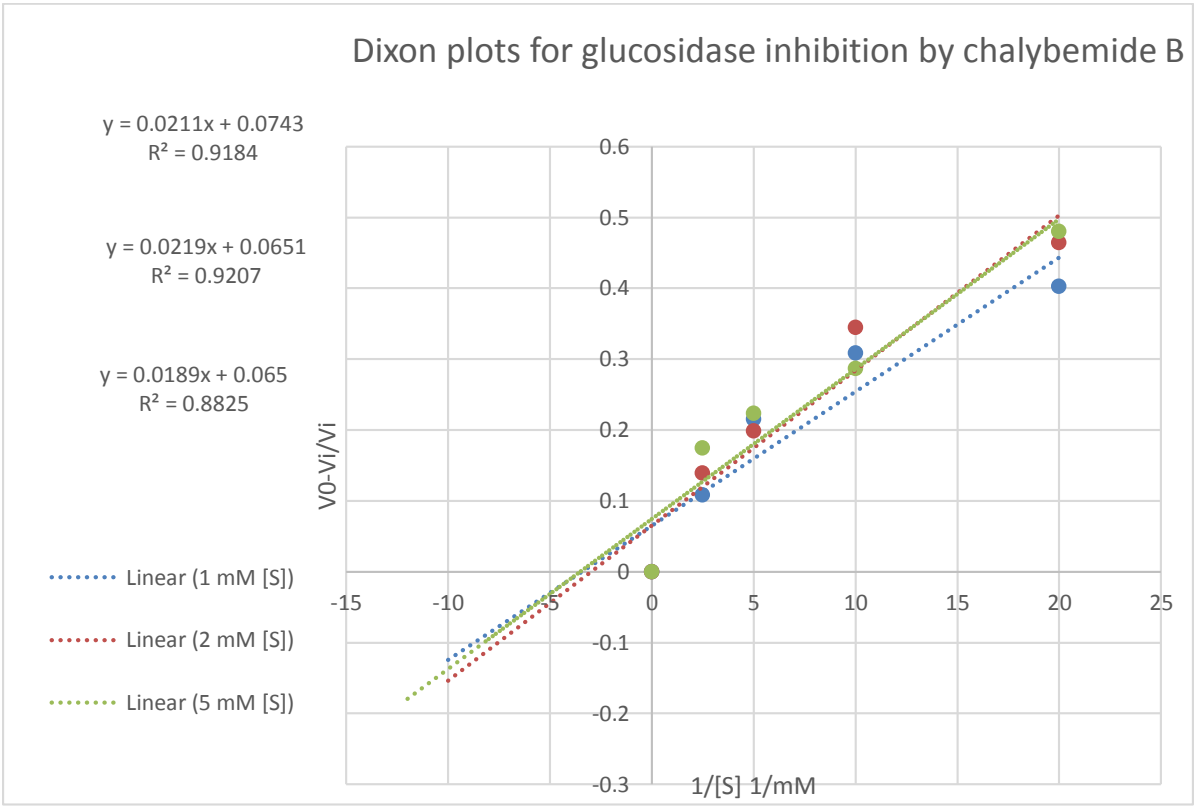
Dixon plots for glucosidase inhibition by chalybemide B
y = 0.0211x + 0.0743
R² = 0.9184
y = 0.0219x + 0.0651
R² = 0.9207
y = 0.0189x + 0.065
R² = 0.8825
Linear (1 mM [S])
Linear (2 mM [S])
Linear (5 mM [S])
V0-Vi/Vi
1/[S] 1/mM
0.6
0.5
0.4
0.3
0.2
0.1
0
-0.1
-0.2
-0.3
-15
-10
-5
0
5
10
15
20
25

12.8: Lineweaver-Burk plots and Dixon plots for Zanthocapensol

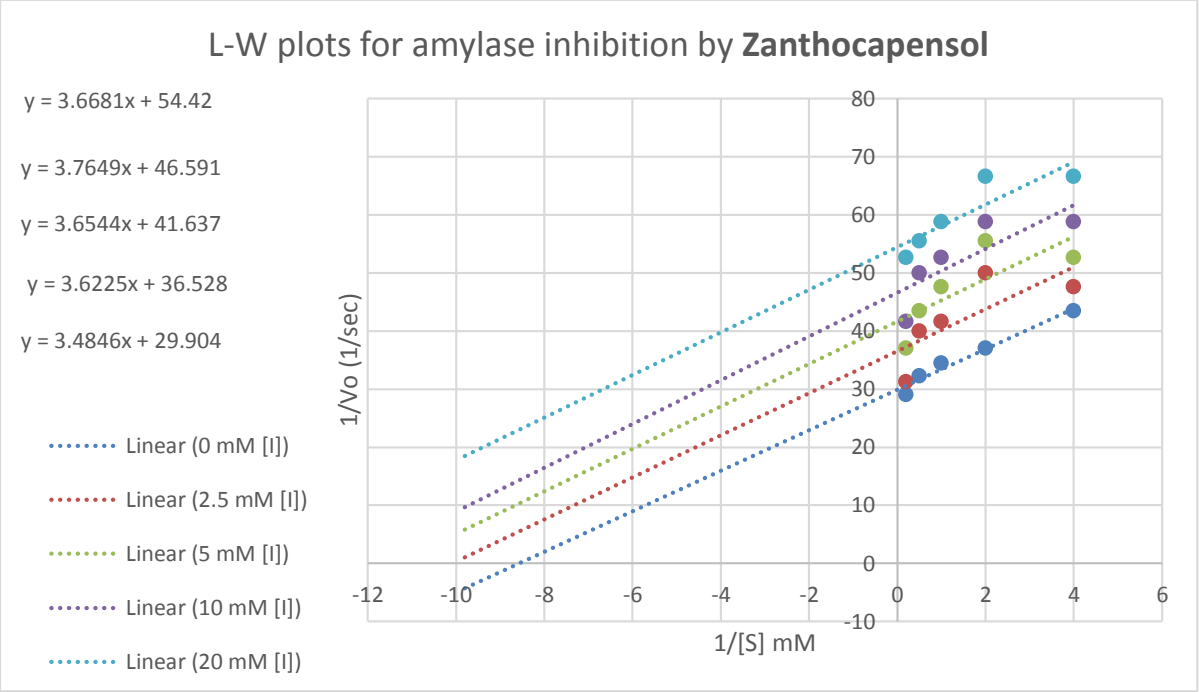

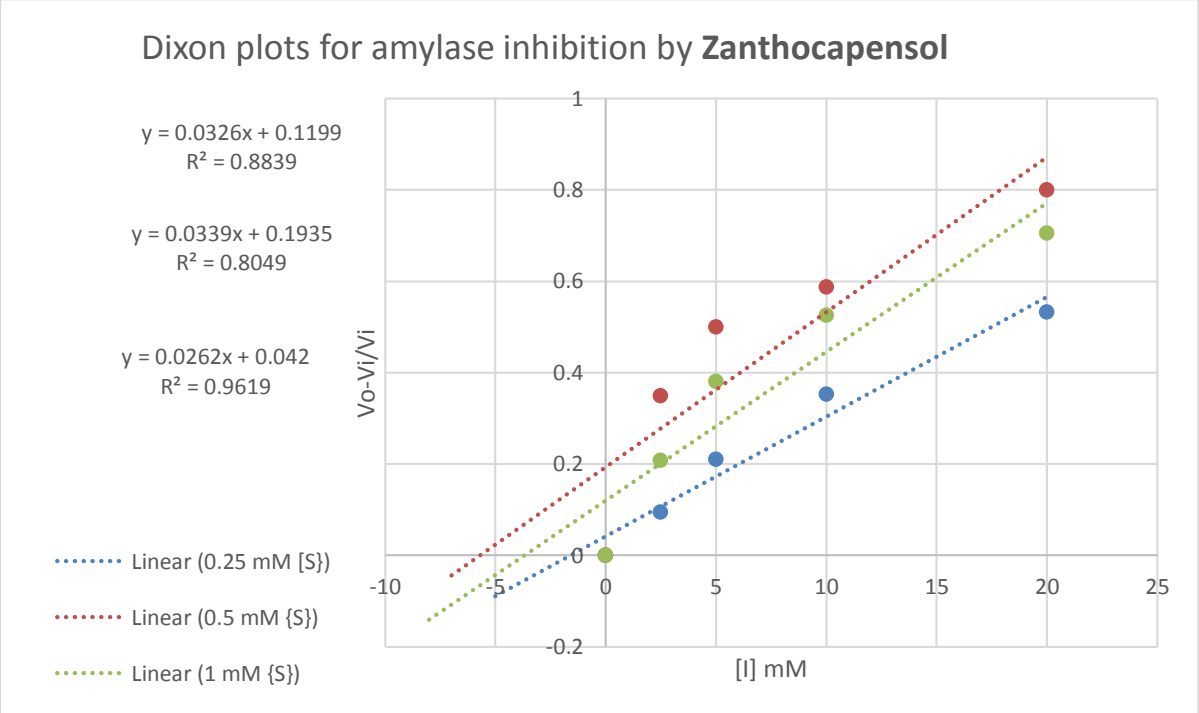

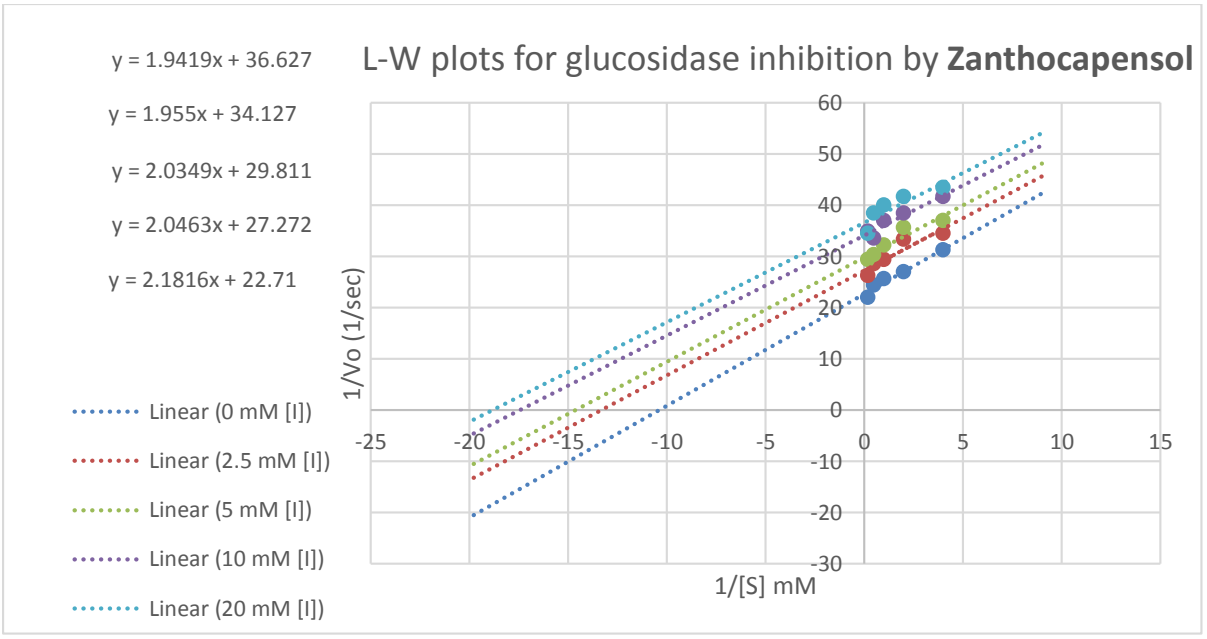
y = 1.9419x + 36.627
y = 1.955x + 34.127
y = 2.0349x + 29.811
y = 2.0463x + 27.272
y = 2.1816x + 22.71
L-W plots for glucosidase inhibition by **Zanthocapensol**
1/Vo (1/sec)
1/[S] mM
Linear (0 mM [I])
Linear (2.5 mM [I])
Linear (5 mM [I])
Linear (10 mM [I])
Linear (20 mM [I])

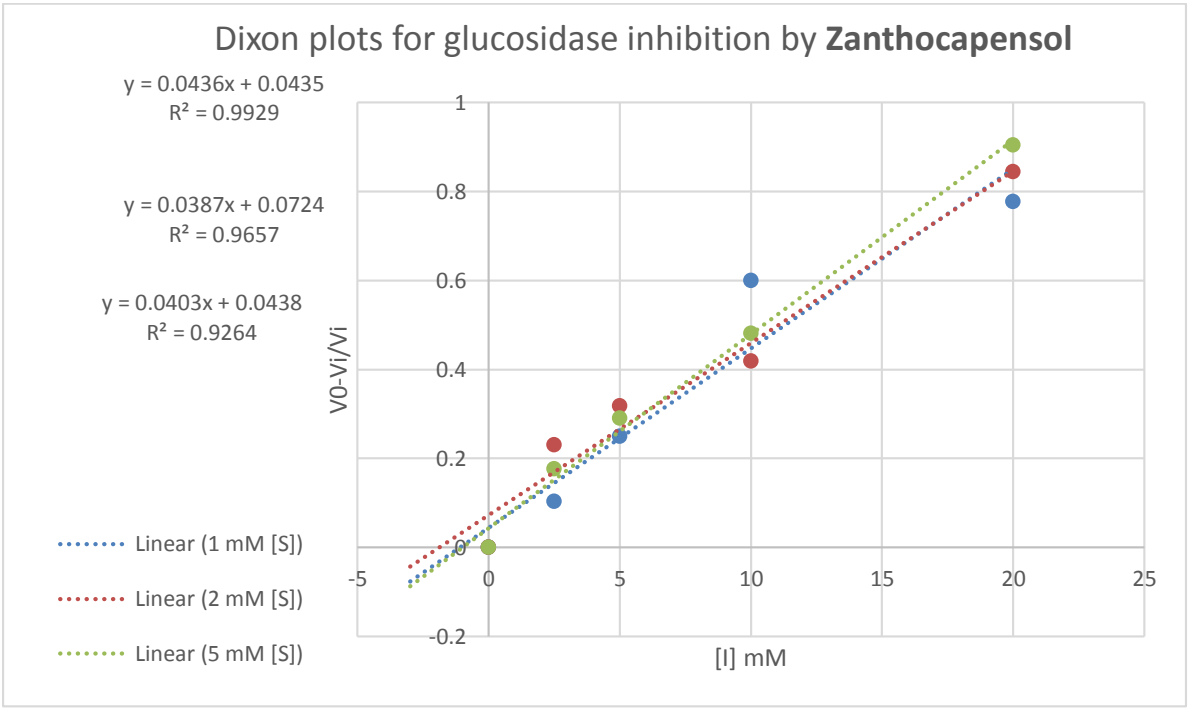
Dixon plots for glucosidase inhibition by **Zanthocapensol**
y = 0.0436x + 0.0435
R² = 0.9929
y = 0.0387x + 0.0724
R² = 0.9657
y = 0.0403x + 0.0438
R² = 0.9264
V0-Vi/Vi
[I] mM
Linear (1 mM [S])
Linear (2 mM [S])
Linear (5 mM [S])

12.9: Lineweaver-Burk plots and Dixon plots for Chalybemide C

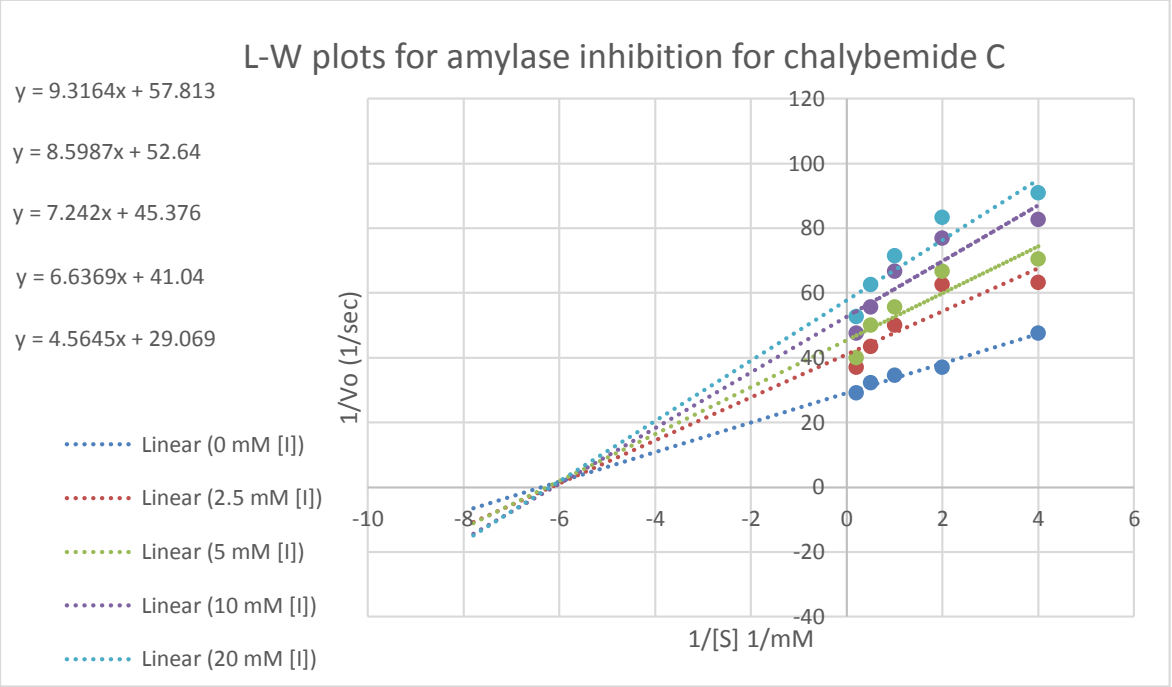

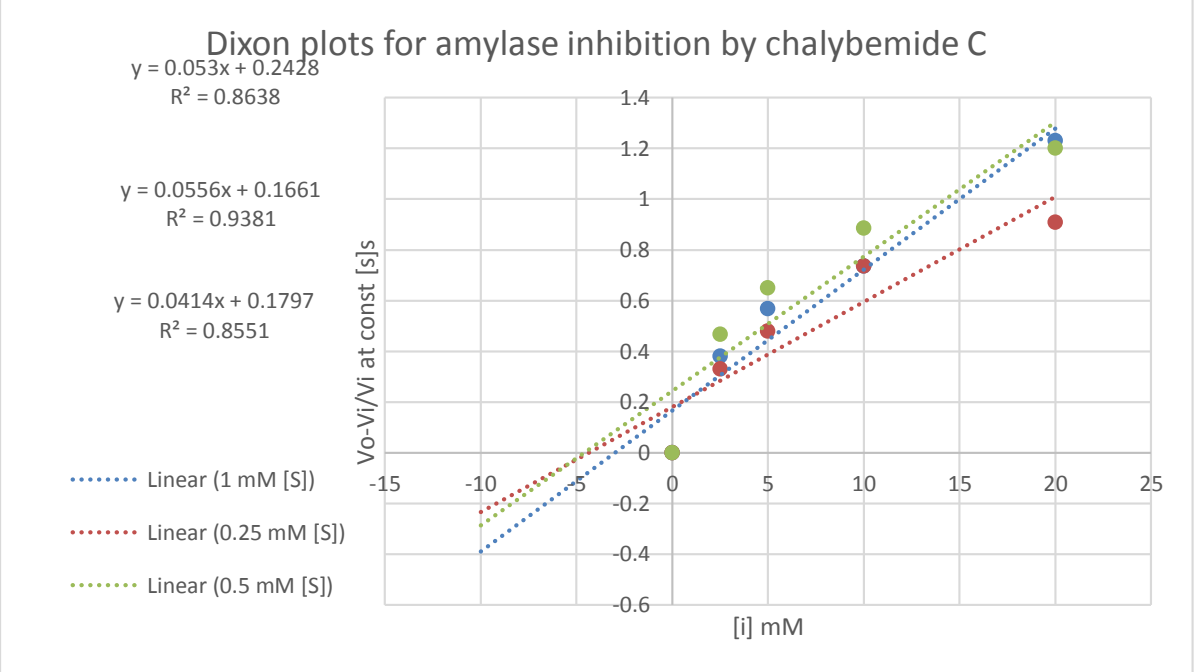

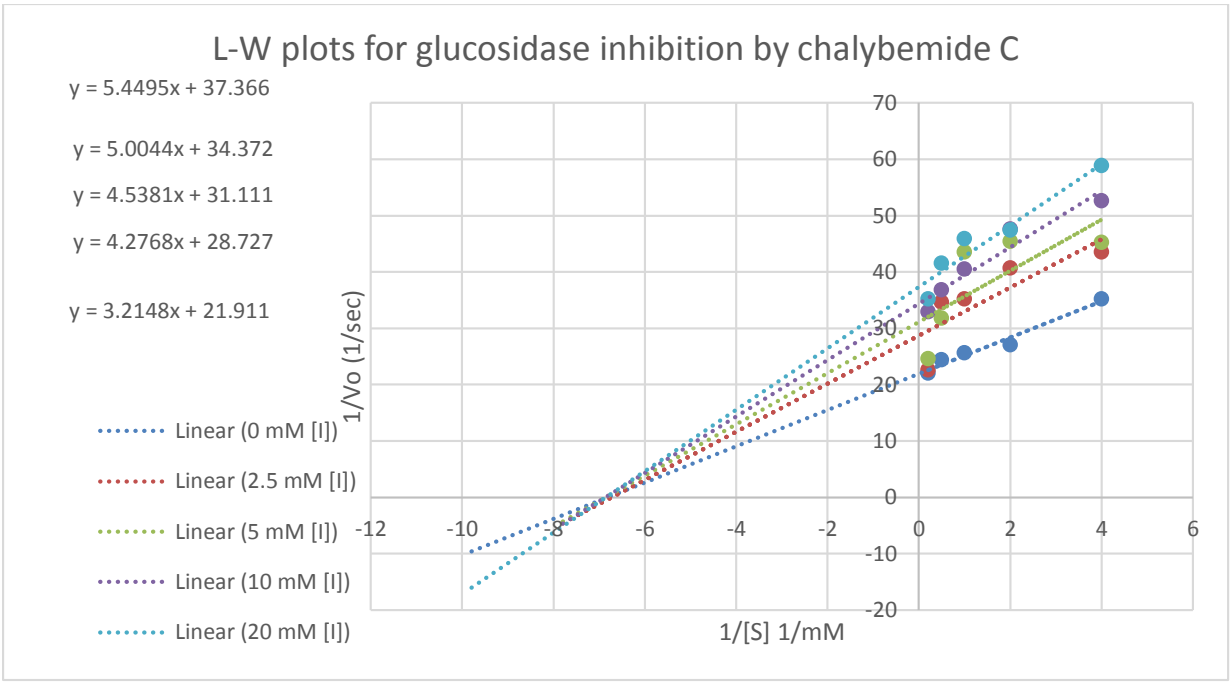
L-W plots for glucosidase inhibition by chalybemide C
y = 5.4495x + 37.366
y = 5.0044x + 34.372
y = 4.5381x + 31.111
y = 4.2768x + 28.727
y = 3.2148x + 21.911
Linear (0 mM [I])
Linear (2.5 mM [I])
Linear (5 mM [I])
Linear (10 mM [I])
Linear (20 mM [I])
1/Vo (1/sec)
1/[S] 1/mM
70
60
50
40
30
20
10
0
-10
-20
-12
-10
-8
-6
-4
-2
0
2
4
6

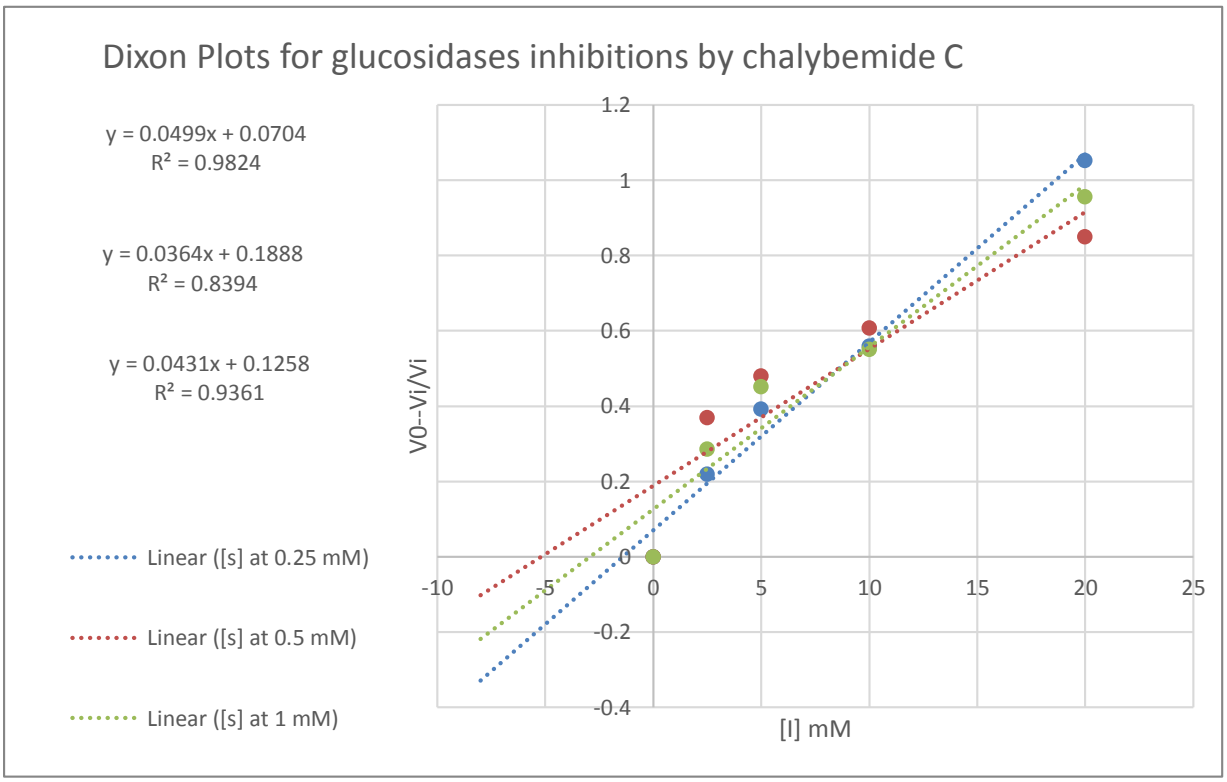
Dixon Plots for glucosidases inhibitions by chalybemide C
y = 0.0499x + 0.0704
R² = 0.9824
y = 0.0364x + 0.1888
R² = 0.8394
y = 0.0431x + 0.1258
R² = 0.9361
Linear ([s] at 0.25 mM)
Linear ([s] at 0.5 mM)
Linear ([s] at 1 mM)
V0--Vi/Vi
[I] mM
1.2
1
0.8
0.6
0.4
0.2
0
-0.2
-0.4
-10
-5
0
5
10
15
20
25

12.10: Lineweaver-Burk plots and Dixon plots for 2,3-epoxy-6,7-methlenedioxy coniferyl alcohol

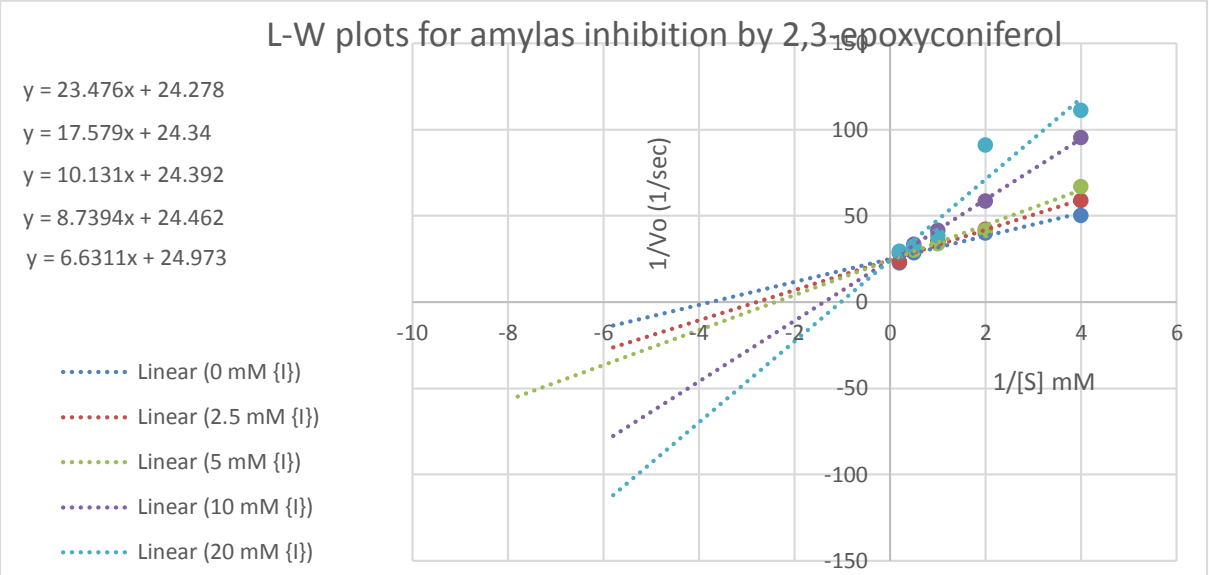

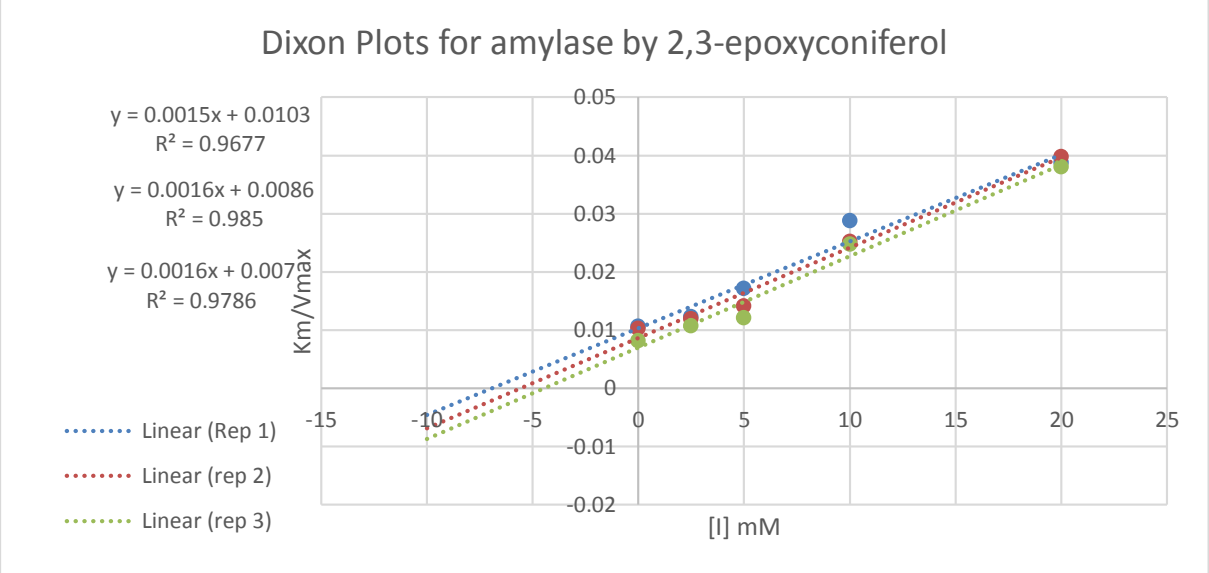

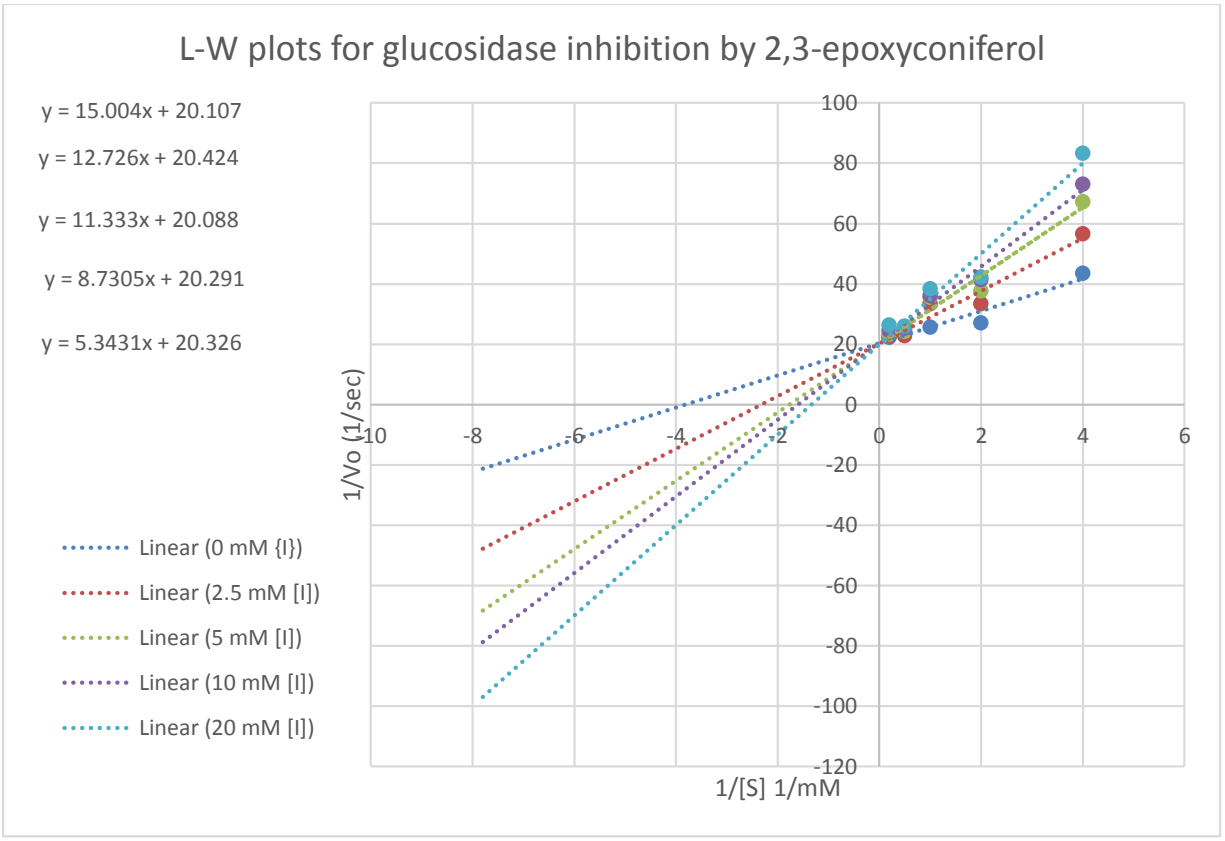
L-W plots for glucosidase inhibition by 2,3-epoxyconiferol
y = 15.004x + 20.107
y = 12.726x + 20.424
y = 11.333x + 20.088
y = 8.7305x + 20.291
y = 5.3431x + 20.326
Linear (0 mM {I})
Linear (2.5 mM [I])
Linear (5 mM [I])
Linear (10 mM [I])
Linear (20 mM [I])
1/Vo (1/sec)
1/[S] 1/mM
100
80
60
40
20
0
-20
-40
-60
-80
-100
-120
-10
-8
-6
-4
-2
0
2
4
6

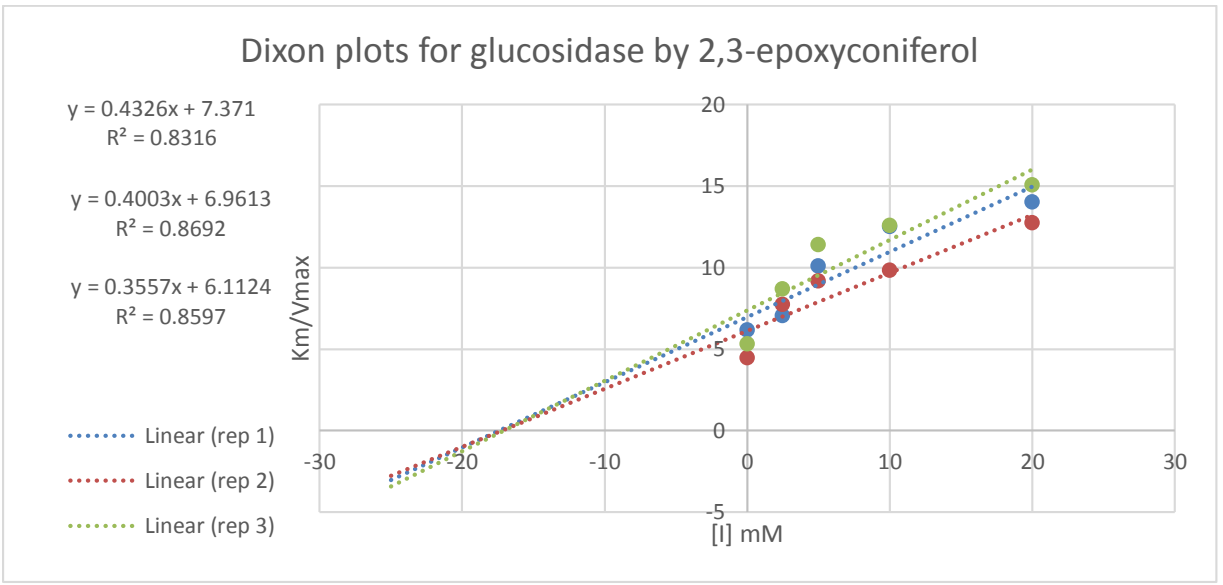
Dixon plots for glucosidase by 2,3-epoxyconiferol
y = 0.4326x + 7.371
R² = 0.8316
y = 0.4003x + 6.9613
R² = 0.8692
y = 0.3557x + 6.1124
R² = 0.8597
Linear (rep 1)
Linear (rep 2)
Linear (rep 3)
Km/Vmax
[I] mM
20
15
10
5
0
-5
-30
-20
-10
0
10
20
30

12.11: Lineweaver-Burk plots and Dixon plots for 1,3-dimethoxy-12-methyl-9H-[1,3]benzodioxolo[5,6-c]phenanthridin-12-ium (Chelerythrine derivative) (42)

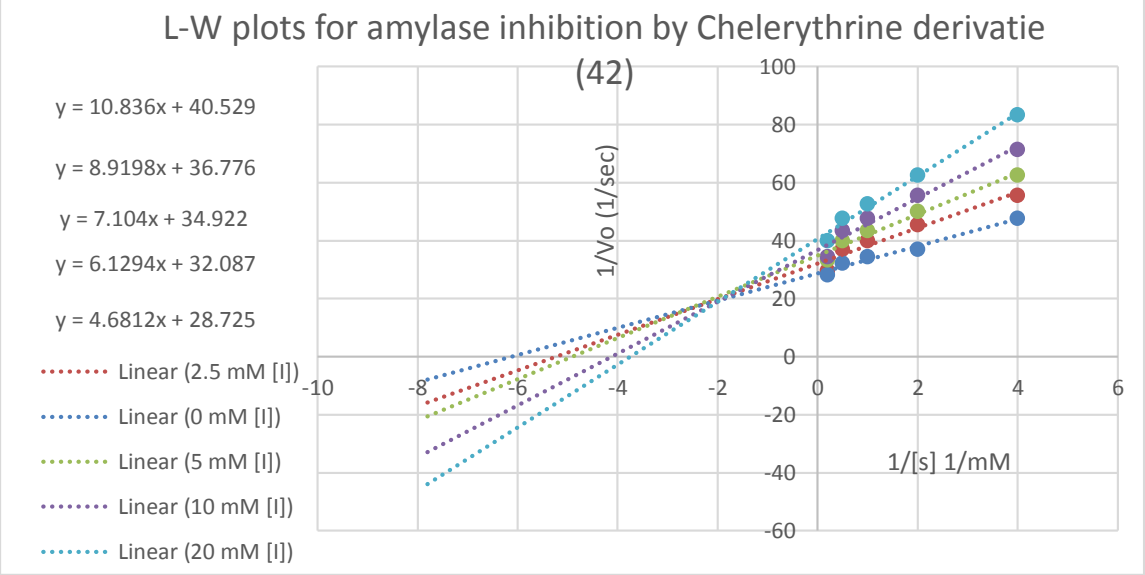

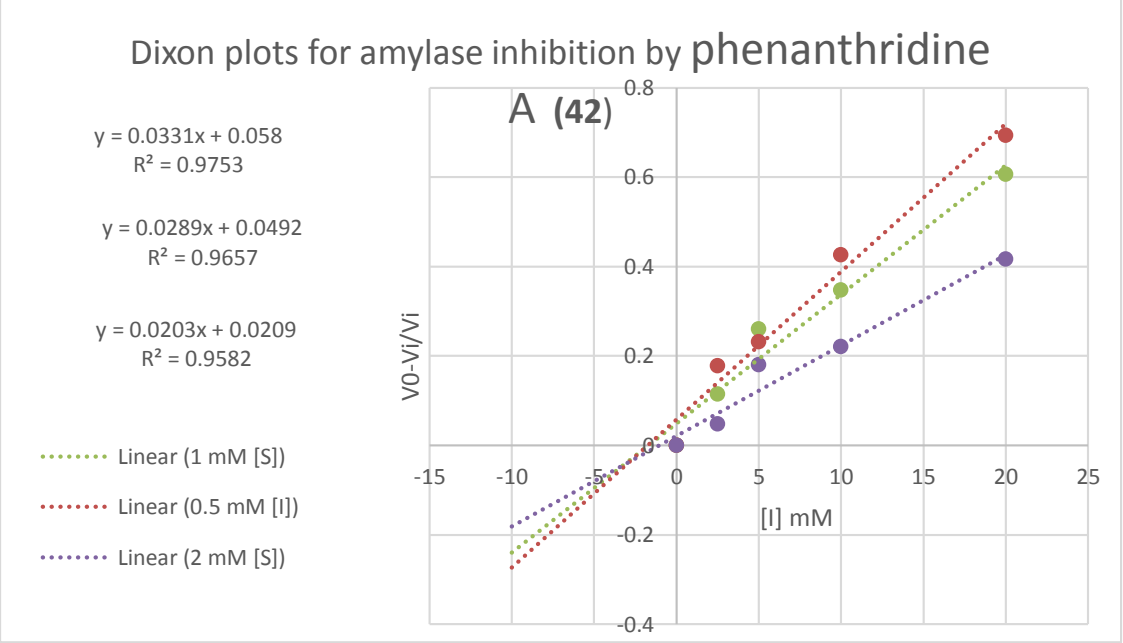

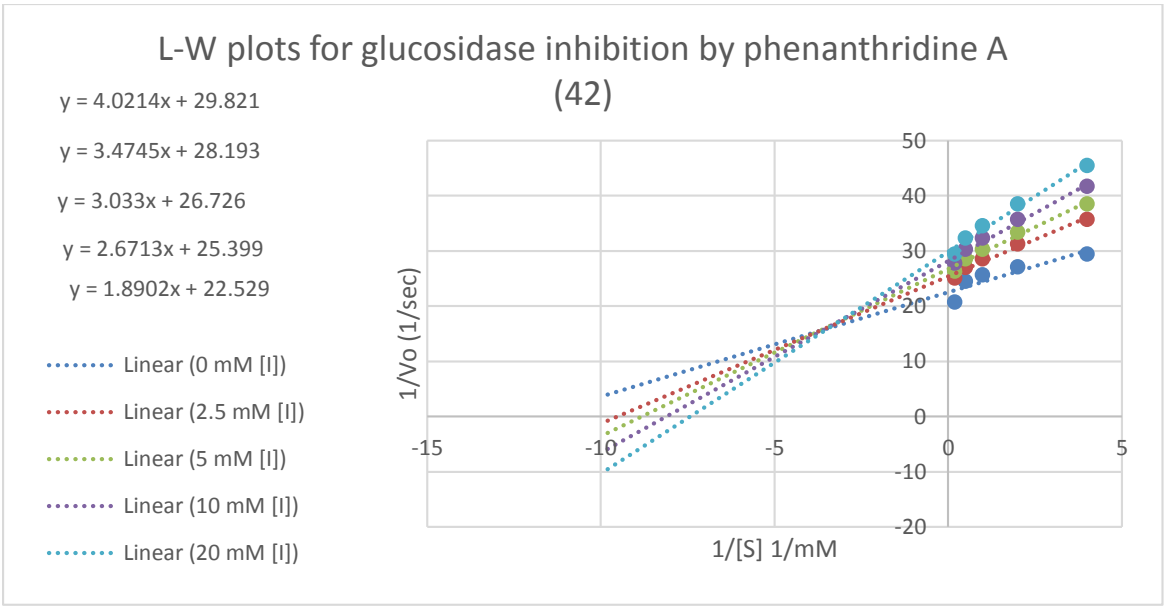
L-W plots for glucosidase inhibition by phenanthridine A (42)
y = 4.0214x + 29.821
y = 3.4745x + 28.193
y = 3.033x + 26.726
y = 2.6713x + 25.399
y = 1.8902x + 22.529
Linear (0 mM [I])
Linear (2.5 mM [I])
Linear (5 mM [I])
Linear (10 mM [I])
Linear (20 mM [I])
1/Vo (1/sec)
1/[S] 1/mM
50
40
30
20
10
0
-10
-20
-15
-10
-5
0
5

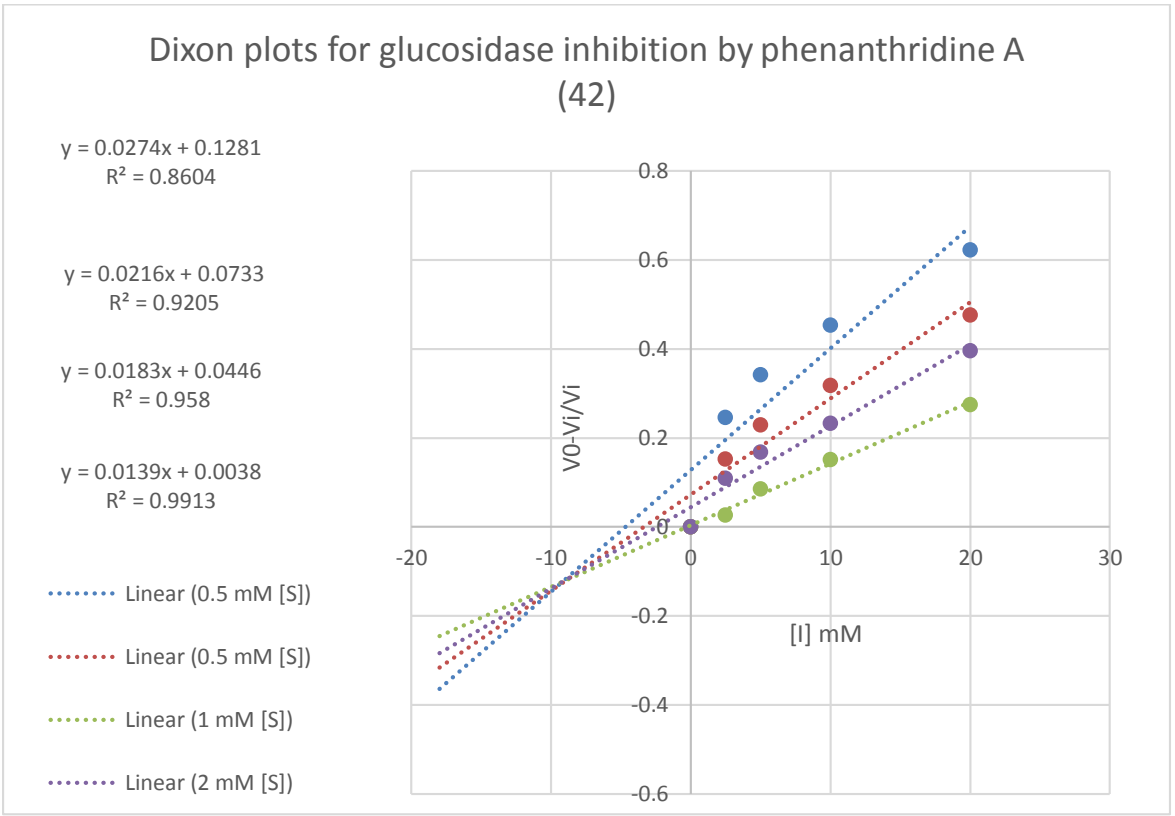
Dixon plots for glucosidase inhibition by phenanthridine A (42)
y = 0.0274x + 0.1281
R² = 0.8604
y = 0.0216x + 0.0733
R² = 0.9205
y = 0.0183x + 0.0446
R² = 0.958
y = 0.0139x + 0.0038
R² = 0.9913
Linear (0.5 mM [S])
Linear (0.5 mM [S])
Linear (1 mM [S])
Linear (2 mM [S])
V0-Vi/Vi
[I] mM
0.8
0.6
0.4
0.2
0
-0.2
-0.4
-0.6
-20
-10
0
10
20
30

12.12: Lineweaver-Burk plots and Dixon plots for Acarbose

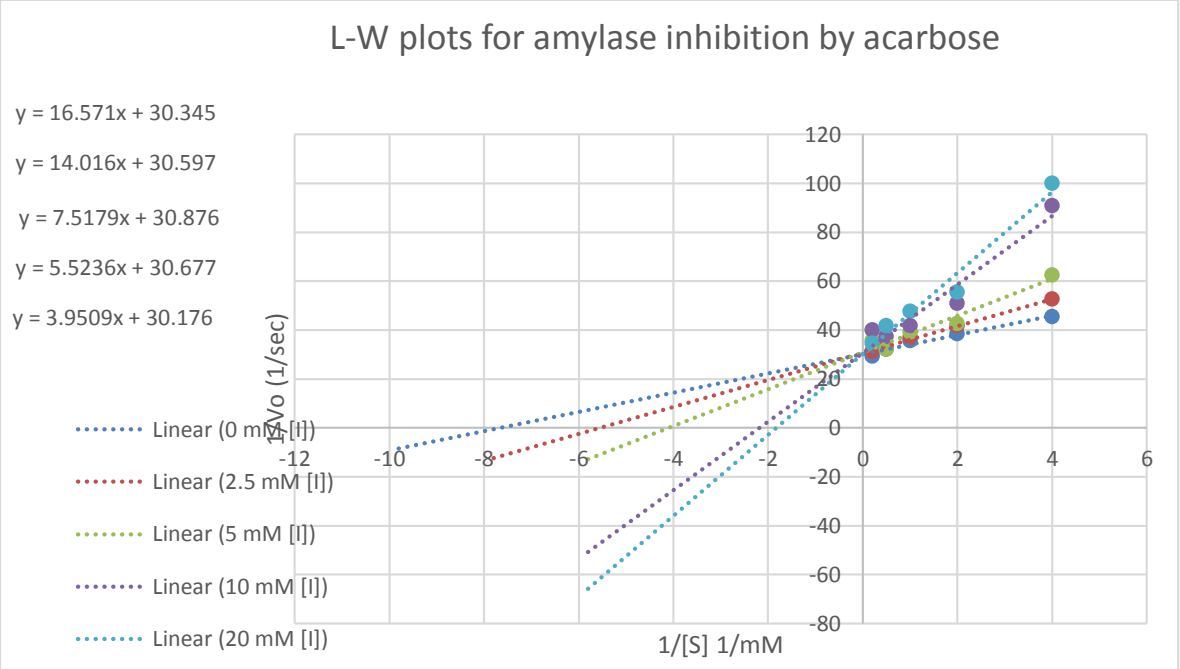

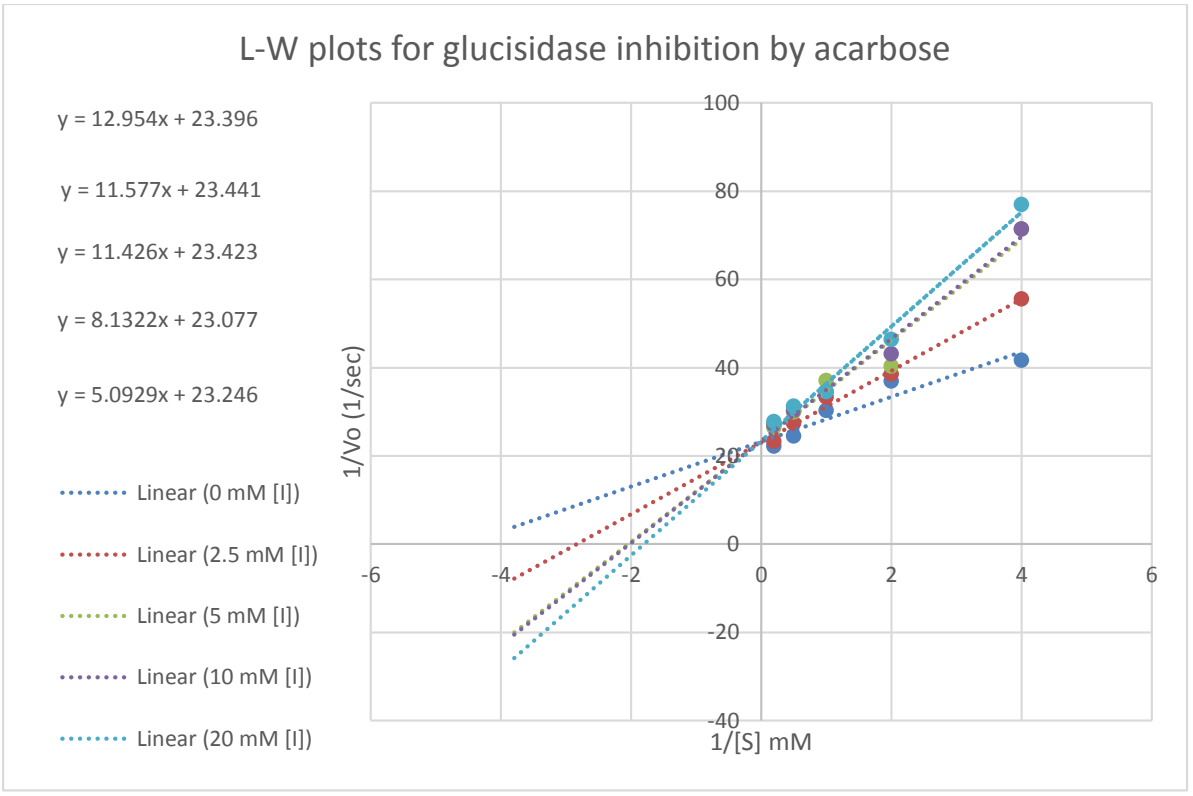
L-W plots for glucisidase inhibition by acarbose
y = 12.954x + 23.396
y = 11.577x + 23.441
y = 11.426x + 23.423
y = 8.1322x + 23.077
y = 5.0929x + 23.246
Linear (0 mM [I])
Linear (2.5 mM [I])
Linear (5 mM [I])
Linear (10 mM [I])
Linear (20 mM [I])
1/Vo (1/sec)
1/[S] mM
100
80
60
40
20
0
-20
-40
-6
-4
-2
0
2
4
6

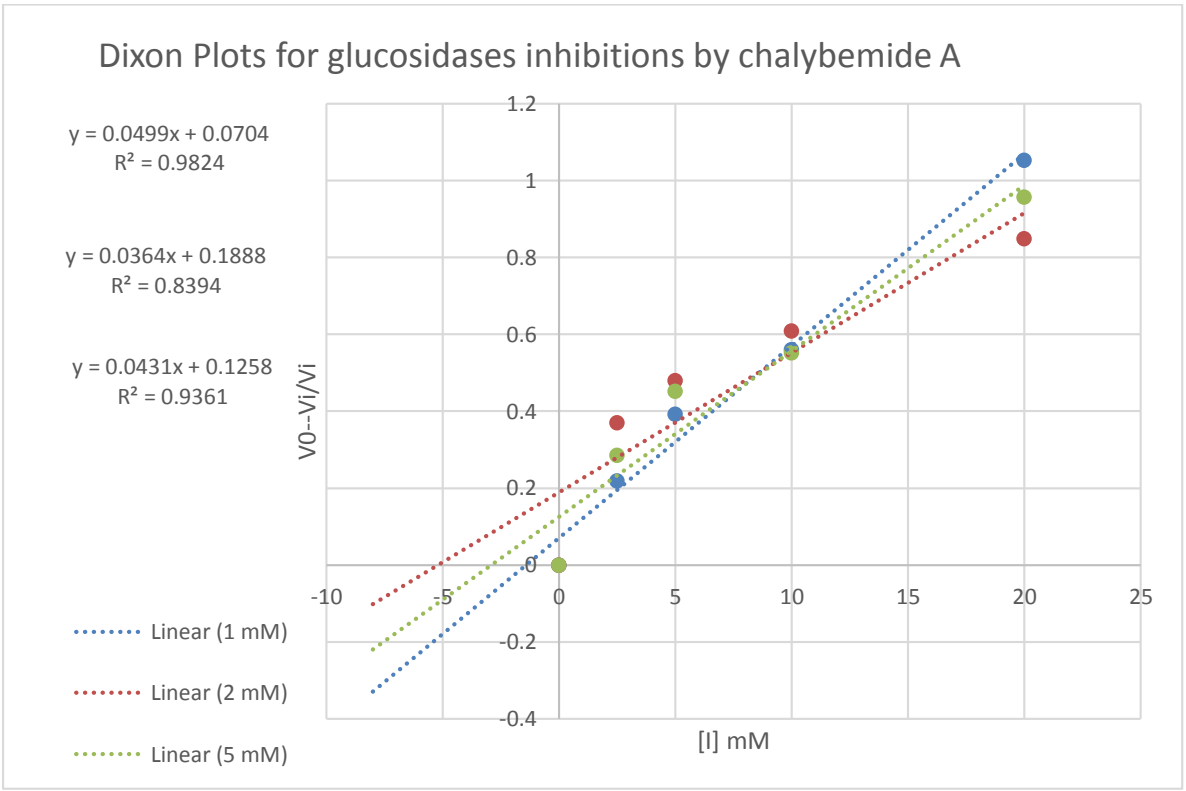
Dixon Plots for glucosidases inhibitions by chalybemide A
y = 0.0499x + 0.0704
R² = 0.9824
y = 0.0364x + 0.1888
R² = 0.8394
y = 0.0431x + 0.1258
R² = 0.9361
Linear (1 mM)
Linear (2 mM)
Linear (5 mM)
V0--Vi/Vi
[I] mM
1.2
1
0.8
0.6
0.4
0.2
0
-0.2
-0.4
-10
-5
0
5
10
15
20
25